Optimisation of a chronically implanted catheter for intraparenchymal delivery of therapeutics to the brain

For the consideration of the award:

Doctor of Philosophy (PhD)

Name: Trefor Owen Lewis

Student ID: 0227265

Date: 17th December 2019

Declarations

I hereby confirm that the work submitted is my own and has not been accepted in substance for any other degree or award, and is not being submitted concurrently in candidature for any degree or other award.

Until such time that a decision is made on the eligibility of this application for the award of PhD (Doctor of Philosophy), this work will not be submitted to another institution for the consideration of any award.

Where publications have arisen from the work undertaken, these are stated. I confirm that this submission, as a whole, is not substantially equivalent to previously published works.

Throughout the duration of this research I have been in the employment of Renishaw PLC who have also funded the student fees and experiments described within this thesis. Renishaw own several patents in relation to the catheter, equipment and methods utilised as part of this research and I am a named inventor on several patent applications, all of which are owned by the Renishaw PLC group.

Final word count: 35,855

Abstract

Delivering drugs to the brain to treat degenerative diseases and other conditions is challenging because of the blood brain barrier, which acts as a filtration system preventing over 99 % of large, therapeutic molecules from entering the brain from the blood. A *first-in-man* study, delivering drugs directly through chronically implanted catheters inserted deep into the brain, formed the basis of this project. The short and long-term distribution data from this clinical study provided the direction of this research.

Surgical planning guidelines were created which provide device specific, numerical values to optimise retention of infusate within target neuroanatomy.

Optimisation of these implanted catheters was assessed through device characterisation, material investigation, development of miniaturised delivery systems for *in vivo* investigations and the creation of a finite element model of infusions into porous 'brain' matter.

Despite dissimilar mechanical properties to brain tissue, agarose gel has superior permeability and optical properties over composite hydrogels for the characterisation of a recessed step catheter. *In vitro* experiments varying catheter features and infusion regimes identified significant changes in the distribution patterns of infused fluids which propagate through porous substrates, such as gels or the brain. By adjusting the catheter step length and peak volumetric flow rate, optimisation of implanted catheters could maximise coverage of target neuro anatomy.

Gliosis around the implanted catheter was anticipated as a result of the immune response to injury. Through experimentation gliosis was shown not to be exacerbated by intermittent infusions. The extent of injury during implantation plays a greater role. Changes in clinical infusion distribution patterns may have been linked to observations of lower gliosis levels around the same time as test infusions occur clinically (1month post implant). Longer recovery periods could provide improved reliability of test infusions to inform users ahead of setting prescriptions for extended infusion regimes.

Published work arising from this thesis

Peer reviewed journal articles

Lead author

Lewis, O. et al. 2016. Chronic, intermittent convection-enhanced delivery devices. *J Neurosci Methods* 259, pp. 47-56. doi: 10.1016/j.jneumeth.2015.11.008

Lewis, O. et al. 2018. Maximising coverage of brain structures using controlled reflux, convection-enhanced delivery and the recessed step catheter. *J Neurosci Methods*, doi: 10.1016/j.jneumeth.2018.08.029

See appendicies for work submitted for publication

Co-authored

Barua NU, Woolley M, Bienemann AS, Johnson D, Wyatt MJ, **Lewis O**, Irving C, Castrique E, Gill SS. Convection-enhanced delivery of AAV2 in white matter--a novel method for gene delivery to cerebral cortex. J Neurosci Methods. 2013;220(1):1-8. doi: 10.1016/j.jneumeth.2013.08.011

Barua NU, Woolley M, Bienemann AS, Johnson DE, **Lewis O**, Wyatt MJ, Irving C, O'Sullivan S, Murray G, Fennelly C, Skinner P, Gill SS.. Intermittent convection-enhanced delivery to the brain through a novel transcutaneous bone-anchored port. J Neurosci Methods. 2013;214(2):223-32. doi: 10.1016/j.jneumeth.2013.02.007

Barua NU, Bienemann AS, Woolley M, Wyatt MJ, Johnson D, **Lewis O**, Irving C, Pritchard G, Gill SS. Convection-enhanced delivery of MANF--volume of distribution analysis in porcine putamen and substantia nigra. J Neurol Sci. 2015;357(1-2):264-9. doi: 10.1016/j.jns.2015.08.003

Gill T, Barua NU, Woolley M, Bienemann AS, Johnson DE, O'Sullivan, Murray G, Fennelly C, **Lewis O**, Irving C, Wyatt MJ,Moore P, Gill SS. In vitro and in vivo testing of a novel recessed-step catheter for reflux-free convection-enhanced drug delivery to the brain. J Neurosci Methods. 2013;219(1):1-9. doi: 10.1016/j.jneumeth.2013.06.008

Luz M, Allen PC, Bringas J, Boiko C, Stockinger DE, **Lewis O**, Nikula KJ, Woolley M, Fibiger HC, Bankiewicz K. Intermittent convection-enhanced delivery of GDNF into rhesus monkey putamen: absence of local or cerebellar toxicity. Arch Toxicol. 2018;92(7):2353-67. doi: 10.1007/s00204-018-2222-z

Singleton WGB, Bienemann AS, Woolley M, Johnson D, **Lewis O**, Wyatt MJ, Damment SJP,Boulter LJ, Killick-Cole C, Asby DJ, Gill SS. The distribution, clearance, and brainstem toxicity of panobinostat administered by convection-enhanced delivery. J Neurosurg Pediatr. 2018;22(3):288-96. doi: 10.3171/2018.2.peds17663

Whone A, Luz M, Boca M, Woolley M, Mooney L, Dharia S, Broadfoot J, Cronin D, Schroers C, Barua NU, Longpre L, Barclay CL, Boiko C, Johnson GA, Fibiger HC, Harrison R, **Lewis O**, Pritchard G, Howell M, Irving C, Johnson DE, Kinch S, Marshall C, Lawrence AD, Blinder S, Sossi V, Stoessi AJ, Skinner P, Mohr E, Gill SS. 2019. Randomised trial of intermittent intraputamenal glial cell line-derived neurotrophic factor in Parkinson's disease. Brain. 2019 Mar 1;142(3):512-525. doi: 10.1093/brain/awz023

Whone A, Boca M, Luz M, Woolley M, Mooney L, Dharia S, Broadfoot J, Cronin D, Schroers C, Barua NU, Longpre L, Barclay CL, Boiko C, Johnson GA, Fibiger HC, Harrison R, **Lewis O**, Pritchard G, Howell M, Irving C, Johnson DE, Kinch S, Marshall C, Lawrence AD, Blinder S, Sossi V, Stoessi AJ, Skinner P, Mohr E, Gill SS 2019. Extended Treatment with Glial Cell Line-Derived Neurotrophic Factor in Parkinson's Disease. J Parkinsons disease. 2019 Feb 26. doi: 10.3233/JPD-191576

Conference presentations

Lead presenter

Lewis O, Woolley M, Johnson DE, Irving C, Stewart G, Howell M, Kinch S, Moore P, Timbrell R, Fletcher J, Pritchard G, Skinner P, Campbell S, Bienemann AS, Barua NU, Wyatt MJ, Rosser AE, Evans SL, Gill SS. *A systems based approach to drug delivery - a method that works.* SNO-SCIDOT Joint Conference on Therapeutic Delivery to the CNS; San Antonio, Texas, USA. 2015.

Lewis O, Woolley M, Johnson D, Bienemann A, Barua N, Singleton W, Harcourt-Brown T, Gill SS. *Functional and translational performance of a novel recessed-step catheter and stereotactic system for use in pre-clinical and clinical CED indications.* AMND; Liblice, Czech-Republic. 2017.

Lewis O, Woolley M, Johnson DF, J, Moore PB, AS, Gill SS. *Accurate and informed placement of indwelling catheters is vital for successful direct delivery to the brain*. 22nd Covance symposium; Munster, Germany. 2018.

Contributor

Singleton WGB, Barua NU, Morgan JA, **Lewis O**, Johnson DE, Woolley M, Edwards RJ, Lowis SP, Gill SS (2016) - PF-062 Neuro-oncology - Robot-assisted multi-catheter chronic intermittent convection enhanced drug delivery for the treatment of paediatric diffuse intrinsic pontine glioma: surgical case series of 10 patients. 44th Annual Meeting of International Society for Pediatric Neurosurgery, Kobe, Japan, Oct 23-27, 2016 (Childs Nerv Syst (2016) 32:1957–2040)

Singleton WGB, Woolley M, Johnson DE, **Lewis O**, Bienemann AS, Barua NU, Gill SS. Multi-catheter intermittent convection-enhanced delivery of carboplatin as a treatment for diffuse intrinsic pontine glioma (DIPG): pre-clinical rationale and early clinical experience. International Symposium on Paediatric Neuro-Oncology, ISPNO; Liverpool, UK. 2016.

Singleton WGB, Woolley M, Johnson DE, **Lewis O**, Bienemann AS, Barua NU, Gill SS. Preclinical development of a translatable drug delivery platform. International Symposium on Paediatric Neuro-Oncology, ISPNO; Liverpool UK. 2016.

Singleton WGB, Woolley M, **Lewis O**, Johnson DE, Irving, C, Pritchard G, Moore P, Kinch S, Howell M, Selby J, Fletcher J, Skinner P, Bienemann AS, Harcourt-Brown T, Barua NU, Gill SS.. Development of new CED devices. SCIDOT-SNO; San Francisco, USA. 2017.

Woolley M, Barua NU, **Lewis O**, Keane I, Johnson DE, Irving C, Kinch S, Moore P, Howell M, O'Sullivan S, Fennelly C, Pritchard G, Campbell S, Skinner P, Gill SS. Factors Facilitating Optimised Intraparenchymal Drug Delivery – A Prescriptive Systems Approach. Partnership Opportunities in Drug Delivery; Boston, USA. 2013.

Woolley M, **Lewis O**, Johnson DE. Optimising Intraparenchymal Convection Enhanced Delivery. World Preclinical Congress; Boston, USA. 2018.

Conference Posters

Author

Lewis O, Woolley M, Johnson DE, Fenech J, Keenan B, Potts M, Hobden P, Evans SL,. Novel brain phantoms for neurological catheter development. World Congress of Biomechanics; Dublin, Ireland. 2018.

Lewis O, Woolley M, Johnson D, Moore PF, Fenech J, Barua NU, Bienemann AS, Singleton W, Gill SS. Successful delivery to the brain requires effective targeting, convection-enhanced-delivery and controlled reflux - Translation of drug delivery systems from lab to clinic. World Preclinical Congress; Boston, USA. 2018.

Co-author

Hollingworth M, Hurter C, Collins P, Singleton W, Wooley M, **Lewis O**, Skinner P, Munroe P, Desai M, Chandler C, Bristow A, Jarosz J, Deasy N, Killick-Cole C, Bienamann AS, Walker D, Gill S, Zacharoulis S. DIPG-65. Preliminary experience of chronic intermittent convection-enhanced delivery of carboplatin and sodium valproate for the treatment of diffuse intrinsic pontine glioma following radiation therapy. Neuro-Oncology. 2018;20(suppl_2):i62-i. doi: 10.1093/neuonc/noy059.158

Acknowledgements

Thanks should go to a longer list of people than can reasonably be allowed here, however, thanks go first to my supervisors Dr Max Woolley, Dr David Johnson, Prof Anne Rosser and Prof Sam Evans who, along with Renishaw have enabled this project.

Thanks must also go to:

Dr Bethany Keenan and Dr Mariusz Pietrzyk, both of who have provided endless encouragement and inspiration.

Prof Steven Gill and Mr Neil Barua, without who's inventive spirits there would be a step missing on the path to treating numerous life changing illnesses.

Dr Alison Bienemann, Mr Will Singleton and the functional neurosurgery group at the University of Bristol who have supervised and guided countless studies on the route to developing and optimising this delivery platform. In particular to Marcella Wyatt and Lisa Boulter who's technical skills and knowledge have been instrumental in the processing of immunohistochemical samples.

Dr David (Harri) Harrison and Dr Mutwakil Abdulla of the Brain Repair Group for assistance in devising and running studies within Cardiff University.

The highly skilled staff at the translational biomedical research centre (TBRC), Langford, Bristol.

To the old, new and current staff of the neurological applications department at Renishaw who have moved mountains to develop a totally novel neurosurgical procedure to treat previously untreatable neurological conditions.

To all those I've missed out by name my apologies but also my thanks, every contribution has contributed to not only this work but another step on the road to new treatments.

Finally, special thanks go to the bravery of all participants and those responsible for running the ground breaking GDNF trial in Bristol between 2011-2015.

Dedication of thesis

I fy nheulu/ For my family

Contents

List of figures

List of tables

Nomenclature

δ	Displacement
λ	Tortuosity
Φ	Porosity
τ	Time
A	area
aCSF	artificial Cerebro Spinal Fluid
BBB	Blood-Brain Barrier
C	Concentration
CED	Convection-Enhanced Delivery
CNS	Central Nervous System
CSF	Cerebro Spinal Fluid
CUBRIC	Cardiff University Brain Research Imaging Centre
D	Diffusion coefficient
DDS	Drug Delivery System
FEA	Finite Element Analysis
FEM	Finite Element Model
FNS	Functional Neurosurgery Group (Bristol University)
GDNF	Glial cell line-Derived Neurotrophic Factor
IGT	Inner Guide Tube
IHC	Immunohistochemical/ Immunohistochemistry
ISF	Interstitial fluid
IV	Intravascular
j	flux (volumetric flow rate per unit area)
k^{irr}	First order degradation rate constant
NAD	Neurological Applications Department (Renishaw)
NHP	Non-Human Primate
OD	Outer diameter
OGT	Outer Guide Tube
PD	Parkinson's disease
PNS	Peripheral Nervous System
Q	Volumetric flow rate
R	Universal gas constant
RSC	Recessed Step Catheter
SEM	Standard error of the mean
STD	Standard deviation
t	Time
T_E	Echo time (MRI parameter)
T_R	Repetition time (MRI parameter)
UPDRS	Unified Parkinson's Disease Rating Scale
v	Velocity
V	Volume
X	Distance

Glossary

Backflow	See ‘reflux’
First-in-man	Seminary use of a technology or pharmaceutical in a human subject
Glia Limitans	A naturally occurring boundary within the cortex which limits the development of glial cells beyond the cortical layer of the brain
Intraparenchymal	Within the body of an organ, within the context of this thesis this predominantly refers to the brain
Interstitial	The space between cells, in the context of this thesis this refers specifically to the space between cells in the brain tissue
Locally advanced	Spread of cancer to local, surrounding tissues
Metastasis	Cancer which has spread from one organ or place of the body to another
Neuroglia	Aside from neurons (the cells which carry nerve impulses) these cells are the most prolific within the brain and are responsible for homoeostasis and immune response to injury/ insult
Parenchyma	The functional tissue within on organ of the body
Penumbra	In the context of a neurological tumour, it is the area of tissue which immediately surrounds the tumour mass or resection cavity following surgery which is most at risk of local advancement or causing metastasis
Reflux	The undesirable backflow of fluid around the exterior face of a catheter positioned in the brain tissue (not a cavity)
Solute	A substance dissolved in a solvent
Solution	Solvent + Solute = Solution
Solvent	A fluid into which a solute can dissolve

1 Introduction

The brain is arguably the most important of our organs. Whether it is the autonomous regulation of the heart, or the decision to lift a coffee cup at the start of the day, the brain is involved in all aspects of conscious and unconscious thought, action and deed.

Keeping it healthy is therefore paramount, and when disease or infection arise, it is desirable to bring the brain back into a state of normality as soon as possible so that 'business as usual' can resume.

The consumption of drugs to alleviate illness, whether as a tablet or injection are now commonplace, either as over-the-counter medications or via a doctor's prescription. While small molecules such as alcohol, oxygen or paracetamol can enter the cerebrospinal fluid within the brain (Langford *et al.*, 2016; Kumpulainen *et al.*, 2007), large macromolecules are prevented from passing from the blood into the brain by the blood brain barrier (BBB). This naturally occurring filtration system was discovered when neurotoxins were shown to affect only the brain when injected directly into the brain tissue, and not when delivered systemically (Lewandowsky, 1909). It was not until the late 1960s that the barrier was identified as the tight junctions between endothelial cells which line the blood vessels (Reese and Karnovsky, 1967). The BBB is a useful feature in nature to protect the brain from toxins that might be ingested from the environment, but problematic in the field of pharmaceuticals where man made drugs are too big to pass into the brain freely. The BBB typically prevents over 99 % of systemically delivered drugs from entering the brain (Stockwell *et al.*, 2013).

Technologies in the form of medical devices to aid in the transfer of these macromolecules to the brain tissue directly are few and far between, despite a clear need across numerous medical conditions. Children with brain stem tumours continue to have a short life expectancy following diagnosis (median survival ~9months (Singleton *et al.*, 2018)) and the burden of neurodegenerative diseases (Parkinson's, Alzheimer's, Huntington's, etc.) on healthcare systems continues to rise in line with the global population and improved registration in less developed countries.

One of the key challenges to treating neurological conditions therefore remains, overcoming the BBB to deliver drugs directly to the site of action. Such a technique was described in the mid-1990s by a group investigating ways of improving dispersion of drug during injection into the brain tissue (Bobo *et al.*, 1994). Slow injection flow rates (0.1-1.0 µl/min) were used to gradually increase the local hydrostatic pressure to push fluid radially away from the injection site. The method was termed convection-enhanced delivery (CED), which overcame the issues of backflow (reflux) along the catheter track which was prevalent in previous injection studies.

Since 1994 however several high profile clinical trials failed to meet their clinical outcomes, dampening the adoption of CED as a paradigm for the treatment of neurological disease (Nutt *et al.*, 2003; Lang *et al.*, 2006; Kunwar *et al.*, 2010). While poor drug efficacy could not be ruled out, follow up studies repeatedly showed that successful delivery of the fluids to the target region of the brain was not achieved (Mueller *et al.*, 2011; Sampson *et al.*, 2010) suggesting that improved technology for single and repeated delivery may yet provide a pathway to treating these debilitating conditions.

The author formed part of a collaboration between academia, industry and healthcare to create a novel system for the direct injection of drugs into the tissue of the brain, and resolve limitations in the technology seen in previous drug trials which failed to meet their goals. The development of the system is beyond the scope of this thesis, though is detailed in numerous co-authored publications.

The drug delivery system developed was used in a clinician led study in Bristol, UK, where Parkinson's disease patients were enrolled to receive monthly infusions of a protein, directly into their brains for 18 months, in the hope of halting, and possibly reversing the symptoms of their disease. As a *first-in-man* study of not only this technology, but also the method of intermittently infusing fluid monthly into the tissue of the brain, this represented a unique opportunity to evaluate and optimise chronic, intermittent delivery.

The aim of this thesis was to collate and interpret the device related data from the clinical study and develop strategies for optimising distribution of drugs into the brain tissue to maximise the likelihood of drugs producing clinical improvements in diseased patients in future studies.

The objectives of the project were;

- To collate device related distribution data from the first-in-man clinical study to form a baseline of intermittent delivery performance
- Critique the methods used to deliver drugs intermittently and identify opportunities for improvements, with respect to device performance
- Review the current choice of materials used in the production of brain mimics for opportunities to improve the reliability of evidence generated on device performance in laboratory evaluations
- Implement a parametric study of the recessed step catheter design for drug delivery to baseline performance when the device features are modified, or the device is used with differing, clinically useful flow rates
- Create a finite element model of the device and infusions to describe the mechanical strains present around an implanted catheter
- Evaluate the immune response to intermittent infusions through an implanted catheter
- Combine learning points from all studies into a series of surgical guidelines for improved likelihood of distribution performance during repeated, intermittent infusions in the brain

2 Literature review

2.1 An introduction to the field of direct delivery of therapeutics to the brain

This chapter contains work previously published within the Journal of Neuroscience Methods review article "Chronic, intermittent convection-enhanced delivery devices" (Lewis et al., 2016)

The healthcare and social burden of neuro-degeneration and neuro-oncology is large and increasing. Global figures are difficult to ascertain as poorer nations have inadequate methods of identifying and disseminating frequencies. However, with over 4.6 million patients identified with Parkinson's disease (PD) in the top 10 populated countries of the west, and in excess of 20 million with Alzheimer's disease (Kowal *et al.*, 2013; Dorsey *et al.*, 2007) there is a clear need for a treatment option capable of delivering therapeutics to the tissues affected by these, and other neurological conditions. Further, forecast burden models predicted that PD cases will double within 15-25 years while Alzheimer's disease may triple (81.1 million) by 2040 (Lopez, 2011; W.H.O., 2006). This will place a very high demand on healthcare resources all over the world.

Delivery of medicines to the body is usually accomplished through oral or intravascular (IV) administration. These routes place active molecules within the bloodstream which are then indiscriminately transported all over the body through the vascular system. Vessel walls are lined with endothelial cells, which are joined by tight junctions. Within the brain, it is these tight junctions which permit the transfer of oxygen and nutrients to the surrounding tissues but are also responsible for preventing the migration of large therapeutic molecules to areas affected by disease. This filtration network protects the brain from injected poisons and other dangers ingested from the environment and is termed the Blood-Brain Barrier (BBB) (Bauer *et al.*, 2014). It is the BBB which prevents oral or IV routes of administration from being viable treatment options as <1 % of systemically administered drugs reach the brain (Stockwell *et al.*, 2013). In order to achieve therapeutic levels in the target tissues, it would be necessary to deliver drugs systemically at such elevated levels that they become toxic to the other tissues of the body.

Bypassing the BBB and directly injecting therapeutics into the target tissues of the parenchyma is a long-hypothesised alternative.

Cannulae placed into the brain could deliver therapeutics by displacing the interstitial fluids between the cells and inducing flow through the porous brain tissue. As the brain tissue is soft, it is the sealing force against the cannula wall which retains the fluid in the tissues around the injection site. In 1994 it was shown that injection was an inadequate method of delivery as the flow rates used were routinely too high and injected boluses overwhelmed the sealing pressure and refluxed back along the catheter track (Bobo *et al.*, 1994). If injection rates were lowered and pressures gradually increased to mimic vasogenic oedema, fluids would convect through the porous substrate from a point source.

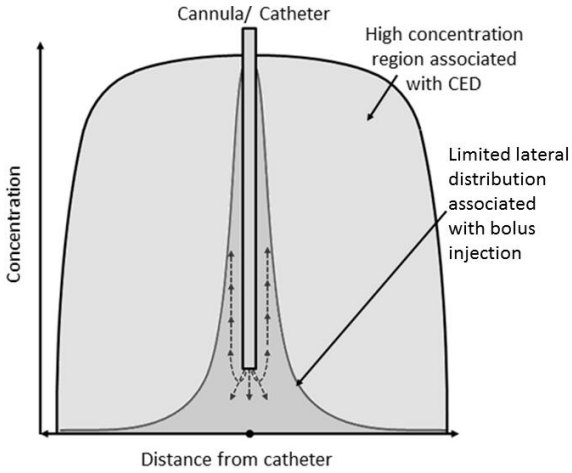

Figure 2-1. Graphic depiction comparing the distribution associated with Convection-Enhanced Delivery (CED) and bolus injection (reproduced and modified from (Lam, Thomas and Lind, 2011). Note that the region of high concentration has spread laterally a much larger distance from the catheter than simply injecting a bolus which is the hallmark of CED.

Convection dramatically increased the radial concentration of therapeutic macromolecules in tissues away from the catheter site (Figure 2-1) (Bobo *et al.*, 1994; Morrison *et al.*, 1994). This method was termed Convection-Enhanced Delivery (CED) and it remains a popular term for this paradigm for research.

Translation of CED into clinic has not only been slow, but a standard treatment which indicates the use of CED does not currently exist. Despite positive results in pre-clinical animal research (Gash *et al.*, 1996) as well as investigational, clinician led (unblinded) studies in humans (Gill *et al.*, 2003; Slevin *et al.*, 2005; Patel *et al.*, 2013), formal, blinded clinical trials have failed to meet their primary endpoints (Lang *et al.*, 2006; Kunwar *et al.*, 2010). As the system is considered a combination therapy in the United States, no translation through trials to market of a medical device has yet been achieved.

Retrospective investigations found that overly ambitious study design, higher than expected placebo affects, catheter target accuracy and predictability of distributions were major factors in failing to achieve successful outcomes (Mueller *et al.*, 2011; Sampson *et al.*, 2010).

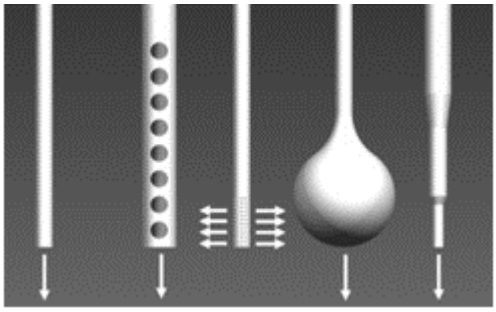

Figure 2-2. Device design groups used in CED studies (left to right); End Port Cannula, Multi-Port Cannula, Porous Tipped Catheters, Balloon Tipped Catheters and Stepped Profile Catheters,– image reproduced and modified from (Debinski and Tatter, 2009).

Recent improvements, notably to the delivery platform, have reinvigorated the application of clinical CED with eight active studies registered in 2015 (ClinicalTrials.gov, 2015b). Improvements in cannula/ catheter design also progressed in parallel to these studies, incorporating features aimed at minimising the likelihood of reflux (Figure 2-2). Only a small number of

devices have been commercialised which display acceptable acute performance when used with the principles of CED (Brady *et al.*, 2014; Richardson *et al.*, 2011). Progress in this field has therefore focused on acute or short-term infusions.

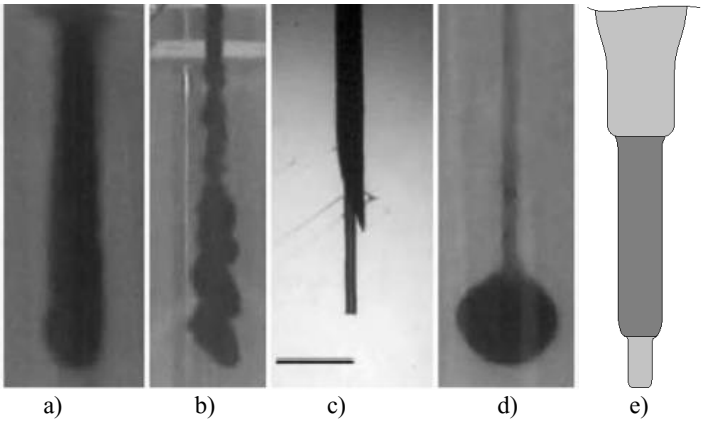

Figure 2-3. Infusion profiles of simple end port cannula [stainless steel hypotube] which experience large backflow characteristics (a, b) and improvement of control and predictability possible through introduction of a reflux inhibiting feature [step] (c, d) – images reproduced and modified from (Krauze et al., 2005), e) MRI interventions - SmartFlow cannula - commercial embodiment of the stepped profile cannula.

Acute devices tend to be made from stiff, ceramic tubes to aid their stereotactic delivery, but this makes them unsuitable for long term implantation as they do not comply with the movement of brain tissue. This has been shown to have detrimental effects on the sealing action around the implanted cannula during long term, low flow infusions (Guarnieri, Carson and Jallo, 2008). Stiff cannulae could induce significant trauma if left in place after the patient was recovered from general anaesthesia. Features such as increases in diameter (steps) are incorporated to increase stiffness proximal to the entry point at the skull surface to aid target accuracy and also to increase the radial compression from surrounding tissues, decreasing the likelihood of reflux occurring during delivery when compared to other catheter designs (Figure 2-3 & Figure 2-4).

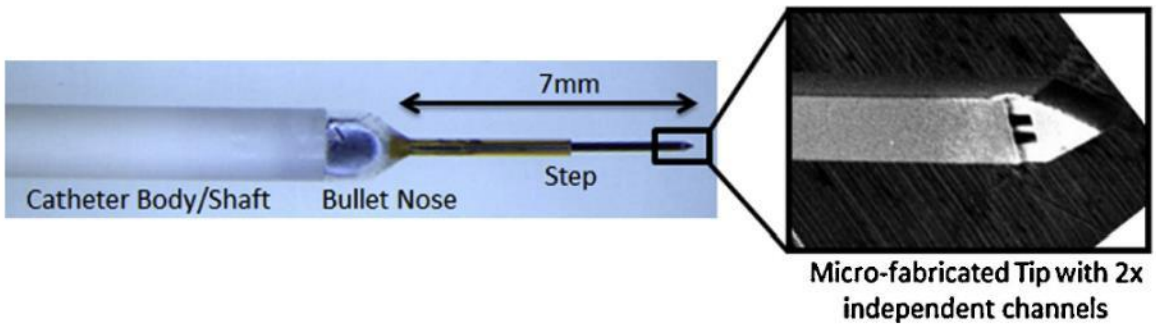

Figure 2-4. Alcyone lifesciences Inc, MEMS catheter design, commercially available twin bore cannula used for acute infusions - (Brady et al., 2014).

Polymeric designs which are more pliable are better suited to longer term implantation but require additional support during delivery to achieve target accuracy, which is typically achieved with stiff guide rods (Gill *et al.*, 2003; Gill *et al.*, 2013; Rosenbluth *et al.*, 2011).

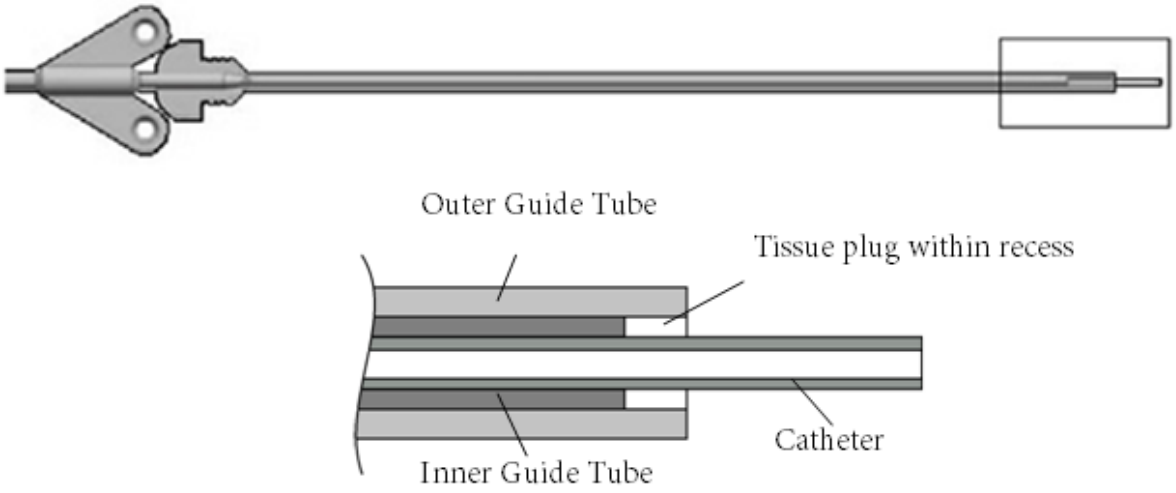

Figure 2-5. Assembled catheter design with a reflux inhibiting feature – a recessed step - images reproduced and modified from Gill et al. 2013.

Implanted catheters also incorporate stepped and recessed profiles to minimise the likelihood of reflux, though little information is available on their chronic (long term) performance (Gill *et al.*, 2013).

The integrity of neural tissue following long term delivery has not been directly quantified, however immunohistochemical analysis of the first (available) subject to receive continuous infusion of GDNF into the brain using an implanted pump, showed evidence of clinical improvement, but local toxicity, likely as a result of point source accumulation of the protein (Love *et al.*, 2005; Barua *et al.*, 2013c).

Chronic, intermittent delivery could be useful to treat a range of neurological conditions such as Alzheimer's disease, Parkinson's disease (Gill *et al.*, 2003) and Gaucher Disease (Lonser *et al.*, 2005), and even treat traumatic spinal injuries. Repeated infusions could maintain elevated levels of therapeutic within a target tissue, where it is quickly cleared or metabolised (e.g. chemotherapy).

The application of chronic CED may also be useful in the treatment of brain tumours such as Glioblastoma Multiforme (GBM) and Diffuse Intrinsic Pontine Glioma (DIPG) tumours, targeting strategies will be key to place long term catheters in areas of likely recurrence.

Novel, chronic systems will provide clinicians with 'enabling technology' to treat patients and provide the pharmaceutical industry with a new platform to develop therapeutics. Broadening the knowledge of this niche has been hindered in part by the lack of commercially available chronic CED systems to undertake clinical research.

Renishaw PLC is undertaking the development of a chronically implantable catheter system based on the recessed step catheter (Figure 2-5), which will provide a means of administering therapeutics intermittently over several years.

2.2 Mathematical and computational modelling of porous flow in the brain

To understand how to optimise the performance of long-term indwelling catheters, this section will review published data to understand the mechanisms of diffusion, convection, porous flow and the modelling of CED catheters.

Within the medical field, drug delivery encompasses a wide range of treatment paradigms which range from topical creams and intravenous injection to inhalation systems (e.g. asthma pumps) and drug-eluting polymers (e.g. Carmustine [Gliadel®] wafers), among numerous others.

In the context of drug delivery directly to the brain, there are unique environmental factors which define the substrate and the travel of the molecule within it.

For products such as the anticancer, drug eluting (Gliadel®) wafers described above, diffusion is the dominant mechanism for drug dispersal. The particle flux (j) in a substrate is defined by Fick's Law (Equation 2-1) linking the linear distance (x) from a starting point of a particle through a substrate based on a diffusion coefficient (D) and an initial concentration (Fick, 1855).

Equation 2-1. $$j_x = -D\frac{\partial C}{\partial x}$$

Where the substrate is homogeneous, a constant diffusion coefficient can be used. Where the free diffusion value and substrate tortuosity (hindrance to the travel of the infusate) are known, Equation 2-2 can be used to determine the local tissue diffusion tensor value, Dt (Sykova and Nicholson, 2008).

Equation 2-2. $$D_t = \frac{D}{\lambda^2}$$

Where empirical data is acquired through experimentation and the distance travelled by the infusate from an input source over time are known, Equation 2-3 may be used to determine the diffusion tensor (Saltzman, 2001).

Equation 2-3. $$D_t = \frac{\delta^2}{2\tau}$$

Where D is the free diffusion coefficient of the molecule in water, δ is distance from the source and τ is time.

Medical devices employing diffusion alone limit the extent and clinically relevant concentration of a drug to the tissues immediately around the implant (Bobo *et al.*, 1994). Treatment efficacy is significantly diminished for drugs with short half-lives, or where the diseased area extends beyond a few millimetres (such as the penumbra of a resected tumour). Conditions such as Parkinson's or lysosomal storage disorders, which may require repeated delivery of a drug after the initial volume is lost or metabolised are not catered for using a one-time drug eluting implant.

Direct delivery of a drug to the interstitial spaces of the brain tissue is therefore an attractive alternative to systemic routes which, as previously described, provide negligible transfer of the drug from the blood into the brain tissues. Bolus injection (volumetric flow rates (Q) >50 µl/min) are not appropriate for direct delivery as the excess local pressures open a fluid path between the needle and the tissue and infusate refluxes to the surface of the brain, leaving a high concentration only in the needle track (Figure 2-1). Convection-Enhanced Delivery bridges the gap between the diffusive and bolus injection speeds, providing a method of increasing the concentration of drug deep into the surrounding tissues (Bobo *et al.*, 1994). CED therefore relies on increasing the local hydrostatic pressure to induce bulk flow of the interstitial fluid away from the fluid

outlet of the delivery device. High flow (>1 µl/min) is needed to induce convection which overwhelms the natural interstitial fluid flow to initiate bulk flow in the tissue (Morrison *et al.*, 1994; Belova, Shaffer and Trapa, 2017).

Numerous groups have sought to mathematically and computationally describe the distribution of molecules in the brain following CED infusions (Morrison *et al.*, 1994; Linninger *et al.*, 2008c; Raghavan *et al.*, 2006; Belova, Shaffer and Trapa, 2017; Zhang, Yang and Jiang, 2012) (Figure 2-6).

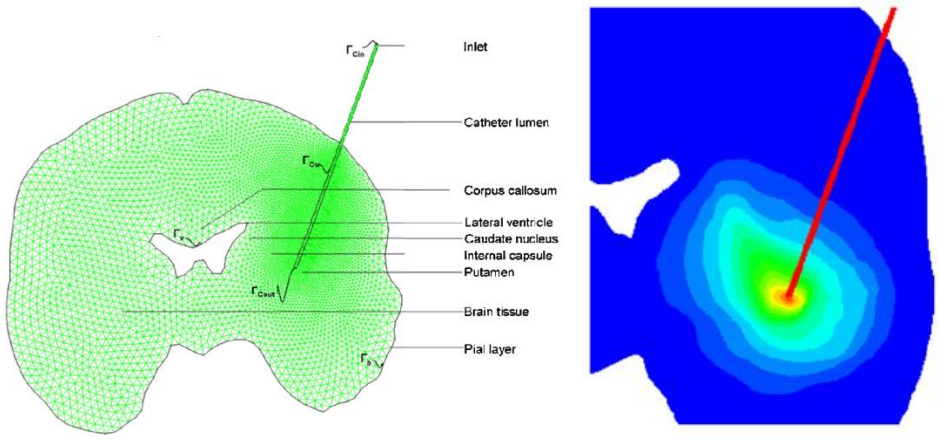

Figure 2-6. 2D Finite element model of the brain with a cannula placed into the tissue providing a point source inlet for fluids (Linninger et al., 2008a).

The base equation for convection was described by Morrison et al (Morrison *et al.*, 1994). The partial differential equation defines the concentration of a solute within a porous substrate as a function of time (**Equation 2-4**).

Equation 2-4.

$$R_d \frac{\partial c_i}{\partial t} = D_e \nabla \cdot (\phi \nabla c_i) - \nabla \cdot (\phi v_i c_i) - \left[\frac{L_p s(1-\sigma)(p_e - p_i)}{(e^{Pe_{mv}} - 1)}\right] c_i - k_{irr} c_i$$

Net Concentration	Diffusion	Convection	Loss into microvasculature	Loss due to metabolism

Where the time dependant concentration of a solute within a differential volume (left-hand term) is determined by the net diffusion, convection and losses into and out of that volume (**Equation 2-4**).

Belova et al (Belova, Shaffer and Trapa, 2017) refined the equation to ignore specific and non-specific binding and metabolism in their mathematical investigation of GDNF concentration following CED.

Equation 2-5. $$\boldsymbol{\phi \frac{\partial c_{ISF}}{\partial t} = \nabla \cdot (\phi D_t . \nabla c_{ISF}) - \nabla \cdot (\phi \vec{v}_{ICF} c_{ISF}) - k_{irr} C_{ISF}}$$

Where: C=infusate concentration, ISF=interstitial fluid, $\boldsymbol{\Phi}$*=tissue porosity,* $\boldsymbol{\vec{v}_{ICF}}$*= interstitial fluid velocity, D_t is the macromolecular diffusion tensor, K_{irr} is the first order degradation rate constant.*

Both the diffusion tensor and the porosity are tissue type dependant as white and grey matter are known to have different porosity (Grey-0.2, White – 0.18 (Linninger *et al.*, 2008c)) which affect the magnitude of the diffusion tensor. White matter provides additional complexity as it is anisotropic, with fluids preferentially flowing parallel to the axes of the nerve fibre bundles, giving the diffusion tensor a directionality, which are specific to the orientation of the local nerve fibre tracts. The diffusion vector can be established through magnetic resonance imaging using a diffusion tensor imaging sequence (MRI-DTI) which can be incorporated into computational models of the brain (Figure 2-7) to predict fluid flow *in situ (Linninger et al., 2008b; Kim, Mareci and Sarntinoranont, 2010; Sarntinoranont et al., 2006; Messaritaki et al., 2018).* The example of such a workflow has been provided in Figure 2-7 and illustrates an MRI image on the left with a representative finite element model on the right. The finite element model contains more than the location of the grey and white matter.

Numerous MRI scan types exist (each tailored to collect specific information about the tissues under investigation). Basic imaging such as a T1 weighted image can identify spatially where grey and white matter occurs in the brain in addition to structures like voids (nasal cavity) or CSF spaces. As a volume, the MRI scans are built from 3D voxels (with an x, y and z component), like a 2D picture is made up of pixels (which have only x-y lengths). The finite element model can then be constructed by importing these voxels and allocating values for porosity or permeability based on the values (e.g. intensity levels) of the MRI scan and its known association to empirical values. Further scan types, such as Diffusion Tensor Imaging (DTI) can add a directionality tensor to the white matter, such that infusates preferentially flow in a certain direction if they pass into those voxels as the finite model is run.

Prospective and predictive models are commonplace in various fields to try and estimate outputs based on a set of inputs to variables with known relationships [e.g. weather forecasts which predict: windspeeds, rainfall, cloud cover and temperature; or Structural FEA models which estimate mechanical properties, deflections, stresses and strains (outputs) based on material properties, boundary conditions and loads (inputs)(e.g. Ridgeway *et al.*, 2020); or clinical predictive models of symptom progression based on previous pathology (e.g. Dumont, 2016)].

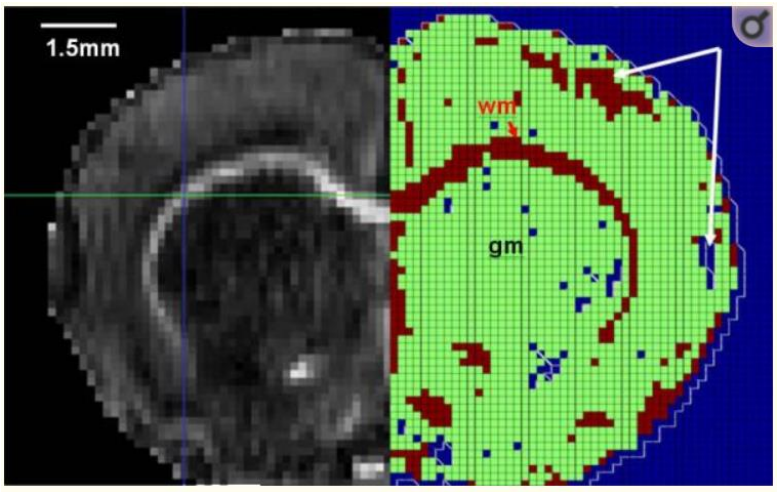

Figure 2-7. A voxelized DTI scan of a rat brain (left) and a Finite Element model of the same scan (right) demonstrating how diagnostic data can be engineered into a prospective, predictive model which can be tailored bespoke to each patient (Kim, Mareci and Sarntinoranont, 2010).

Retrospective attempts to analyse CED infusions, which occurred in patients with high grade recurrent glioma, showed agreement of 50 % isodose (radiation) level in 66 % of the simulation, providing clinically useful information 85 % of the time (Sampson *et al.*, 2007).

Take home message

Continued development of patient specific models and their integration into surgical workflow and planning software will improve device performance. Improved coverage (or retention) of infused drug in the target structures will provide the best initial conditions to evaluate clinical improvements in patient outcomes, but such models require empirical knowledge about the infusion catheter and its mode of action to provide useful insight into catheter placement.

2.3 Biological response to injury and implanted devices and its effects on CED

In order to understand how the performance of CED catheters may be affected by the duration of implantation, it is prudent to characterise the environment surrounding the catheter. Presented here is a discussion on the homeostatic environment surrounding the catheter and, later a discussion on how this environment will likely change as a result of the damage caused by surgery and long-term implantation of the system which will affect the predictive accuracy of porous flow models based on acute parameters.

2.3.1 The tissue environment

The nervous system is divided at the simplest level into the Central Nervous System (CNS) and the Peripheral Nervous System (PNS). The CNS comprises the brain and spinal cord while the PNS is made up of all other nervous tissues. Visually the brain appears very complex with highly undulating sulci covering the external surface, internal chambers (ventricles) filled with Cerebrospinal Fluid (CSF), the bulbous cerebellum at the rear of the brain as well as the fibrous sheaths which separate the various compartments of the brain (these are the *meninges*; dura mater, arachnoid mater, pia mater) which also extend to surround the spinal cord. The bulk of the brain, the nervous tissue, is however made up of two major cell types: neurons and neuroglia.

"Neurons are responsible for memory, thought, muscle control and the regulation of glandular secretions…." (Tortora, 2009)

Sensory neurons are the cells which collect stimuli of various types (heat, light, force, etc.) from all over the body and convert the input into an electrical signal which is transmitted along the cell (the action potential). Motor neurons are involved in the execution of motor actions and interneurons connect different neuronal pathways throughout the CNS and are involved with internal processing. Neurons are diverse in their neural circuit connections and functionality which is why damage to a small area can have catastrophic neurological consequences. Dimensionally, neurons range from a few millimetres in length to single cells which can stretch the full length of the body (brain to foot). Neurons have a highly complex cell form with branch like structures at either end of a long axonal trunk (Figure 2-8). The '*dendrites*' are the prominences which gather incoming signals from stimuli at one end of the neuron and pass them through to the '*axon*' which is responsible for transmitting the nerve impulse the greatest distance. The impulse is achieved with the assistance of the myelin sheath which surrounds the axon, this insulates and accelerates the ionic exchange at the inner surface against the cell wall. At the distal end of the neuron, the signal reaches the '*Axon terminals*' which discharge the signal to adjacent cells (e.g. muscles, glands, neurons). The cell nucleus is located within the centre of the dendrite cluster. If damaged, neurons generally do not have the capacity to divide through mitosis and regenerate lost function. Such cells are described as permanent cells.

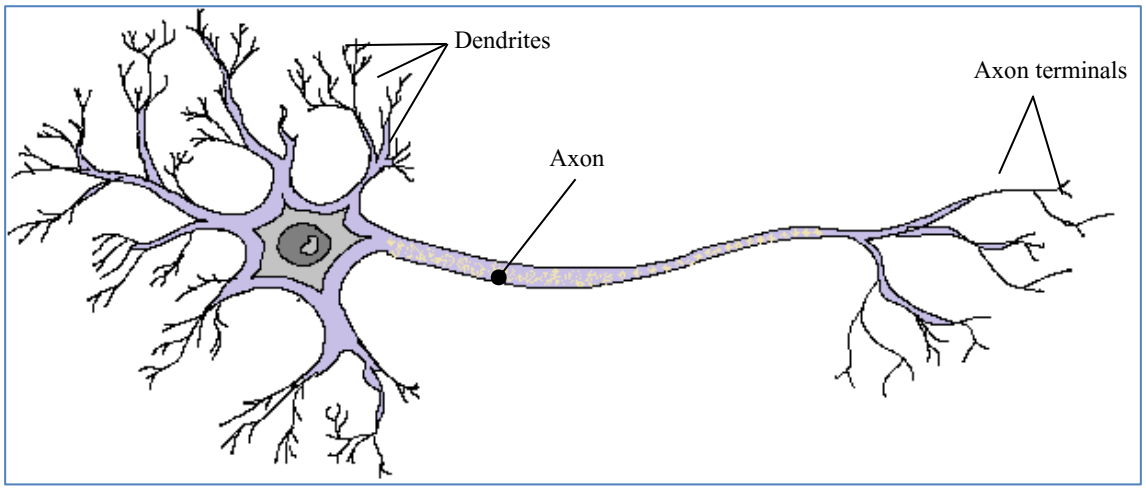

Figure 2-8. Illustration of a neuron with distinguishable features identified.

The other major cell type found in the CNS is Neuroglia (Table 2-1). This family of cells make up ~50 % of the bulk of the CNS, and while they are smaller than neurons, they are 5 to 50 times more numerous. Neuroglia are responsible for an array of functions, including the creation of nerve impulses, and assisting with maintaining the local homeostasis of the environment that surrounds the neurons, the extracellular matrix (Tortora, 2009).

The extracellular matrix fills the interstitial space (space between cells-Figure 2-9) and is comprised of a solution of supportive proteins, molecules and ions (Na^+, K^+, Cl^-) at various concentrations in CSF. The correct balance of ions is required to generate the action potential responsible for the nerve impulse (Raven and Johnson, 1996).

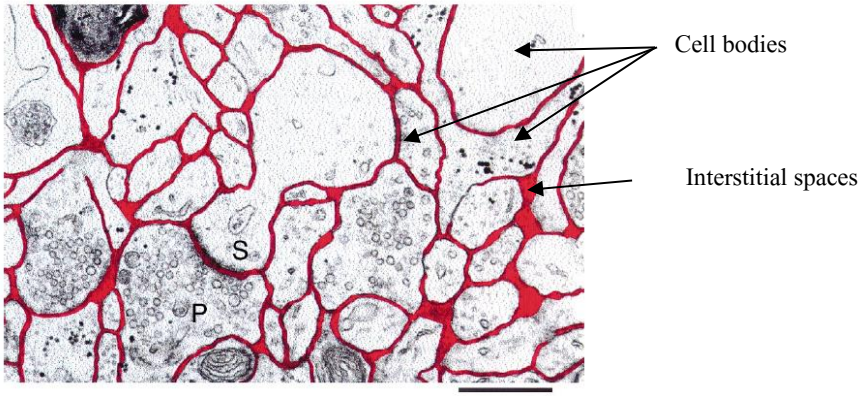

Figure 2-9. An electron micrograph showing the interstitial spaces in the rat cortex – image replicated from (Roitbak and Sykova, 1999).

In all, there are six major types of neuroglia but only four are found in the CNS, Schwann cells and satellite cells are limited to the Peripheral Nervous System (PNS) (Table 2-1). It is important to know the function of these cells as they are important not only in the homeostatic management of the brain tissues but also in the response to injury and healing which will be covered in the following sections.

As shown in Figure 2-10, when sectioned, the brain appears lighter and darker in different areas, these are known as the white and grey matter respectively.

Table 2-1. Glial cell types, function and location in the nervous system.

NeuroGlia cell type	Shape /Primary function	Location
Astrocyte	Varieties are found in both grey (protoplasmic – branched processes) and white matter (fibrous – un-branched processes)/ responsible for providing structural strength to neurons, maintain local ion (K^+) balance, maintain selective permeability of the endothelial tight junctions of the capillaries and act as a conduit for nutrients between the capillaries and the neurons. Astrocytes are highly heterogeneous and poses region specific functionality.	CNS
Oligodendrocite	Branched cell which covers many axons (similar but smaller than astroglia)/ responsible for forming the myelin sheath around axons in the CNS	CNS
Ependymal cells	Cuboidal with microvilli and cilia / Line ventricles and central spinal canal – produce CSF and assist with circulation	CNS
Microglia	Small cells with thin branches/ phagocytes that remove debris from damaged neural tissues and consume microbes	CNS
Schwann cell	Large cells which cover a single axon or a cluster of axons (like a multi-lumen tube)/ responsible for forming the myelin sheath around axons in the PNS and also contribute to axon regeneration in the damaged PNS	PNS
Satellite cell	Flat cells that cover the neuron cell bodies in the PNS/ Regulate exchanges of materials between cell body and interstitial fluid	PNS

Functionally, the white matter is responsible for the transfer of nerve signals, the motorways which carry the electrical signal throughout the body. The white appearance of the tissue is caused by the fatty (lipid) myelin sheath which surrounds the neuronal axons. Conversely the darker appearance of the grey matter is due to the lack of myelinated axons in these areas of tissue. The grey matter is comprised of neuron bodies, dendrites, unmyelinated axons, axon terminals and neuroglia.

The cells which occupy the grey matter account for ~80 % of its volume, leaving the remaining ~20 % occupied by the extracellular matrix (Roitbak and Sykova, 1999). During infusions, it is this interstitial space which is invaded and occupied by the fluid convecting from the catheter and into the surrounding tissue.

The ratio of interstitial space within a volume of tissue (the rest being occupied by cells in the context of this work) is known as the pore fraction or extracellular volume fraction (EVF). The pore fraction varies between tissue types depending on its density and arrangement of cells.

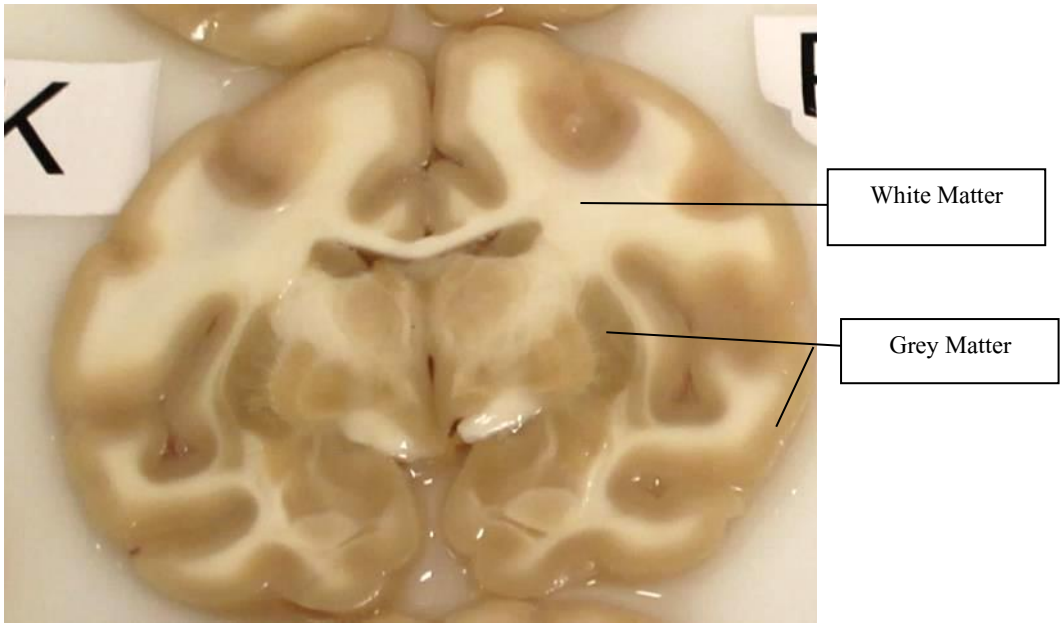

Figure 2-10. Perfusion fixed coronal section of NHP brain.

The EVF of white matter is ~1/3 (which would result in a 3 fold increase in any fluid infused into it) while the EVF of the brainstem is ~1/9 in healthy tissue. Compromised nervous tissue can dilate the extra-cellular spaces reducing the local density of cells and alter the 'normal' EVF (Lonser *et al.*, 2002; Lonser *et al.*, 2007a; Lonser *et al.*, 2007b).

2.3.2 The immunological response to injury and medical device implantation

Homeostasis in normal healthy tissues is achieved by receiving nutrients and other chemical species for ongoing maintenance from a support network of cells and vessels. Cells of the immune system which provide healing and protection from foreign pathogens or injury are present within the bulk of the tissues in addition to the lymph and blood vessels.

In response to injury a chemical imbalance in the microenvironment is triggered which initiates a chain of chemical reactions which starts with acute inflammation and ends ultimately in healing and reconstitution of the tissue, or the formation of fibrous tissues which attempts to protect the body and return the local area to a condition of homeostasis. The cascade of cellular activities leading to healing or fibrosis is sometimes known as the "tissue response continuum"(Anderson, 2001) – (Figure 2-11).

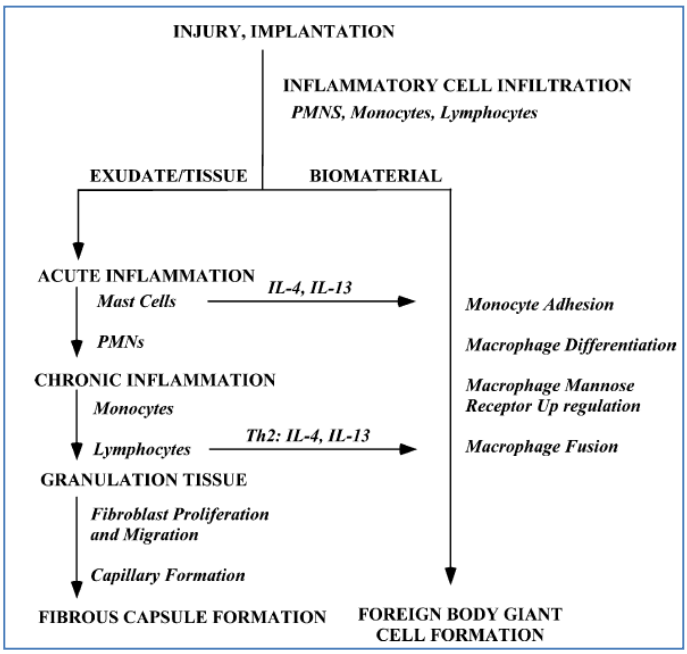

Figure 2-11. The cascade of cellular events and associated cell types present at the site of injury during the generalised tissue healing process – figure replicated from Anderson et al (Anderson, 2001).

2.3.3 Stages of injury and healing

Many variations on the terms used in the healing of tissues can be found in the literature but all cover broadly the same chemical and cellular events in different levels of detail (Table 2-2). The presence of some cell types are ubiquitous in injury (e.g. monocytes and macrophages) while others will be highly specialised to the site of injury (e.g. microglia).

Table 2-2. Stages of generalised and specific healing proposed by various authors.

		Description of activity within tissues following injury/ device implantation		
	Location	**General**	**General**	**Brain**
Stages	**0**	Homeostasis	Homeostasis	Homeostasis
	1	Injury	Injury	Injury
	2	Acute inflammation	Haemostasis	Microglia/ Macrophage infiltration
	3	Chronic inflammation	Inflammation	Up-regulation of GFAP, Trophic factors, cytokinases, proteases, protease inhibitors, cell surface and matrix molecules
	4	Granulation tissue	(Cell)Proliferation/ initial repair	Glial scar formation and infiltration of meningeal cells (where the meningeal layer is compromised)
	5	Foreign body reaction/ Fibrous capsule formation	Remodelling	
	Source	(Anderson, 2001)	(Kuhn, 2005)	(Fawcett and Asher, 1999)

2.3.3.1 Injury

Initially, tissues are subjected to an insult or injury which damages the stroma (structural cells) and parenchymal cells (active organ cells) within the local environment. Blood vessels are inevitably ruptured leading to the traverse of blood and blood products into the wound site which form a thrombus (blood clot).

2.3.3.2 Acute inflammation

Proteins from the blood will quickly be deposited onto any foreign body in the wound area (within the context of this review the foreign body would be an implanted medical device), the deposition (or adsorption) of these proteins onto the surface is termed the formation of the provisional matrix. This protein deposition is spontaneous and immediate and plays a role in the extent of the downstream reactions which occur in the healing process (Anderson, 2001; Kuhn, 2005).

It is the breakdown of this provisional matrix which releases chemical species which control the serial stages of acute inflammation, wound healing, chronic inflammation, granulation and fibrosis.

During the acute inflammation stage, the wound is saturated with neutrophils. These are a type of granulocyte white blood cell, the most prevalent in mammals. Mast cells will also be present at this stage and through their de-granulation they secrete substances to control/ mediate the acute inflammatory response (e.g. signalling cytokines). Histamine is released by mast cells to increase the permeability of blood vessels and increase the flow of white blood cells to combat foreign microbes. Interleukin 4 and 13 are also released and these are known to play a role in the later formation of Foreign Body Giant Cells (FBGC) – section 2.3.3.4.

2.3.3.3 Chronic inflammation

Once haemostasis is achieved, mononuclear cells (e.g. monocytes, lymphocytes) are recruited to the area in large numbers, this signifies the chronic inflammation stage. Within the brain, microglia are recruited in large numbers but also divide to flood the injured area filling spaces previously occupied by now damaged neurons (Fawcett and Asher, 1999). The purpose

of these cells is to fight off any invading microbes within a wound through phagocytosis, the consumption of the foreign cell/ matter. Macrophages are capable of phagocytosing particles approximately 5µm in size (Anderson, 2001). If it is not possible for a phagocyte to engulf a foreign body then other adaptive and non-adaptive mechanisms exist within the body to combat intruders, such as the complement system. The complement system is part of the immune system and is comprised of a family of molecules. When any one of the family of complement molecules are activated, they divide in a cascade activating the remaining complement molecules. Active molecules attach like a key to foreign cell walls, combining to form a gate/ hole which permits the entry of extracellular fluid into the cell causing it to swell, leading ultimately to cell lysis (**Tortora**, 2009). This system is only one of a range of molecular options available within the immune system which can be recruited to combat injury, and ultimately lead to changes in the environment around the implanted system.

2.3.3.4 Foreign body reaction

As previously mentioned, macrophages are capable of engulfing single particles up to 5µm in size. For larger particles (>10µm), typical in medical device implantation, macrophages cannot consume the foreign material which results in a state of frustrated phagocytosis. Macrophages can then combine to form Foreign Body Giant Cells (FBGC). These cells have the capacity to phagocytose larger particles but for whole devices, phagocytosis is not feasible. Consequently these cells can produce acidic compounds in an effort to degrade the material. Such degradation was shown to damage neuronal cells (Hayn, Deppermann and Koch, 2017) as well as implanted polyurethanes (Anderson, 2001). While typically seen around the same time as the formation of granulation tissue, the presence of FBGC has also been used to denote the chronic inflammation stage in medical device implantation. Mediation of the FBGC reaction is possible through inhibitory agents (e.g. Anti Il-4, Anti Il-13) or modified surface properties of medical devices (Anderson, 2001; Kuhn, 2005).

2.3.3.5 Granulation tissue formation

Granulation tissue is characterised by the formation of new blood vessels (neovascularisation) or vessels sprouting from existing vessels (angiogenesis). There will be a large presence of macrophages and an infiltration of fibroblasts also at this stage. Granulation tissue is the precursor of fibrous capsule formation. The granulation tissue is normally separated from the medical device by a 1-2 cell deep layer of monocytes, macrophages and foreign body cells (the cellular components of the foreign body reaction).

2.3.3.6 Fibrous capsule/ Gliotic scar

Within tissues that have a high capacity for regeneration, division and recovery, granulation tissue resolves to create functional parenchymal tissues. In the brain parenchyma however, astrocytes rapidly differentiate to form a tightly packed astrogliotic scar characterised by the upregulation of GFAP and vimentin. The density is a function of the interweaving of the actrocyte prominences (Figure 2-12) which become more numerous and hypertrophic following injury (Fawcett and Asher, 1999). The extent of the fibrous capsule is, in part, affected by the severity of the trauma caused during injury and also by the up-regulation of proteoglycans such as chrondrotin sulphate proteoglycan (CSPGs) which is found in connective tissues (Tian *et al.*, 2006). Fibroblasts and meningeal cells also migrate to the site of injury and can infiltrate the scar in an

attempt to protect the CNS from secondary lesions (Pekovic *et al.*, 2005) and re-establish the glia limitans. Glial Scar formation is thought to be complete before six weeks (Hayn, Deppermann and Koch, 2017).

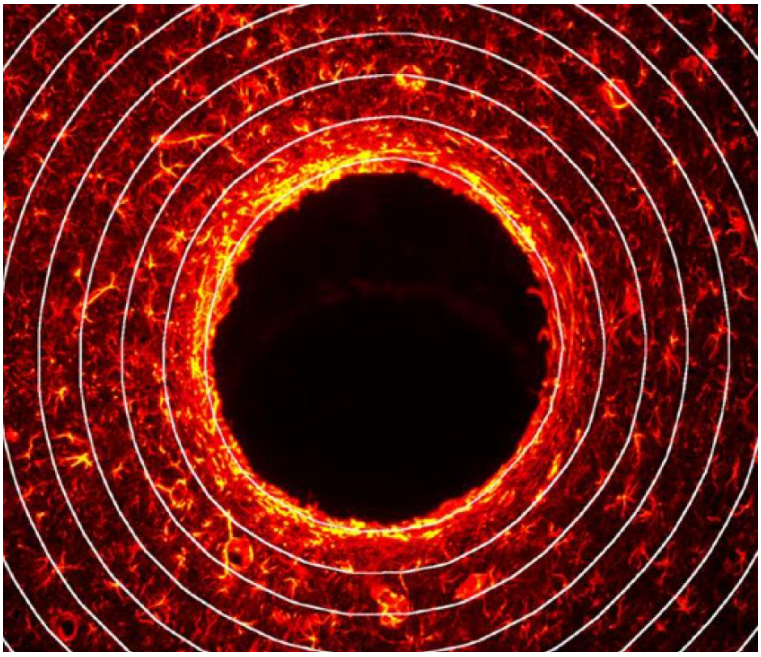

Figure 2-12. Increased density of Glial Fibrillary Acidic Protein (GFAP) positive cells (astrocytes) around an implanted steel cannula track in the rat cortex – image replicated and modified from (Hayn, Deppermann and Koch, 2017).

Take home message

In order to optimise the chronic, intermittent delivery of therapeutics to the CNS it is critical to generate a basic knowledge of the healthy and compromised working environment. Further, the reaction to injury which will result from the implantation of the catheter device should be understood in order to evaluate the likely effect on distribution of therapeutics into the surrounding target tissues.

2.4 Discussion

The white and grey matter of the CNS is comprised of neurons and glial cells. These cells are surrounded by a hydrophobic membrane which prevents the influx of the interstitial fluid. As such, brain tissue can be considered a porous substrate, as infusions into the bulk of the tissue will replace the interstitial fluid in the extracellular spaces between the cells, with uptake of molecules into cells, metabolism and excretion occurring over a longer timeframe.

Infusions into different areas of the brain will have different distribution patterns, governed by the density of the cells, fluid flow and available extracellular spaces in the local area. Infusions into white matter will likely increase in coverage of tissue volume threefold, while infusions into grey matter will increase approximately five fold, because they can occupy only a fraction of the tissue between the cells. Denser regions such as the brain stem may have even higher increases in distribution volume, closer to eight or nine-fold.

Distribution patterns will also be affected by the infusion regimes used to administer the delivery, as well as the affinity of the infused molecule to the local tissues. Efflux pathways within the brain (perivascular spaces and metabolism/ receptor binding onto or into cells) will act as sinks, removing fluid from the target zones.

Following injury, proteins within the tissues and blood (where vessels are damaged) adsorb onto the external faces of foreign microbes or implanted devices. The chemical imbalance of traumatised cells cause the quiescent immune system cells to become active. Microglia, monocytes and macrophages are recruited to the area and attach to the proteins on the external face of the foreign cells or implanted device. These cells attempt to consume the foreign microbes, clear cellular debris from the injury or breakdown the foreign body. Failure to remove the foreign body can lead to macrophages joining to form foreign body giant cells (FBGC) which have additional capacity to create acidic compounds to accelerate degradation of materials. FBGC can remain present at the site of implants throughout their service life.

Mast cells secrete vasodilators to increase the flow of cells to the area causing local vasogenic oedema. Microglia and astrocytes are activated following injury and quickly divide to fill areas of tissue previously occupied by damaged neurons. As the functional parenchymal cells of the brain, neurons do not have the capacity to divide and regenerate, activated astrocytes become hypertrophic, increasing the number of fibrils on its exterior to interconnect with adjacent astrocytes to form a tightly interwoven glial scar around the site of injury to protect the body. The glial scar has limited extracellular space and forms gap and tight junctions between the adjoining cells filaments. Implants that traverse the meningeal layers surrounding the brain may also be susceptible to the infiltration of meningeal cells which try to re-establish the glia limitans following injury.

Repeated delivery into the tissues of the body, in particular the brain, will also be affected by the changing nature of the local environment around the implanted device. This dense tissue is a physical barrier to flow which presents a problem for treatments delivered by long term implanted delivery systems. CED relies on a ‘high’ flow, positive pressure to increase lateral coverage away from the site of delivery (over natural diffusion alone which is limited to several millimetres from the delivery site) (Bobo *et al.*, 1994). Such increases in pressure are however also likely to overcome any reflux inhibition features on current catheter designs. Reflux will likely limit the therapeutic benefit if infusions are not largely retained within the target tissues or structures.

The changes to tissue morphology as a result of intermittent infusions have yet to be characterised. Intermittent regimes may exacerbate the formation of astroglial tissues.

The glial scar is widely discussed as a primary factor inhibiting the formation of new axonal growth in spinal cord injuries, as well as degrading performance of implanted electrodes.

Further work is required to characterise this environment and understand how the parameters of acute infusion differ to those of the long-term environment and whether performance, measured in volume of distribution of target tissues, can be optimised through a variety of strategies. Manipulation of the infusion regimes or repetition schedule may be considered.

Alternatively, mediation of the tissue response to injury may be required to prolong the useful life of implanted catheters while maximising distribution performance.

The aim of this thesis is to investigate and optimise the design and use of chronically implanted catheters in the brain for repeated delivery of therapeutics which are currently under development at Renishaw PLC.

The objectives will be to gather and analyse empirical distribution data from the *first-in-man*, chronic implantation study which utilised a recessed step catheter and evaluate its performance. Understanding of the principles which govern successful repeat deliveries into the brain will be sought to provide strategies to maximise the long-term efficacy of prospective treatments and provide guidelines to prospective neurosurgical users on optimal implantation strategies for this catheter.

As this approach is multi-disciplinary and multifaceted, a schematic has been provided to clarify the specific questions which are posed at the outset of each chapter (Figure 2-13). A complementary follow up schematic is also provided in the final chapter of the thesis, highlighting the outcomes of each chapter as they relate to the central theme of the thesis (Figure 8-1).

Optimisation of a chronically implanted catheter for intraparenchymal delivery of therapeutics to the brain

Q – How does a catheter perform when chronically implanted?

Chapter 3 – Evaluation of a first in man chronic, intermittent convection enhanced delivery system
Purpose: Characterise the performance metrics of the recessed step catheter design used *in vivo*

- Coverage of target structures
- Evaluation of study subject's normality in the patient population
- Comparison of implanted catheters - position of functional features in target structure

Q – What materials can be used as brain mimics to further develop knowledge of the catheter function in vitro?

Chapter 4 – Evaluation of brain mimics for catheter design evaluation
Purpose: Identify an optimal brain mimic to further evaluate the recessed step catheter

- Compare the infusion characteristics between agarose gels and composite hydrogels (made from polyvinyl acetate and phytagel) which are reported to be more mechanically similar to brain tissue than agarose

Q – How does changing the catheter infusion or dimensional variables affect the infusion distribution and how can this be used towards optimisation?

Chapter 5 – In vitro and in vivo characterisation of the recessed step catheter distributions
Purpose: Execution of infusion study in gels and pigs comparing distribution characteristics obtained when modifications are made to the catheter features or the way it is driven (infusion rates)

- Create a set of design curves for distribution characteristics based on catheter step length and infusion flow rate

Q – Can an in-silico model of the recessed step catheter be created and used to verify the characteristics observed within in vitro gel studies, and later built in to planning or analysis software?

Chapter 6 – Modelling of the recessed step catheter
Purpose: Create a computational model of porous flow from a recessed step catheter

- Collate model parameters from appropriate, referenced sources
- Create a biphasic finite element model for solvent flow through a porous substrate with clinically relevant step lengths

Q – Is the permeability of the micro-environment around the catheter negatively affected by the implantation of the catheter or the continued intermittent infusions and how could this affect chronic optimisation?

Chapter 7 – Longitudinal study of inflammatory reaction to a chronically implanted catheter

- Purpose: investigate the inflammatory reaction *in vivo* comparing active and inactive catheters over 90 days post implant

Figure 2-13. Schematic of thesis with primary questions posed at the outset of each chapter.

3 *First in Man* chronic, intermittent, convection-enhanced delivery system

*This chapter contains work which contributed to the publications "**Randomized trial of intermittent intraputamenal glial cell line-derived neurotrophic factor in Parkinson's disease.**" (Whone et al., 2019a) and "**Extended Treatment with Glial Cell Line-Derived Neurotrophic Factor in Parkinson's Disease**" (Whone et al., 2019b)*

3.1 Motivation

The author formed part of a medical research and industrial collaboration study group responsible for the implementation of a clinician led study, infusing Glial cell-line Derived Neurotrophic Factor (GDNF) (a naturally occurring protein) intermittently into the brains of Parkinson's patients through a novel drug delivery system (DDS).

The author was therefore not responsible for the clinical study design or the development of the drug delivery system. The data gathered during this seminal study does however represent the first opportunity to investigate, and baseline the performance of chronically implanted catheters which are accessed intermittently (i.e. not continuously infusing a low flow rate such as occurs with implanted pumps) and establish opportunities for optimisation. It is hoped that an assessment of the distributions over the duration of the 18 month study will provide guidelines for improving performance in future studies.

3.2 Introduction

Within the context of this investigation, the short and long-term performance of a chronically implanted catheter system is of primary interest, however it is necessary to explain the design of the study from which the data was gathered. What follows is an overview of the clinical trial focusing on the relevant areas surrounding the delivery system and the definition of acceptable catheter performance.

3.2.1 Clinician led study design

Study title: **A Placebo-Controlled, Randomized, Double-Blind Trial to Assess the Safety and Efficacy of Intermittent Bilateral Intraputamenal Glial Cell Line-Derived Neurotrophic Factor (GDNF) Infusions Administered via Convection-Enhanced Delivery (CED) in Subjects with Parkinson's Disease**

(EudraCT No: 2011-003866-34)

Following a 6-patient phase I (drug safety) study, 35 patients were successfully enrolled and randomised into the primary GDNF study (Figure 3-1) with approximately half receiving GDNF and the other half receiving a placebo (artificial cerebrospinal fluid [aCSF]). Following screening, subjects progressed to surgery where they were implanted with a DDS (Figure 3-2). Approximately 1 month (study week -4 [W-4] following system implantation, subjects underwent the first of three test infusions. Test infusate consisted of aCSF and Gadolinium Based Contrast Agent (GBCA) (Magneist, Bayer), preceded and followed by a T1 weighted MRI scan which provide a baseline of the patient's anatomy with and without the presence of the contrast agent (Figure 3-3).

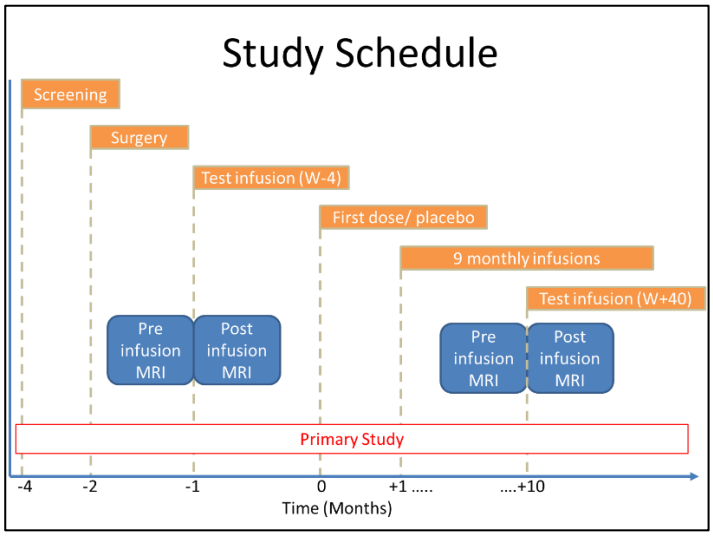

Figure 3-1. Primary GDNF study patient schedule (extension study not shown).

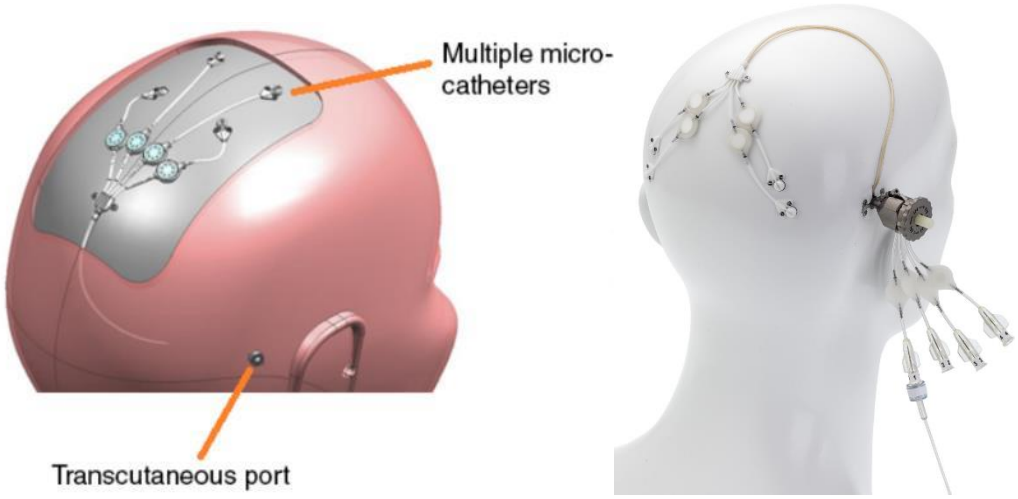

a) **b)**

Figure 3-2. Chronically implanted drug delivery system a) shown on a CAD package avatar with a cut away section of tissue displaying the catheters tunnelled beneath the skin, terminating at the point where they enter the brain cavity (vertical catheter trajectory), b) mannequin implanted with the chronic DDS fitted with an externally mounted application set for intermittent infusions to the brain via the percutaneous port (posterior catheter trajectory).

The distribution was assessed over 3 principle areas;

- infusion retained within a pre-defined Volume of Interest (VOI) (Figure 3-4),
- within the whole target structure (putamen)
- total hemispherical coverage (V_d, distribution volume).

All volumes were recorded in mm^3 units (equivalent to the volume of µl).

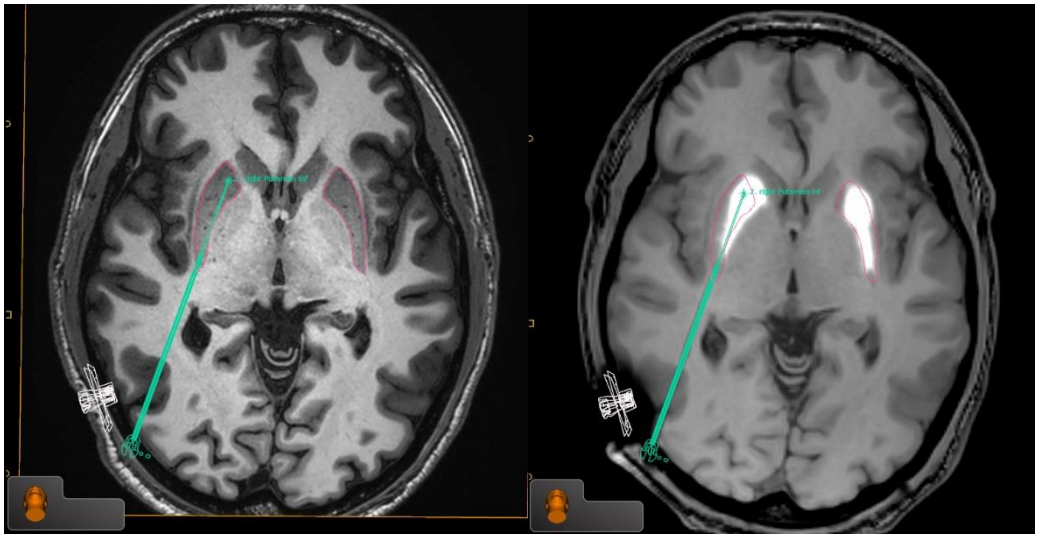

a) b)

Figure 3-3. First test infusion in a GDNF study subject, a) pre-infusion baseline T1 weighted MRI scan, b) post infusion T1 weighted MRI scan.

The VOI was defined as the posterior 2/3^{rds} of the dorsal putamen (upper, rear 2/3rds), the area of the putamen thought be responsible for initiating motor functions. Subjects were randomised (included) into the study only if a minimum coverage (40 %) of the VOI was achieved during the first test infusion (as defined by the study protocol). This base coverage

requirement was introduced to minimise the risk of study failure as a result of technical failures in delivery seen in previous studies. This enabled the study to focus solely on the clinical efficacy of the drug under investigation.

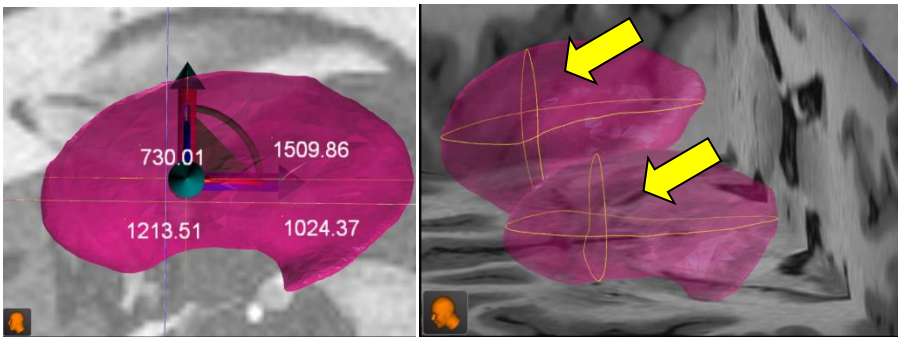

a) b)

Figure 3-4. a) Example of a subject's surgical plan with the target structure (putamen) automatically segmented and presented as a pink 3D mesh. Section planes have been positioned to sub-divide the mesh and highlight the region of interest. b) Left and right putamen are shown with sub-division planes highlighting the VOI (arrows).

Once accepted into the study, subjects received a monthly infusion of test article (or placebo) through the percutaneous access port (Figure 3-5). Following a total of 10 monthly administrations, a second test infusion was administered, and pre- and post-infusion MRI scans were gathered for assessment of long term distribution characterisation (study week 40[W40]).

Following completion of the primary phase of the protocol, subjects automatically rolled onto an open labelled (see below) extension study, receiving a further 10 months of infusions with all subjects guaranteed treatment with the test article (GDNF). At the completion of the extension study a further test infusion was performed (t=week 80[W80]).

In Parkinson's studies, such as the primary study here, participants and study administrators are routinely blinded, meaning that they do not know if the subjects are receiving the active drug under investigation or a placebo. This is done to minimise a placebo effect, where people believe they are receiving drug and exhibit improved clinical scores despite having no pharmacological reason to do so. Once this study moved into the extension phase, study designers felt it was unethical for participants to have no prospect of receiving the study drug having undergone such invasive surgery and having their normal medication withheld for extended periods, and so it became an open labelled study for the remaining 9 months. All participants were given the test article (GDNF) and all study administrators were aware of the drug being given. There was therefore no control group for the extension study, but continued device performance was not affected by the unblinding of this study as this was measured directly through infusion distributions viewed under MRI.

a) b)

Figure 3-5. a) GDNF subject receives an infusion into the brain via the external bone anchored percutaneous access port (https://medium.com/parkinsons-uk/meet-the-team-behind-the-gdnf-trial-ec7f3c2d102c), b) Close up image of the administration set attached to the percutaneous port in a glioblastoma patient (Barua et al., 2014).

3.3 Method of infusion distribution assessment

As described above, the definition of catheter performance, in the context of this body of research, is the ability to target and cover a defined body of brain tissue (neuroanatomical structure). This thesis will therefore not deal with clinical symptoms of disease or drug trial outcomes, however these will be summarised in the discussion section later.

Coverage of the VOI, putamen and hemisphere were assessed at all test infusions.

3.3.1 Distribution volume, V_d

The need to define the extent of coverage in trials delivering drugs to the brain has been highlighted previously (Lang *et al.*, 2006). This previous study, investigating the continuous delivery of GDNF to the putamen of Parkinson's patients, identified that a failure to induce improvements seen in an older study (Gill *et al.*, 2003) may have been down to differences in the delivery system. This hypothesis was based on ad hoc T2 – weighted MRI scans taken of a limited number of patients which clearly showed significantly more reflux in patients who participated in the failed phase II study (investigating drug efficacy, above safety which is typically performed in a phase I study)(Figure 3-6).

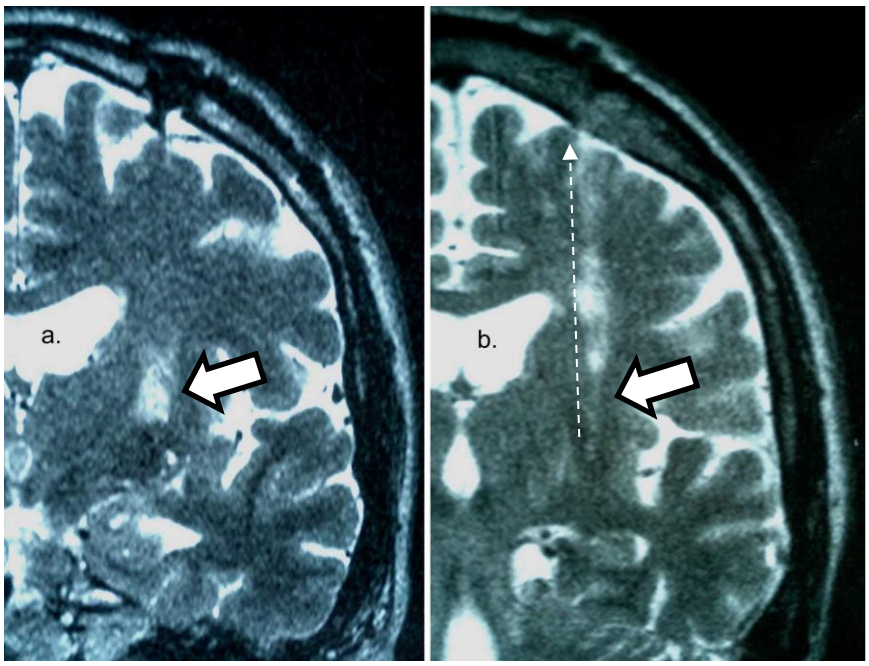

Figure 3-6. T2 weighted MRI scans of Parkinson's subjects from Phase I (left) and Phase II (right) studies provided by Prof Steven Gill a) 0.6 mm diameter catheter used showing infusion (white cloud) located around the catheter tip (white arrow), b) 1.2 mm diameter catheter used showing absence of dense white infusion located at the catheter tip (white arrow) but extensive reflux to the surface of the brain (dotted arrow).

Infusion distributions that are visible in MRI scans are spread at different concentrations around the site of administration (with the highest concentrations typically around the catheter track). To provide a consistent analysis approach, study guidelines were created by the lead neurosurgeon which stipulated a "viewpoint analysis" be adopted as previously described (Yin *et al.*, 2010; Yin *et al.*, 2011; Gimenez *et al.*, 2011).

Post infusion T1 weighted MRI scans were windowed (adjusted brightness and contrast levels) to increase the contrast between the infusion and the surrounding tissues. As the visible white matter was removed from view (by thresholding the image), the remaining tissues visible would contain only the hyperintense gadolinium tracer. 2D profiles were then drawn around the periphery of the visible infusion on each MRI slice to make a volume.

No minimum VOI or putamenal coverage value was pre-defined in the study protocol for the final test infusions (weeks 40 and 80).

Subjects were grouped according to their dominant trajectory entry position on the skull. Three groups were identified in the study based on an evolving surgical technique: vertical, anterior and posterior (Figure 3-7).

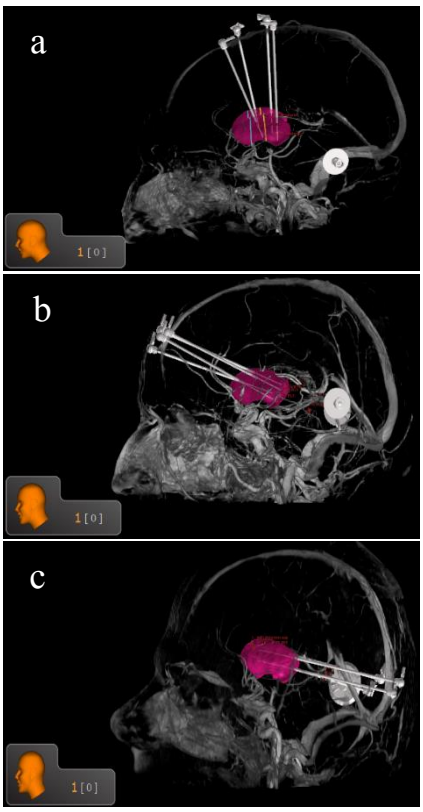

Figure 3-7. Surgical implantation trajectories of the recessed step catheter employed in the primary GDNF study, a) vertical (n=6), b) anterior (n=3), c) posterior (n=26).

3.3.2 Position of catheter features in structure

Additional measurements were calculated from the post implant CT scan. The actual implanted position of the catheter as well as its reflux inhibiting features were recorded. An investigational analysis was performed on these values to establish if a correlation (Pearson correlation coefficients) existed between position of the device and target coverage.

3.3.3 Anatomical variation

The infusion volume was standardised across the study population, 300 µl/catheter (600 µl/putamen) which contained GBCA. The volume of the target (putamen) will be calculated to establish the normality of the study population, and also how this variation might affect percentage coverage of the target structure. The putamen volumes of the 36 PD subjects were extracted from the anonymised surgical plans (generated with a validated auto-segmentation tool within Renishaw's neuroinspire™ surgical planning software).

3.3.4 Statistical analysis

Direct comparison of means were compared using a Student's t-test with significance set at $p \leq 0.05$. Sample groups larger than two were compared using a one-way ANOVA to establish statistically significant differences in population mean.

Pearson correlation coefficients were calculated to establish strength of interrelationships between variables. The Anderson Darling method was used to confirm normal distribution of putamen volumes.

3.4 Results

3.4.1 Putamen volume

All putamen volumes ranged between 3.22-5.37cm^3 with a normal distribution (Figure 3-8) and an average volume of 4.39±0.06cm^3 (SEM). There was no statistically significant difference between the right and left putamen volumes (p=0.78).

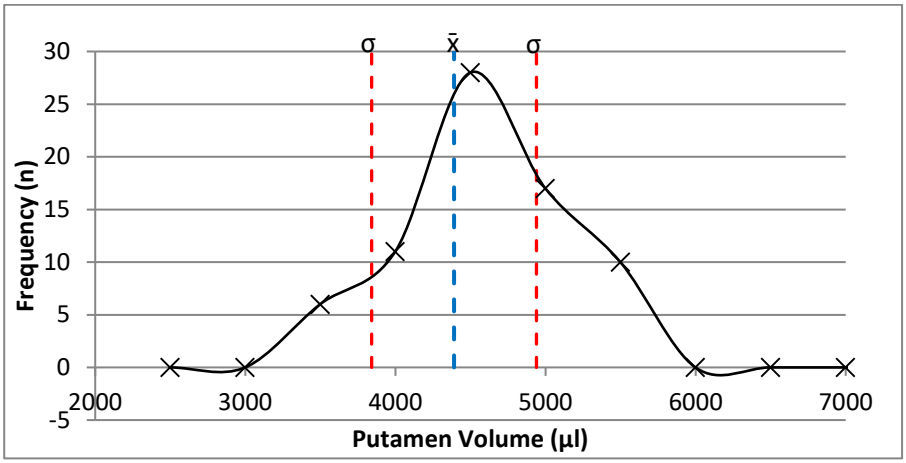

Figure 3-8. NBT GDNF primary cohort putamen volumes - frequency plot, average volume, $\bar{x}$= 4.39 ml, Standard error of the mean (SEM) =0.06cm^3; indicated by blue dashed line, red dashed lines represent 1 standard deviation, σ=0.55cm^3 (n=72 putamen).

3.4.2 Variations in surgical trajectory and its effect on step length

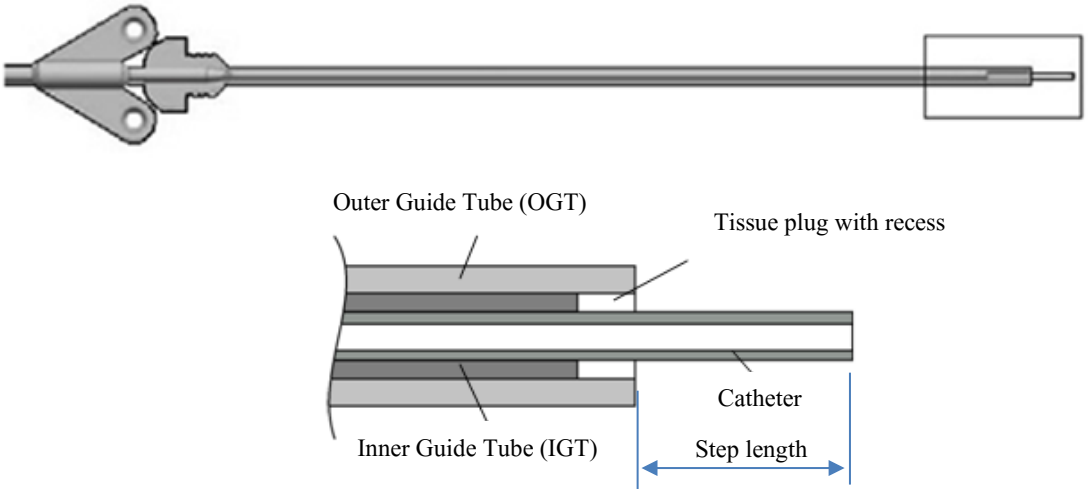

Figure 3-9. Recessed Step Catheter with variable step length (Dimensions: OGT=1.7 mm OD, Catheter = 0.6 mm OD).

a

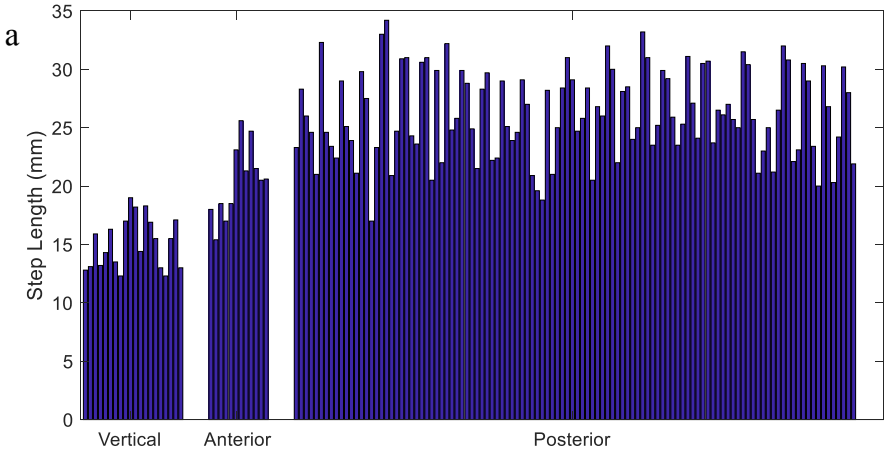

	Vertical	Anterior	Posterior
Average	15.08	20.39	26.19
n	20.00	12.00	112.00
STD	2.17	3.08	3.76
SEM	0.49	0.89	0.36

b

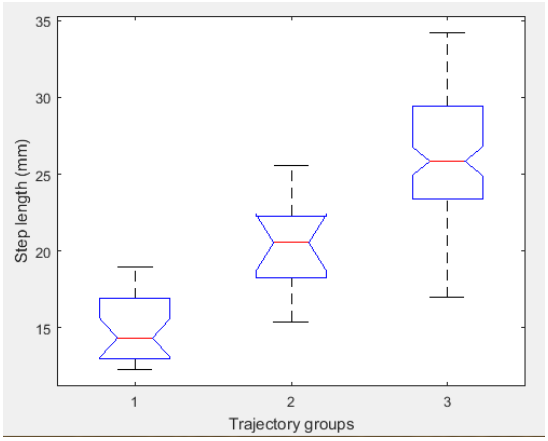

Figure 3-10. Step length variations between catheters implanted into the putamen via different trajectories, a) all catheter lengths across 3 trajectory groups, b) box and whisker plot of 3 trajectory groups (group 1=vertical approach, group 2 = anterior approach, group 3 = posterior approach); lower and upper horizontal blue lines define the 25th and 75th quantiles, red line defines median value. Height of notches (blue lines) define the 95th confidence intervals of the means of each group, as these do not overlap the reader can be confident that the true medians do differ.

In total, 140 catheters were implanted in 35 patients (6x vertical, 3x anterior, 26x posterior) with a significant rise in the average length of the step region (distance between the OGT tip and the catheter tip (Figure 3-9)) ($F(2,139)=104.58$, $p<0.001$). Step lengths ranged from 12.3-34.2 mm (Vertical:12.3-19mm, Anterior:15.4-25.6 mm, Posterior-17.0-34.2 mm). Step lengths rose in line with putamen volume($r=0.0156$, $p=0.197$), this was significant within the posterior trajectory group ($r=0.341$, $p=0.013$) which was aligned with the long axis of the structure (Figure 3-11).

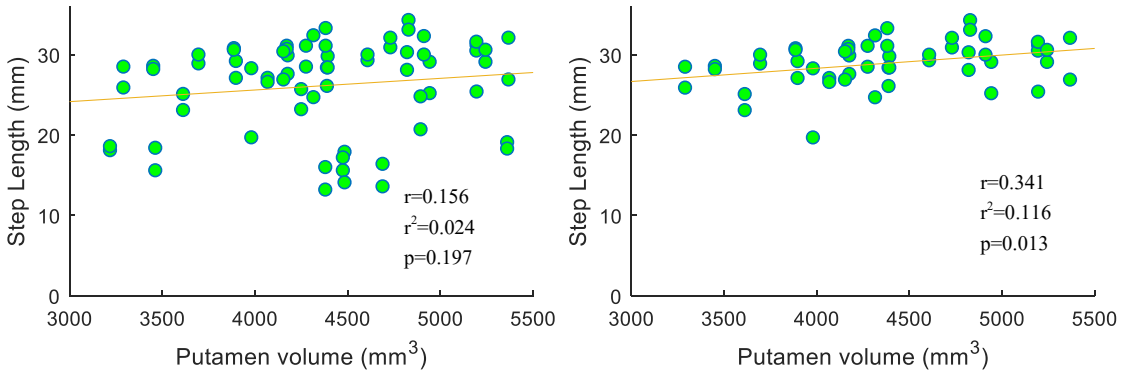

a) b)

Figure 3-11. Variations in maximum step length and putamen volume: a) all subjects (n=70), b) posterior trajectory subjects only (n=52).

3.4.3 Coverage of VOI and putamen

Over the 80 study weeks the 3 groups of test infusions maintained high percentage coverage of the VOI with no significant change in the average coverage (F(2,207)=1.88, p=0.16). Average VOI coverage was W-4/69±2(SEM)%, W40/75±2 %, W80/70 ±3 % (Figure 3-12).

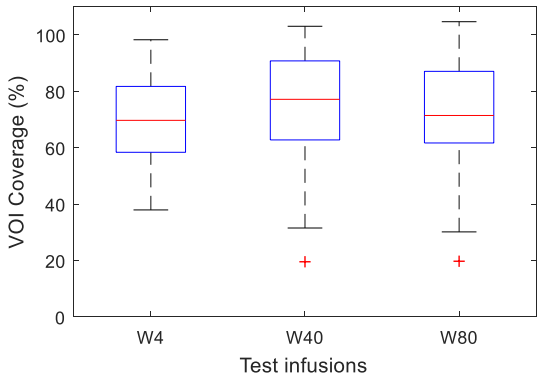

Figure 3-12. Percentage coverage of the VOI over the 3 test infusions [n=70/ group, $\bar{x}_{W-4}$= 69 ± 16 % (STD), $\bar{x}_{W40}$= 75 ± 19%, $\bar{x}_{W80}$= 70 ± 21%].

The average putamen coverage was not significantly different between any of the three test infusions (F(2,206)=0.12, p=0.89). Average putamen coverage was 51.5±1.8 %(SEM)(W-4), 50.8±1.9 % (Week40), 51.4 ±2.2 %(Week80) (Figure 3-13). The percentage coverage ranged from 15-80 % (W-4), 24-82 % (W40) and 16-84 %(W80).

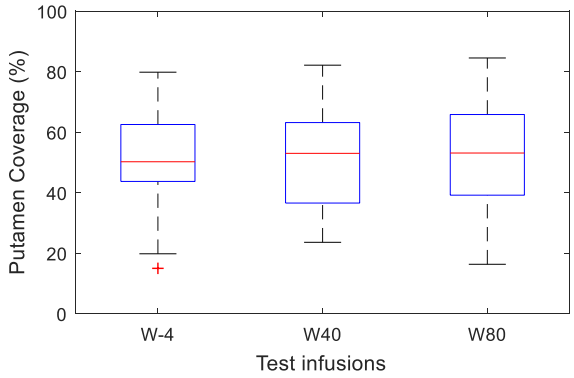

Figure 3-13. Percentage coverage of the Putamen over the three test infusions [n=70/ group, $\bar{x}_{W-4}$=51.5 ± 15 % (STD), $\bar{x}_{W40}$=50.8 ± 16 %, $\bar{x}_{W80}$=51.4 ± 18 %].

Modifications to the choice of surgical implant trajectory was shown to have a significant effect on lengthening the step region of the RSC within the putamen (section 3.4.2). This increase in step length was associated with a significant rise in the VOI coverage ($F(2,69)=4.89$, $p=0.01$) (Figure 3-14a) and the percentage coverage of the putamen ($F(2,67)=22$, $p<0.001$) (Figure 3-14d) at the first test infusion.

Average VOI coverage remained high (<50 %) throughout the main and extension study period with the largest coverage in the anterior and posterior groups (**W-4**-57%(vertical), 79%(anterior), 70 %(posterior)/ **W40**-75 %(vertical), 92 %(anterior), 72 %(posterior)/ **W80**-69 %(vertical), 93 %(anterior), 68 %(posterior)).

Average putamen coverage also remained largely consistent over the study period (**W-4**-31%(vertical), 41 %(anterior), 57 %(posterior)/ **W40**-38 %(vertical), 60 %(anterior), 53 %(posterior)/ **W80**-36 %(vertical), 59 %(anterior), 54 %(posterior)).

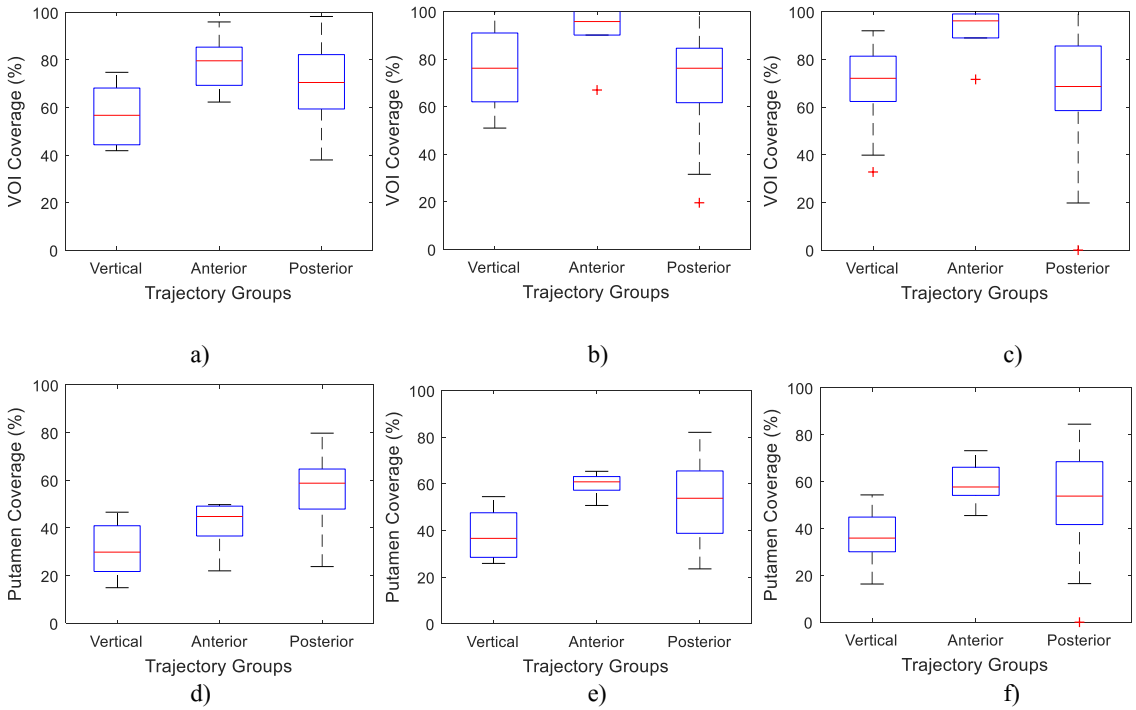

Figure 3-14. Percentage coverage of the VOI (a-c) and the putamen (d-f) over the three test infusion time points (Week-4, Week 40, Week 80, respectively) [$n_{vertical}$=10, $n_{anterior}$= 6, $n_{posterior}$=52, a-c) VOI coverage: $\bar{x}_{W-4}$=57 ± 12 % (STD) (vert), 79 ± 12 % (ant), 70 ± 16 % (post); $\bar{x}_{W40}$=75 ± 17 % (vert), 92 ± 13 % (ant), 72 ± 19 % (post); $\bar{x}_{W80}$=69 ± 18 % (vert), 93 ± 11 % (ant), 68 ± 22 % (post); d-f) putamen coverage: $\bar{x}_{W-4}$=31 ± 11 % (vert), 41 ± 11 % (ant), 57 ± 12 % (post); $\bar{x}_{W40}$=38 ± 11% (vert), 60 ± 5 % (ant), 53 ± 16 % (post); $\bar{x}_{W80}$=36 ± 12 % (vert), 59 ± 10 % (ant), 54 ± 18 % (post)]. Note: the anterior groups in boxplots b) and c) are shown reaching 100 % but without obvious 'whiskers' demarking the upper and lower quantiles. This is because the anterior group has only 6 entries which cluster in the upper 90's percent region. A single data point in the 70 % region is correctly shown as an outlier.

Despite a constant infusion volume, the range of distribution coverage values significantly increased ($F(2,207) = 23.7$, $p<0.001$) over the 80 week study (**W-4**-2049-8076/ **W40**-1915-11,265/ **W80**-2,680-11,137) (Figure 3-15a). With the largely consistent VOI and putamen coverage shown above, the increased coverage was outside the intended regions of interest. Calculating the ratio of coverage retained inside the putamen to that outside over the three test infusions shows a significant decline in the average retention of infusate inside the target tissue structure ($F(2, 206) = 29.22$, $p<0.001$) (Figure 3-15b).

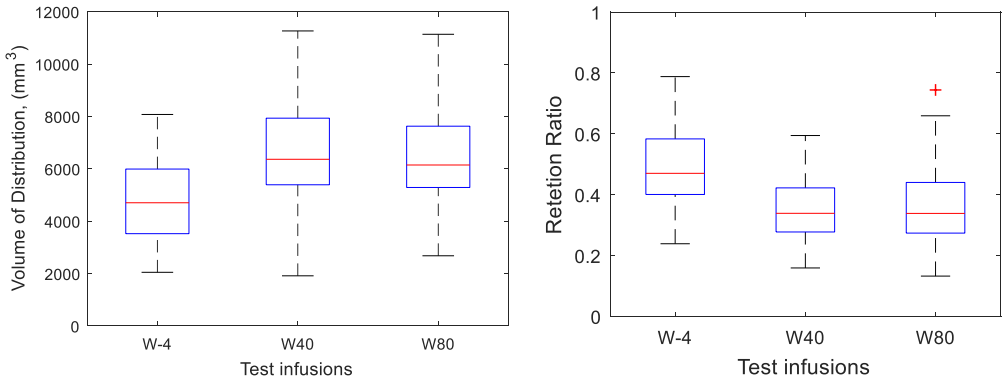

Figure 3-15. a) Total hemispherical (1/2 of the brain) distribution volume (V_d), b) V_d ratio retained within the boundary of the putamen over the study period. [n=70/group, a) $\bar{x}_{W-4}$= 4,796 ± 1,560 mm³ (STD), $\bar{x}_{W40}$= 6,553 mm³ ± 1,721 mm³, $\bar{x}_{W80}$= 6,437 ± 1,991 mm³; b) $\bar{x}_{W-4}$= 0.4857 ± 0.1320, $\bar{x}_{W40}$ = 0.3463 ± 0.0989, $\bar{x}_{W80}$= 0.3584 ± 0.1219].

3.4.4 Delay to MRI scan acquisition

The delay time between completing the infusion and acquiring the T1 weighted MRI scan for distribution assessment significantly (F(2,103)=5.1, p=0.001) increased following the first test infusion (Figure 3-16a) with the average delay rising from 43mins (W-4) to 57mins (W40) and finally 60mins (W80). The increase in average delay was not associated with a small number of outliers, as most patients experienced longer delays between the completion of the infusion and the acquisition of the T1 weighted MRI scan at follow up test infusions (Figure 3-16b).

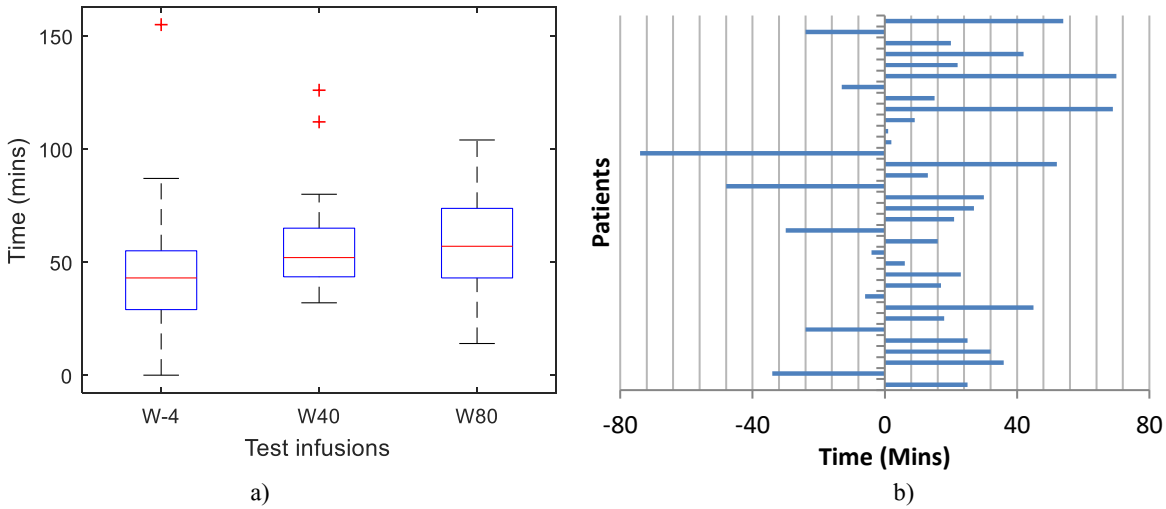

Figure 3-16. Average delay times to acquire the post infusion T1 weighted MRI scan: a) delay at three test infusion time points, week -4, 40 and 80 (n=35/group, $\bar{x}_{W-4}$= 43 ± 28 mins (STD), $\bar{x}_{W40}$= 57 ± 21 mins, $\bar{x}_{W80}$= 60 ± 21 mins), b) changes in delay per subject between first and second test infusion.

3.4.5 Correlation analysis of putamen volume and coverage achieved

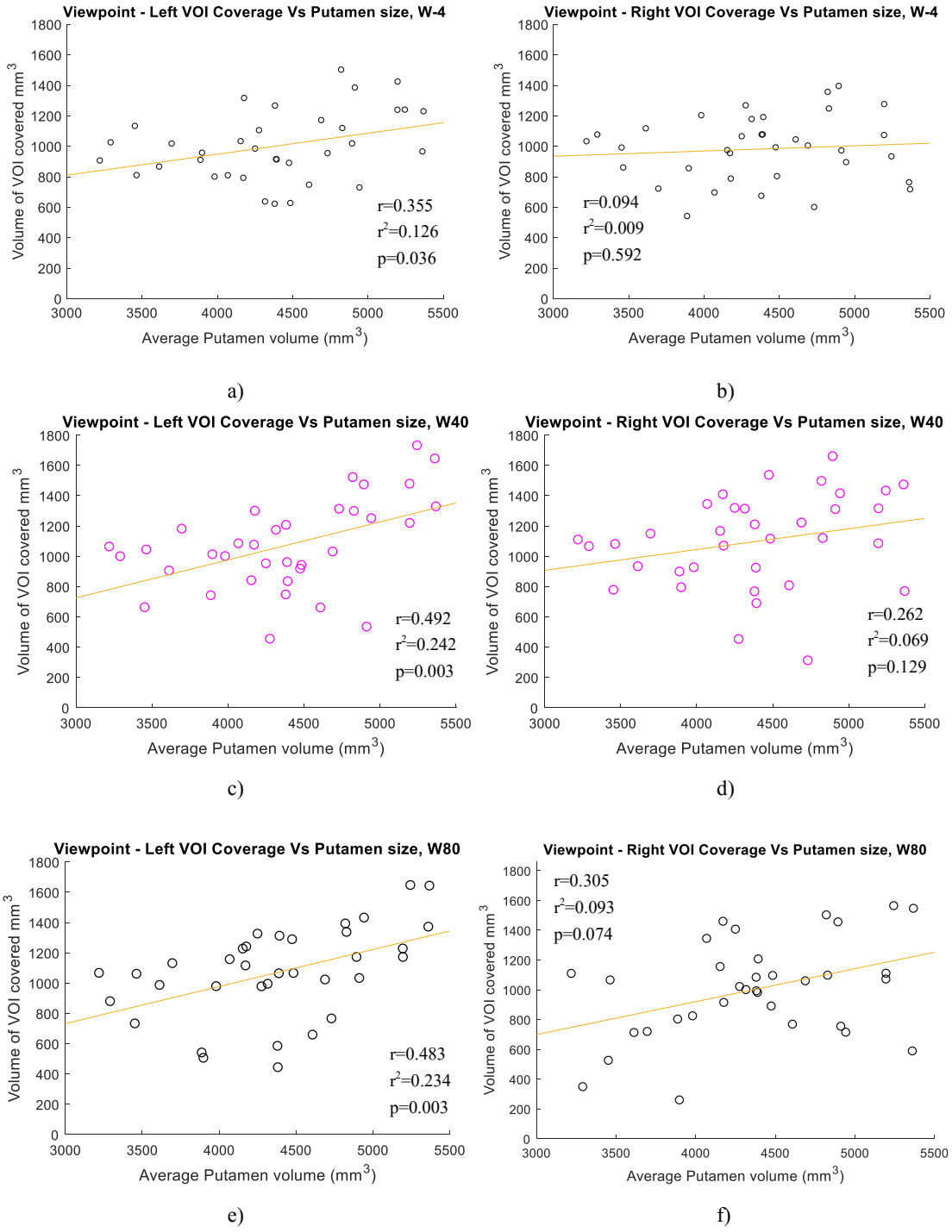

Figure 3-17. Left and right VOI coverage plotted against the average putamen volume: a-b) week-4, c-d) week40, e-f) week80.

Positive Pearson correlation coefficients were calculated for the relationship between increased VOI (r=0.09-0.49) (Figure 3-17a-f) and putamen (r=0.03-0.34)(Figure 3-18a-f) coverage with increased size of patient anatomy. Significance is only obtained on the patient left for the VOI coverage at all test infusion (Figure 3-17a, c & e) the putamen coverage at week 40 (Figure 3-18c). Negative correlation coefficients were observed for the percentage coverage of the putamen with increases in putamen volume which neared significance at the first test infusion (p=0.059), was significant at week 40 (p=0.032) and was not significant at week 80 (p=0.384).

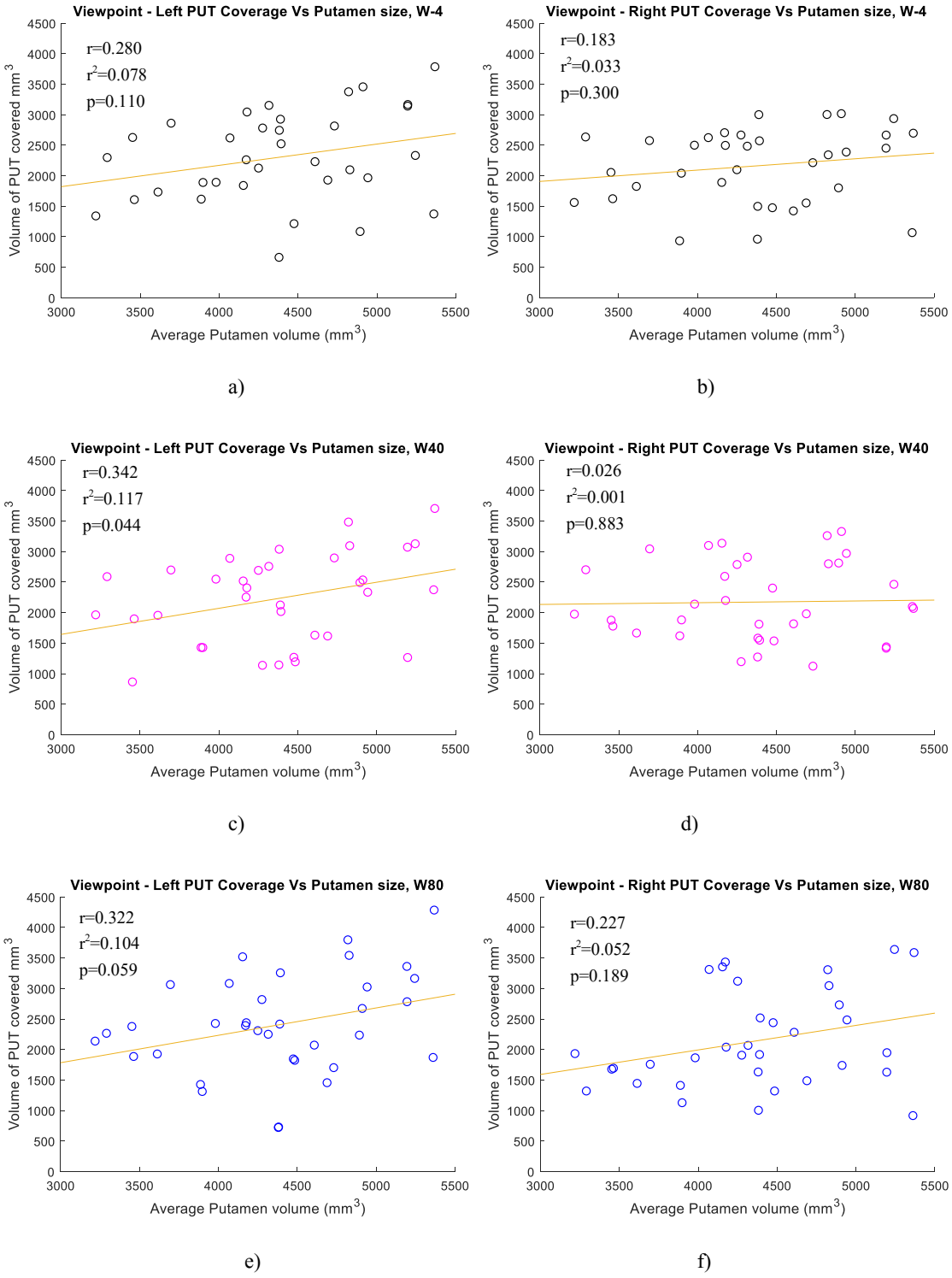

Figure 3-18. Left and right putamen coverage plotted against the average putamen volume: a-b) week-4, c-d) week40, e-f) week80.

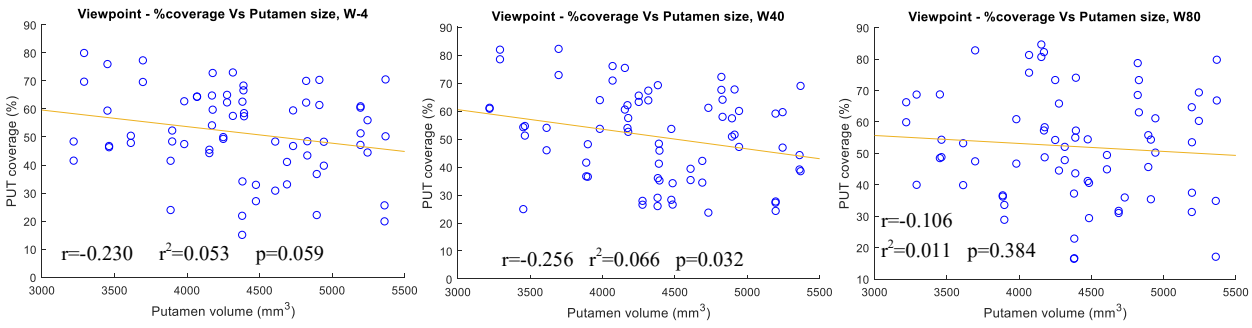

a) *b)* *c)*

Figure 3-19. Percentage coverage of the putamen relative to its size over the study period.

3.4.6 Correlation analysis of catheter feature placement and coverage achieved

Weak and insignificant Pearson's correlation coefficients (r=0.01-0.17) were calculated for the relationship between percentage coverage of putamen and the position of the OGT tip (the reflux inhibition feature) into the grey matter of the putamen at the first and second test infusion (Figure 3-20a-b).

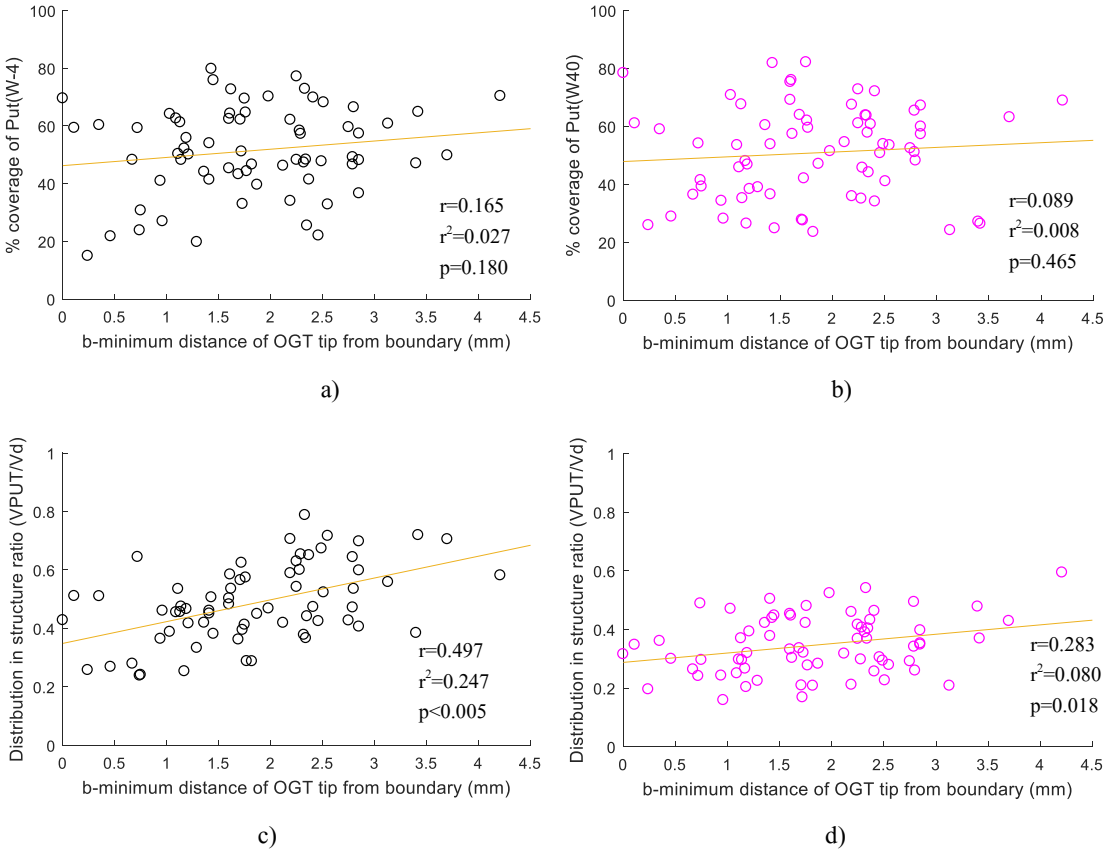

Figure 3-20. Correlation analysis of depth of the OGT tip (containing the recessed step) into structure, a) %coverage of putamen at study W-4 and b) W40, c) ratio of distributed infusate retained inside the putamen at study W-4 and d) W40.

Significant Pearson's correlation coefficients (r=0.497/ p=<0.005 and r=0.283/ p=0.018)) were however observed in the ratio of infusate retained inside the target structure by placing the OGT tip deeper into the boundary of the putamen at the

first and second test infusions (Figure 3-20c-d). This correlation weakens after 40 weeks implantation (r=0.28) but remains significant. (Figure 3-20d).

A medium strength, significant correlation coefficient (r=0.34/ p=0.004) was calculated for the relationship between percentage coverage of putamen and the increasing distance between the tip of the catheter and the boundary wall of the putamen (Figure 3-21a). This correlation disappeared by the second test infusion (r<0.1/ p=0.465)) (Figure 3-21b).

The ratio of infusate retained in the structure was largely unaffected by the position of the catheter tip (within the sample population) (r=-0.07/p=0.561 & r=0.23/ p=0.054), W-4 to W40 respectively) (Figure 3-21c-d).

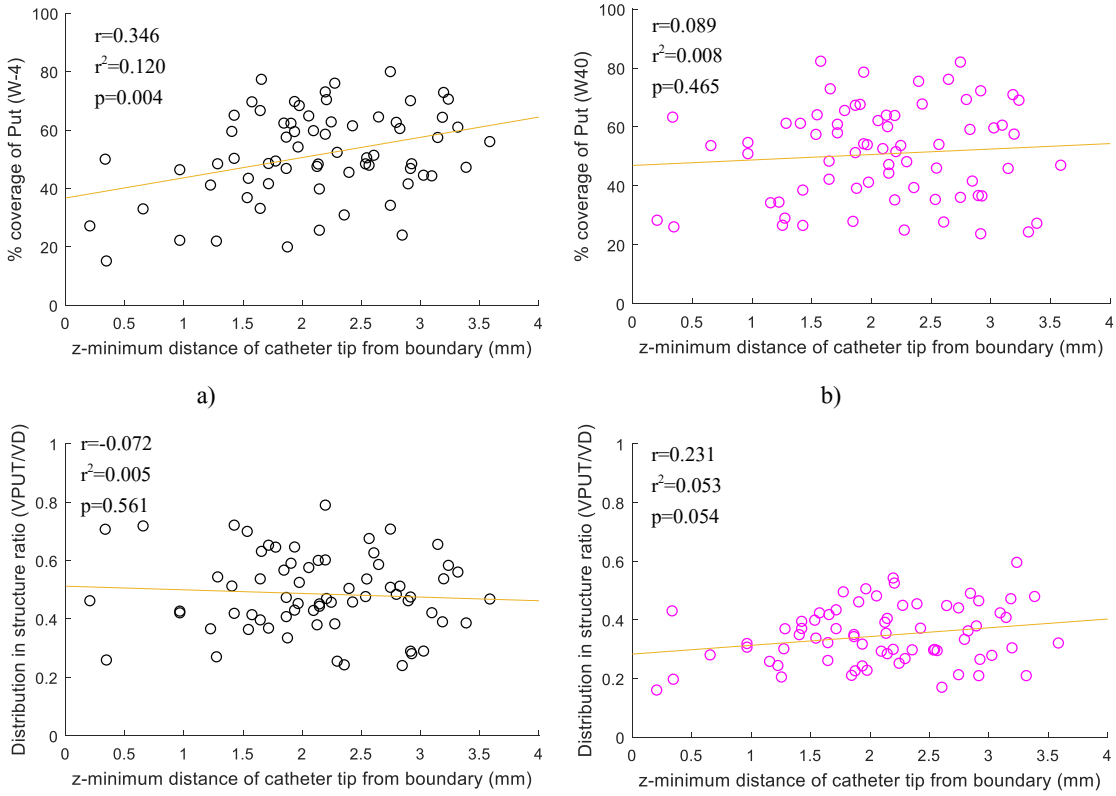

Figure 3-21. Correlation analysis of distance from catheter tip (along trajectory) to putamen boundary, a) %coverage of putamen at study W-4 and b) W40, c) ratio of distributed infusate retained inside the putamen at study W-4 and d) W40.

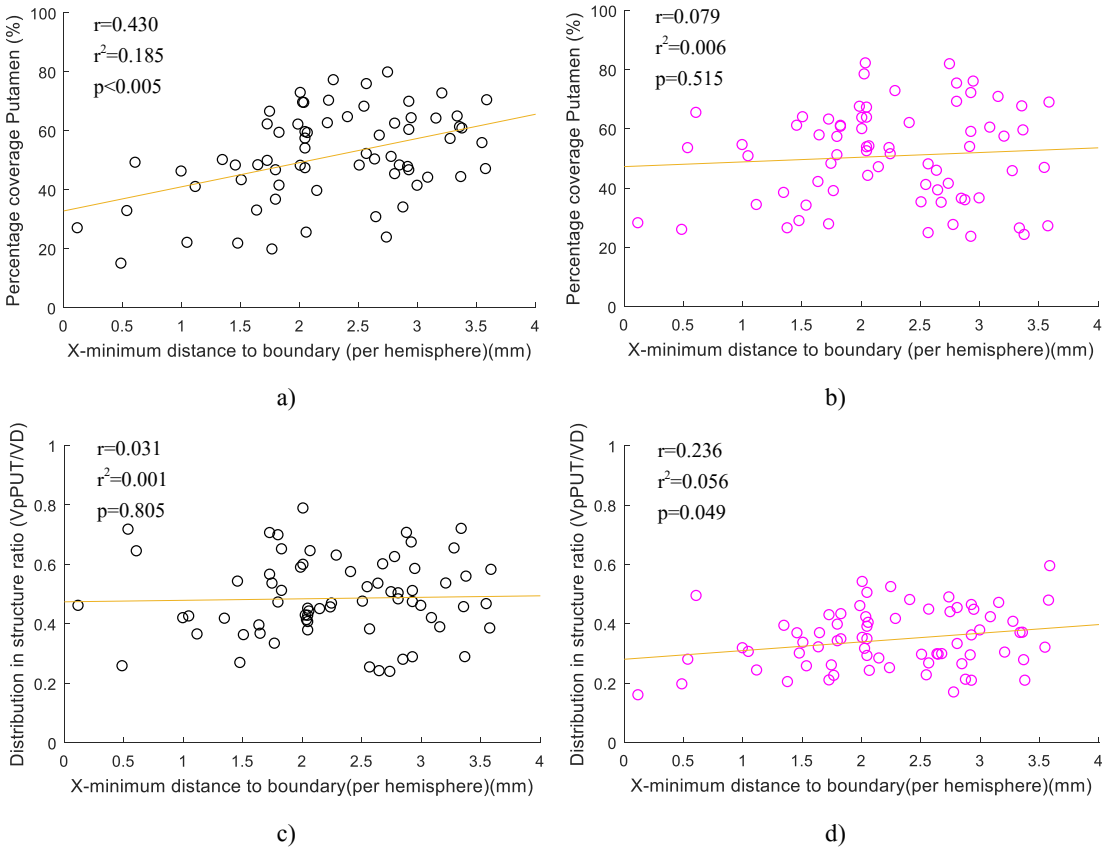

Figure 3-22. Correlation analysis of distance from catheter tip (any direction) to putamen boundary, a) %coverage of putamen at study W-4 and b) W40, c) ratio of distributed infusate retained inside the putamen at study W-4 and d) W40.

As above, a significant correlation coefficient (r=0.43/ p<0.005) was also calculated for the relationship between percentage coverage of putamen and the minimum distance (in any direction) between the tip of the catheter and the boundary wall of the putamen (Figure 3-22a). This correlation also disappeared by the second test infusion (r<0.1/ p=0.515) (Figure 3-22b) and the ratio of infusate retained in the structure continued to be largely unaffected (within the sample population) (r=-0.03/p=0.805)at the first test infusion (W-4) but tighter grouping at W40 was significant (r=0.24/ p=0.050) (Figure 3-22c-d).

A significant correlation coefficient (r=0.550/ p<0.005) was initially calculated for the relationship between percentage coverage of putamen and the increasing step length of the RSC inside the putamen (Figure 3-23a). This relationship weakened and became non-significant by the second test infusion (r=0.16/ p=0.188) (Figure 3-23b). The ratio of fluid retained inside the putamen was correlated weakly and non-significantly (r=0.129/ p=0.295) with step length at the first test infusion (Figure 3-23c) but became significant by the second test infusion due to close grouping of data points (r=0.332/ p=0.005) (Figure 3-23d).

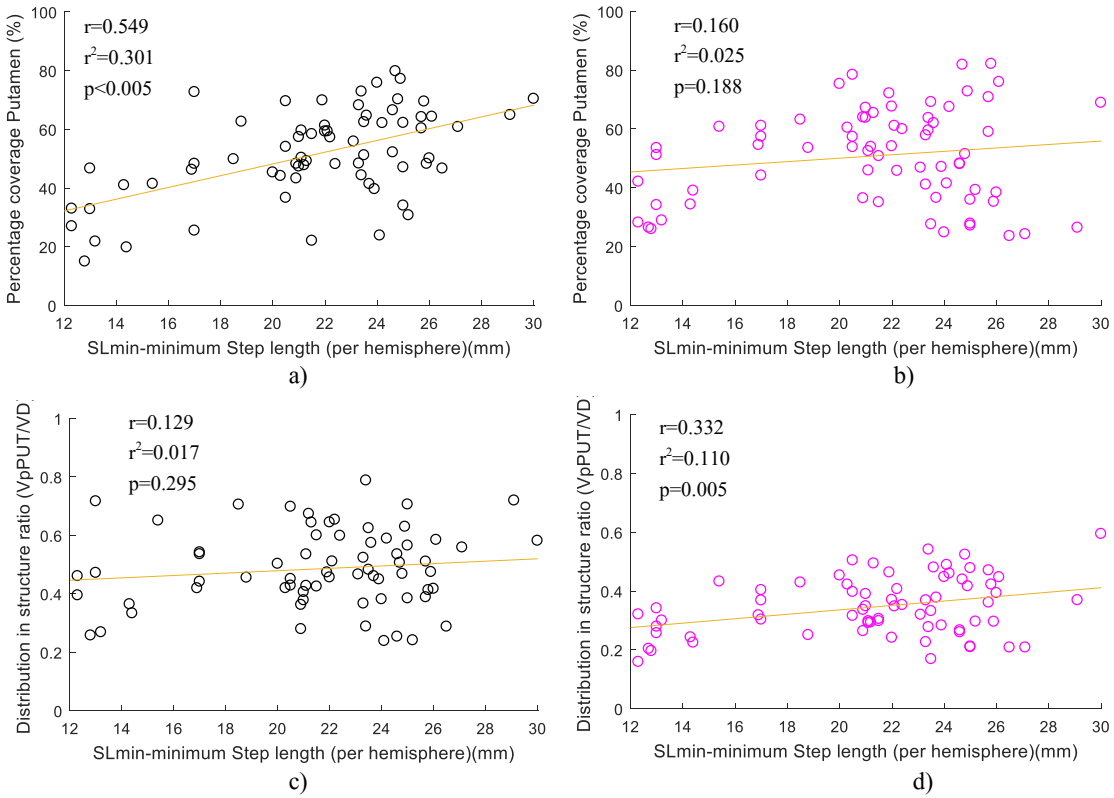

Figure 3-23. Correlation analysis of minimum catheter step length (per hemisphere) inside putamen, a) %coverage of putamen at study W-4 and b) W40, c) ratio of distributed infusate retained inside the putamen at study W-4 and d) W40.

Non-significant, correlation coefficients (r=-0.15/ p=0.222 & r=0.05/ p=0.680) were calculated for the relationship between percentage coverage of putamen and the minimum (or negative) distance of the catheter wall (along the step length region) and the boundary wall of the putamen at the first and second test infusions (Figure 3-24a-b).

No significant correlation was observed for the ratio of fluid retained through increasing the distance of the stepped region from the boundary (into the structure) (r=0.066/ p=0.592 & r=0.040/ p=0.742) (Figure 3-24c-d).

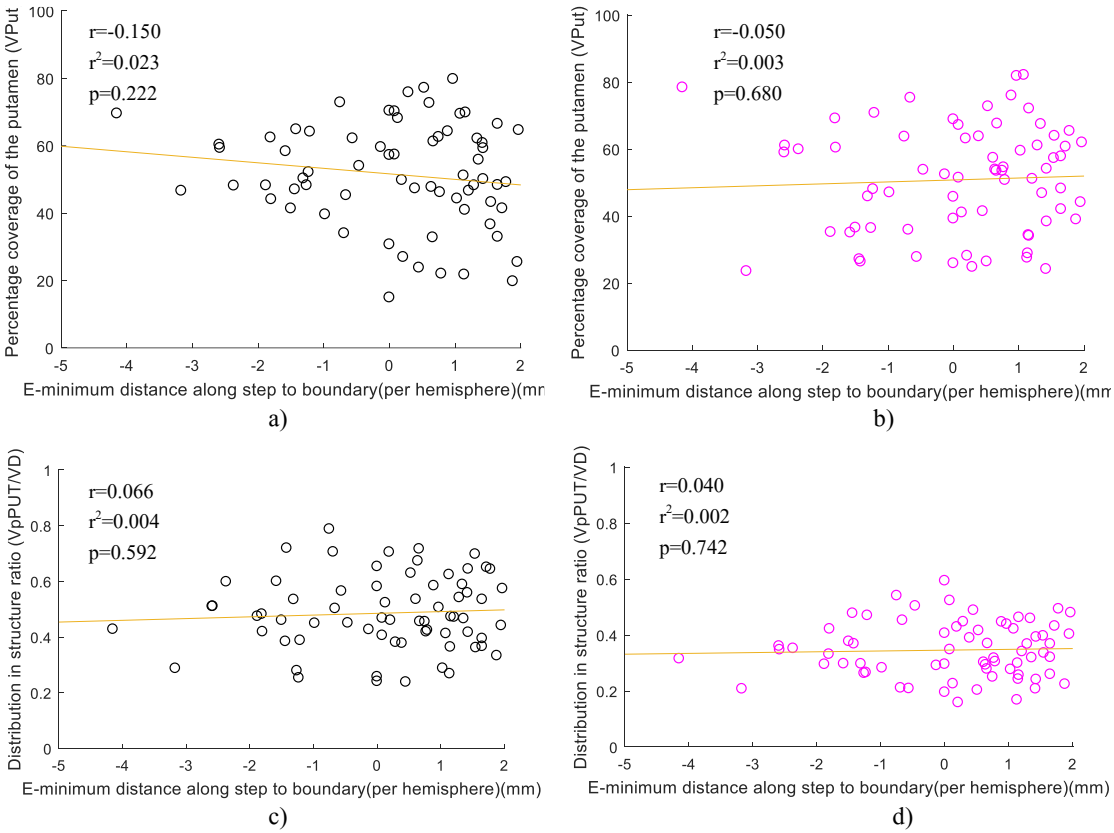

Figure 3-24. Correlation analysis between minimum (or negative) distance from catheter stepped region to the putamen boundary, a) %coverage of putamen at study W-4 and b) W40, c) ratio of distributed infusate retained inside the putamen at study W-4 and d) W40.

A positive and significant correlation coefficient (r=0.45/ p<0.005) was calculated for the relationship between a group of equally weighted mixed variables (i.e. Catheter and OGT tip position from putamen boundary, inclusion of the whole stepped region within the putamen boundary and increasing step length inside the putamen boundary) and percentage putamen coverage at the first test infusion. This correlation weakened and became non-significant for the second test infusion (r=0.171/ p=0.158).

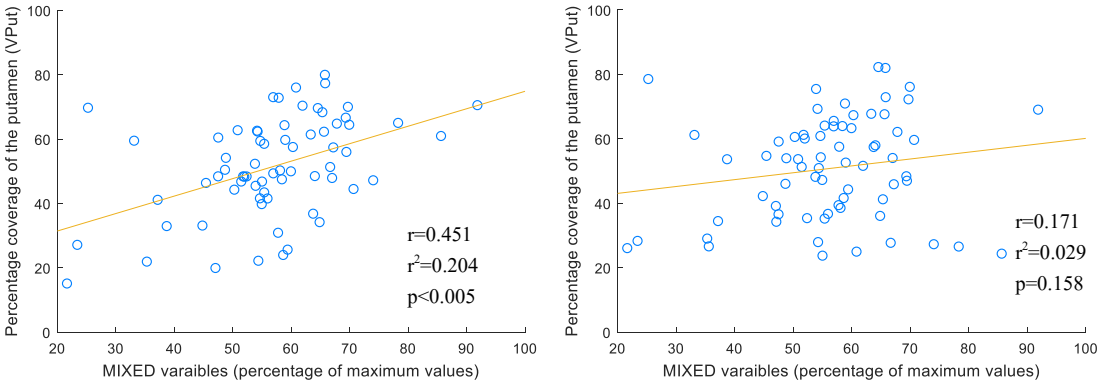

Figure 3-25. Putamen coverage (%) plotted against a mixture of variables (Step Length, Distance of the OGT into the structure, minimum distance of the catheter from the putamen boundary and the minimum distance of the catheter to the boundary of the structure (along the step length) a) week-4, b) week 40.

Table 3-1. Tabulation of the correlation coefficients (significant values shown in green).

Fig	Variable A	Variable B	R	R2	p
3-11a	Step Length (mm)	Putamen Volume (mm^3)	0.150	0.024	0.197
3-11b	Step Length (mm)	Putamen Volume (mm^3) *Posterior only*	0.341	0.116	0.013
3-17a	Left VOI coverage (W-4)	Average Putamen Volume (mm^3)	0.355	0.126	0.036
3-17b	Right VOI coverage (W-4)	Average Putamen Volume (mm^3)	0.094	0.009	0.592
3-17c	Left VOI coverage (W40)	Average Putamen Volume (mm^3)	0.492	0.242	0.003
3-17d	Right VOI coverage (W40)	Average Putamen Volume (mm^3)	0.262	0.069	0.129
3-17e	Left VOI coverage (W80)	Average Putamen Volume (mm^3)	0.483	0.234	0.003
3-17f	Right VOI coverage (W80)	Average Putamen Volume (mm^3)	0.305	0.093	0.074
3-18a	Left Putamen coverage (W-4)	Average Putamen Volume (mm^3)	0.280	0.078	0.110
3-18b	Right Putamen coverage (W-4)	Average Putamen Volume (mm^3)	0.186	0.033	0.300
3-18c	Left Putamen coverage (W40)	Average Putamen Volume (mm^3)	0.342	0.117	0.044
3-18d	Right Putamen coverage (W40)	Average Putamen Volume (mm^3)	0.026	0.001	0.883
3-18e	Left Putamen coverage (W80)	Average Putamen Volume (mm^3)	0.322	0.104	0.059
3-18f	Right Putamen coverage (W80)	Average Putamen Volume (mm^3)	0.227	0.052	0.189
3-19a	Put coverage (%), (W-4)	Putamen Volume (mm^3)	0.230	0.053	0.059
3-19b	Put coverage (%), (W40)	Putamen Volume (mm^3)	0.256	0.066	0.032
3-19c	Put coverage (%), (W80)	Putamen Volume (mm^3)	0.106	0.011	0.384
3-20a	OGT tip depth into structure (mm)	%coverage of Putamen (W-4)	0.165	0.027	0.180
3-20b	OGT tip depth into structure (mm)	%coverage of Putamen (W40)	0.089	0.008	0.465
3-20c	OGT tip depth into structure (mm)	Distribution in structure ratio (W-4)	0.497	0.247	0.000
3-20d	OGT tip depth into structure (mm)	Distribution in structure ratio (W40)	0.283	0.080	0.018
3-21a	Dist. catheter tip from boundary (mm)	%coverage of Putamen (W-4)	0.346	0.120	0.004
3-21b	Dist. catheter tip from boundary (mm)	%coverage of Putamen (W40)	0.089	0.008	0.465
3-21c	Distance of catheter tip from structure boundary (mm)	Distribution in structure ratio (W-4)	-0.072	0.005	0.561
3-21d	Distance of catheter tip from structure boundary (mm)	Distribution in structure ratio (W40)	0.231	0.053	0.054
3-22a	Min distance of catheter tip to structure boundary (mm)	%coverage of Putamen (W-4)	0.430	0.185	0.000
3-22b	Min distance of catheter tip to structure boundary (mm)	%coverage of Putamen (W40)	0.079	0.006	0.515
3-22c	Min distance of catheter tip to structure boundary (mm)	Distribution in structure ratio (W-4)	0.031	0.001	0.805
3-22d	Min distance of catheter tip to structure boundary (mm)	Distribution in structure ratio (W40)	0.236	0.056	0.049
3-23a	Min Step Length (mm)	%coverage of Putamen (W-4)	0.549	0.301	0.000
3-23b	Min Step Length (mm)	%coverage of Putamen (W40)	0.160	0.250	0.188
3-23c	Min Step Length (mm)	Distribution in structure ratio (W-4)	0.129	0.017	0.295
3-23d	Min Step Length (mm)	Distribution in structure ratio (W40)	0.332	0.110	0.005
3-24a	Min distance to boundary (mm)	%coverage of Putamen (W-4)	0.150	0.023	0.222
3-24b	Min distance to boundary (mm)	%coverage of Putamen (W40)	-0.050	0.003	0.680
3-24c	Min distance to boundary (mm)	Distribution in structure ratio (W-4)	0.066	0.004	0.592
3-24d	Min distance to boundary (mm)	Distribution in structure ratio (W40)	0.040	0.002	0.742
3-25a	Mixed variables (percentage of maximum values)	%coverage of Putamen (W-4)	0.451	0.204	0.000
3-25b	Mixed variables (percentage of maximum values)	%coverage of Putamen (W40)	0.171	0.029	0.158

Table 3-2. Condensed table of significant correlation coefficients only (from Table 3-1).

Fig	Variable A	Variable B	R	R2	p
3-11b	Step Length (mm)	Putamen Volume (mm^3) *Posterior only*	0.341	0.116	0.013
3-17a	Left VOI coverage (W-4)	Average Putamen Volume (mm^3)	0.355	0.126	0.036
3-17c	Left VOI coverage (W40)	Average Putamen Volume (mm^3)	0.492	0.242	0.003
3-17e	Left VOI coverage (W80)	Average Putamen Volume (mm^3)	0.483	0.234	0.003
3-18c	Left Putamen coverage (W40)	Average Putamen Volume (mm^3)	0.342	0.117	0.044
3-19a	Put coverage (%), (W-4)	Putamen Volume (mm^3)	0.230	0.053	0.059
3-19b	Put coverage (%), (W40)	Putamen Volume (mm^3)	0.256	0.066	0.032
3-20c	OGT tip depth into structure (mm)	Distribution in structure ratio (W-4)	0.497	0.247	0.000
3-20d	OGT tip depth into structure (mm)	Distribution in structure ratio (W40)	0.283	0.080	0.018
3-21a	Dist. catheter tip from boundary (mm)	%coverage of Putamen (W-4)	0.346	0.120	0.004
3-22a	Min distance of catheter tip to structure boundary (mm)	%coverage of Putamen (W-4)	0.430	0.185	0.000
3-22d	Min distance of catheter tip to structure boundary (mm)	Distribution in structure ratio (W40)	0.236	0.056	0.049
3-23a	Min Step Length (mm)	%coverage of Putamen (W-4)	0.549	0.301	0.000
3-23d	Min Step Length (mm)	Distribution in structure ratio (W40)	0.332	0.110	0.005
3-25a	Mixed variables (percentage of maximum values)	%coverage of Putamen (W-4)	0.451	0.204	0.000

Pearson correlation coefficients, coefficient of determination and the probability (for r) from all scatter plots in section 3 are tabulated above (Table 3-1) with significant correlations condensed further in Table 3-2.

3.5 Discussion

3.5.1 Manual profiling of the infusion distributions

An assessment of the viewpoint analysis method (section 3.3.1) was performed using three industry experts, two neurosurgeons who were associated with the development of the method in Bristol, and a third at an external site. All users were first required to read through the work instructions on the method and confirm they agreed with it. The users were asked to profile 2 objects in the surgical planning software: a chamber filled with a gadolinium solution (at the same concentration used *in vivo*), and an example *in vivo* infusion into the putamen of a study subject.

The chamber was previously measured using a co-ordinate measurement machine (CMM) and the internal volume was calculated at 39.744 ± 0.004 ml. Each of the users profiled volumes which were in excess of this by 5-13 %.

Comparison between the *in vivo* infusion did not have a 'true value' and only a comparison between users was sought. Here, each personality played a greater role as the users stated that while they agreed with windowing to maximise the contrast to define the border of the infusion, they each left varying amounts of white matter present in the image, and different users included or excluded infusate depending on whether they felt it was inside the region of interest (Figure 3-26).

This produced a large variation in the volumes assessed 1.053-4.042 ml (ratio~1:4). This variation between users was too large to provide meaningful comparison between patients and prompted the use of a single, dedicated operator.

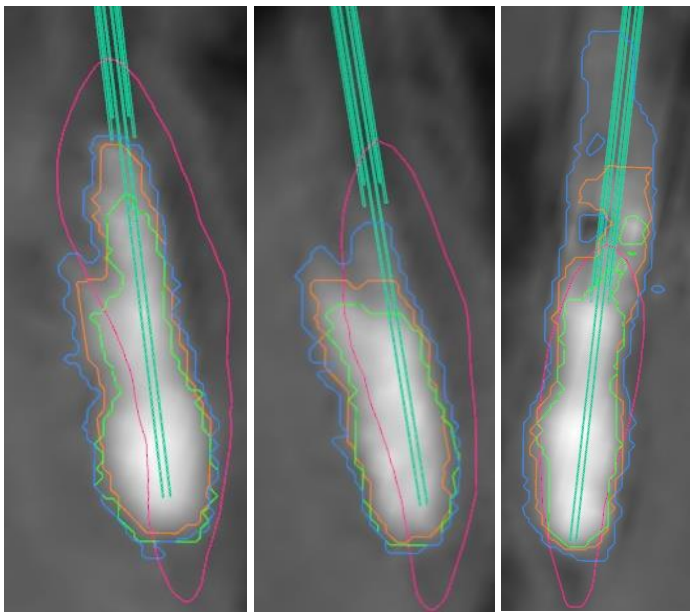

Figure 3-26. 2D profiles of a real infusion in the putamen of a subject (pink outline) provided by three neurosurgeons.

A reanalysis of a different subject's infusion was performed using a single user (author) using the manual adjustment of contrast and brightness described above (section 3.3.1) where the anatomy was removed from view by thresholding the image to leave the much brighter gadolinium. The variation between repeats improved markedly (4.41-4.94 ml, ratio 1:1.1) with overlapping profiles proving to be more consistent (Figure 3-27).

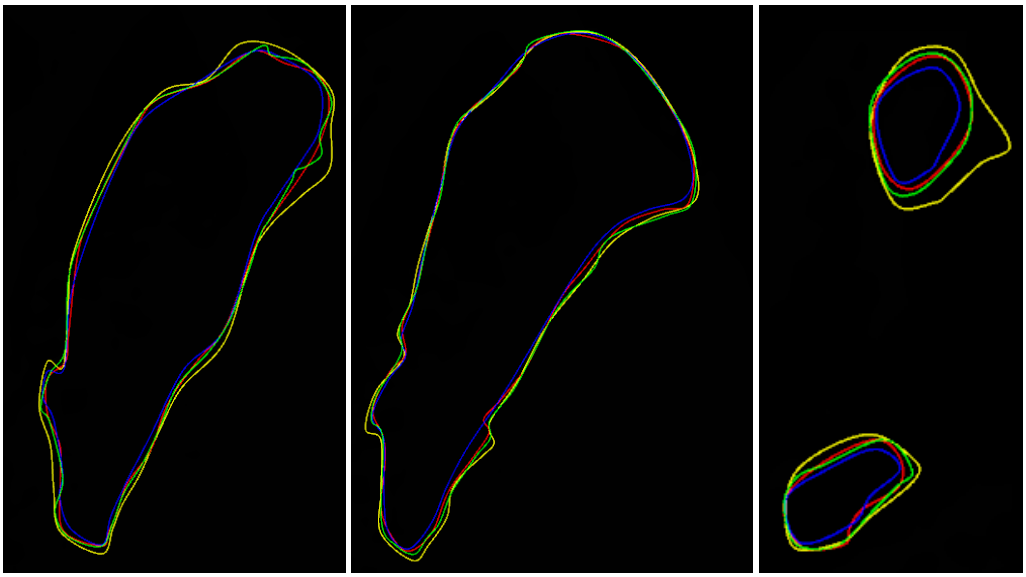

Figure 3-27. Numerous profiles around an infusion from four repeated analysis performed by a single user.

This improvement was acceptable for the purposes of defining the relative proportion of coverage between each subject's test infusions and also between subjects.

3.5.2 Putamen volume

Earlier published work investigated the volume of the putamen in patients with and without Parkinson's disease (PD). Non-diseased putamen (n=13 patients) had an average volume of 3.57±0.12cm^3 (range; 2.38-4.89cm^3) while PD participants (n=11 patients) had average putamen volumes of 3.98±0.15cm^3 (range; 3.01-5.29cm^3) (Yin *et al.*, 2009). No statistical

significance was found between the right and left hemispheres within each group, but smaller brains were attributed to the increased age of the subjects in the healthy group who were on average 8 years older than those in the PD group.

The average putamen volume (Figure 3-8) of the 36 participants (pre-randomisation) within this study was 4.39±0.06cm^3 (range; 3.22-5.37 cm^3), ~0.4 cm^3 (10 %) larger than the average volume previously published. In an effort to standardise the administration (infusate) volume to all subjects in this study, the infusion volume was fixed at 300 µl/catheter (600 µl/putamen) which assumed a 5:1 V_d/V_i ratio providing a 3,000 µl (3 cm^3) distribution volume (assuming all infusate was retained within the target structure). Such a limited infusion volume, covering 3 cm^3, would only cover 56-93 % of the complete putamen volume of subjects in this study.

Where maximal coverage of the target structure is required, optimisation should involve the patient specific target volume in the calculation of infusate volume (or dose). Unless such a standardisation step is included in the clinical workflow, it is unlikely that complete (or optimised) target coverage can be obtained without over infusion to compensate for the natural range of putamen sizes.

Such patient specific medicine has recently been advocated in a review focused on the optimisation of therapeutic delivery to treat neuro-oncology indications (Raghavan, Brady and Sampson, 2016).

It is perhaps counterintuitive therefore that the general trends in the total volume of tissue covered in the VOI (Figure 3-17a-f) and the putamen (Figure 3-18a-f) increased as the putamen volume increased. Trendlines are typically positive with correlation coefficients showing the strongest values in the period immediately following implantation (1st test infusion at W-4) though few are significant. Percentage coverages of the target structure do however decline with increasing putamen volumes (Figure 3-19a-c), indicating that while more tissue was covered, this was outstripped by increases in the target volume. This observation neared significance at the first test infusion (W-4/ p=0.059), was significant at week 40 (p=0.03), and was not significant at week 80 (p=0.384). Improvements in total coverage may be possible by increasing the infusion volume for larger structures. Changes to the surgical trajectory, configuration and position of the implant also play a role in retaining infusate within the target structure. Increasing infusion volume to match putamen volume maintaining a theoretical V_d/V_i ration is however a logical step towards optimisation, maintaining a therapeutic dose per unit of tissue.

3.5.3 Catheter assembly step length (SL)

As the investigator led study progressed, the target structure was increased to include the whole of the putamen over the smaller VOI alone. While the clinical protocol remained unchanged, the choice of surgical trajectories was affected, with anterior (and later posterior) trajectories being favoured over a vertical approach (Figure 3-7).

The change in trajectory significantly ($F(2,139)=104.58$, $p<0.001$) increased the average length of the step inside the putamen (Figure 3-10a-b). Step length ranged from 12.3-34.2 mm (Vertical:12.3-19 mm, Anterior:15.4-25.6 mm, Posterior-17.0-34.2 mm). Positive trends in the step length were most obvious in the posterior group which aligned the step with the long axis of the target structure (Figure 3-11).

3.5.4 Coverage of VOI and putamen

Increases in the step length were associated with a significant ($F(2,67)=22$, $p<0.001$) rise in the percentage of the putamen which was covered (Figure 3-14d). Previously published *in vitro* and *in vivo* empirical testing limited the step length to a few millimetres but infusions were retained below the inhibiting recess step feature (Gill *et al.*, 2013). Observations of the clinical infusion morphology indicates that the fluid flows from the catheter tip to the step, with the step acting to control, and limit the extent of the reflux. Further work is required to characterise and optimise this effect.

The average percentage coverage of the VOI and the whole putamen were not statistically significant between any of the three test infusions (Figure 3-12,Figure 3-13), suggesting a maintenance of the implanted system performance. Sub-plots show a varied picture however with a lowering of the percentage coverage limit in the posterior group and modest increases in the others over the three test infusions (Figure 3-14 a-f).

Decline in the retention of the infusate inside the target structure was visible in some cases over the second and third test infusions (Figure 3-28a-c). This was not common in all cases however with many implants maintaining a high level of coverage over the 80-week study period (Figure 3-28d-f). Visually there was no obvious differences between these cases on the pre- and post-implant MRI images which might lead to such disparities in the long-term performance.

The ratio of the infusion which was retained inside the target tissues declined after the first infusion (W-4) ($F(2, 206) = 29.22$, $p<0.001$) (Figure 3-15b). Average percentage coverage of the VOI and putamen can only therefore have been maintained by the significant increase ($F(2,207) = 23.7$, $p<0.001$) in the volume of tissue covered by each test infusion.

It is hypothesised that declining performance in some patients may be linked to the extent of reactive gliosis which may be present at the cellular level which would decrease the permeability of the tissue surrounding the catheter. Further work is required to understand how this could be limited or overcome in this treatment population.

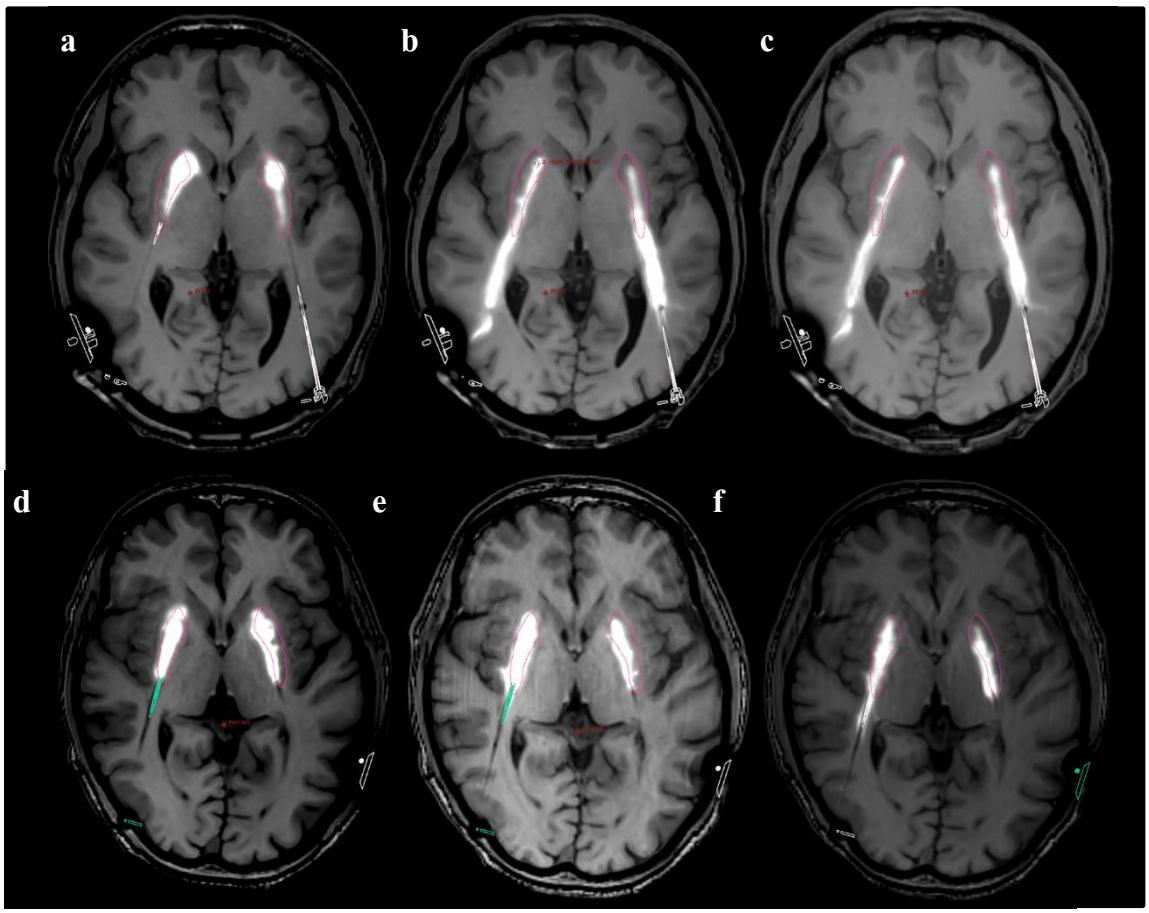

Figure 3-28. Post infusion T1 weighted MRI scans of two subjects over the three test infusions: a) S036-W-4, b) S036-W40, c) S036-W80, d) S022-W-4, e) S022-W40, f) S022-W80.

3.5.5 Delay to MRI scan acquisition

A contributing factor to the increased V_d values recorded at successive test infusions was the significant rise in delay time between completing the infusion and acquiring the T1 weighted MRI scan for distribution assessment ($F(2,103)=5.1$, $p=0.001$) (Figure 3-16a). Average delays rose from 43mins (W-4) to 57mins (W40) and finally 60mins (W80) providing longer periods for the concentrated infusate to diffuse into the surrounding tissues, increasing the volume of coverage observed. Delay time alone is however poorly correlated with total volume of tissue covered at both the first ($r=0.3$) and second ($r=0.06$) test infusions suggesting that other factors contribute to the volume of tissue covered.

3.5.6 Position of the catheter and the reflux inhibiting step in the target structure

Previous publications have retrospectively reviewed the position of an implanted, point-source cannula in the primate putamen and assessed the retention of infusate inside the structure (Yin *et al.*, 2011). From this analysis a series of red, blue and green zones were established which provided the best ratio of retention using the specific stepped cannula design under investigation. The regions were also transferred manually onto corresponding human MRI slices create putative target regions for the thalamus and brainstem to demonstrate the translation of the method (Figure 3-29a-b).

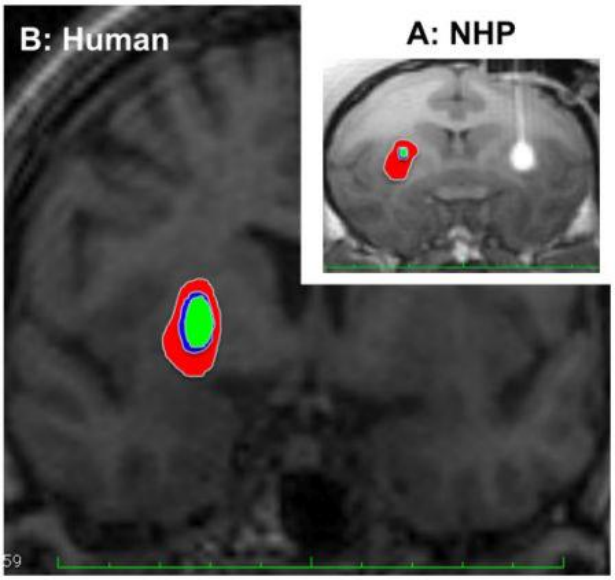

Figure 3-29. Red, Blue, Green targeting Zones for the a) non-human primate (NHP) and b) human Putamen (Yin et al., 2011).

As previously described by Gill et al. 2013, the catheter used within this study was a recessed step catheter, different from the externally stepped cannula described above (Gill *et al.*, 2013). As such, the differing infusion characteristics would negate the application of the previously described surgical planning guide which defines only the optimal cannula tip position. As the RSC is not a point source device but one that uses "controlled reflux*", new knowledge on optimal placement is required.

**controlled reflux will be discussed in greater length in later sections but briefly it describes the expected path of fluid between the catheter tip and the recess, housed in the end of the outermost guide tube. Infusions then develop not as a sphere, from a point, but as a long cylindrical form which is defined by the step region.*

A review of the catheter assembly features and their position within the target structure was performed to identify which were the dominant features responsible for maximising coverage of the putamen (Figure 3-30).

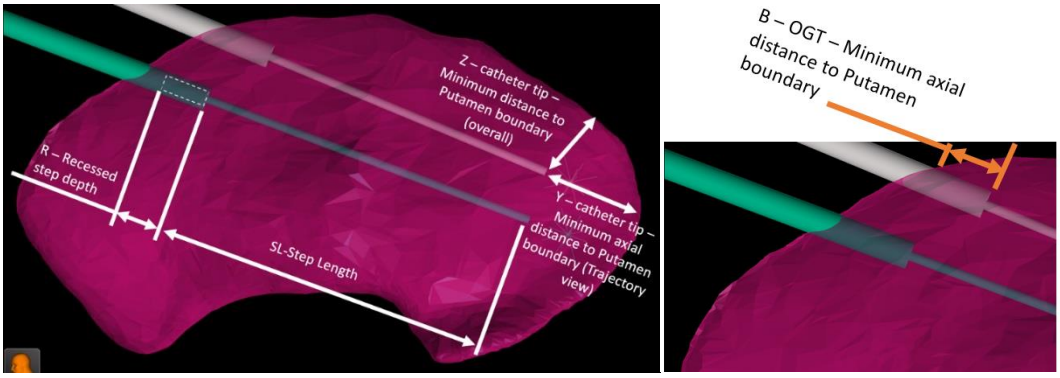

Figure 3-30. Physical placement of catheters inside the putamen.

As the OGT tip houses the reflux inhibition feature of the RSC, locating this as close to the boundary (without overlapping it) could maximise the coverage of the target structure. The percentage of the putamen which was covered did not however significantly correlate with OGT depth into the putamen over the first and second (r=0.01/ p=0.780 & r=0.17/

p=0.465)(Figure 3-20). Weakly positive trendlines indicate that greater coverage might be achieved by placing the OGT tip deeper into structure, but there was too much variance within the data to show this. The ratio of fluid retained inside the putamen was however significantly affected by the position of the OGT at both first and second test infusions (r=0.497/ p<0.005 & r=0.283/ p=0.018). Placing it deeper within the grey matter indicates that less of the infusate is likely lost to reflux back along the catheter track.

Increases in the step length also correlated strongly and significantly (r=0.52/ p<0.005) with coverage of the putamen at the first test infusion. (Figure 3-23a). While remaining a positive correlation over time the significance dropped at the second test infusion (r=0.159/ p=0.188).

Increasing the distance between the catheter tip and the boundary of the structure (up to 3.5 mm) correlated strongly and significantly (r=0.34/ p<0.005 & r=0.43/ p<0.005) with increased putamen coverage (Figure 3-21a, Figure 3-22a).
In the transverse anatomical plane, the putamen can be visualised as an arced grey matter structure akin to a horn or crescent moon (Figure 3-28, pink outline). Catheters entering from the posterior typically skirted the medial aspect of the putamen. With the step region in such close proximity to the boundary of the putamen, reductions in the coverage or retention of fluid would be expected. While rational, the large variation in the coverage and retention values did not support this hypothesis (Figure 3-24), this is likely as result of the balance required in the placement across multiple features of the RSC, not just it's tip. Significant correlations were tabulated (Table 3-2) with representation from all variables reviewed at some point in the study. Generally, placing the catheter tip, OGT tip and step length (between the two tips) further into the structure led to positive increases in putamen coverage or retention of fluid inside the putamen. Distances above 3 mm yielded minimum coverage or retention values of 40 % (Figure 3-20c, Figure 3-21a, Figure 3-22a) at the first test infusion. As retention or coverage were not interchangeable, this 3 mm value is proposed as a guideline which aims to increase the lowest coverage values but requires further validation.
As no single feature was dominant in determining the coverage of the structure, four variables were collated and weighted equally in a final correlation analysis. The four variables were step length: distance of the OGT into the structure; minimum distance of the catheter from the putamen boundary; minimum distance of the catheter to the boundary of the structure (along the step length). The collective, 'mixed variables' were associated with a significant positive correlation (r=0.452/ p<0.005) in the putamen coverage, re-affirming the balance required in maximising several factors when planning the surgical placement of the RSC, unlike the centre of mass approach for point source delivery devices.

It is hypothesised therefore that optimised initial placement of catheter features in line with the mixed variable parameter will provide improved coverage of the putamen in future studies;

- OGT tip should be placed in excess of 3 mm into the putamen boundary
- The tip of the catheter should be placed 3 mm from the distal boundary of the putamen
- The step length should be maximised within the confines of the putamen
- The length of catheter between the catheter and OGT tip should be centralised within the long axis of the putamen

Generally, benefits observed from placement of any feature at the time of implant was not maintained through to the test infusion at 40 weeks and beyond, as can be seen in the drop in significance of the mixed variables positioning plot at the second test infusion (r=0.171/ p=0.158). It is hypothesised that the natural formation of a gliotic sleeve surrounding the device, and the lack of opportunities to modulate the infusion regime to compensate may account for this. Further work is required to characterise and optimise the implant, design and use of the catheter systems for chronic use.

3.5.7 Clinical trial outcome

While beyond the scope of this body of research, it is of note that the empirical evidence arose as the result of a first in man study investigating the repeated, intermittent delivery of GDNF to the putamen in patients suffering with incurable Parkinson's disease (Whone *et al.*, 2019a; Whone *et al.*, 2019b).

The primary objective of the study was to achieve a 20 % improvement in the motor function of the study subjects (as measured using the Unified Parkinson's Disease Measurement Scale (UPDRS)).

While anecdotal evidence of some subjects, televised in a BBC documentary in February 2019, suggests improvements in activities of daily living, including motor function, overall the study failed to meet its primary objective.

Previous failures of this therapy may have led to an overly conservative study design which did not include a dose escalation arm, where increasing amounts of drug is given to evaluate if stronger effects can be seen in higher doses, below that which produce a toxic or negative effect. It is possible that the dose administered here was simply too low to produce the level of improvement across the whole study population which was required.

A follow up study investigating the improvement in the subjects in the extension phase (between 40 and 80 weeks of drug infusions) highlighted that while there was significant overlap in the motor scores of subjects who received drug and those who received placebo, subjects who had a greater than 10-point improvement in their motor scores were limited to those who received the GDNF. This suggests that there may be a subset of patients for who GDNF is more efficacious than others. However, as this part of the study was open label, and all participants would have known they were on drug, a placebo effect cannot be ruled out, as Parkinson's disease patients are known to suffer large placebo effects in clinical trials. This open-label observation may however warrant further investigation and be a critical lifeline for a potentially curative treatment which has had significant hurdles to generate the clinical evidence of its much-publicised potential.

3.6 Conclusions

This *first-in-man,* chronically implanted drug delivery system successfully provided intermittent administration of test article to targeted regions of the brain over an 84-week study period.

Limitations in the study design have been highlighted which offer potential future improvements in clinical study design or optimised patient treatments, such as the standardisation of infusion volume or drug dose based on patient anatomy volume. To assess system performance a consistent analysis time should be targeted, keeping MRI times equal both between test infusions and between patients.

Surgical planning of future implants should seek to optimise the implant location of the catheter features (as shown in Figure 3-31) by positioning the;

- OGT tip should be placed in excess of 3 mm into the putamen boundary
- The tip of the catheter should be placed 3 mm from the distal boundary of the putamen
- The step length should be maximised within the confines of the putamen
- The length of catheter between the catheter and OGT tip should be centralised within the long axis of the putamen

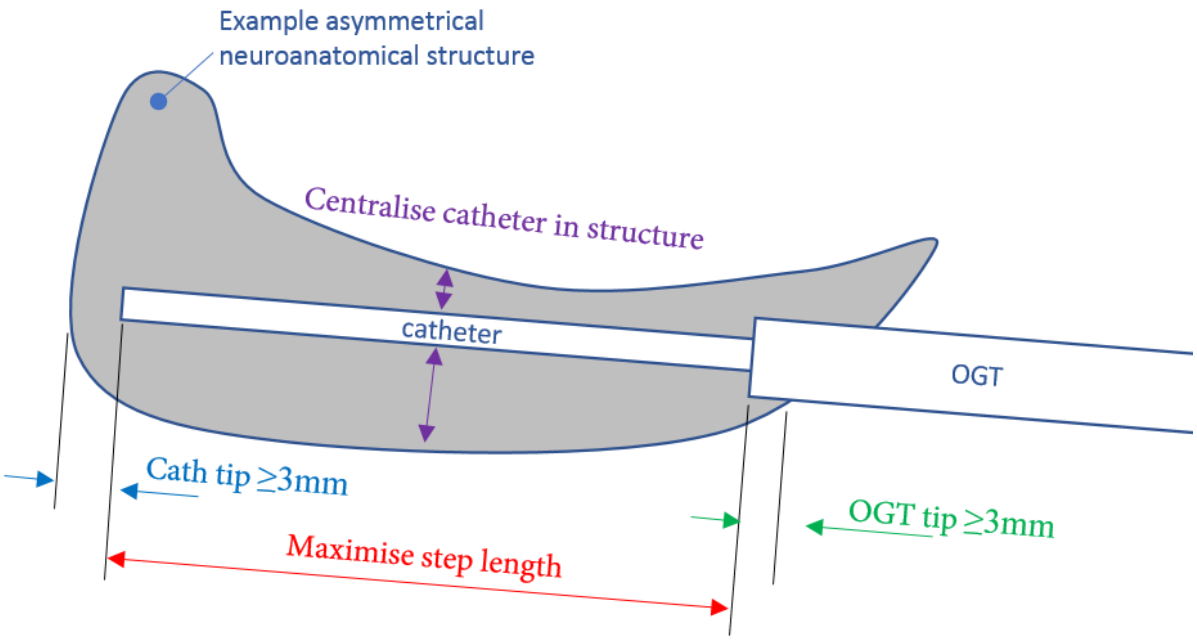

Figure 3-31. Proposed recommendations for RSC feature placement.

This surgical planning strategy represents a short term, best option for maximising coverage of the target anatomy in upcoming clinical trials. It is unlikely to represent a long-term solution for retention of infusates inside the target structure, which appears to be negatively affected by long term implantation, with an increasing proportion of the infusate accumulating outside the target structure in many subjects. It does however represent the best starting point from the available long-term evidence in human subjects who have received intermittent infusions for 80 weeks.

Take home message

Chronic, intermittent delivery to the brain is possible over at least 80weeks.

Variations in distribution patterns occur between patients, and also within the same patient over time but without visible differences on the post implant MRI scans which may provide indications of poorly performing devices.

The surgical planning guidelines for the placement of the RSC offer an initial element for the optimisation of the implanted catheters. Further work is required to fully characterise the catheter performance.

3.7 Future work

Further work is required to characterise the infusion characteristics and limitations of the RSC design in addition to understanding the effects of long term implantation on the permeability of the tissue surrounding the site of infusion.

Recommendations for the position of catheter features in surgical planning should be monitored in future clinical implants to assess the assumptions made in this retrospective review of the first cohort of patients using this paradigm.

4 Evaluation of brain mimic materials for catheter design evaluation

*This chapter contains work published within the poster presentation "**Viscoelastic Vs Agarose hydrogels as brain phantoms for catheter development**"(Lewis, Woolley and Johnson, 2018)*

4.1 Motivation

The recessed step catheter (RSC) used in the clinical study described above was developed with the intention of inhibiting reflux of fluids back along the catheter track. This is achieved through the inclusion of an internal recess between the outer and inner guide tube and the catheter (Gill *et al.*, 2013). The distributions from the catheter were first tested *in vitro* in an agarose gel model before being trialled *in vivo* in the porcine model. The embodiment of the catheter used in these experiments had a step length (see Figure 3-1) between 3-6 mm which was comparable to other devices trialled in CED experiments (Gill *et al.*, 2013).

Within section 3 it was observed that the step lengths used within the clinical trial did not use the catheter with this 3 mm step embodiment, but significantly extended the tip section between 12-34 mm in length to match the form of the subject's putamen. As the step length provided one of the highest correlation coefficients for overall putamen coverage (Figure 3-23a) it is clear that this is a dominant feature of device performance and optimisation.

A detailed evaluation of the catheter performance, varying the step length feature in line with pre-clinical and clinical lengths, is therefore required to characterise and optimise the infusion distributions using the RSC. A suitable *in vitro* model is therefore required which can accommodate the magnitude of clinically translatable step lengths.

4.2 Introduction

Prior to embarking on a large volume of laboratory assessments of the chronically implanted catheter design outlined above, a review of the experimental substrates was conducted.

Agarose gel is a validated mimic for grey matter tissue which has been used to investigate the design of cannula and the distribution of infusions *in vitro* (Chen *et al.*, 2004; Krauze *et al.*, 2005; Gill *et al.*, 2013; Ivanchenko, Sindhwani and Linninger, 2010). Validation was performed by Chen (2004), comparing a 0.6 % gel to porcine brain tissue using three metrics; needle insertion force, line pressure and distribution volume (comparing the infusion of an MRI visible tracer in the gel to a live pig).

Agarose gel, like gelatines are however brittle and prone to fracture during probe or catheter insertion, introducing variables not seen in clinical applications. Some groups have sought to overcome this hurdle by setting the gels around their cannula prior to testing (Lueshen *et al.*, 2017). While this provides concise, spherical infusions, it avoids one of the key characteristics of implantation which is the trauma caused during implantation, which can have significant, detrimental effects on the outcome of infusions (White *et al.*, 2011a).

Alternative phantom materials have been shown to more closely mimic the mechanical characteristics of brain tissue. Composite hydrogels (CH) comprised of a polyvinyl alcohol (PVA) and phytagel (PHY) mix have exhibited similar

viscoelastic properties to porcine brain during needle insertion and compressive testing (Forte *et al.*, 2016; Leibinger *et al.*, 2016). Scanning Electron Microscope (SEM) images of the gels indicate a microporous structure to the gels. These gels may therefore offer improved resistance to cracking during catheter implantation.

Here this viscoelastic gel was evaluated as an alternative to agarose gel for the investigations of infusions using a RSC.

4.3 Materials and methods

4.3.1 Agarose gel manufacture

A container of 0.6 % (by weight) agarose gel was prepared by mixing molecular grade agarose gel powder (Severn Biotech LTD, UK) with concentrated (x5) Tris Borate-ETDA buffer (Severn Biotech, UK) and deionised water. The mixture was heated in a microwave for 5minutes, stirred and then heated further until all powder had fully dissolved. The heated solution was decanted into clear, rectangular glass jar (~500 ml) and allowed to cool naturally to ambient temperature where the gel set.

4.3.2 Composite Hydrogel manufacture

The CH samples were prepared by weighing dry phytagel powder and PVA granules separately. Dry powder/ granules were separately added to deionised water and heated and stirred (using a magnetic stirrer) to 90^{o}C until they had dissolved, and the liquid became clear (Figure 4-1a). This would typically take ~1hr. PHY and PVA solutions were then mixed in a 1:1 ratio and mixed for a further 30minutes (Figure 4-1b). Evaporation was minimised throughout the heating cycle by loosely capping the glass vessels. Weight assessment of the clear solutions confirmed negligible liquid losses, limited to between 3-5 g from the 1700 g of each solution (0.18 %).

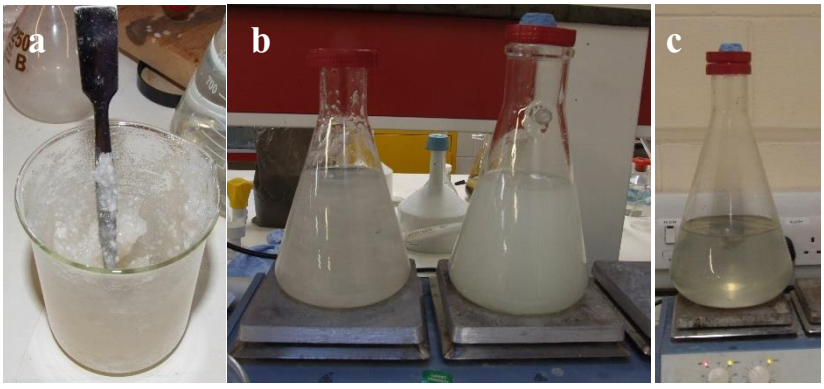

Figure 4-1. Composite hydrogel manufacture a) making a paste with PHY powder and de-ionised water, b) mixing the PHY and PVA solutions on a magnetic hot plate, c) Mixing the combined solutions to make the final CH preparation.

The manufacture of the CH was not straightforward and required some development beyond the basic text provided in journal papers. Phytagel in particular would cluster once added to a large body of water and would not fully dissolve even after several hours of heating and mixing. Creating a paste by adding a small amount of water and manually mashing the phytagel together before transfer to the larger body of water was effective in fully dissolving the PHY within the stated timeframe (Figure 4-1c).

Once mixed, the molten solution was decanted into bespoke, flexible silicone containers (56x56x150 mm) and allowed to cool to ~35-40 ºC. These containers were then loosely covered with cling film and transferred to a domestic freezer (temperature = -25 ºC) where samples were frozen overnight.

Two CH mix ratios were assessed, *5 %PVA/0.59 %PHY* and *6 %PVA/0.85 %PHY,* with a minimum of four samples each.

4.3.3 Indentation testing (structural testing of the samples)

CH samples were removed from the freezer and allowed to thaw for a minimum of 24 hrs at room temperature (four samples per CH variation and four samples of agarose gel). To verify that samples were consistent with previously published data (Forte *et al.*, 2016; Leibinger *et al.*, 2016) an indentation test was performed on all CH samples.

A 6 mm spherical diameter indenter was attached to a load cell (5 N load cell; MultiTest 2.5, Mecmesin LTD, Sussex, UK) and driven in compression at 0.1 mm/s until a nominal contact load was recorded (0.01N). The load and displacement were then zeroed and the spherical indenter was inserted at a fixed rate of 1 mm/s to a maximum depth of 6 mm.

The indenter was then held in place for 500 s to gather load relaxation data.

Agarose gel samples were also assessed but were not subject to release through inspection as no indentation data currently exists to qualify agarose for testing.

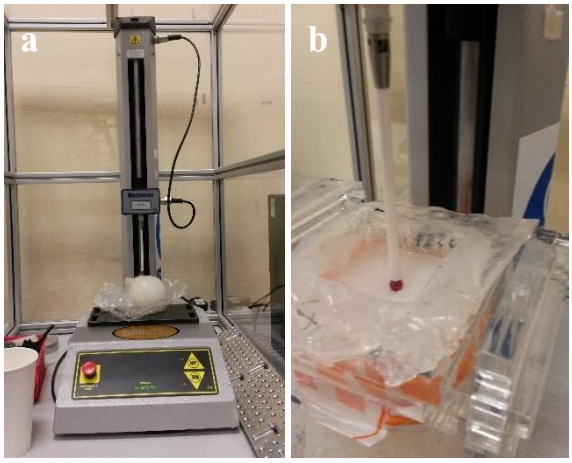

Figure 4-2. Indentation test rig, a) Mecmesin MultiTest 2.5 force test stand, b) indentation test of CH.

4.3.4 Infusion regime and line pressure monitoring

RSC were stereotactically implanted in the sample gels using a dedicated test rig (Figure 4-3).

Trypan blue dye (0.4 %) alone or in combination with a Gadolinium based contrast agent (Prohance™, Bracco) were infused into the gels, ramping to a peak flow rate of 5 µl/min over 40minutes, and delivering a total infusion volume of 400 µl per catheter. Line pressure was recorded for all infusions. Infusions were imaged using a magnetic resonance imaging (MRI) machine (3T MRI, Prisma, Siemens) at the Cardiff University Brain Research Imaging Centre (CUBRIC). A 3D T1-weighted scan sequence was used to image the gel containing the gadolinium infusion (T_R=10 ms, T_E=3.45 ms, Flip angle=10º, slice thickness=1 mm [isometric voxels]).

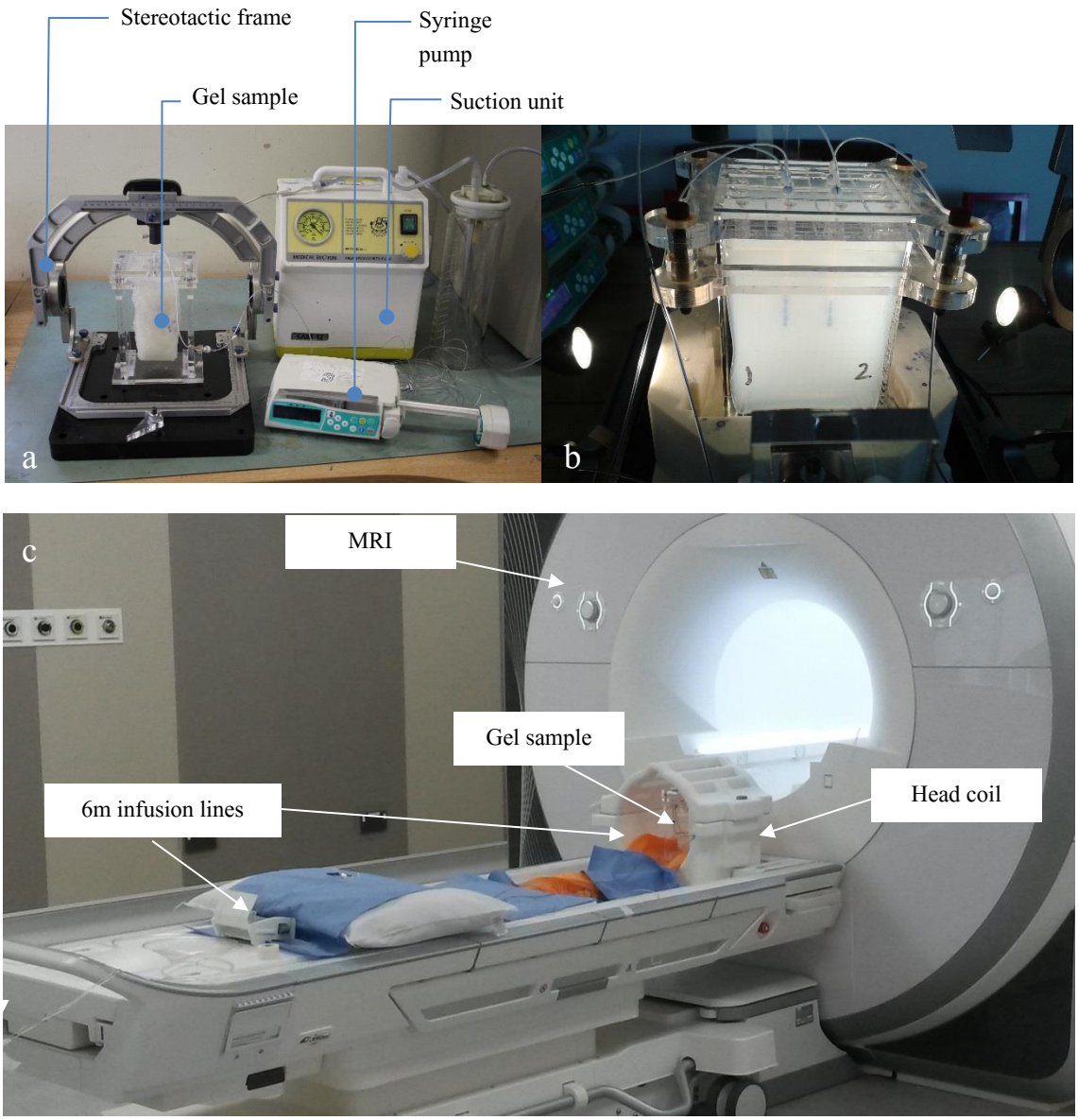

Figure 4-3. Infusion testing, a) Schematic of gel infusion rig, b) agarose pot with acrylic 'skull' housing RSC hubs, c) real time infusion test rig housed in a Magnetic Resonance Imaging (MRI) machine with 6m lines extending to the pumps in the control room.

4.3.5 Infusion morphology assessment

Distributions were visualised in two ways. The MRI scans were reviewed, and the gels were also sliced and photographed (comparison in situ was not possible under ambient lighting as the CH are white and opaque).

4.3.6 High speed image acquisition of implant

Samples of agarose gel were pigmented with 10µm blue polystyrene spheres while molten and cast into clear chamber slides. Microspheres were used to aid visualisation of the strains within the gel during device implantation (e.g. a 0.6 mm diameter tungsten carbide rod, used clinically to create the track for the catheter, was used). High speed acquisition was performed to assess gel compression and obvious signs of tearing as the rod was inserted laterally into the gel at a rate of 1 mm/s to a maximum depth of 5 mm (Figure 4-4 and Figure 4-5).

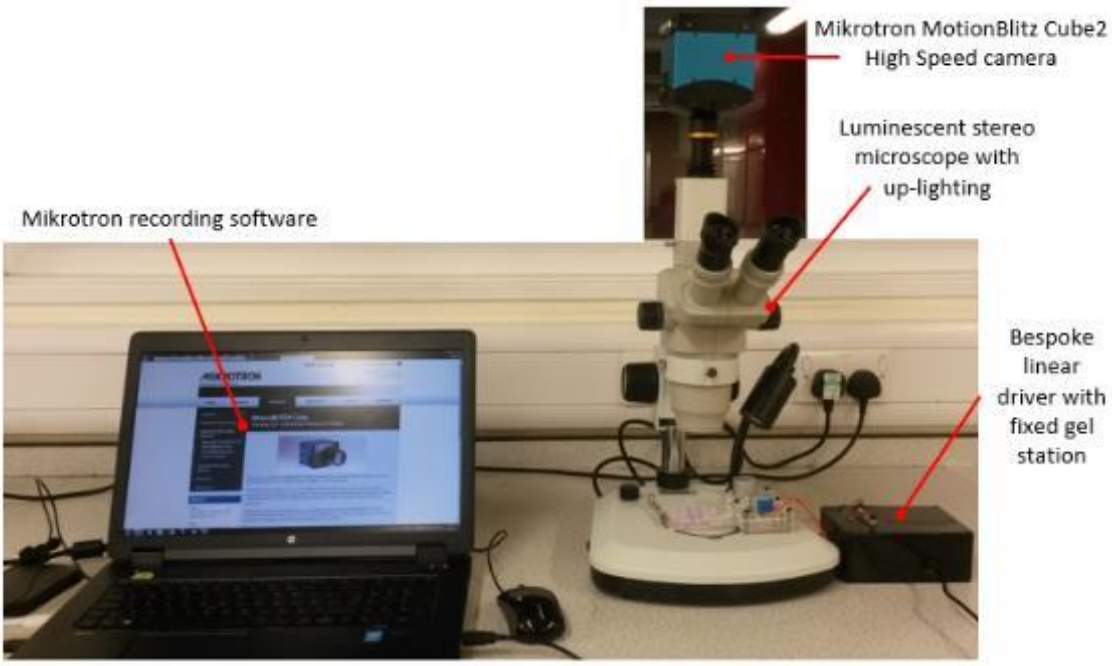

Figure 4-4. High speed image capture test rig.

It was not possible to image CH strains due to the gel's opacity.

Image acquisition was performed using a Mikrotron MotionBlitz Cube2 high speed camera. Chamber slides were visualised beneath a Leica light microscopy stand with back-lighting. Rod insertion and withdrawal were controlled with a bespoke actuator mechanism driven by dual stepper motors and controlled by a programable Arduino microcontroller (Figure 4-5).

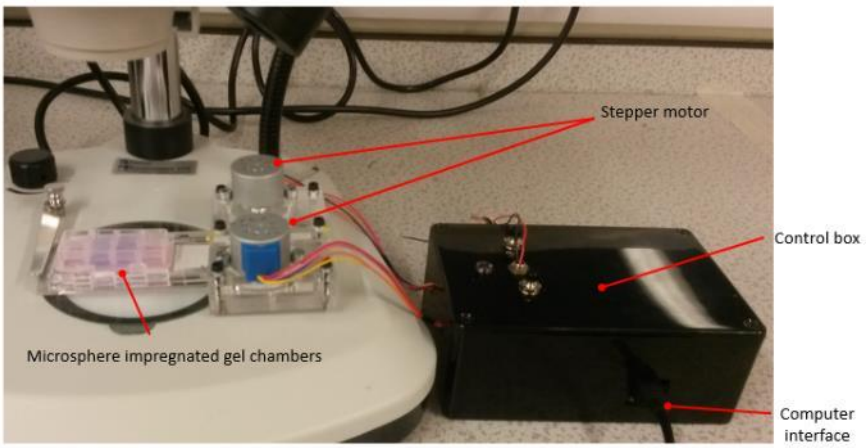

Figure 4-5. Microsphere gel samples positioned beneath the microscope and within the controlled insertion actuator mechanism.

4.4 Results

4.4.1 Indentation testing

Linear rises in force were observed for the two CH mixtures during the indentation test (spherical indenter) with the higher PVA and PHY content having produced a stiffer gel (peak force: 0.68-0.85 N) (Figure 4-6). Both CH mixtures exhibited a viscoelastic relaxation curve profile over the hold period (500 s) (Figure 4-7). Agarose gel however exhibited repeatable,

brittle fracture characteristics. The indenter ruptured the surface routinely around 4 mm insertion depth (peak forces: 0.34-0.50 N). Once the surface was ruptured the residual resultant forces quickly dissipated (Figure 4-7).

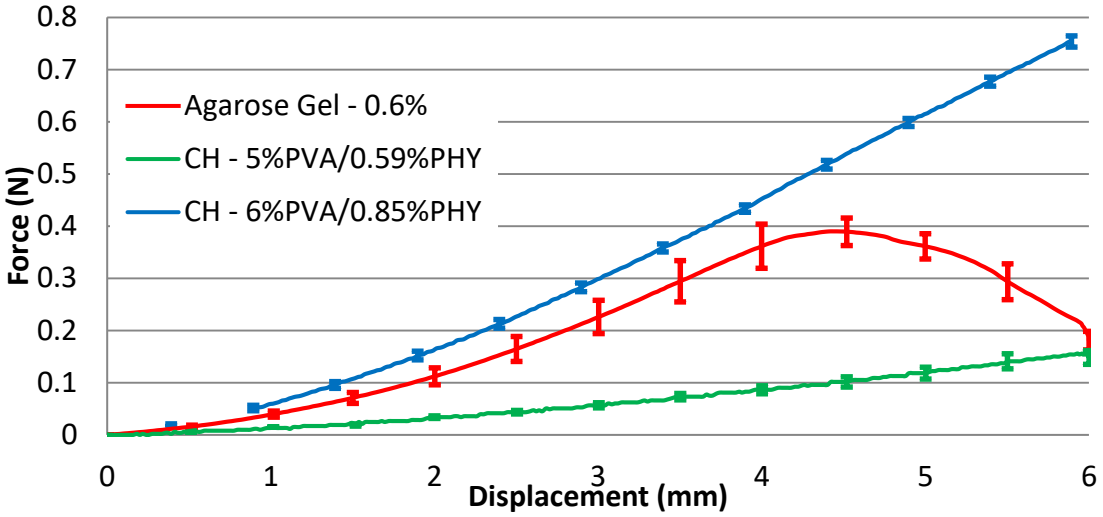

Figure 4-6. Indentation test of agarose and composite hydrogels (SEM range shown, n=4 per material tested).

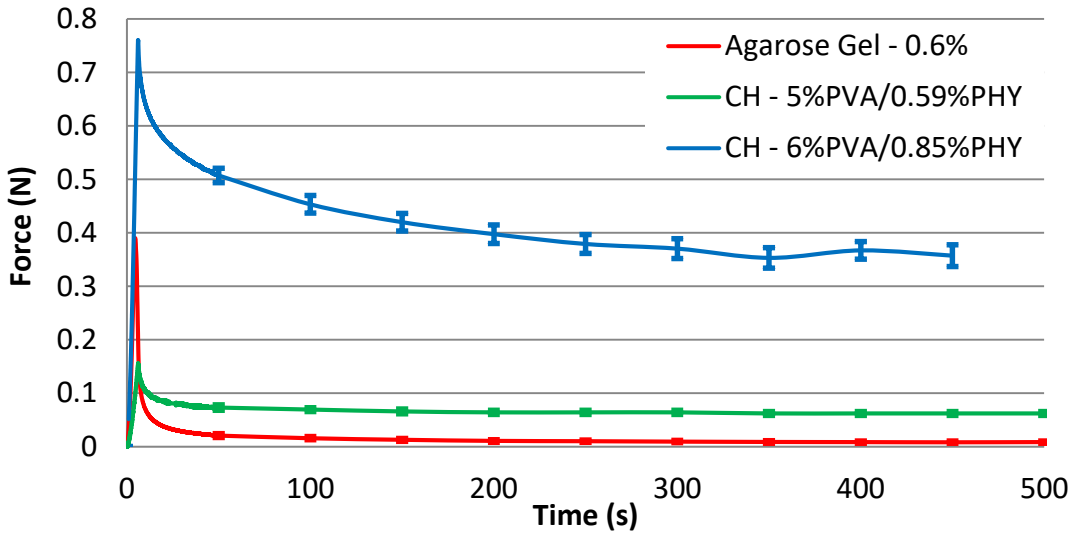

Figure 4-7. Force relaxation curve following indentation of agarose and composite hydrogels (SEM range shown, n=4 per material tested).

4.4.2 In line pressure monitoring

The total infusion time for the 400 µl infusion was ~1hr40mins. Monitoring revealed higher mean line pressure in both sets of CH samples than in the agarose gel (Figure 4-8). Peak line pressure in the agarose would routinely reach a plateau once the peak infusion rate had been reached, but the pressure in CH samples would rise to a peak and then sharply fall over the duration of the experiment.

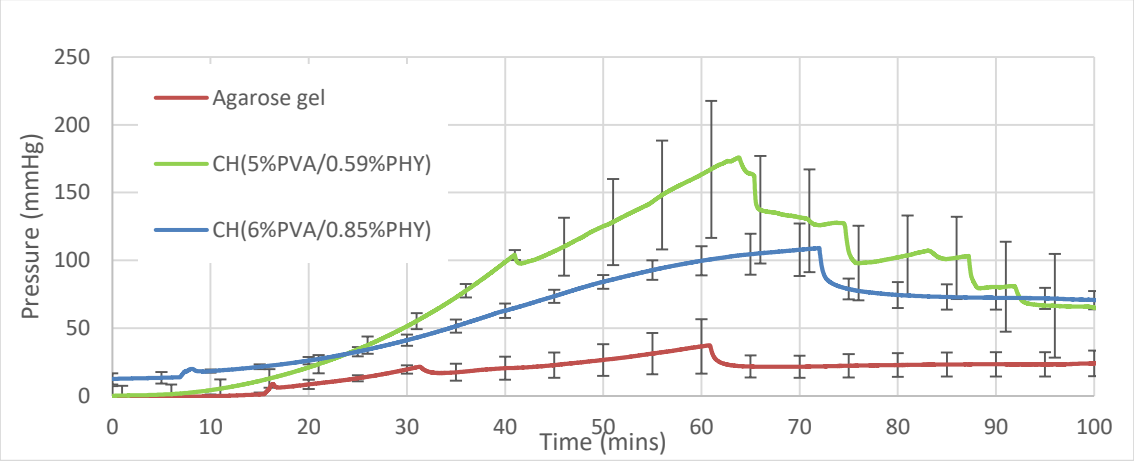

***Figure 4-8. Infusion line pressure* (SEM range, *n=4 per material tested*).**

4.4.3 Infusion morphology

Infusions into the agarose gel (Figure 4-9 a-d) occupied the region defined between the catheter tip and the recess, at the OGT tip, as expected from clinical infusions previously shown (Figure 3-28 a & d). Minor reflux was visible on a single infusion extending to the surface of the gel. Infusion distributions of the GBCA and trypan blue dye into the CHs exhibited highly irregular infusion patterns which were not consistent with either agarose or clinical distribution morphologies.

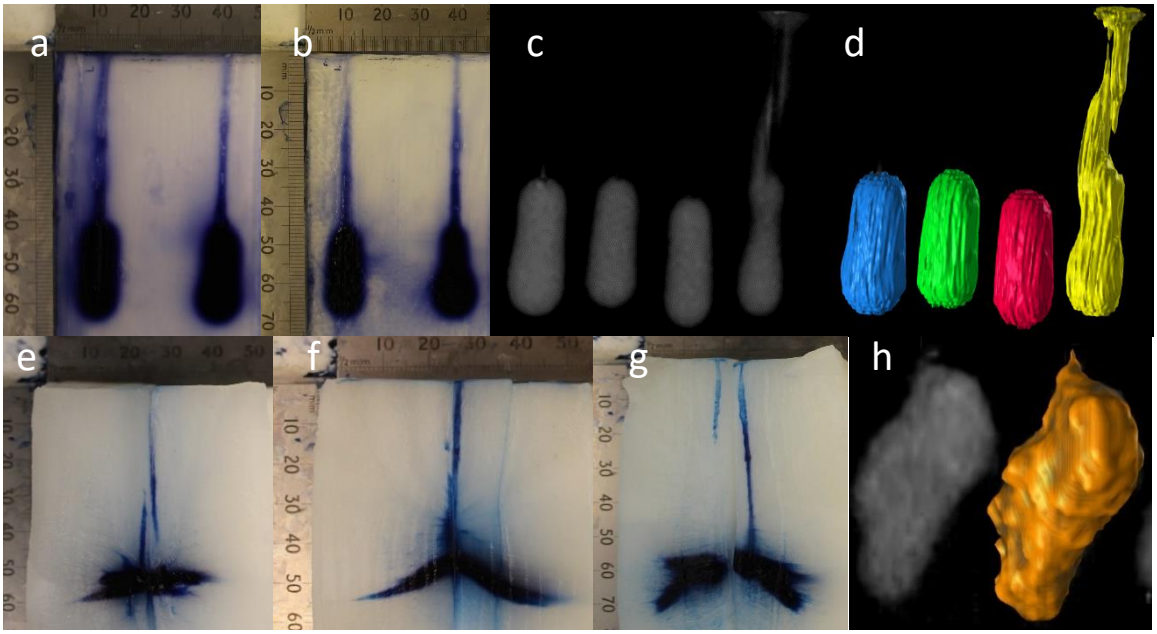

Figure 4-9. a-b) Trypan blue infusions into agarose gel using RSC, c-d) 2 mM gadolinium infusion in agarose gel – MRI image (left) and segmented infusions (right), e-g) Trypan blue infusions into CH using RSC, h) 2 mM gadolinium infusion into CH showing highly irregular morphology.

4.4.4 High speed image acquisition of implant

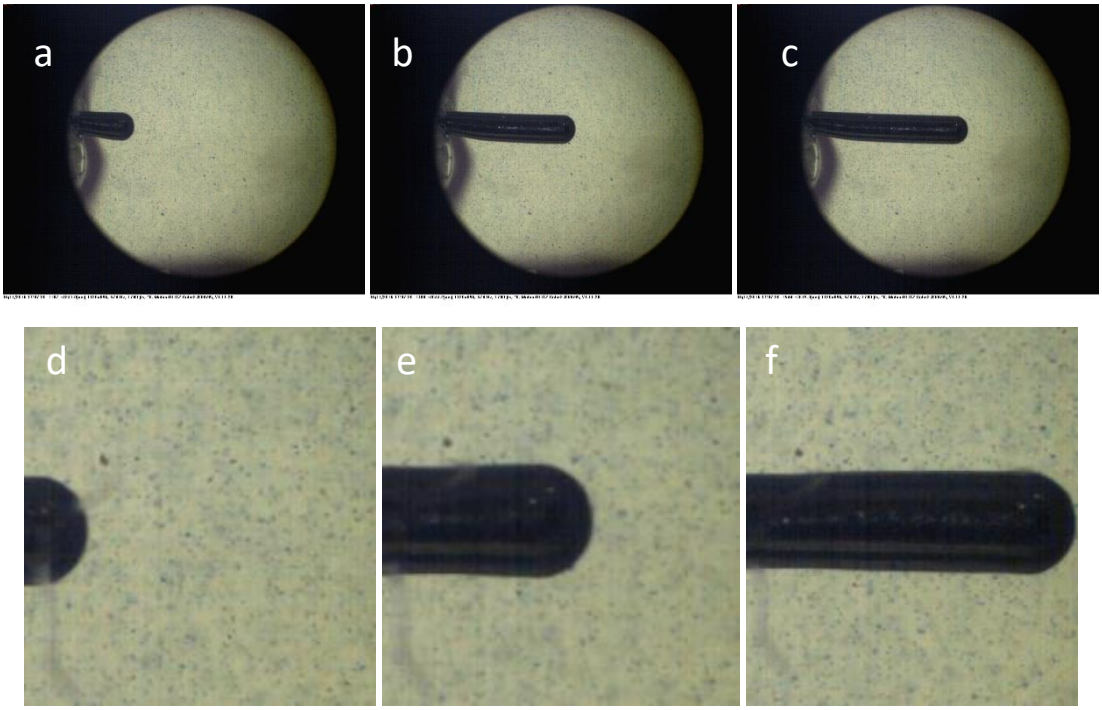

Figure 4-10. Track forming rod insertion into microsphere pigmented gel samples under magnification imaged using high speed camera a-c) sample images of rod insertion, d-f) magnified images of rod travelling through gel showing limited tearing using this rod and insertion speed.

4.5 Discussion

Agarose gel has a number of benefits when considering its use for the investigation of infusion parameters or new catheter designs. It is relatively low cost to purchase the powder (~£400/Kg) and buffer (£5/L) when only 4 g of powder and 75 ml of buffer can yield enough gel to fill a 500 ml glass jar which can comfortably house 4 infusions. The gel is also easy to manufacture in small or large quantities with minimal equipment (measuring and mixing vessels, and a microwave). Agarose is also transparent which enables real time monitoring of the distribution as it propagates through the gel using relatively low-cost equipment such as desk lamps and a digital camera with time lapse capability. Inserting catheters into the gel can yield a high failure rate however, due to the brittle nature of the gel (Dawe and Erickson, 2006), which is not observed in brain tissue (Bienemann *et al.*, 2012; Gill *et al.*, 2013).

Alternative mimics such as the CH (investigated here) could resolve the failure observed through initial implantation through closer adherence to the viscoelastic properties of brain tissue. The CH also has a comparable cost of basic materials (PHY~£180/Kg, PVA~£210/Kg).

Disadvantages of the CH include the extended manufacturing time (agarose: 15-20minutes, CH; 2.0-2.5hrs) for a comparable volume of gel which adds to the overall cost significantly. Costs could be amortised if manufacture were scaled up, but this is unlikely in the context of laboratory settings. The opacity of the CH means that data on the developing distributions is hidden, unless high cost infrastructure such as MRI scanners are available, which in themselves have a high operational cost.

Variations in batches due to measurement error were minimal as large quantities of gel were made each time. 2 L of gel were made by mixing the PVA and PHY solutions in a ratio of 1:1. Laboratory balances with a minimum of 2 decimal places were used to measure the dry weight of PVA and PHY resulting in a measurement error of 5±0.01 %PVA/0.59±0.01 %PHY for the lower concentration CH and 6±0.01 %PVA/ 0.85±0.01 %PHY for the higher concentration. Indentation testing was then performed on samples used within this experiment to confirm that they possessed similar viscoelastic properties to those previously published, with the lower concentration of the CH (5%PVA/0.59% PHY) closely matching the viscoelastic curves published for *ex vivo* pig brain tissue (Figure 4-6, peak force: 0.13-0.20 N, Figure 4-7, asymptotic relaxation curve with load trending towards 0.05 N over 500 s) (Leibinger *et al.*, 2016). Minor adjustment to the CH recipe yielded a five-fold increase in the stiffness of the CH (6 %PVA/0.85 % PHY).

Unexpectedly, while the agarose withstood around 4 mm of indentation, providing resultant forces similar in magnitude to gelatine, evaluated alongside the CH in previously published work, further indentation resulted in complete rupture of the agarose surface. Once the indenter had broken the surface the residual resultant forces quickly dropped close to zero, where gelatine had previously maintained a higher overall residual load throughout the relaxation assessment over 500s (0.10-0.13N at 500s). The agarose gel exhibited brittle surface fracture under spherical indenter loading which is dissimilar to brain tissue or the CH (5 %PVA/0.59 % PHY) previously published (Leibinger *et al.*, 2016).

Under high magnification and at high image acquisition speeds (50Hz) the gel did not exhibit obvious signs of tearing when stabbed with a 0.6 mm diameter tungsten carbide rod (Figure 4-10). Impregnated spheres are pushed ahead and radially away from the track forming tool, providing a degree of resultant compressive force which would aid sealing and minimise reflux during infusions. Viewed at much slower speeds, the insertion of the rod is met with a compression then a slip action along the contact interface. While this test did not produce large amounts of visible tearing, higher insertion speeds and larger dissection rods may result in increased trauma. This deformation appears to be strain dependant with larger strains induced through surface indentation resulting in gel rupture. Such rupture would result in catastrophic failure and cause infusate reflux, however slow implantation speeds to minimise strains and tearing may result in improved outcomes.

Both CH mixtures were more elastic to the touch than agarose (as might be expected from the indentation testing), rebounding to the insertion of implantation rods for the guide tubes and catheter.

Line pressure alone has been shown to be a poor indicator of distribution performance or a hallmark of refluxing infusions but was shown to highlight occluded channels effectively (Lam *et al.*, 2014).

Infusions into the agarose gels were uneventful producing the expected elongate distributions observed in the clinical trial (Figure 3-28a & d). Some minor reflux was observed on a single infusion (Figure 4-9c & d) which reached the surface of the gel and appeared to decompress the infusion slightly, limiting the fullness of the distribution seen in the other 3 infusions. Infusions into both CHs routinely yielded high line pressures (Figure 4-8), sometimes reaching occlusion alarm limits of the B|Braun syringe pumps. This line pressure which rose and subsided at random, appeared to be caused by the inability

of the infusate to travel through the CH substrate. Anisotropic distributions were both irregular in shape, making volumetric analysis difficult, and unpredictable in the amount of line pressure that would be required to force the fluid into the gel. A second batch of CH gels were made at a different time point to evaluate whether the limited dispersal of fluids was batch specific, but the outcomes were the same.

While mechanically similar to the viscoelastic properties of brain tissue, the CH mixtures are not suited to infusion studies. Further development would be required to balance the need for mechanical alignment with brain tissue and the need to also achieve comparable and homogenous permeability to grey matter and/ or agarose if it is to replace it as a preferred mimic material.

4.6 Conclusions

Despite exhibiting comparable mechanical properties of CH previously published and validated against *ex vivo* porcine brain, two separate recipes of CH failed to effectively distribute infusions consistently, or in a comparable manner to those observed in clinical studies.

Conversely, infusions into the agarose produced consistent distribution shapes which were similar to clinically observed infusions into the human putamen. Despite a consistent technique used to implant the catheters in the gel, one of the four tested displayed some uncontrolled reflux which extended beyond the step (inhibition) feature, which further confirms the challenge of utilising the agarose gel for catheter development. While agarose gel is an imperfect brain mimic which is prone to brittle fracture (under indentation loading with a spherical indenter), it does poses similar permeability to brain tissue (grey matter). In addition, its relatively low cost and ease of manufacture continue to make it the most appropriate surrogate for brain tissue in the early phases of development and laboratory-based investigations.

Take home message

Brain mimic materials are a compromise in place of using the real thing.

Agarose gels are brittle (under spherical indentation compressive loading) and mechanically fail in a way unlike brain tissue but do offer a low cost, optical substrate with a similar pore fraction to brain tissue (validation against infusions in porcine brain previously published), for viewing infusions as they distribute.

The composite hydrogels investigated here are currently unsuitable for investigating catheter performance due to their dissimilar permeability characteristics to brain tissue.

5 *In vitro* and *in vivo* characterisation of the recessed step catheter distributions

*This chapter contains work previously published within the Journal of Neuroscience Methods article "**Maximising coverage of brain structures using controlled reflux convection-enhanced delivery and the recessed step catheter**" (Lewis et al., 2018)*

5.1 Motivation

As has previously been highlighted, systemic routes of administration which aim to deliver therapies to the brain are highly inefficient at transporting drugs to brain parenchymal tissues. Firstly because of the non-target specific nature of systemic delivery, but more importantly the filtration provided by the blood brain barrier.

A range of cannula designs for acutely delivering infusates directly to the brain were reviewed (section 2.1) alongside the fully implantable recessed step catheter (RSC), designed in Bristol University, UK (Gill *et al.*, 2013). The RSC is capable of acute infusions but uniquely able to provide long term intermittent access to the brain when coupled with a percutaneous access port.

The evidence for the RSC, published ahead of the *first-in-man* study (Gill *et al.*, 2013), compared its infusion and distribution performance to a comparator design, an externally stepped cannula, both single and double steps. The step length of the RSC (defined by the distance between the catheter tip and the outer guide tube tip), was restricted to 3 mm in the agarose gel tests, and 3-6 mm in the *in vivo* porcine study, where fluid appeared to flow readily between the catheter tip and the recess within the outer guide tube. This step length effectively defining the initial infusion region. Once transferred to clinic however the step length then dramatically increased, ranging from 12.3-34.2 mm, average 23.7 mm (Section 3.4.2). A reassessment of the RSC's performance characteristics with respect to the distributions which can be obtained is therefore warranted to aid in the understanding of what should be expected *in vivo* both pre-clinically and clinically.

5.2 Introduction

The aim of this chapter is to investigate the effects of a limited number of variables upon the distribution morphology obtained in a grey matter brain mimic (agarose gel) selected in the previous section.

As an initial evaluation of step lengths, a range between 3-18 mm will be investigated, covering grey matter target lengths in pre-clinical and clinical cases. Peak infusion flow rates ranging from 0.1-0.6 ml/hr (1.3-10 µl/min) will also be evaluated which have been used in both pre-clinical and clinical cases (Barua *et al.*, 2013a; Bankiewicz *et al.*, 2016; Gill *et al.*, 2013).

5.3 Materials and methods

5.3.1 *In vitro* evaluation

5.3.1.1 Agarose gel and infusate preparation

Agarose gel is a validated mimic for grey matter tissue used to investigate the distribution of infusions *in vitro* (Chen *et al.*, 2004; Krauze *et al.*, 2005; Gill *et al.*, 2013; Ivanchenko, Sindhwani and Linninger, 2010), and as we showed in the previous chapter, represents on balance, the best substrate currently available for the investigation of infusions from catheter devices.

Agarose gel (0.6 %) was prepared by mixing molecular grade agarose gel (Severn Biotech LTD, UK) with concentrated Tris Borate-ETDA buffer (Severn Biotech, UK) and deionised water. The mixture was heated in a microwave for 5 minutes, stirred and then heated further until all powder had fully dissolved. The heated solution was decanted into 50x50x150 mm clear, rectangular acrylic containers which represented a large volume of homogenous brain tissue (375 ml). Gels set as they were cooled naturally to ambient temperature.

A 3 mm acrylic lid was secured to the pot and used to simulate the skull. The RSC hub was anchored within the acrylic lid, mimicking the implantation procedure.

Trypan Blue powder (Sigma Aldrich) has previously been used as a high visual contrast in gel infusion tests (Gill *et al.*, 2013; Krauze *et al.*, 2005). Powder was weighed and dissolved in deionised water to a concentration of 0.4 %.

5.3.1.2 Catheter

As previously described, the RSC is formed by the assembly of three components; an Outer Guide Tube (OGT), Inner Guide Tube (IGT) and catheter (Figure 3-9). To evaluate the step length and its effect on infusion morphology, the OGT and IGT were cut to a fixed length for all tests, 60 mm and 58.5 mm, respectively, forming a 1.5 mm gel plug within the recess. Catheters were cut to 63, 66, 72, 78 mm, creating step lengths of 3, 6, 12 and 18 mm beyond the distal tip of the OGT.

5.3.1.3 Test set up

Test samples were rigidly fixed within an infusion 'station'. An acrylic baseplate was used to mount the gel pot, the delivery frame and digital camera for sequential, time lapse images of the developing distributions (Figure 5-1). Rigid delivery rods and identical tools were used to implant the plastic tubes into the gel using a human stereotactic frame (Radionics® CRW™, Integra Lifesciences Corp.), mimicking the insertion technique used within the human cases.

A digital camera (Model 1200D, Canon Inc) was used to acquire time lapse images throughout the infusions with standard desktop lamps used to add light through the pots of gel. B|Braun™ Perfusor Space syringe pumps were used to run *ramp and taper* infusion regimes (Figure 5-2).

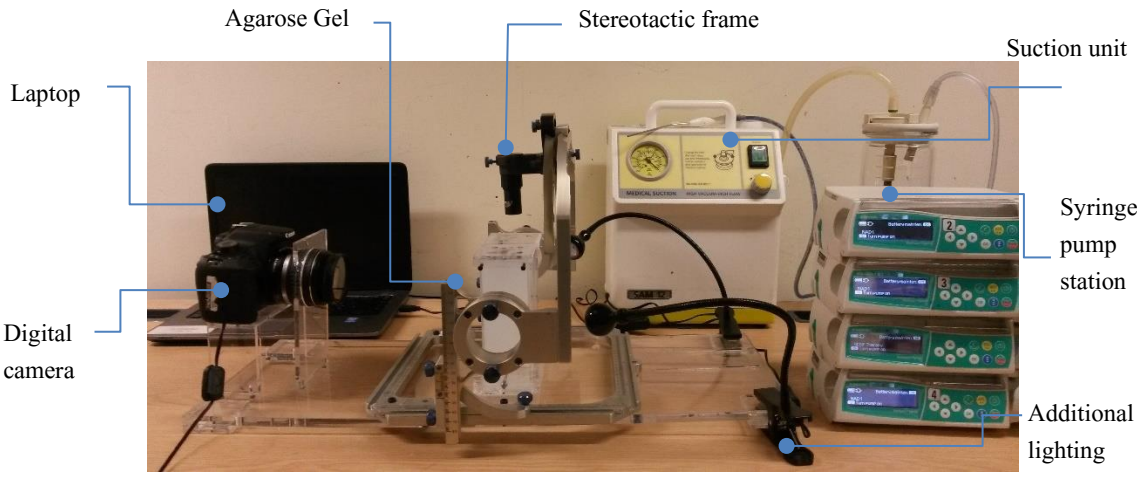

Figure 5-1. Schematic of gel infusion test set up.

5.3.1.4 Infusion volume

To assess a representative infusion volume, a retrospective review of Deep Brain Stimulation (DBS) surgical plans were anonymised and reviewed (outside the remit of this thesis) which were provided by Prof Steve Gill. This supportive evidence however identified that the volume of two likely targets for delivery of a therapeutic the putamen and the caudate nucleus had average volumes of 4.30±0.03 ml (range: 2.89-5.94 ml) and 2.90±0.03 ml (range 2.03-4.64 ml), respectively. The volume of the putamen compares favourably to a smaller sample (n=11) previously published, 4.02+/-0.23 ml (range: 3.01-5.29 ml) (Yin *et al.*, 2009). Average caudate nucleus volumes were similar to previously published data (3.5±0.26 ml) from the same source.

Within the short time of an infusion, it will be assumed that the space occupied by infused fluid will occupy only the interstitial space between cells as these have a finite volume themselves. The available space in this sponge like framework, the interstitial (or extracellular space) is ~20 % of the volume fraction (Roitbak and Sykova, 1999), therefore the other ~80 % is occupied by cells. The ratio of coverage for a unit infused (V_d/V_i) is therefore 5:1, and has previously been reported as such, 5±0.2 (mean ± standard deviation)(Chen *et al.*, 1999).

Total coverage of the putamen would require an infusion volume of at least 0.8 ml (800 µl), or 0.4 ml (400 µl) split over 2 catheters (which was the arrangement used in the first-in-man study).

5.3.1.5 Infusion regime

A gradual rise in the flow rate is widely used in CED studies (Bankiewicz *et al.*, 2000; Bienemann *et al.*, 2012; Gill *et al.*, 2013; Barua *et al.*, 2013b) to minimise the risk and incidence of reflux. A stepped ramped regime can be used.

Three linear ramp and taper profiles, each delivering 400 µl were defined and installed onboard a bank of four syringe pumps (Perfusor® Space, B|Braun). Infusions were accelerated to the peak flow rate (Q) over 40mins (Figure 5-2) and held there until the infusion was complete (which included a standard, decreasing linear taper to shut off of 1min, which was a default requirement of all pump regimes). Total infusion times were 1hr (Q_{10}=0.6 ml/hr[10 µl/min]), 1hr40mins (Q_5=0.3 ml/hr[5 µl/min]) and 4hrs21mins (Q_1=0.1 ml/hr[1.3 µl/min]) which were all considered clinically translatable as a patient

could be seen, infused and observed within a single working day. A minimum of 9 repeats for each step length at each flow rate were performed (n=108).

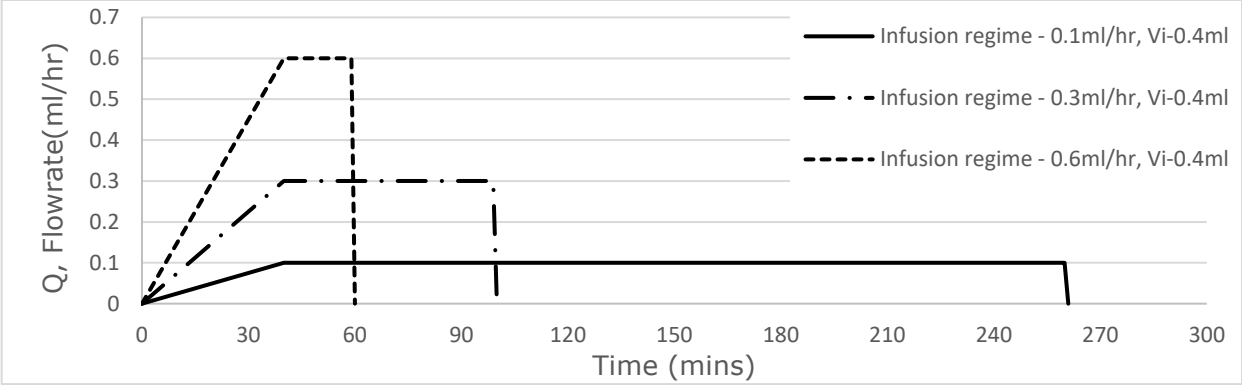

Figure 5-2. Investigational, clinically translatable infusion regimes for intermittent delivery.

5.3.1.6 Infusion image acquisition rig

Gel pots typically contained two separate, non-contacting infusions to maximise the use of each gel. Once infusions were complete, the gel was sliced within 10minutes, into 3 mm sections along the long axis of the pot, providing 50x150x3 mm slices of gel.

The central section contained the infusion at its widest point. This section was laid flat onto a scaled bed and photographed beneath a diffusion light box (Figure 5-3).

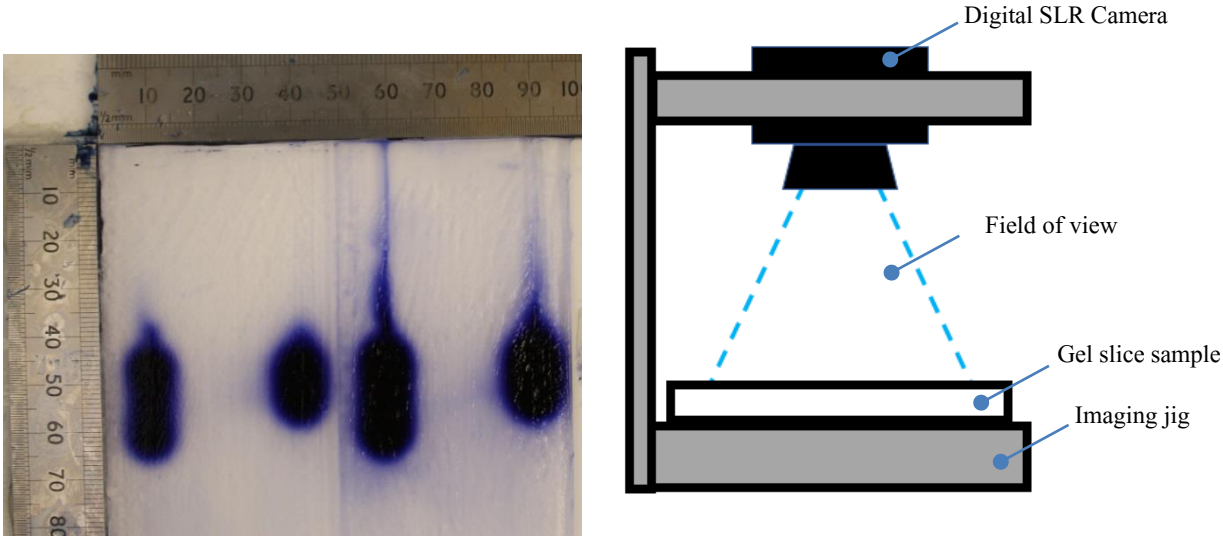

Figure 5-3. Infusion imaging rig: left) showing well demarcated infusion clouds within 3 mm thick slices of agarose gel against a graduated border; right) side profile schematic of the gel slice imaging jig.

5.3.1.7 Image analysis

Images of the gel slices acquired using the scaled imaging jig (Figure 5-3). Briefly, 3 mm thick slices of gel were laid flat onto the white acrylic base of the imaging jig. This jig had two embedded rules with 0.5-1.0 mm scale increments. The images were acquired manually using a digital SLR camera with remote shooting capability. Live view images were observed from within the lightbox before pictures were collected. These image files were then manually imported into

Matlab for further processing (Matlab 9.2, The Mathworks, Inc., Natick, Massachusetts, United States). Infusion areas were magnified within the image segmentation toolbox (Image processing toolbox 10.0) and the manual plotter was used to place a polygon around the boundary of the infusion. This 2D profile was used to create a segmented binary image with the same dimensions as the base image and was exported to the workspace. The image then only contained pixels with values of zero or 1 (outside and inside the infusion distribution, respectively). Pixel width was calibrated for each image using the scaled rules on the imaging rig (Figure 5-3). A script was used to calculate the distribution volume (V_d) of the dye by counting the width of every vertical row of white pixels in the segmented image. The length of each row was divided in two to define the radius of the distribution at that height. This was squared and multiped by Pi to get the cross-sectional area at that height. Each sequential area was multiplied by the pixel height to create a disc volume at every level of the infusion. The sum of the discs from each row provided the total distribution volume, V_d. Maximum distribution length and width were also recorded.

Sectioned gel slices displayed a clear profile boundary for the distributions as a dark, saturated core with a weaker, diffuse boundary. The band of diffuse infusate was routinely 1-2 mm in width and inherently variable. To minimise subjectivity, manual profiles were created for each infusion at the border of the highly saturated core region, with all assessments performed by a single person. Analysed volumes are therefore likely to underestimate total coverage, no information on concentration gradients within the overall coverage, but would provide a more direct comparison between tests.

5.3.2 *In vivo* evaluation

5.3.2.1 Study licences and ethical oversight

Surgical procedures were performed in accordance with the Animals (Scientific Procedures) Act (1986) under specific UK Home Office project and personal licences (project licence number 30/2909) at a licensed establishment. Study protocols were pre-approved by the University of Bristol Ethical Review board.

5.3.2.2 Surgical procedure

The author did not perform the surgical procedures but devised and assisted in the conduct of the study in a theatre support, planning and operational role. *In vivo* proof of principle of the catheter infusion characteristics was investigated through the implantation of RSC into deep grey matter structures (putamen and thalamus) in 5 large white Landrace pigs. A combination of twelve catheters in all were implanted.

OGT tips were placed inside each structure and the catheter length was adjusted to provide a range of step lengths to a maximum of 12 mm (longer step lengths were not possible in grey matter targets due to the size and shape of the porcine brain).

Anaesthesia, head fixation, MRI scanning and stereotactic procedures were performed as previously described (White *et al.*, 2011b; Barua *et al.*, 2013c).

5.3.2.3 Test infusions

Magnevist is a gadolinium-based contrast agent (GBCA) widely used in CED research (Lonser *et al.*, 2002; Lonser *et al.*, 2007b; Bankiewicz *et al.*, 2016). An MRI visible solution was prepared by diluting Magnevist® (Bayer) down to a 2 mM concentration in artificial cerebrospinal fluid (aCSF). Infusion volumes were lowered to 120-200 µl, with smaller infusion volumes used in the putamen due to its smaller size.

Sequential T1 weighted MRI scans were acquired throughout the infusions. Ramped infusion regimes were used as described above with flow rates peaking at 0.18-0.3 ml/hr.

5.3.3 Statistical analysis

The statistical difference between the mean of sample populations was assessed by Student's t-test or a one-way ANOVA where more than two groups were compared.

A significance level of 5 % was used to compare V_d, distribution width and length between flow rates and between step lengths.

Pearson correlation coefficients were calculated for the distribution volume, width and length at each infusion flow rate over the step length groups.

5.4 Results

5.4.1 *In vitro* infusion morphology: Distribution length and width

In the agarose gel a strong correlation between increased step length (SL) and increased length of the distribution was observed (Figure 5-4a: Q1[r=0.95, p<0.001], Q5[r= 0.98, p<0.001], Q10[r=0.98, p<0.001]). Infused fluid refluxed back to the recess as expected across all step lengths assessed, with greater amounts of reflux beyond the step occurring in shorter steps and at higher flow rates. As the distribution lengthened, as would be expected, the width reduced as the infusion volume was fixed for all tests. The width linearly dropped a small but significant amount at each step length (Figure 5-4b: Q1[r=-0.89, p<0.001], Q5[r=-0.83, p<0.001], Q10[r=-0.60, p<0.001]).

When reviewing the effect of flow rate on the morphology, the length of the infusion clouds decreased as the volumetric flow rate (Q) increased. This affect was consistently observed across all step length groups (SL(3 mm); $F(2,27)=31.6$, $p<0.001$, SL(6 mm); $F(2,29)=25.3$, $p<0.001$, SL(12 mm); $F(2,30)=19.7$, $p<0.001$, SL(18 mm); $F(2,29)=9.5$, $p<0.001$). The average distribution width was also significantly reduced as the volumetric flow rate (Q) was increased. Again, this was observed at each of the step lengths investigated (SL(3 mm); $F(2,27)=116.0$, $p<0.001$, SL(6 mm); $F(2,29)=49.9$, $p<0.001$, SL(12 mm); $F(2,30)=75.2$, $p<0.001$, SL(18 mm); $F(2,29)=46.8$, $p<0.001$).

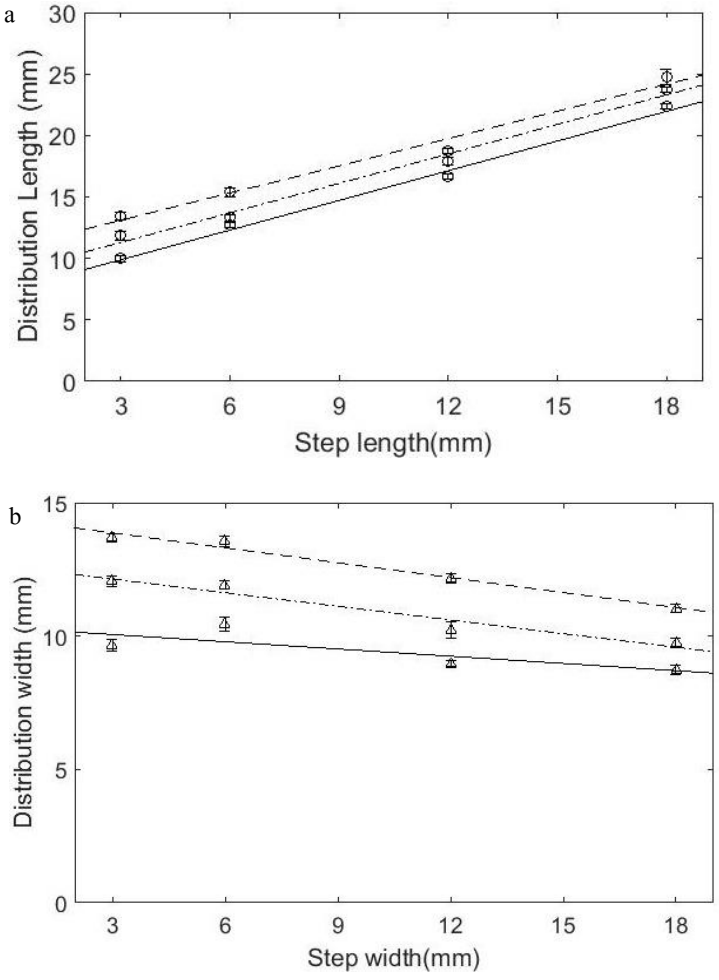

Figure 5-4. a) Q1 (top), Q5 (middle) and Q10 (bottom) trendlines for distribution length versus step length, b) Q1 (top), Q5 (middle) and Q10 (bottom) trendlines for distribution width versus step length. Error bars denote SEM.

5.4.2 *In vitro* infusion morphology: Distribution volume

Both flow rate and step length affected the overall volume of gel coverage within this experiment. At each fixed step length, increasing the flow rate resulted in a significant decrease in the distribution volume (SL(3 mm); $F(2,27)= 71.3$, $p<0.001$, SL(6 mm); $F(2,29)= 65.4$, $p<0.001$, SL(12 mm); $F(2,30)= 103.6$, $p<0.001$, SL(18 mm); $F(2,29)= 69.4$, $p<0.001$) (Figure 5-5).

Increasing the step length provided a positive correlation with increases in the distribution volume within each of the flow rate groups assessed (Q1[r=0.66, p<0.001], Q5[r=0.74, p<0.001], Q10[r=0.78, p<0.001]).

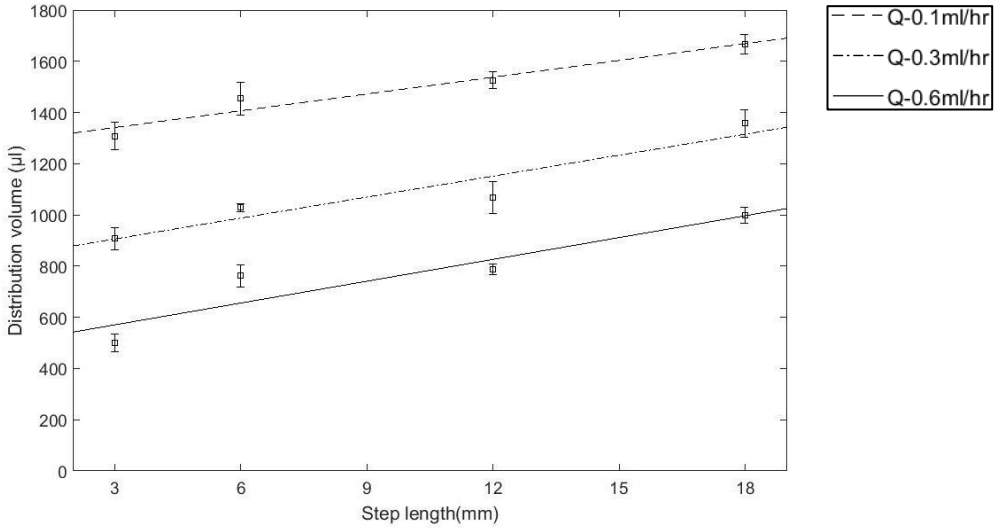

Figure 5-5. Q1 (top), Q5 (middle) and Q10 (bottom) trendlines for distribution volumes versus step length. Error bars denote SEM.

5.4.3 *In vivo* infusion morphology: Length and width

Due to the relative size difference in the anatomical targets used in the porcine putamen, two infusion volumes were used within the *in vivo* study arm; putamen-120 µl, thalamus-200 µl.

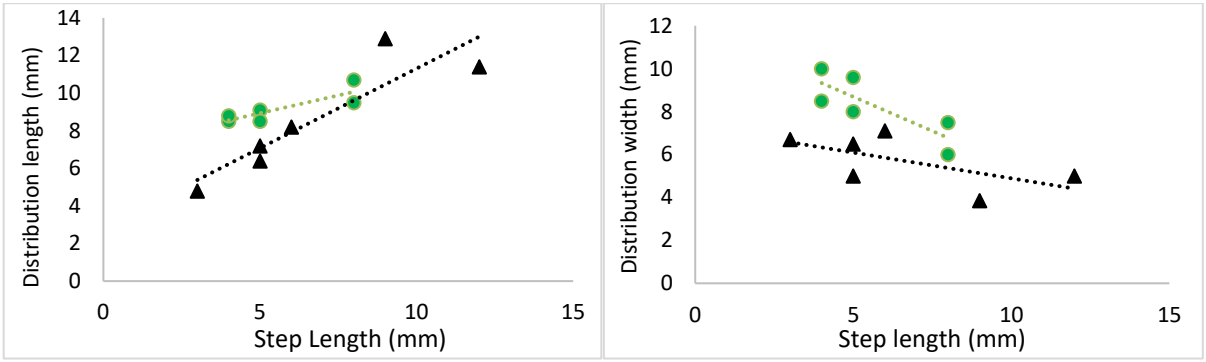

a) b)

Figure 5-6. a) Length of infusions achieved in the porcine grey matter; triangles=120 µl (at 5 µl/min), circles = 200 µl (at 3 µl/min); b) width of distributions achieved in the porcine white matter; triangles=120 µl (at 5 µl/min), circles = 200 µl (at 3 µl/min).

As demonstrated in the gel model, increases in the step length were strongly correlated with an increase in the distribution length despite there being fewer data points available within this proof of principle part of the study (Vi(120 µl): R=0.90, p=0.006, Vi(200 µl): R=0.84, p=0.03) (Figure 5-6a). While there is a negative linear trend in the distribution width, consistent with gel studies, the variability is too great which prevents the establishment of significance in this instance (Vi(120 µl): R=-0.62, p=0.13, Vi(200 µl):R=-0.82, p=0.05)(Figure 5-6b). All infusions flowed between the catheter tip and the recess as seen in the gel study for all lengths tested (3-12 mm) (Figure 5-7a-d).

5.4.4 *In vivo* infusion morphology: distribution volume

Non-significant, and numerically small increases were observed in the distribution volume as the step length was increased (Vi(120 µl):R=0.77, p=0.27, Vi(200 µl):R=0.77, p=0.07) (Figure 5-7e).

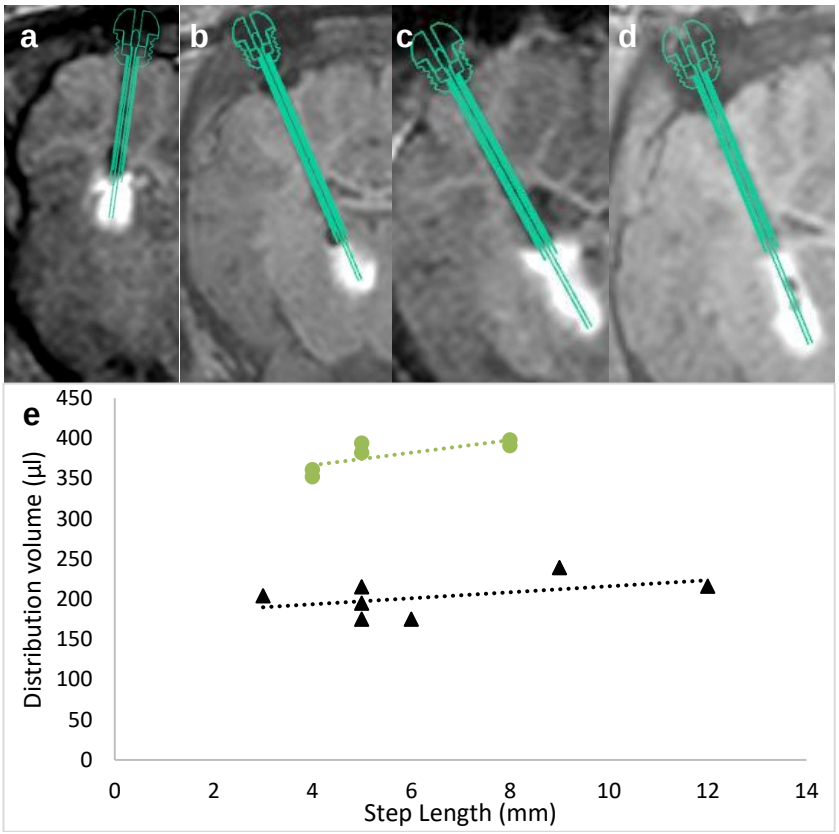

Figure 5-7. In vivo MRI scans of infusions using the recessed step catheter in the porcine model - a) 5 mm step in putamen, b) 6 mm step in thalamus, c) 8 mm step in thalamus, d) 12 mm step in thalamus, e) distribution volume achieved from infusions into the porcine grey matter; triangles=120 µl (at 0.3 ml/hr) circles = 200 µl (at 0.18 ml/hr).

5.5 Discussion

5.5.1 Controlled reflux

Studies of CED devices typically advocate a point source from which to deliver spherical infusions of therapies (Ivanchenko, Sindhwani and Linninger, 2010), however this method is sub-optimal for the coverage of neuroanatomical structures which are themselves not spherical. By modifying the desirable distribution morphology to more closely match these target structures, improvements in coverage could be achieved.

While the delivery of fluid to a variable region could be achieved in a variety of ways (e.g. variable porous/ multiport catheter sections), the RSC uses the inherent reflux observed in CED applications to cover the region defined by the extension of the catheter beyond the guide tubes, the step length (SL - Figure 5-8a).

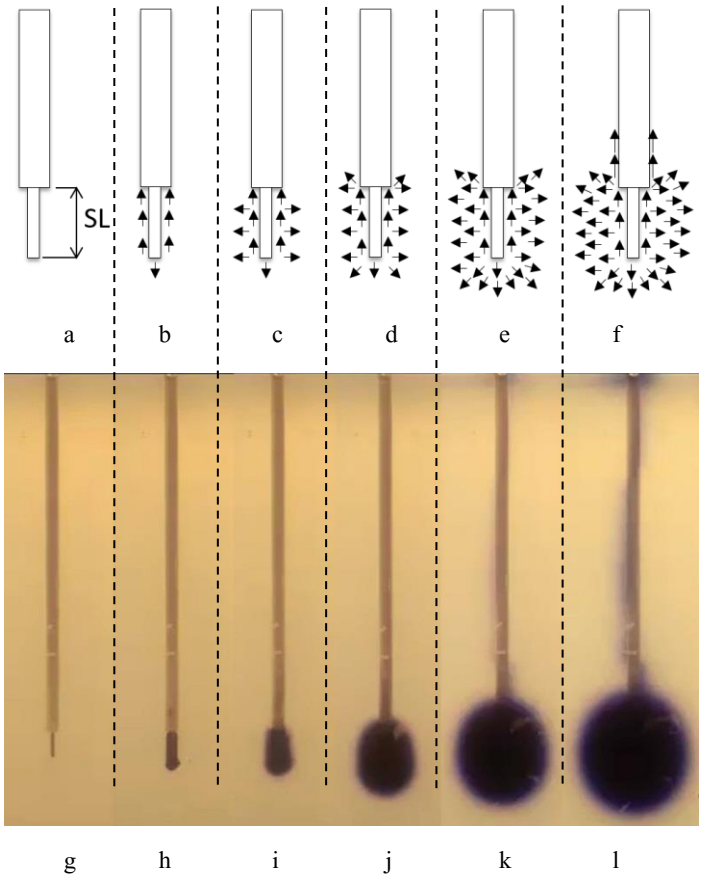

Figure 5-8. The stages of controlled reflux; a) implanted device – SL=Step Length, b) initial reflux, c) ramped/ stepped increase in the flow rate leading to containment of flow front at the inhibition feature and establishment of lateral flow pathways, d) peak flow rate achieved and stable convection reached, e) optimal limit of delivery, f) overload – pressure exceeds inhibition feature limit; g-l) stages a-f demonstrated in a gel model

Encouraging the fluid to remain in this region is achieved through the inclusion of an internal recess within the step, increasing the tortuosity of the fluid path, effectively "controlling the reflux". This feature will eventually fail in response to excessive pressures induced through large volumes or flow rates. A schematic illustrating the development of an infusion and the point of failure are provided above (Figure 5-8a-f) alongside a representative examples of each stage from a sample gel infusion (Figure 5-8g-l).

5.5.2 Controlling infusion morphology

At the time of conducting this experiment, no detailed assessment of the operational performance of a "controlled reflux" catheter system had been published. Earlier work published in Bristol, identified only the recess as a feature to limit 'backflow', and compared a 3 mm step length against other arrangements with similar features, specifically an externally stepped cannula (Gill *et al.*, 2013; Krauze *et al.*, 2005). Though numerous papers had, and have since been published on the pre-clinical and clinical uses of these systems to administer investigational molecules (Singleton *et al.*, 2018; Souweidane *et al.*, 2018; Bankiewicz *et al.*, 2016; Whone *et al.*, 2019a), none have published systematic investigations on the

manipulation of flow rates and infusion volumes using the recessed step catheter design. This experiment therefore provides information on the distribution morphology (shape, length, width and total volume of distributions) which might be expected from clinically useful volumes in grey matter targets. These agarose gel experiments confirm that within the range evaluated, the fluid would routinely travel between the catheter tip and the recess and develop an infusion cloud from this initial region.

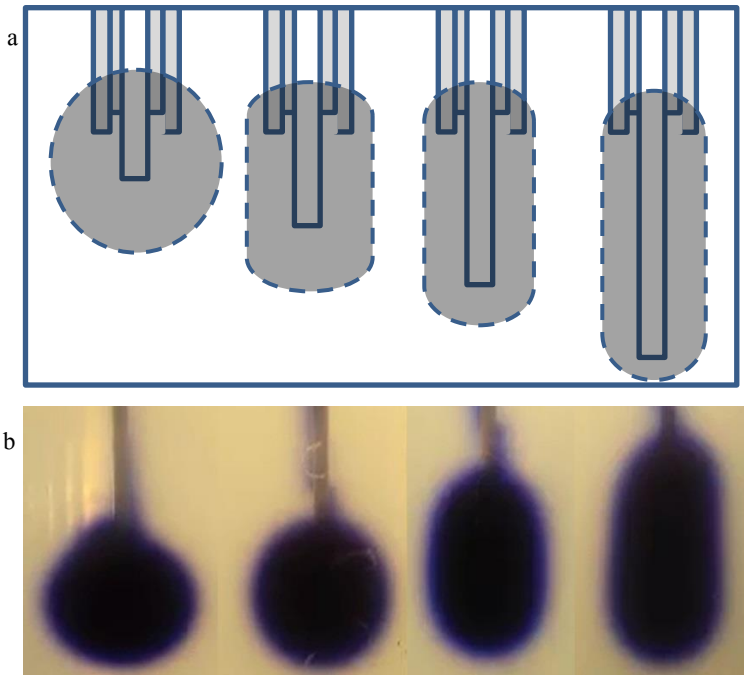

Figure 5-9. a) Schematic of distribution morphology characteristics associated with increasing the step length of the recessed step catheter, b) actual distributions associated with increasing step lengths.

Logically, as the step and distribution length increased, the distribution width would narrow, resulting in spherical distributions for shorter step lengths and elongate, cylindrical infusions as the step increased (Figure 5-9a-b).

There were a number of interesting findings beyond this simple observation, however.

As the infused volume was fixed at 400 µl, and the gel was homogenous (0.6 % agarose), then the overall distribution was thought to remain constant. However, as the step length increased so too did the distribution volume. A significant linear rise in coverage was observed from 3-18 mm (Figure 5-5).

It is likely that manually profiling the edge of infusions where the boundary is diffuse (the combination of the convective and diffusive flow during the infusion), may introduce an error into this process as an exact edge is not visible. Automatically segmenting the infusion distributions was trialled, however variations in lighting taken at the time of sample acquisition prevented isolation of the infusions using a fixed threshold value.

As with the assessment of the clinical trial, a single user (author) was tasked to perform all manual segmentations around the dark boundary before the infusion grows lighter in colour (Figure 5-10). The depth of the diffuse ring around the infusions was not markedly different between cases, which is unsurprising as Dawe and Errickson have previously reported that the diffusion coefficient of Typan blue in 0.6 % agarose gel is 1.08 mm^2/hr (Dawe and Erickson, 2006) meaning that the dye will continue to spread throughout the gel due to Brownian motion, but this will occur at a much slower rate than

during an infusion where the convective and diffusive flows combine. The use of the dark, convective boundary by a single user was used to provide a useful comparison point between samples. Future work should however seek to automate the analysis process and incorporate real time imaging assessment of the distribution volumes using a fixed lighting source.

Figure 5-10. The distal edge of distributions in the agarose gel from an 18 mm step length catheter infused at a) 0.1 ml/hr, b) 0.3 ml/hr, c) 0.6 ml/hr.

Significant differences in the distribution volumes were also observed when changing flow rate (and keeping the step length fixed). As the flow rate increased, the coverage significantly dropped (Figure 5-5), which may be explained by the prolonged infusion time for slower rates, where the distribution volume would be augmented by the increased time for diffusion, and further improved by longer step lengths. At each step length investigated (3, 6, 12 and 18 mm) there was a significant drop in the distribution volumes achieved as the flow rate was increased from 0.1 to 0.3 and then 0.6 ml/hr. This mirrors trends previously published by Chen and colleagues who noted a 50 % reduction in the Vd/Vi ratio when flow rates increased from 1-10 µl/min (Chen *et al.*, 2002). This evidence confirms that the infusion regimes used with an implanted device play a significant role in the overall coverage of target structures.

These characteristic profiles identified in the gels were also observed *in vivo*, with infusate refluxing in a controlled manner to the step before stabilising and distributing laterally (Figure 5-7).

As might be expected, infusions into live tissues are less uniform than in homogenous gels however linear increases in distribution length and a reduction in width were observed across the small number of catheters tested which demonstrates proof of principle.

Take home message

The RSC is unique in the field of direct delivery to the brain as it uses the three-tube system to its advantage to vary the distribution morphology by modifying the step length. This can be used to target, and maximise the coverage of, asymmetric neuro-anatomical structures.

Considering the operational limits of the RSC, secondary reflux beyond the recess occurred most often in the shortest step lengths (3-6 mm) and at the highest flow rates (0.6 ml/hr). This in part explains historical challenges previously identified in translating pre-clinical results to a clinical setting. Pre-clinical infusions are inherently lower in volume to accommodate the anatomy and there is a desire to limit clinical patient times to reduce costs, driving infusions faster and faster (Bankiewicz *et al.*, 2016). The trends shown above highlight significant risks of lower coverage and higher risk of reflux when infusion rates are ubiquitously pushed to go faster and faster, and also increase the risk of tissue damage as previously published (Krauze *et al.*, 2005).

A compromise must therefore be struck between the preferred, short infusion times resulting in smaller distribution volumes, or longer infusion times that provide greater coverage, reduced risk of reflux but greater risk of unavoidable losses via natural clearance mechanisms.

5.5.3 Application of learning

To optimise the performance of implanted catheters a knowledge of their distribution characteristics must be known in advance. This chapter has provided empirical evidence on the morphology of distributions which can be achieved with the RSC.

For anatomical neurological structures such as the putamen (Figure 3-4), total coverage is unlikely using a single implanted catheter. In the *first-in-man* study, two catheters were implanted into each hemisphere to maximise coverage of the putamen with average volumes increasing as a result of increased retention and longer steps inside the target structure (Figure 3-14). Average coverage reached a high at 57 % in the first test infusions when posterior trajectories maximised the step length into structure.

A third catheter into the anterior portion of the structure may have yielded further gains. Future development of finite element analysis (FEA) models may provide useful tools for surgical planning as advocated by other groups (Linninger *et al.*, 2008a; Linninger *et al.*, 2008b; Linninger *et al.*, 2008c; Vidotto *et al.*, 2020; Zhan, Rodriguez and Dini, 2019). The creation of optimal trajectories, step lengths and infusion regimes to maximise coverage ahead of implantation would be valuable for patient care. An example surgical plan, increasing the number of catheters and alternative trajectories are provided below (Figure 5-11).

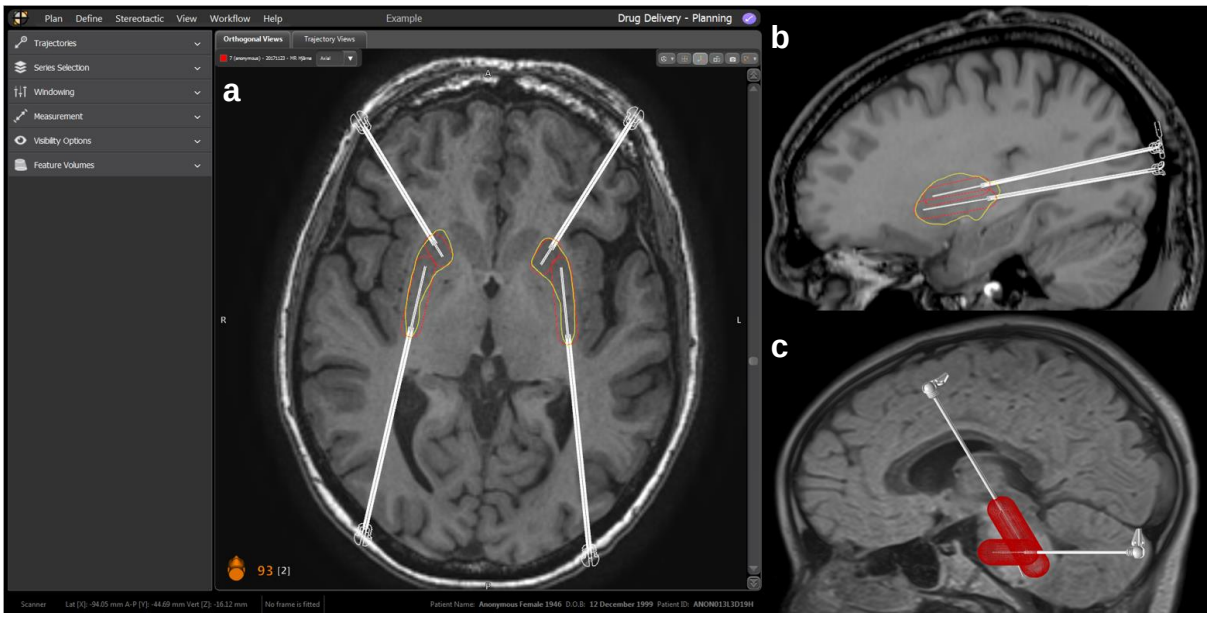

Figure 5-11. Examples of surgical trajectories aiming to maximise target structure coverage using the RSC, a) Example drug delivery surgical plan within neuroinspire™ (Renishaw plc, UK), putamen (yellow outlines) coverage is targeted with an empirical infusion distribution planning guide (red outlines) delivered via four catheters (white outlines), b) alternative, vertically stacked RSC entering the putamen via a posterior trajectory, c) transfrontal and transcerebellar catheter trajectories aimed at maximising coverage in the brain stem for indications such as Diffuse Intrinsic Pontine Glioma (DIPG).

One of the limitations to this study was the upper length of the step investigated. Controlled reflux is unlikely to succeed indefinitely and therefore further evidence of an operational limit of the device would be useful and presents an opportunity for further work.

As there is inherent variability within neurodegenerative populations our investigations would discourage the use of a *"one size fits all"* approach, and real time or post-infusion imaging would augment a treatment regime which enables the clinician to "drive" the implanted system based on real feedback. Implanted catheters could then be optimised with initial infusion parameters, but fully implanted MRI compatible systems also offer the ability to maintain long term performance through periodic test infusions.

5.6 Conclusions

Prior to this experiment an agarose gel and small porcine in vivo study had shown evidence of a novel recessed step catheter performing well against comparison catheter designs. The embodiment of that system was limited to short step lengths 3 mm (gel) and ~6 mm (*in vivo*). A subsequent *first-in-man* study utilised the RSC design in a significantly different way, extending the step length to over 5 times the lengths previously investigated.

This study demonstrated the stages of controlled reflux across a range of pre-clinical and clinically useful step lengths, infusion volumes and flow rates.

This empirical evidence has highlighted new nuances in the performance of the RSC from the way in which is it assembled and the way in which it is infused through.

Increasing the step length significantly increases the distribution volumes achieved, while increasing the flow rate from 0.1-0.6 ml/hr significantly drops the distribution volume (for any fixed step length).

This empirical evidence provides useful data for the creation of a predictive model to aid surgical planning, and can immediately be adopted in the methods used to operate implanted devices.

Further work is required to understand how these observations may be translated to acute and chronic infusions in the human diseased brain.

Take home message

In addition to the surgical planning guidelines outlined in section 3.6, optimisation of implanted catheters can be aided with the knowledge of empirical distribution patterns obtained from varying basic parameters of step length, infusion volume and peak volumetric flow rate.

6 Modelling of recessed step catheter

6.1 Motivation

As previously highlighted, there is a symbiotic relationship between empirical evidence of device function and computational models. While empirical testing, both *in vitro* and *in vivo* represent real-world evidence of device function, variables can be quickly modified within a computational model and small changes evaluated for effects on the outcome or performance of a system providing cost savings in materials, time and an ethical use of resources. Computational models also provide insight at a magnification not feasible using standard medical diagnostic tools such as MRI, whose resolution is typically no better than 0.6 mm voxels.

In order to provide valuable input data for such a computational model, it is common to create a body of data with which to validate the model (Chen *et al.*, 2002; Elenes, Rausch and Rylander, 2019), which for the RSC has been accomplished in earlier sections (sections 3-5).

Computational and mathematical models of porous flow are based on the principles of mass conservation and the transportation equations for convective and diffusive flow as outlined in section 2.2. These models require input conditions for the source of the fluid, which in the case of CED studies, is typically the catheter. End port, side port and porous tipped cannula have previously been described (Linninger *et al.*, 2008a; Sampson *et al.*, 2007; Raghavan and Odland, 2017) but the novel action of the recessed step catheter which uses the controlled reflux mechanism has not to date been modelled.

6.2 Introduction

The aim here is to create a finite element model representing the recessed step catheter and the unique characteristics of the variable step length, comparing the results to the empirical data gathered in section 5. Inspection of the model will be undertaken, specifically investigating the shear stress, displacements, concentration profiles and fluid flux values, to further inform previous empirical observations.

6.3 Method

6.3.1 Platform

FEBio (www.FEBio.org Musculoskeletal research laboratories, University of Utah) is an open access finite element analysis (FEA) software suite. It was chosen as the software package to model distributions from the recessed step catheter as it contained tools for non-linear, multiphasic FEA which are useful for the large deformations present in gels and the brain (Forte *et al.*, 2016; Leibinger *et al.*, 2016). Further, the chemical reaction equations available within FEBio permit the user to apply a solute flux into a multiphasic (porous) substrate. Stochiometric equations for chemical species further allow sources of solution to be defined from bodies, enabling mapping of solvent and solute within the same model.

6.3.2 Model units

Consistency of units is essential for outputs to be meaningful. Unit values for this analysis were chosen as mm, seconds, Newtons and millimole.

Table 6-1. Standard units used in calculations/ FE analysis.

Unit	Description	Type
mm	Millimetre	Length
N	Newton	Force
s	Seconds	Time
kg	Kilogram	mass
mM	Millimole	Molar concentration

6.3.3 Model construction

Using the experimental parameters of the four step lengths evaluated in section 5, four base models were generated (Figure 6-1). To simplify the geometry and make the infusions visible adjacent to the catheter, a 3D wedge shape was chosen, which also permitted boundary conditions to be applied in the three major axes (X,Y,Z). The geometry was defined as a series of points, lines and surfaces to create a volume which was then meshed using the open access software, GMSH (Geuzaine and Remacle, 2009) (available online; www.gmsh.info, accessed 1st July19).

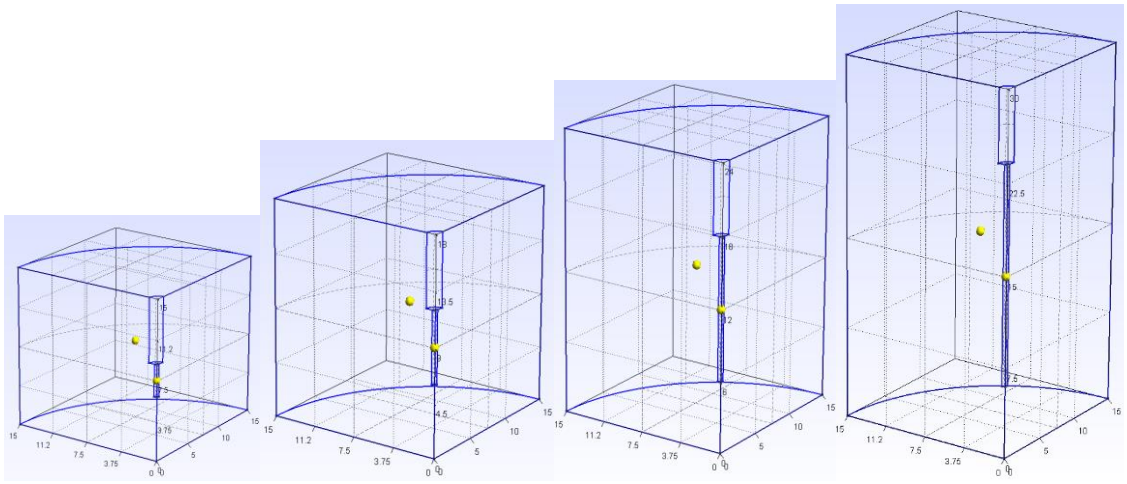

Figure 6-1. Models and meshes created for FE simulations of 3, 6, 12 and 18 mm stepped catheter designs.

6.3.4 Meshing

Mesh generation was accomplished within GMSH. Element density was varied throughout the volume by prescription of the mesh size at designated nodes. This allowed greater density of elements to focus on the area immediately around the catheter step where the infusions are applied within the model. A convergence study was used to assess mesh density.

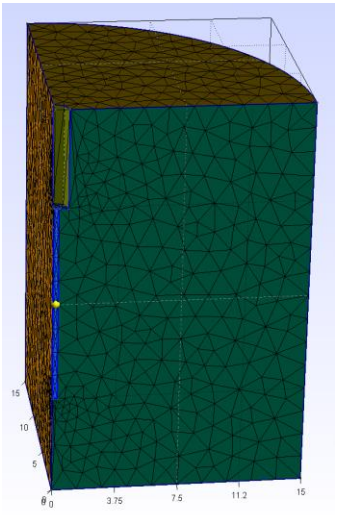

Figure 6-2. 12 mm step length model shown with illustrative, coarse surface mesh.

6.3.5 Model Material parameters

6.3.5.1 Material type

The brain can be considered a multiphasic material with a solid, porous matrix filled with a fluid & solute mixture. Previous mechanical testing and modelling of the brain has identified that it has viscoelastic properties (Forte *et al.*, 2016). Where the solid matrix has been modelled for CED studies, a neo-Hookean material has been selected (Elenes, Rausch and Rylander, 2019). Multiphasic neo-Hookean materials require inputs for;

- solid volume fraction
- Young's modulus
- Poisson's ratio
- Hydraulic conductivity
- Diffusivity (free and restricted)
- Solubility

6.3.5.2 Young's modulus

Published values of Young's modulus of CNS tissues are extensively reviewed by Smith and Humphreys with values ranging from 0.002-0.106 N/mm^2, in several studies of non-perfused and perfused samples (Smith and Humphrey, 2007). In their own evaluation of normal and neoplastic brain tissues they use a nominal Young's modulus value of 0.005 N/mm^2. Choosing a value at the lower end of the reviewed range is logical as a lower Young's modulus would be expected for non-perfused tissues which become tough following fixation. These also closely match the value obtained by Budday et al (0.002 N/mm^2) by indenting white and grey matter (Budday *et al.*, 2015).

For this model a Young's modulus of 0.002 N/mm^2 was chosen to represent the lower end of the published values and likely to produce the largest strains in the material.

6.3.5.3 Poisson's ratio

An unconfined compression test of fresh calf brain white matter by Cheng and Bilston (2007) identified the Poisson's ratio of brain tissue to be 0.35 (Cheng and Bilston, 2007). Separate uniaxial stress tests performed on human brain tissue samples within 12 hrs of death identified that the Poisson's ratio of drained and undrained tissue was very similar, 0.5 and 0.496 respectively (Franceschini *et al.*, 2006). A starting value of 0.45 was selected.

6.3.5.4 Permeability

Permeability, k (m^2), is a physical property of a substrate incorporating factors such as the pore fraction. Hydraulic conductivity, K (m^4/Ns) is the proportionality constant which links the permeability to a particular fluid's properties (viscosity ($\mu[m^2/s]$), density (ρ) and gravity ($g[m/s^2]$)) and are linked by Equation 6-1 and Equation 6-2 (Bear, 1988).

Equation 6-1. $$\boldsymbol{K = k\frac{g\rho}{\mu}}$$

Equation 6-2. $$\boldsymbol{\nu = \frac{\mu}{\rho}}$$

The permeability requested for biphasic materials in the FE software package (FEBio) calls for units in terms of $Length^4/Force*Time$, therefore values of hydraulic conductivity will be used. Within reviewed literature it appears that permeability and hydraulic conductivity are often used interchangeably, therefore care has been taken to ensure that only hydraulic conductivity references are provided.

Linninger et al define the hydraulic conductivity of grey matter as $1.12x10^{-13}m^4/Ns$ in their predictive CED model of brain infusions (Linninger *et al.*, 2008b). Sarntinoranont et al, use a much lower value of $4.22x10^{-15}m^4/Ns$ [$4.22x10^{-12}cm^4$/dyne.S] to investigate a computational model of interstitial transport in the spinal cord (Sarntinoranont *et al.*, 2006) which may be due to the tight bunching of nerve fibres in the spinal cord. Morrison et al calculated a hydraulic conductivity for grey matter of $1.7x10^{-11}m^4/Ns$ using measured values of line pressure and volumetric fluid flow rate (Morrison *et al.*, 1994). Cheng and Bilston conducted a rheologic investigation of calf brains and identified experimentally that the permeability (hydraulic conductivity) of white matter was $4.08x10^{-12}m^4/Ns$ (Cheng and Bilston, 2007). Chen et al investigated drug distribution in brain phantom gels and used a hydraulic conductivity value of $4.5x10^{-10}m^4/Ns$ (Chen *et al.*, 2002). This correlates with their later publication indicating that distribution values in the agarose gel model can exceed those in the grey matter of the brain (Chen *et al.*, 2004), which may account for the increased hydraulic conductivity values for agarose gel.

Rationally, while this model should emulate the empirical data obtained through gel studies, a lower value of hydraulic conductivity than agarose gel, and a higher value than that used to model spinal cord fluid travel will be used to assess likely coverage patterns for grey matter targets. The hydraulic conductivity value for grey matter ($1.12x10^{-13}m^4/Ns$) used in a CED model by Linninger et al (2008) will be used here.

6.3.5.5 Diffusivity

Free aqueous diffusivity, and hindered diffusivity values were obtained through experiment.

- Free diffusion was assessed in beakers of deionised water with injections of dye directly onto the base beneath the water. Periodic images of the dye were recorded for assessment.
- Agarose gel (0.6 %) was prepared as previously described. Clear containers were used to set the gels at depths of approximately 10-15 mm. Vertical puncture marks filled with trypan blue dye were observed beneath a microscope where time lapse images were recorded.

Images were processed using Matlab to obtain segmented binary images. The threshold was maintained throughout the assessment of all repeats (n=6-9). The threshold was selected by plotting a histogram across the final image in the series and noting where the intensity diverges from the background. The hindered diffusion was calculated as 2.362×10^{-9} m^2/s [0.002362 mm^2/s] (modifications to the threshold by ±10 units[0-255] resulted in a minor change to the hindered diffusion rate; $D=1.705 \times 10^{-9}$ - 3.227×10^{-9} m^2/s). Free diffusion was calculated as 9.3×10^{-7} m^2/s [0.9298 mm^2/s].

6.3.5.6 Porosity (and the solid volume fraction)

Porosity (also called the pore-fraction) can be defined as the ratio of a unit volume which is occupied by fluid. This is the inverse of the solid volume fraction, which is the ratio of solid within a unit volume.

The porosity is linked to permeability but while porosity values might be high for very high fluid ratios, the permeability may be very low if the chambers of fluid within a solid are not connected which would allow the flow of fluid under the influence of gravity or a pressure gradient.

Stab wounds in the rat cortex were evaluated using iontophoresis probes (i.e. current applied between two probes with chemical species sampling ability) over a series of time points following injury and a pore fraction in grey matter of 0.2 was identified (Roitbak and Sykova, 1999). In computational models of CED investigated by Linninger et al, higher pore fraction values of 0.26-0.3 are used (Ivanchenko, Sindhwani and Linninger, 2010; Linninger *et al.*, 2008b). Belova et al, highlight Morrison's definition of brain tissue porosity ranging between 0.2-0.4 and resolved to use a mean value of 0.3 in their mathematical description of CED (Belova, Shaffer and Trapa, 2017; Morrison *et al.*, 1994). Here a porosity of 0.3 was used and a solid volume fraction of 0.7.

Table 6-2. Reference values for CED model.

Symbol	Description	Value	Units	Source/ reference
E	Young's modulus	0.002-0.005	N/mm^2	(Budday *et al.*, 2015; Smith and Humphrey, 2007)
K	Hydraulic conductivity	$1.12x10^{-13}$ (0.112)	m^4/Ns (mm^4/Ns)	(Linninger *et al.*, 2008b)
ϕ	Porosity	0.3	Unitless	(Belova, Shaffer and Trapa, 2017)
v	Poisson's ratio	0.45	Unitless	(Smith and Humphrey, 2007)
Q	Volumetric flow rate	0.022, 0.083, 0.167 (1.33, 5, 10)	mm^3/s (µl/min)	(Lewis *et al.*, 2018)
V_i	Infusion volume	400	mm^3	(Lewis *et al.*, 2018)

6.3.5.7 Solute and fluid flux

The value of the fluid flux is defined as the volumetric flow rate per unit area over which the input fluid is applied. In the context of the controlled reflux action exhibited by the RSC, the value of the flux will drop as the step length increases, as there is a larger region over which the input fluid is applied (Table 6-2).

Table 6-3. Flux (flow per unit area) values for the four catheter step length models.

Symbol	Description	Step Length (mm)			
		3	**6**	**12**	**18**
A_{EF}	Area of catheter end face(mm^2)	0.283	0.283	0.283	0.283
A_{SL}	Area along step length (mm^2)	5.65	11.31	22.62	33.93
A_T	Total area of face of applied flux ($=A_{EF}+A_{SL}$)	5.933	11.593	22.903	34.213
Flux	**Fluid Flux($=Q/A_T$)mm/s**				
	Q=0.022	**0.0037**	**0.0019**	**0.0010**	**0.0006**
	Q=0.083	**0.014**	**0.007**	**0.004**	**0.002**
	Q=0.167	**0.028**	**0.014**	**0.007**	**0.005**

6.3.5.8 Chemical reactions

FEBio contains stochiometric functions for the generation and interaction of chemical species/ solutes (ε) which are free ($\alpha=\iota$) and solid bound ($\alpha=\sigma$). Calculations of reactants (R) and products (P) are governed by equations of mass/ chemical conversation (Equation 6-3). Materials can therefore be assigned as a source which will produce solutes at a molar production rate (according to local model units). Where ν represents the stochiometric coefficient of product/ reactant of the chemical species (ε^{α}).

Equation 6-3

$$\sum_{\alpha} \nu_R^{\alpha} \varepsilon^{\alpha} \rightarrow \sum_{\alpha} \nu_P^{\alpha} \varepsilon^{\alpha}$$

It was assumed that the concentration of the solute (trypan blue; 860 g/mole; 4 %by volume) within the solid matrix will be zero at the start of the analysis, therefore there are no reactants to consider, only the concentration of the applied solute flux.

Table 6-4. Specific forward reaction rate of step length models (mM/s^1.mm^2).

Flow rate (ml/hr)	Step Length (mm)			
	3	6	12	18
0.1	0.0218	0.0111	0.0056	0.0038
0.3	0.0653	0.0334	0.0169	0.0113
0.6	0.1306	0.0669	0.0338	0.0227

Model steps were set to 1s, with a maximum of 1000 increments permissible in a single step. The total number of steps was a function of the maximum flow rate and infusion volume (Table 6-4).

Table 6-5. Model run time as a function of peak infusion flow rate and volume infused ($t=V_i/Q$).

Volumetric flow rate, Q (ml/hr)	Infusion volume, V_i (µl)	Infusion time, t (s)
0.1	400	18,000
0.3	400	4,800
0.6	400	2,400

6.3.6 Global model data

Universal gas constant, R=8.314 J/mol.K

Units of the model are mM therefore R=8.314x10^{-6}J/mM.K

Absolute temperature (K): 298K (~25^{o}C) – ambient room temperature

6.3.7 Initial Boundary Conditions (BC)

Boundary conditions were applied to the model to control the physical displacements possible and also define the free draining face for the fluid within the biphasic material to emulate CSF loss *in vivo*.

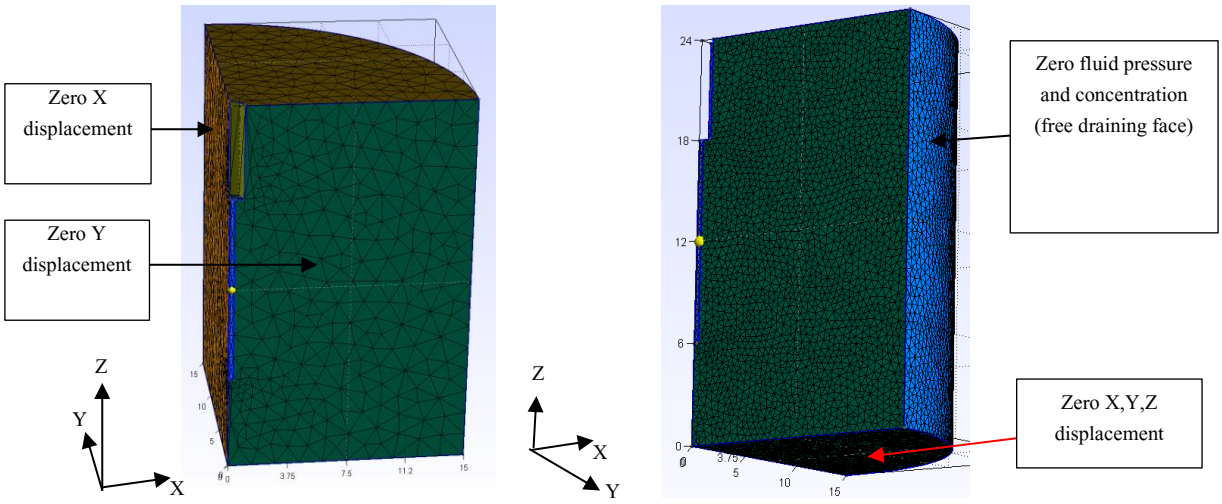

Figure 6-3. Boundary conditions.

6.3.8 Boundary loads (chemical production from a material source)

The application of the liquid solution was applied through the inclusion of a solid material within the model intrinsically linked to the surrounding material. The base material was defined as porous biphasic with no concentration of the solute, while the catheter was defined as a chemical source which provided influx of the solution at a fixed rate (Figure 6-4, Table 6-4), but which varies between models under investigation.

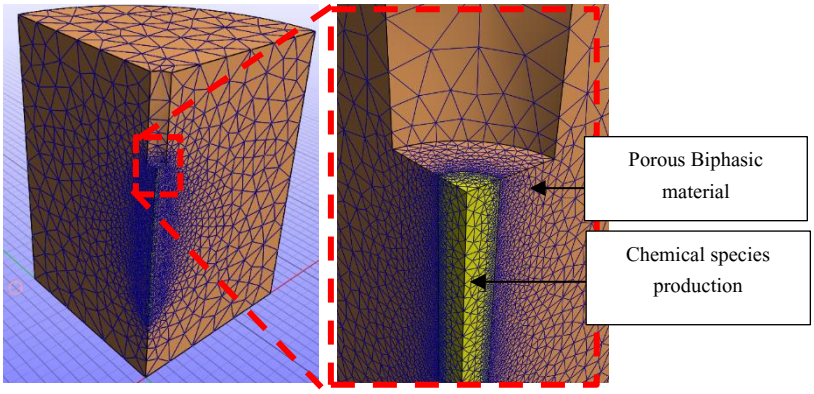

Figure 6-4. Location of applied boundary loads.

6.4 Results

6.4.1 Convergence study

A convergence study was performed, refining the mesh, increasing the number of elements, preferentially around the catheter step length. Four variables were reviewed for convergence of the peak values in the model; shear stress, displacement, concentration and fluid flux (Figure 6-5).

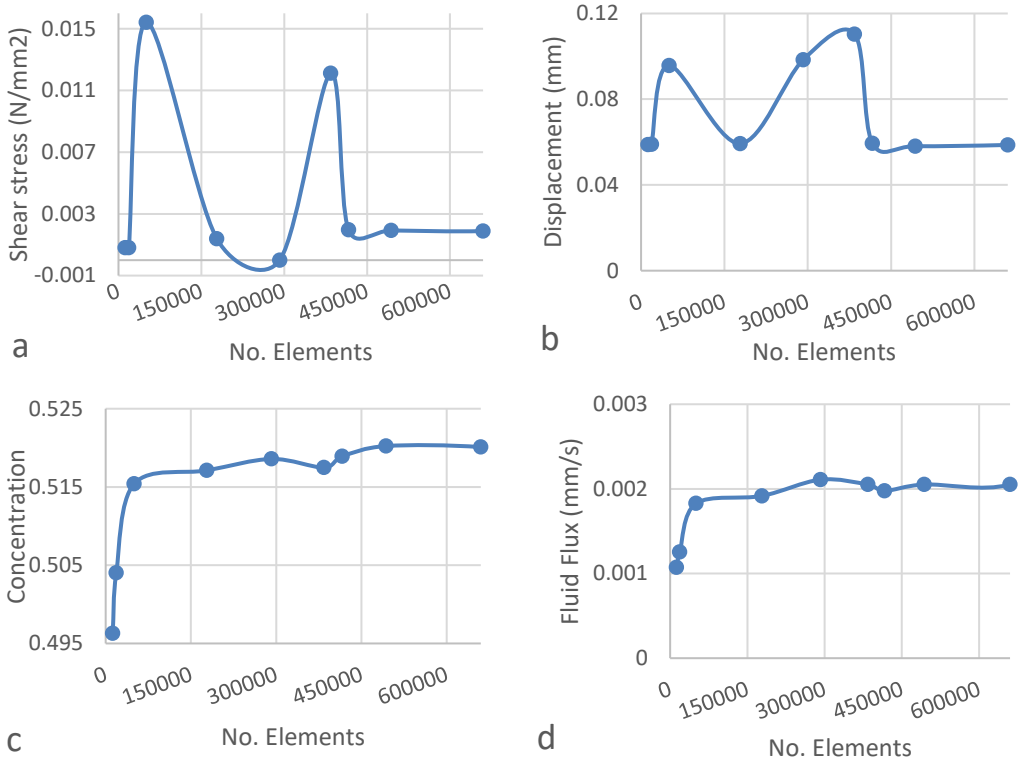

Figure 6-5. Convergence study output: a) Max shear stress, b) max displacement, c) max concentration, d) max fluid flux.

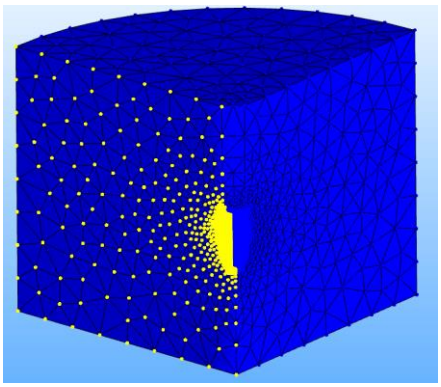

Figure 6-6. Representative example of a single radial plane with all nodes selected for extraction and comparison of nodal information (e.g. displacement, maximum shear stress, etc).

6.4.2 Displacement

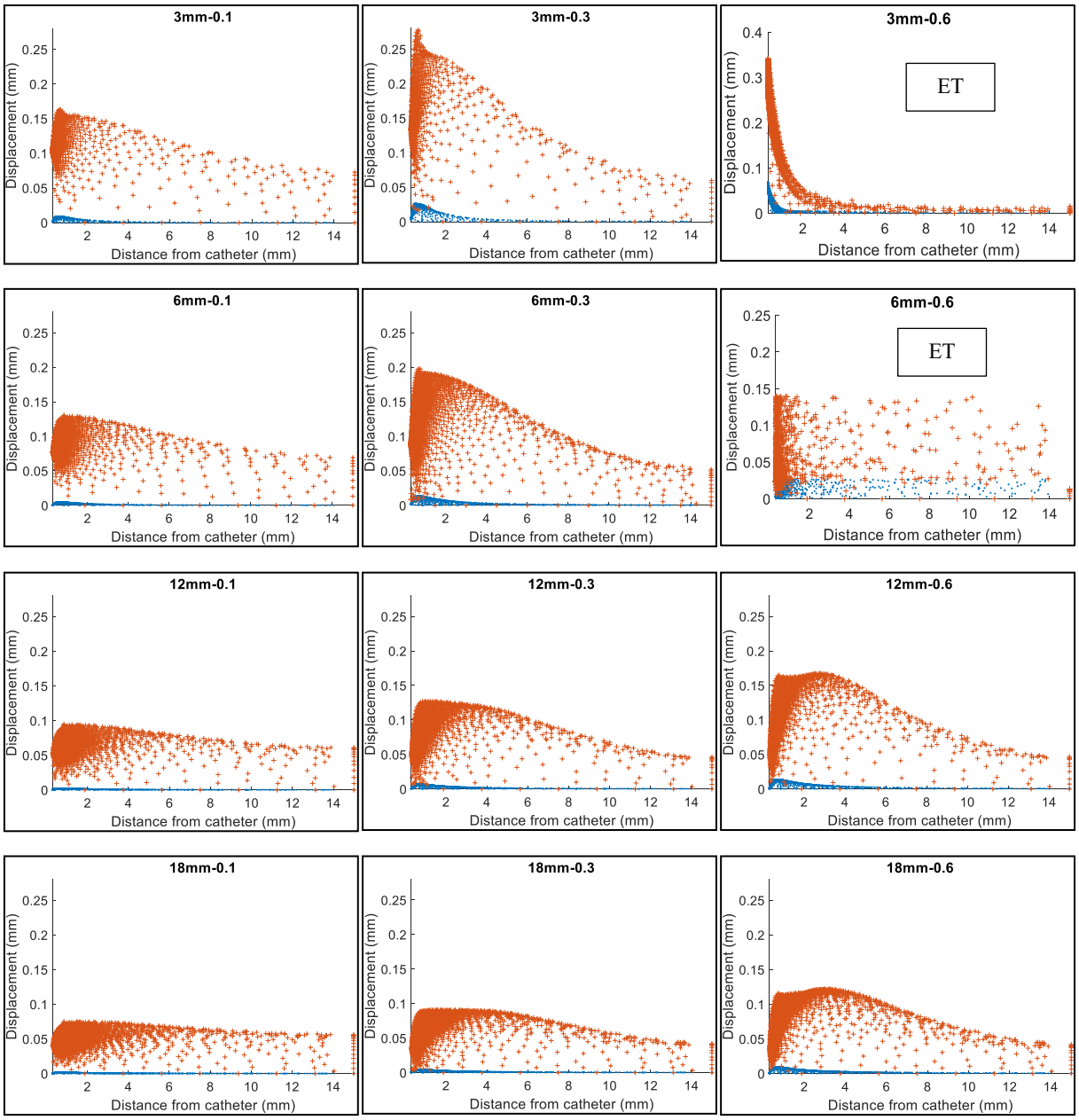

Figure 6-7. Nodal displacement values within the porous substrate emanating radially from the catheter track at 31seconds into an infusion ['.'=t(31s)], and at infusion completion ['+'=tmax(Q0.1/t18,000, Q0.3/t4,800, Q0.6/t2,400)]. ET=error termination, analysis failed to converge.

6.4.3 Shear stress

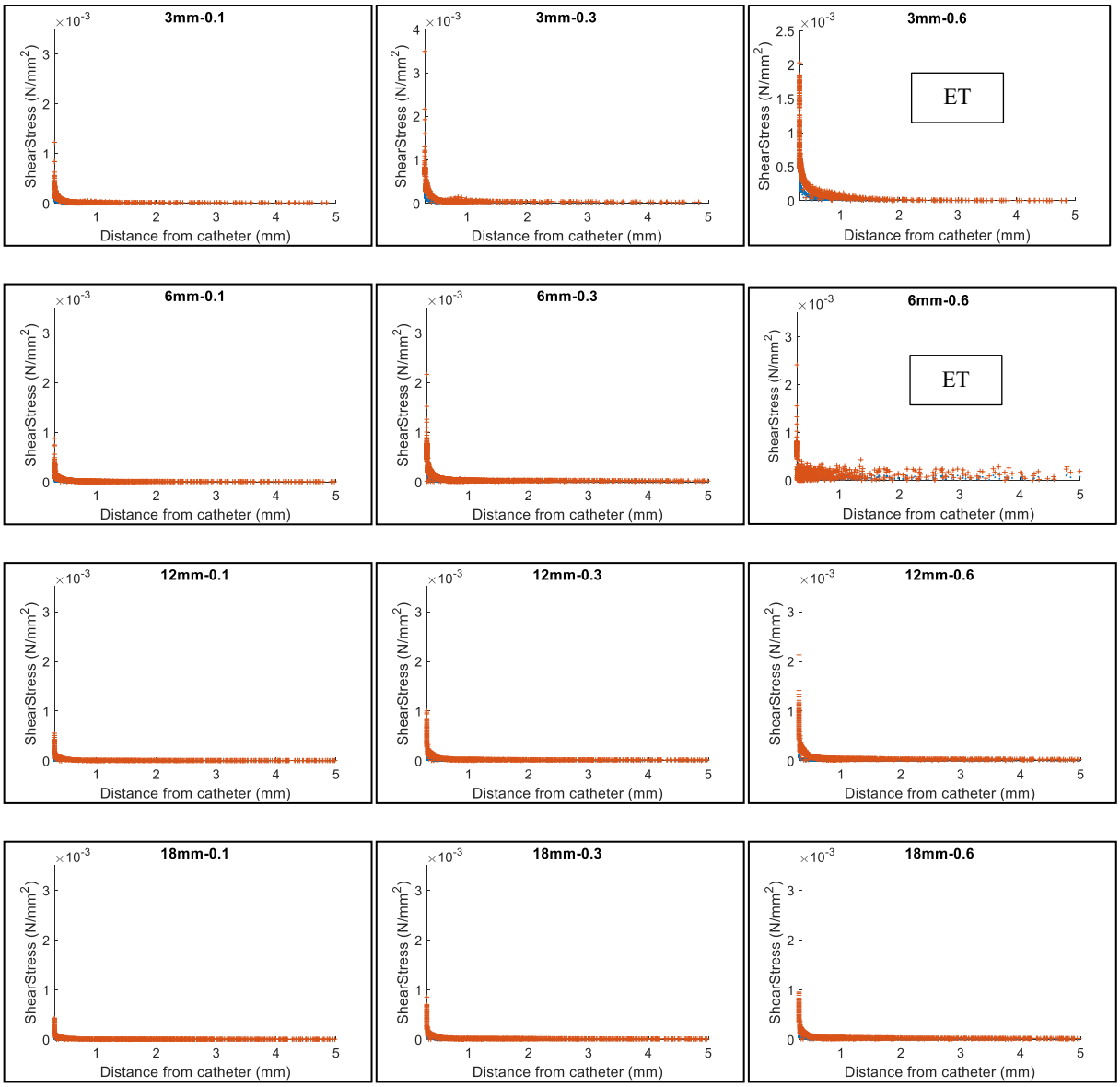

Figure 6-8. Maximum Cauchy shear stress values within the porous substrate emanating radially from the catheter track at 31seconds into an infusion ['.'=t(31s)], and at infusion completion ['+'=tmax(Q0.1/t18,000, Q0.3/t4,800, Q0.6/t2,400)]. ET=error termination, analysis failed to converge.

6.4.4 Fluid flux

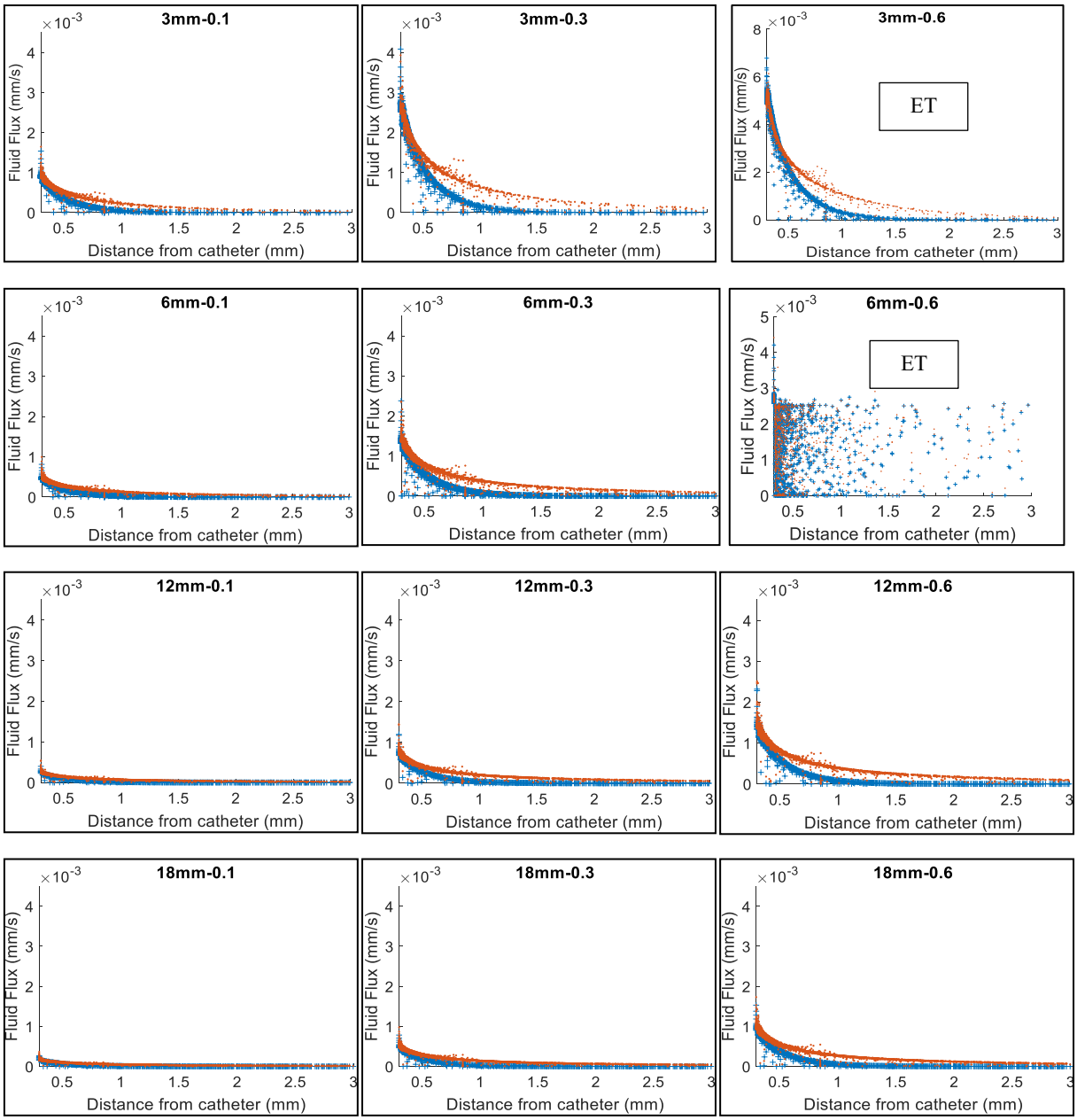

Figure 6-9. Fluid flux values within the porous substrate emanating radially from the catheter track at 31seconds into an infusion ['+'=t(31s)], and at infusion completion ['.'=tmax(Q0.1/t18,000, Q0.3/t4,800, Q0.6/t2,400)]. ET=error termination, analysis failed to converge.

6.4.5 Concentration

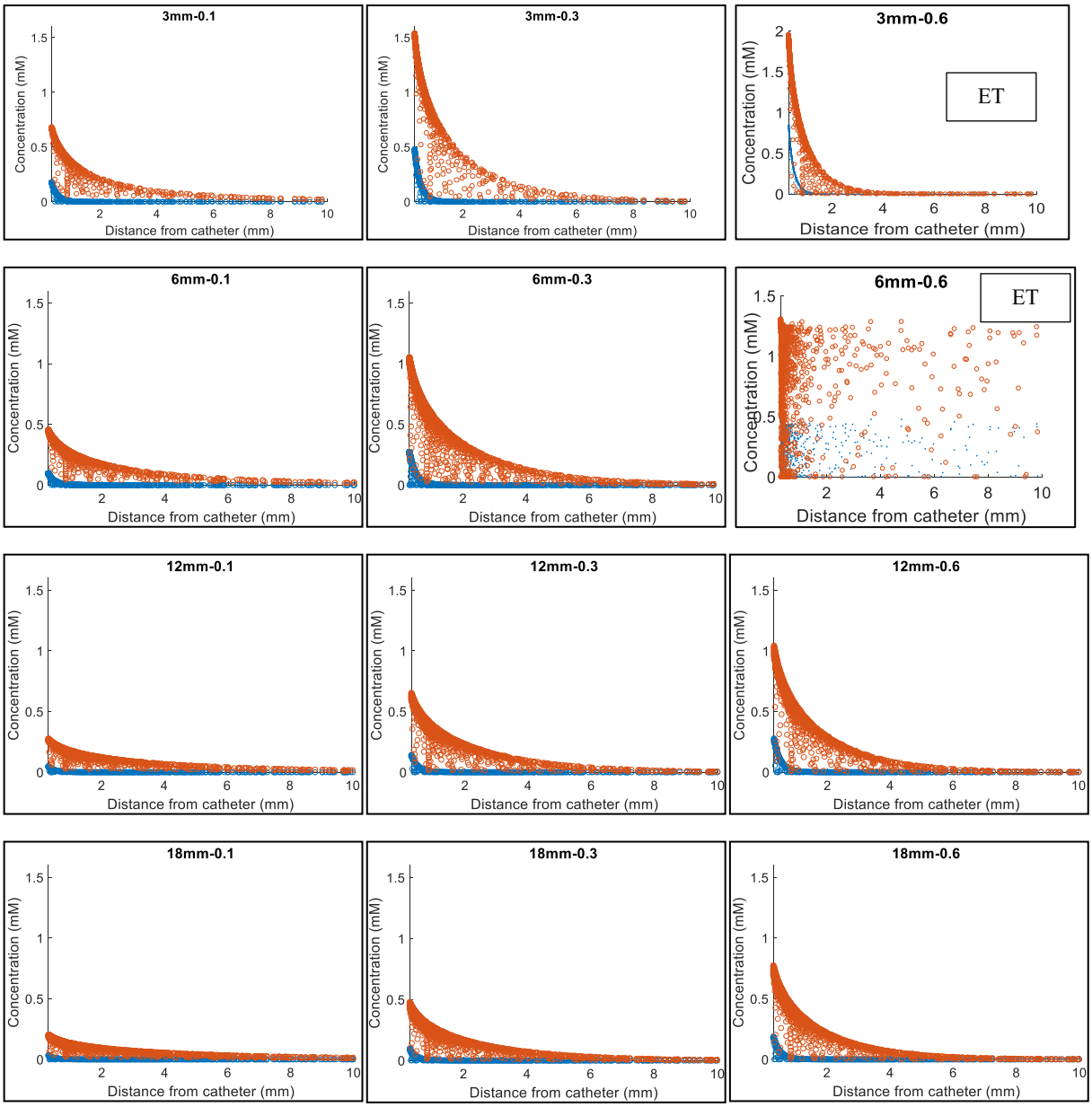

Figure 6-10. Concentration values within the porous substrate emanating radially from the catheter track at 31seconds into an infusion ['.'=t(31s)], and at infusion completion ['o'=tmax(Q0.1/t18,000, Q0.3/t4,800, Q0.6/t2,400)]. ET=error termination, analysis failed to converge.

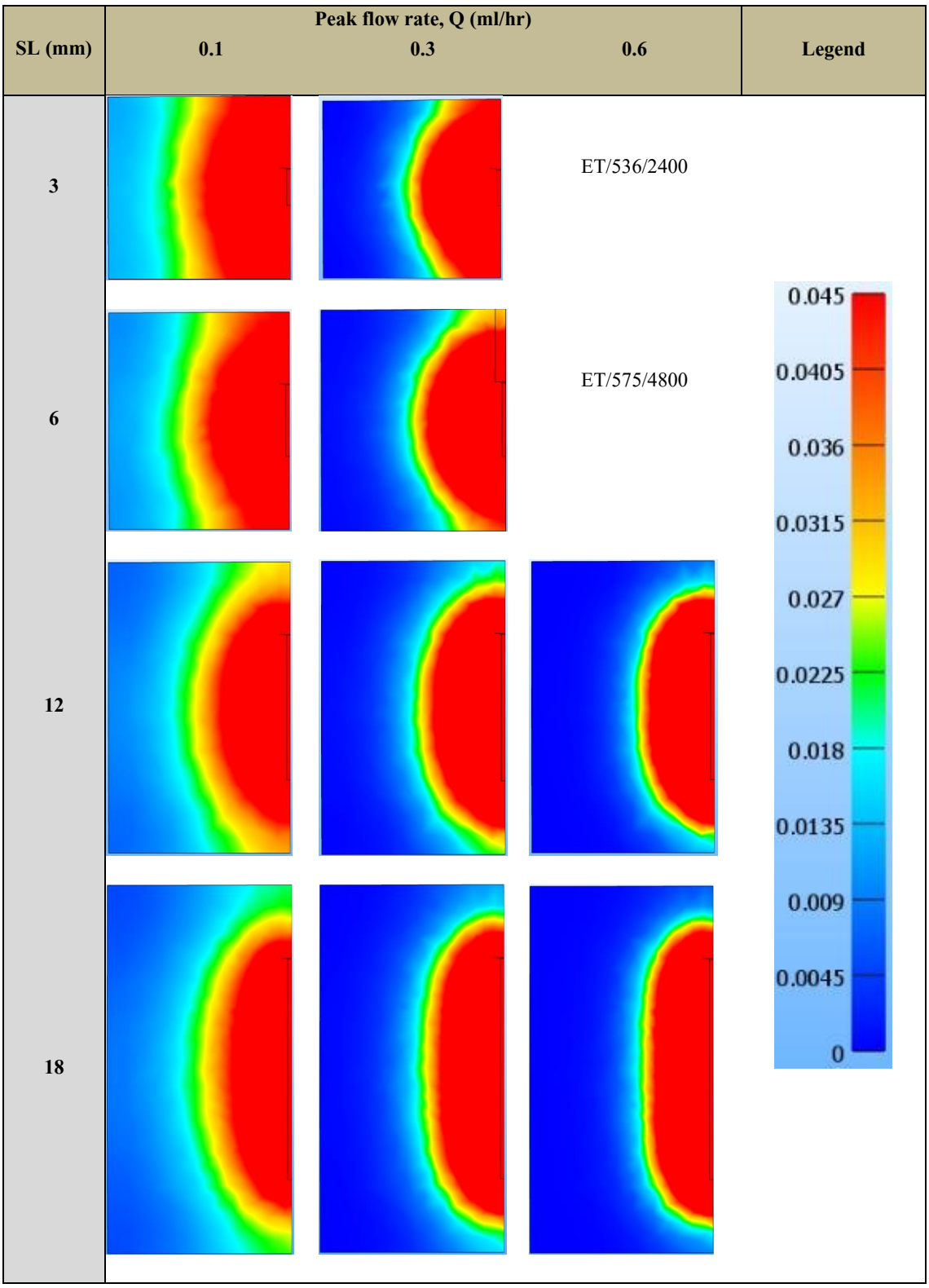

Figure 6-11. Concentration maps of 400 µl infusions into porous substrate. As the 3 mm/Q0.6 and 6 mm/Q0.6 evaluations failed to complete 400 µl infusions these have been omitted to allow direct comparison between results.

6.5 Discussion

The aim of this body of work was to develop a computational model of infusions into a porous substrate representing the brain using the recessed step catheter, to provide further information on the micro-environment around the catheter during convection-enhanced delivery.

A convergence study was performed on the mesh, with focused refinement around the catheter where the production of the solution was applied. Convergence of the four variables under review occurred at different mesh refinements, however stable outputs were obtained across all four variables evaluated by ~40,000 elements, in a 12 mm step length model (Figure 6-5).

The results of the model analysis are presented in Figure 6-7 to Figure 6-10. All nodes on the radial face were selected from each model (e.g. Figure 6-6) with associated values for displacement, shear stress, fluid flux and solute concentration extracted and plotted. Two dimensional plots were selected over three-dimensional plots due to the radial nature of the model which was best represented in this way.

The magnitude of nodal displacement can be seen to increase as a result of fluid flux. As more fluid is forced into the porous substrate the local tissue swells to accommodate the additional fluid. This is most pronounced at short step lengths (where the fluid flux is proportional to the step length) and also at higher volumetric flow rates (where the step lengths are maintained) (Figure 6-7). This nodal displacement agrees with previously published data by Chen et al (2002) who describe undertaking gel experiments and creating a mathematical model which utilise an isotropic and homogenous poroelastic transport model where the pore fraction changes as a consequence of gel dilation. Two optical tracking methods; linear polariscope and nanobead image tracking, were used to quantify local strains around catheter tips during infusions into porous media. Large deformations due to the added fluid content in the substrate were reported (Ivanchenko, Sindhwani and Linninger, 2010).

Previously, empirical distribution curves for the morphology of trypan blue infusions into agarose gel have been provided (Figure 5-4). This indicated that the visible boundary produced differing infusion widths and lengths dependant not only on the step length but also on the infusion flow rate. Concentrations as low as 1-5 % (~0.045 mM) of the neat trypan blue solution (4 % by weight, ~4.65 mM) in deionised water are visible when manually segmenting images of infusions.

This analysis displays higher values of concentration in the substrate immediately adjacent to the catheter, increasing within each step length model group as the flow rate increases (Figure 6-10). The previous observation that higher flow rate infusions produce lower distribution volumes (Figure 5-5) is caused by the elevated concentration of dye proximal to the catheter, which does not continue radially to any great extent.

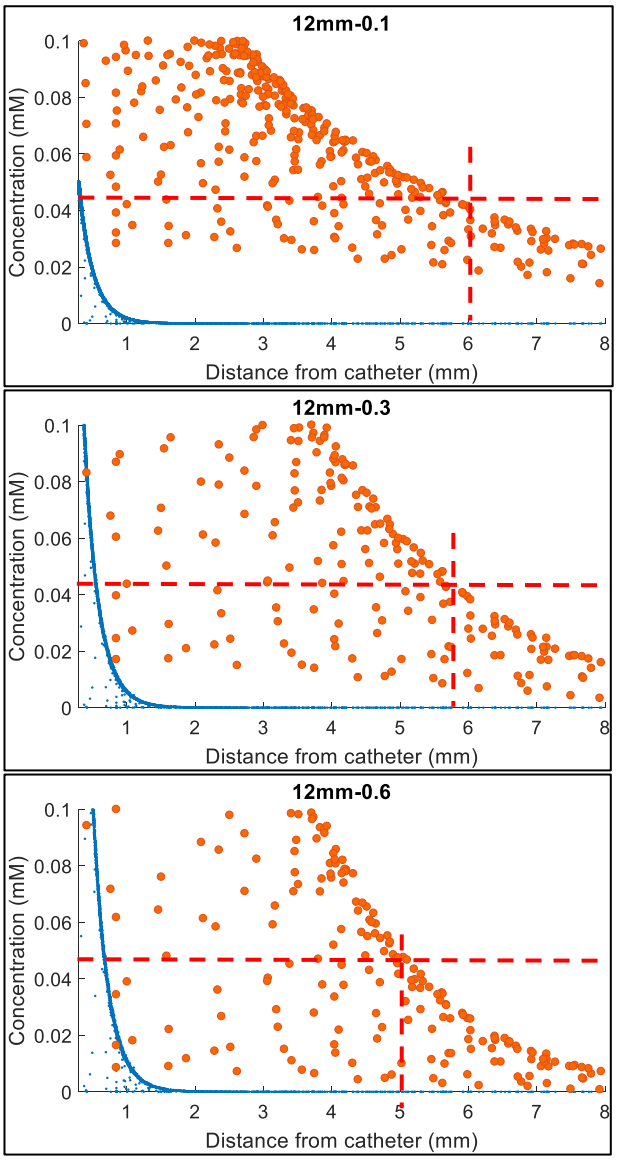

Figure 6-12. Magnified concentration curves plotted radially away from the catheter infusion site for the 12 mm step length model at 0.1, 0.3 and 0.6 ml/hr flow rates.

Conversely, the boundary of the lower concentration of dye extends radially, further away from the catheter in the lower peak flow rate models (Figure 6-12), with the 1 % of neat concentration level (0.045 mM) reaching 6 mm from the catheter in the 0.1 ml/hr model, and only 5 mm in the 0.6 ml/hr model, producing 'larger' distributions at the lower peak flow rate for the same infusion volume.

Two models failed to terminate normally despite initially running as expected. The 3 mm and 6 mm step length models ran for 536 s and 575 s respectively before terminating early. This was not felt to be a failure but a limitation of the model which represents real world limitations of the RSC, and all CED devices in general. As previously discussed, shorter step lengths are at higher risk of uncontrolled reflux, which is exacerbated by running at higher flow rates. The elevated levels of displacement, shear stress, fluid flux and solute concentration are the same order of magnitude as the other models, yet these occur when only a quarter of the analysis had completed, leading to a failure to converge beyond ~550 s.

A limitation of this model is the intrinsic link between the catheter and the surrounding porous substrate (Figure 6-13) which is required for chemical production from a material embedded within a substrate. While this permits a degree of prediction of the infusion distribution profile, it also fails to replicate the real-world failure caused by fluid backflow along the catheter exterior towards the surface of the brain.

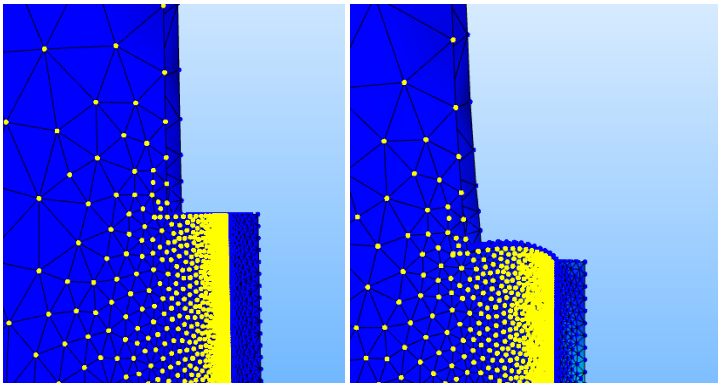

Figure 6-13. Model deformation pre and post infusion.

The high shear stresses observed in the models which failed to converge indicate that as more fluid is forced into the surrounding substrate there is insufficient time for the resident fluid to be displaced, leading to high local stresses. This would lead to separation between the catheter and surrounding tissue, creating a path of least resistance for fluid backflow. Further work may focus on the creation of this multiphasic contact which can fail when exposed to excess shear stress, but is beyond the scope of this project.

This model represents a useful analytical tool to assess modifications to catheter design, molecule size, infusion volume, flow rates or chemical reactions. Predictive distributions to aid surgical planning software may be possible if further work is undertaken to integrate catheter placement software with FEA algorithms. Automatic segmentation of anatomical structures grey and white matter structures (e.g. Figure 6-14), CSF spaces, microvasculature, directionality coefficients of preferential white matter tracks, etc. could be incorporated into surgical planning software to optimise the planned position of catheters to maximise coverage based on not only empirical knowledge of the catheter in an idealised, homogenous gel, but based on iterative simulations to optimise placement and coverage. However, its usefulness as a direct application in surgical planning software will be restricted due to the limitations within the model, and the real-world environment (e.g. the amount of time available for surgical planning and iterative simulations, or the ability to achieve the required targeting accuracy of the implanted system).

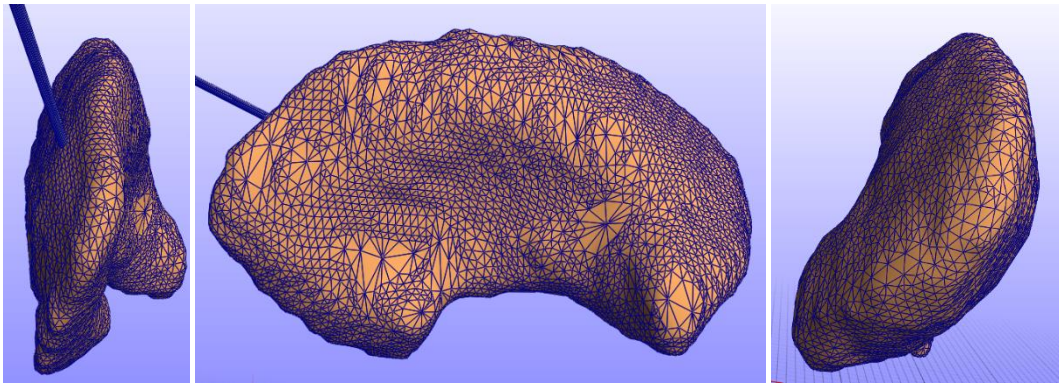

Figure 6-14. Example 3D mesh of a human putamen which could be integrated into a surgical planning suite.

This model is homogenous and isotropic whereas brain tissue is both inhomogeneous and anisotropic due to the differences in density and directionality between grey and white matter. The incorporation of medical diagnostic data, segmenting tissues to differentiate density, porosity and directionality has been previously described (Raghavan *et al.*, 2006; Sampson *et al.*, 2007; Raghavan, Brady and Sampson, 2016; Linninger *et al.*, 2008b; Linninger *et al.*, 2008a). Though limitations in the application of this into a surgically useful workflow exist due to the limited precision of the image data (i.e. large voxel size with loss pathways such as micro vessels which are sub-voxel in size and cannot be directly visualised on MRI scans).

There is also no function for the peristaltic loss which is likely to occur from pumping blood vessels resident in the brain, though all of these limitations represent opportunities for further work.

6.6 Conclusions

Previous work published on modelling convective delivery to the brain has highlighted the necessity to validate models using empirical evidence of device specific performance. This model is validated against the infusions into agarose gel outlined in earlier sections (section 5).

As expected, the porous substrate swells as a result of fluid administration, with the largest nodal displacements occurring in the smallest step length models and those infusions administered at the highest flow rates.

Concentration profiles of the administered solute corresponds to images and analysis of trypan blue infusions into transparent gels, which are validated brain mimics for porous flow. Higher flow rates produce lower distribution volumes as concentrations are focused in the substrate immediately adjacent to the catheter. Slower flow rates, or longer step lengths (which mimic a lower local flux) are associated with lower peak concentrations around the catheter, but higher concentrations at larger radial distances away from the catheter. This is consistent with empirical data collected from infusions of trypan blue into gel, where lower flow rates typically have larger distribution volumes.

This model is a useful starting point for modifications to infusion regimes, solutes, volumes or catheter design, which would complement *in vitro* and *in vivo* investigations. Further work is required to expand its usefulness as a predictive model for surgical planning, but is outside the scope of this project.

Take home message

Large shear stresses lead to large displacements in the substrate around the catheter and are the likely cause of reflux. Limiting the infusion flow rate or volume, coupled with an understanding of the step length for a specific patient's anatomy can optimise implanted catheter performance.

Slower peak infusion flow rates have larger distribution volumes due to a low concentration penumbra surrounding the higher concentration core. Flow rates and catheter dimensions should be considered along-side infusate characteristics such as natural transportation (e.g. viral vectors) following initial infusion, useful half-life, receptor binding and losses to optimise distribution and delivery.

7 Longitudinal study of inflammatory reaction to a chronically implanted catheter

7.1 Motivation

Following the development of the RSC for the *first-in-man* study through a series of initial publications (Gill *et al.*, 2013; Barua *et al.*, 2013b), a fuller understanding of the performance characteristics of this device has been created empirically (see sections 4, 5&6).

These studies have focused on lab-based investigations in gel or acute performance in non-clinical studies. In service however, chronically implanted catheters will deliver therapies repeatedly over months or years depending on the indication. Observations made within the first-in-man study noted a large variation between the short term and long-term performance within and between subjects, with more or less retention of the infused fluids within the target structure (Figure 3-28). Local tissue reaction, including the formation of a glial scar around the implanted catheter, may have contributed to the deterioration of infusate retention in some subjects.

To better optimise the chronic aspect of permanently implanted devices, a fuller understanding of the micro environment around the implanted catheters is required with emphasis on how this changes over time and in response to repeat delivery of fluids.

7.2 Introduction

To evaluate the changing nature of the microenvironment around the implanted catheters a longitudinal implantation study in the rodent model was performed. The rodent model was selected due to its previous use in investigational CED trials, low purchase and maintenance cost and stable skull size over the study period. The clinical sized catheters were too large for this model however and a body of design and manufacture work was required to miniaturise a re-accessible catheter which used the same materials as the clinical device.

A pilot study was undertaken ahead of the primary study to de-risk the surgical procedure and refine the design of the implanted devices to ensure the longevity required for repeated access over three months.

Finally, a longitudinal study in 22 Wistar rats was performed. The aim of this study was to create a baseline data set on the biological reaction to the catheter and determine whether monthly intermittent CED infusions, mirroring those performed in clinic, exacerbated the cellular response leading to scar tissue formation around the implanted catheters.

7.3 Materials and methods

7.3.1 Miniaturised catheter system manufacture

Bespoke aluminium injection mould tools were designed and machined to fit a vertical plunge injection mould machine (MCP 100 KSA semi-automatic injection moulder, MCP group, UK). Carbothane tubes (Lubrizol Lifesciences, The Lubrizol Corp., Ohio, USA) were provided from the stock of clinical devices by Renishaw plc.

Titanium, subcutaneous access ports were designed and machined at Renishaw plc.

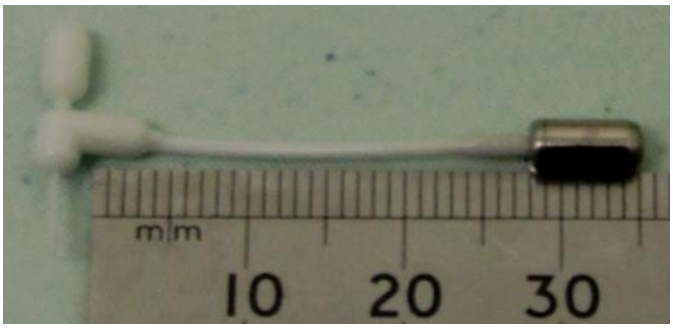

Figure 7-1. Miniaturised catheter system prior to implantation.

All devices were packaged, double bagged and sealed before being sterilised using gamma radiation (25kGy minimum radiation level, Steris AST, Daventry, UK).

Catheter and port elements were assembled in theatre prior to implantation (Figure 7-1).

A detailed description of the device development is provided in the discussion section below.

7.3.2 Roles and responsibilities

The author acknowledges the multidisciplinary nature of this aspect of the project, with assistance provided in the undertaking of the animal sourcing, husbandry, surgery and immunohistochemistry. The author's role was limited to study design, surgical support, device manufacture, histological slide preparation and image processing.

7.3.3 Anaesthesia

Surgical procedures were performed in accordance with the Animals (Scientific Procedures) Act (1986) under specific UK Home Office project and personal licences.

22 Wistar rats were sourced weighing between 425-550g at baseline. Isoflurane gas was used to sedate and anaesthetise the animals before and during the implantation procedures and intramuscular post-operative analgesia was provided. Subjects were weighed at least weekly throughout the study period, with increased frequency around the surgery and re-access infusions.

7.3.4 Surgical procedures

Single lumen polyurethane catheter systems were stereotactically implanted into the striatum (Figure 7-2) of each subject (0 mm A/P (on Bregma), ±3 mm L/R, depth: 5 mm from Bregma) using a bespoke adapter to a standard rodent fixation frame (David Kopf Instruments, CA, USA). The striatum was selected as a large grey matter structure which was also used in the first-in-man clinical trial. Catheters were anchored using UV cure gel placed around the moulded hub and a bone anchored stainless steel screw which provided rigid fixation as the gel alone would separate from the skull when wet.

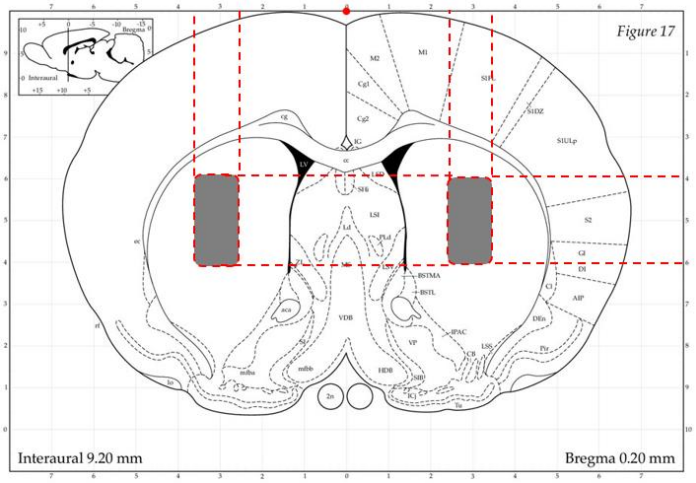

Figure 7-2. Anatomical atlas of the rat brain with target region of the catheter tips in striatum highlighted.

While catheters were bilaterally implanted into the left and right striatum, only the left catheter was connected to a subcutaneous port, providing the active catheter for intermittent delivery of fluid. All catheters in the right hemisphere were left inactive as controls to investigate immune response only.

The ports were housed in a silicone casing which was sutured into the loose tissue at the back of the neck, minimising subcutaneous movement of the device and aiding re-access.

Subjects were randomised following surgery into one of four groups (containing 4 to 6 subjects) based on duration of treatment before sacrifice; 14, 30, 60 and 90 days (groups 1-4 respectively).

7.3.5 Intermittent infusions

Intermittent infusions were scheduled throughout the pilot and the primary study.

Monthly infusions (30, 60 and 90days) were used to mimic clinical administrations of drug or placebo used in the clinical trial.

A 5 µl infusion volume was appropriately selected, scaling down the clinical volume to suite the model. The 5 µl infusion of artificial cerebrospinal fluid (aCSF) was administered at 0.5 µl/min, to achieve convection-enhanced delivery, into the active catheters prior to completion of the surgery and at each re-access time point.

All re-accesses were performed under isoflurane induced anaesthesia with the ports being surgically exposed and cleaned prior to needle penetration and infusion.

7.3.6 Terminations and preparation of histological sections for assessment

After 14 days following surgery (group 1) or following the monthly infusion of aCSF, subjects received a terminal intraperitoneal injection of sodium pentobarbital (Euthatal) (1 ml) according to their group allocation.

Subjects were then transcardially perfused with a prewash of 0.1M phosphate buffered solution (PBS, pH7.3) for 2 minutes using a peristaltic pump (50 ml/min), which was immediately followed by 4 % paraformaldehyde solution (PFA, pH7.3, Fisher Scientific, Loughborough UK) for 5 mins at the same rate.

Brains were removed, post-fixed in 4 % PFA for 4 hr and transferred to 30 % sucrose solution in PBS until cryosectioning (minimum 48 hours).

Cryostatically cut sections are typically thicker, require less work to produce and due to the absence of a dehydrating process (used in wax embedding) are subject to less shrinkage.

Brains were mounted onto a freezing-stage microtome (Leitz, Wetzlar) and sectioned on the axial plane at 30 μm thickness. Sections within the vertical limits of the striatum were preferentially collected and stored in 1:12 series in anti-freeze at -20 °C.

7.3.7 Immunohistochemical staining

Tissue sections were immunohistochemically stained as follows;

- **H&E (Hematoxylin and Eosin);** Used to visualise cell nuclei and general tissue morphology
- **GFAP (Glial Fibrillary Acidic Protein);** stain for protein expressed by glial cells and is the main constituent of intermediate filaments in differentiated astrocytes
- **Ionized calcium-binding adapter molecule 1 (IBA-1);** microglia stain

DAB (3,3'-diaminobenzidine) was used as the chromagen to visualise the specific cell types under light microscopy (GFAP and IBA-1).

All histological stains were performed as a single batch (per stain) and samples were randomised to minimise the risk of systematic or environmental errors.

7.3.8 Image processing

Brain tissue sections were visualised on glass slides beneath a light microscope (Leica, DFC 310 FX, 11547002). Photographs of the circular catheter track and the surrounding tissue were taken at 5x and 10x magnification.

Images were individually imported into Matlab 9.2 (The Mathworks, Inc., Natick, Massachusetts, United States) for image processing, quantification of stained pixels in each image and comparison between sample groups.

The image processing steps were as follows. A script was generated to undertake the repeat steps of import, calibration, thresholding, ellipse placement, segmentation then finally pixel quantification.

After importation, each image was calibrated using the micron scale overlaid automatically by the Leica software.

Overlaid ellipses were manually adjusted to identify the centre point of the catheter tracks. RGB images were converted to greyscale and image thresholding was consistently set for all subjects at 0.65. This created a binary image of the stained cells and allowing direct comparison between samples.

The thresholding value selected was based on a visual assessment of a sample of the segmented images. Binary images were assessed as representing the underlying stained tissue slide. Where the level was too high or low this would incorporate or discount excess stain. The value of 0.65 was selected as the thresholding value, and all images were processed to provide a direct comparison between slides.

The number of stained pixels were normalised per unit area.

Concentric ellipses, originating at the centre of the manually placed ellipse were overlaid onto the segmented image. Concentric ellipses were placed at 50μm increments emanating away from the catheter-tissue boundary, as previously described (Hayn, Deppermann and Koch, 2017).

7.3.9 Statistical analysis

A paired Student's t-test (95 % confidence level) was used to assess the difference in the reaction between left and right hemispheres within each subject at each time point. An ANOVA analysis was used to identify whether there was a significant difference in the level of GFAP or IBA-1 stain over the duration of the study.

7.4 Results

7.4.1 Surgical procedure

The surgical procedure was well tolerated with anaesthesia, implantation, infusion and recovery taking ~1hr. Manual removal of the guidance hub from the main body of the implantable catheter hub was performed using an electric hot knife (Hellermann GmbH) and PEEK screws were abandoned in favour of stainless steel screws to aid anchoring the UV cure glue.

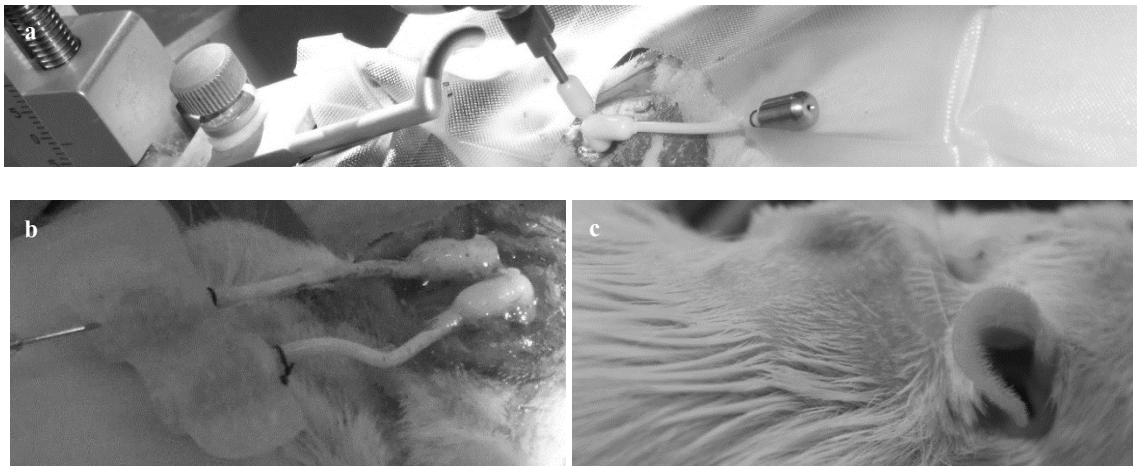

Figure 7-3. a) stereotactic implantation of the catheter and port assembly, b) final implant arrangement with silicone port housing shown (left), c) implanted system following recovery prior to a re-access (hence hair removal).

7.4.2 Re-access infusions

Re-access infusions took ~30-40minutes to complete, with each subject recovering well and maintaining growth throughout the study (Figure 7-4a-c). Some skin erosion around the tips of the silicone housing was noted towards the end of the pilot study which was revised using a more curved housing design in the primary study. While this improved device longevity, some subjects continued to experience some skin erosion of the housing over the course of the primary study. Further development would be required to ensure acceptable longevity of the housing.

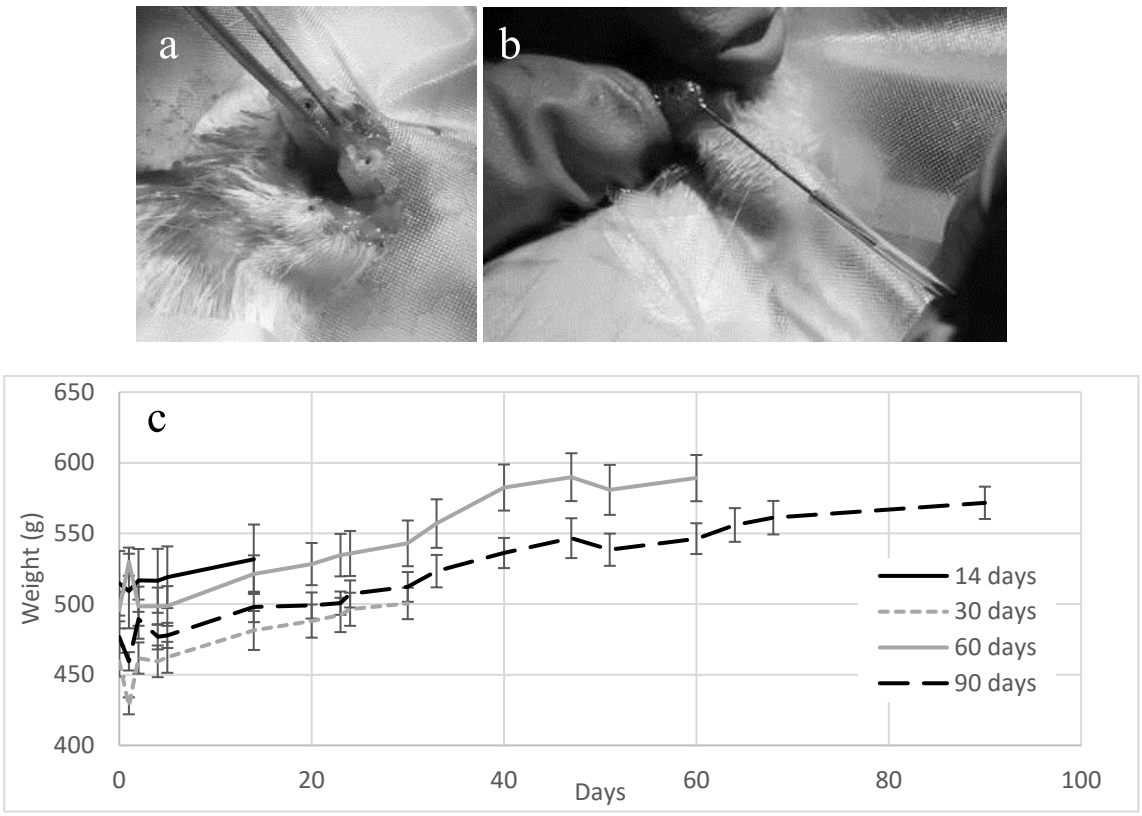

Figure 7-4. Intermittent infusions, a) exposure of re-access port for cleaning ahead of fluid delivery, b) insertion of administration set needle into the subcutaneous port, c) weight measurement chart for 90 day study, Error bars denote SEM.

In a single pilot study subject a unilateral infusion of Indian ink was used to aid visualisation during cryosectioning of the brain and confirm device function (Figure 7-5).

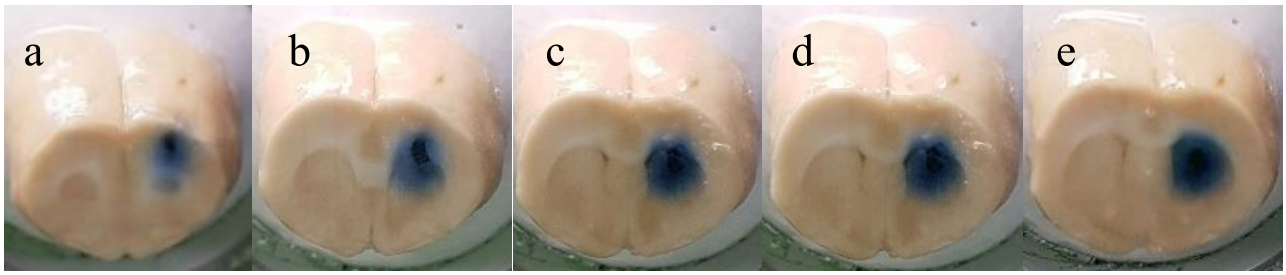

Figure 7-5. Convection-enhanced delivery of Indian ink into left striatum.

Take home message

Repeated access into the rodent is typically performed using multiple injections which require numerous surgeries and penetrations of the brain tissue. Intermittent infusions in the rodent model using a miniaturised re-accessible catheter system are both possible and safe.

7.4.3 Immunohistochemical (IHC) analysis

7.4.3.1 IHC (primary study): H&E

Within the first 14days following implant, a dense cluster of cells can be seen surrounding the catheter track. Leucocytes and microglia have migrated to the catheter-tissue interface, consistent with the expected inflammatory response to injury.

Tissue appeared normal with no signs of tearing or trauma beyond the formation of the catheter track. There were signs of minor haemorrhages as expected along the catheter track. Levels of trauma were minimal, despite the relatively large catheter size for this model.

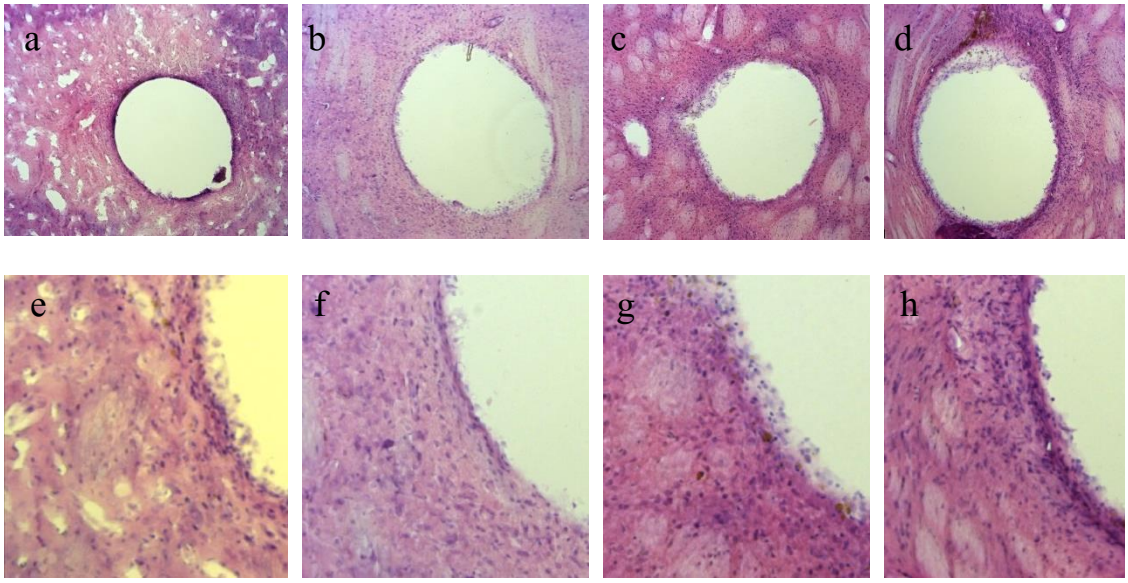

Figure 7-6. H&E: Example set of histological sections which display a representative reaction in the tissue around the catheter track post implant; a) 14days, b)30 days, c) 60days, d) 90days, and magnified images of the lower left quadrant of the catheter track; e) 14days, f)30 days, g) 60days, h) 90days.

7.4.3.2 IHC (primary study): GFAP

An assessment of sample sections from the pilot study subjects confirmed that discrete identification of GFAP stained activated astroglia would not be possible as the fibrils of the glia interweave and become so entangled it is not possible to differentiate them.

As previously described, the quantity of GFAP stained tissue per unit area was therefore assessed following image processing. Assessments were performed as a function of distance from the catheter-tissue interface in 50 µm radial increments. Values were collated into groups and averages plotted with standard error of the mean

(SEM) shown (Figure 7-7). As expected, visual assessment of the immunohistochemically stained sections confirmed a deeper stain at the catheter-tissue interface (Figure 7-8). At 14 days post implant the GFAP staining was most abundant at the catheter interface (30±8 % SEM). The magnitude of the reaction becoming incrementally less with every 50 µm step away from the interface. Unexpectedly, at 1 month post implant there was a significant and widespread reduction in the depth of GFAP staining at all distances from the interface, with the largest reaction once again at the interface but the average having significantly dropped to 13±2 % ($F(3,38)=7.21$ ($p<0.001$).

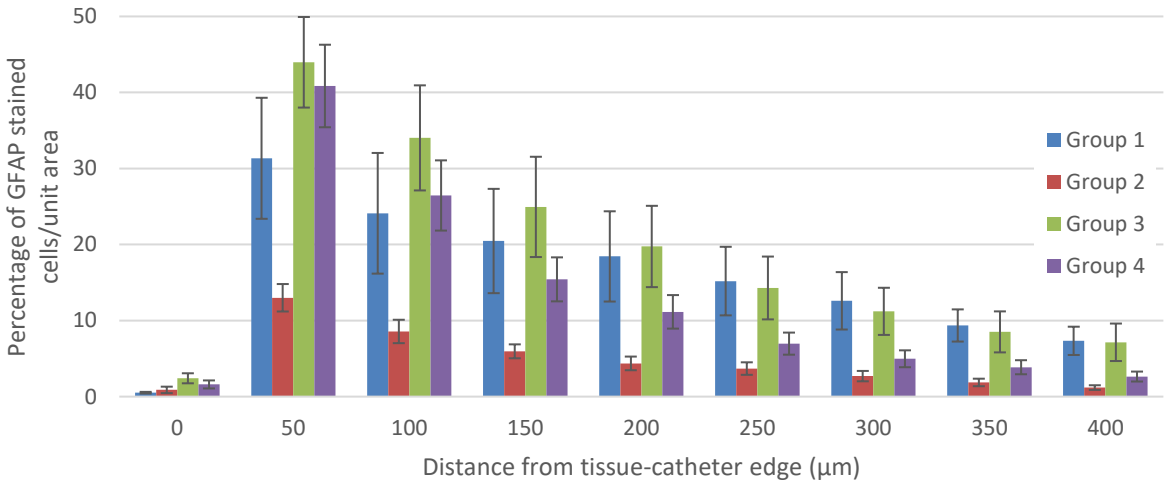

Figure 7-7. Percentage of DAB-GFAP stained cells per unit area radially propagating away from the edge of the catheter track (0µm) at 14days-90days post implant. 0µm increment indicates the cellular reaction within tissue void of the catheter track (error bars denote SEM).

Two months following implant, the average area of GFAP stained tissue was elevated above that at 14days post implant (44±6 % at the interface). The level of GFAP staining was not significantly different between 60 and 90 days ($p>0.05$) at any distance up to 400µm away from the interface.

There was no significant difference ($p<0.05$) in any group, in the level of GFAP staining between the left (active) and right (control) hemispheres at any time point.

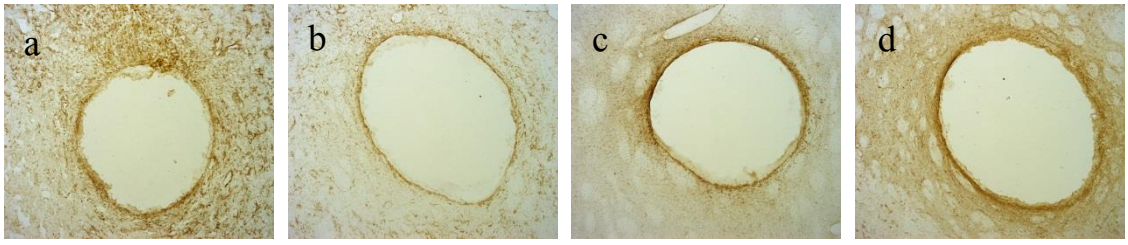

Figure 7-8. GFAP: Example set of histological sections which display a representative reaction in the tissue around the catheter track post implant; a) 14days, b)30 days, c) 60days, d) 90days.

7.4.3.3 IHC (primary study): IBA-1

Tissue stained by IBA-1 was also quantified per unit area following image processing with assessments performed as a function of distance from the catheter-tissue interface in 50µm radial increments. Values were collated into groups and averages plotted with standard error of the mean (SEM) shown (Figure 7-9).

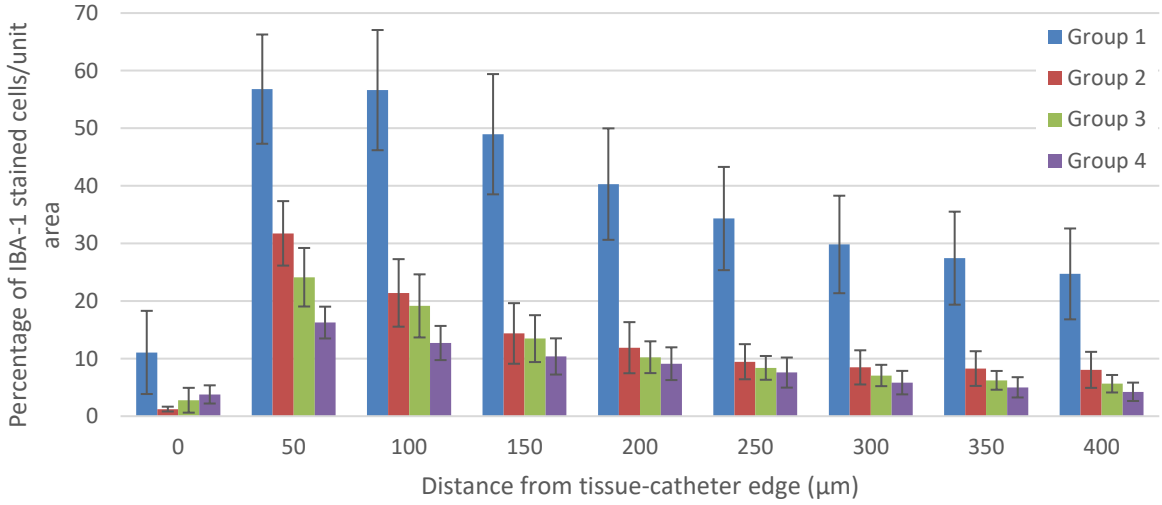

Figure 7-9. Percentage of DAB-IBA-1 stained cells per unit area radially propagating away from the edge of the catheter track (0µm) at 14days-90days post implant (error bars denote SEM).

IBA-1 levels were consistently higher at the catheter-tissue interface (Figure 7-10) with a numerical reduction in the average reaction per unit area emanating radially from the catheter track at each time point. Over the course of the investigatory period a significant drop in the microglia at the interface occurs ($p<0.05$) which is marked between 14 and 30 days post implant where the average volume of stained cells per unit area drops from 57±9 %(SEM) to 32±6 %.

There was no significant difference ($p<0.05$) in any group, in the level of IBA-1 staining between the left (active) and right (control) hemispheres at any time point.

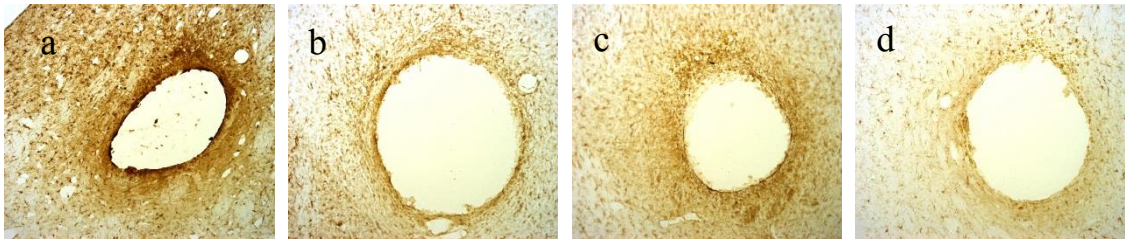

Figure 7-10. IBA-1: Example set of histological sections which display a representative reaction in the tissue around the catheter track post implant; a) 14days, b)30 days, c) 60days, d) 90days.

7.5 Discussion

7.5.1 Development of a miniaturised catheter

To create a baseline set of data on a chronically implanted catheter a miniaturised catheter using the same materials as the clinical catheter was developed.

7.5.1.1 User and Design requirements

Following an initial discussion with Dr Alison Bienemann (Fellow of Research, Functional Neurosurgery Research Group, Bristol University) a basic model was developed for a single channel, bilateral re-access system (Figure 7-11).

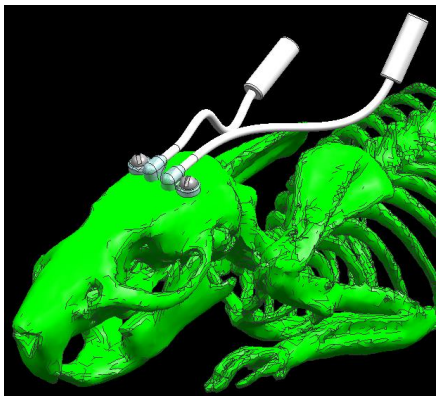

Figure 7-11. Initial model of bilateral single channel re-access system for the rodent model.

With the model as a discussion point a more detailed set of user and design requirements were developed (Table 7-1).

In the rodent model a clinical sized, three tube RSC was not feasible due to the size of the large guide tubes (1.7 mm OD). Further, at a total depth of 4-5 mm into the brain, additional guidance tubes were not felt to be necessary. It was necessary however to include a 90^{o} bend into the design to tunnel the tubing to a connector on the dorsal aspect of the subjects.

Table 7-1. User and design requirements for a permanently implantable rodent catheter system and initial design specification.

User Requirements	Design requirements	Design specification
Easy to implant using stereotactic frame (e.g. Kopf frame)	Include guidance feature to interface with stereotactic surgical frame	Vertically aligned, removable, orientation hub
Can target the striatum	Can be cut to a predetermined length based on species atlas	Minimum straight catheter length of 5 mm
Does not cause skin erosion	Low, smooth profile design	Maximum height of 3 mm
Must be securely anchored to minimise harm	Include features to screw device to skull	Screw down tabs
Intermittent re-accessed by cutting down onto an access port	Sealed, implantable re-access port positioned on dorsal aspect at base of neck	-Sealed Titanium connector within integral silicone seal -30 mm of 1.3 mm OD flexible Carbothane tubing to connect port to catheter
Must be biocompatible	Must use same materials as clinical RSC and percutaneous port	Barium filled Carbothane to be used for moulding and tubing Titanium (grade 5 - Ti 6Al4V) and silicone to be used for connector
Must be implantable for minimum of 3 months	No glue joints	Moulded component over extruded lines

7.5.1.2 Design and manufacture

Prior to commitment to a final design, a rudimentary injection moulding tool was used to investigate the moulding of internal 90^{o} bends, while maintaining fluid patency of the catheter as this challenging feature was novel beyond the clinical RSC design.

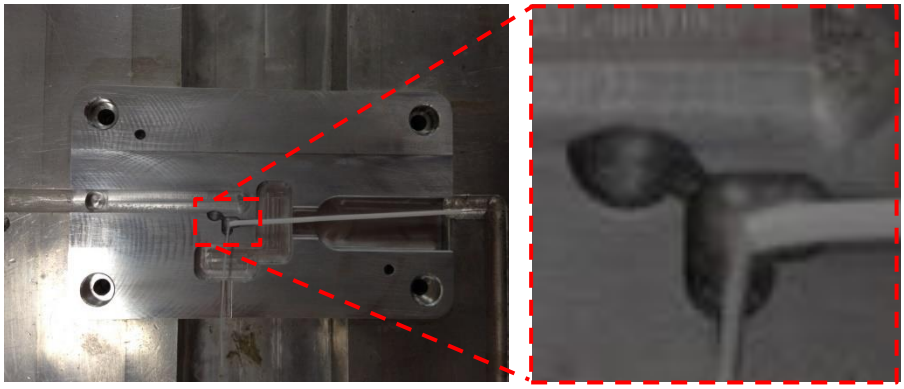

Figure 7-12. Development injection mould tool for 90^{o} inclusive designs.

Wire was placed within the tubing and bent to match the tool form. Optimisation of the internal guide rod diameter was required to ensure wire removal with fluid pressure tests used to ensure continued function (Figure 7-13).

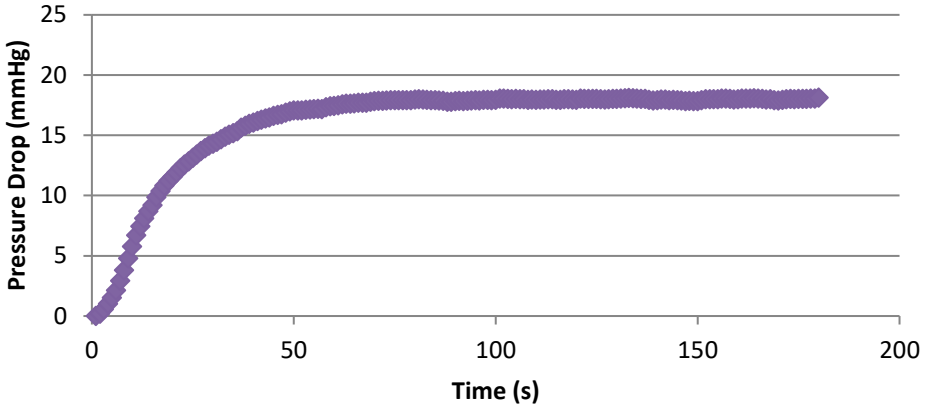

Figure 7-13. Example line pressure evaluation for miniaturised catheter.

With a manufacturing method confirmed, the final design was updated and a new injection mould machined (Figure 7-14b). Components were manufactured, bagged and sterilised prior to implantation.

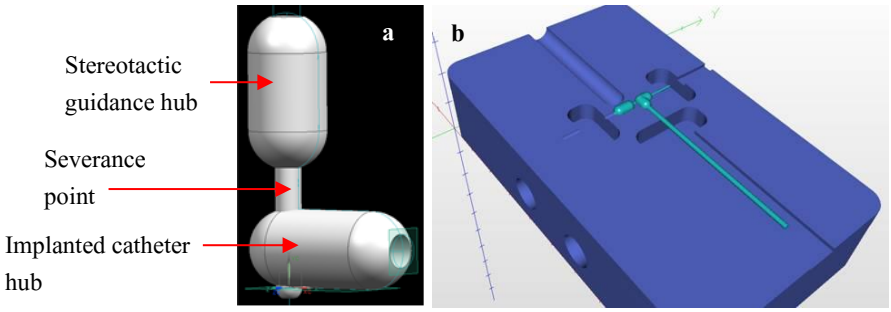

Figure 7-14. a) CAD design of catheter and b) injection moulding tool.

7.5.1.3 Refinement

The pilot study was successfully completed with intermittent re-accesses performed every 2 weeks in study subjects prior to termination. Subjects recovered well from surgery and re-accesses and continued to gain weight throughout the experiment.

Surgical stereotactic tools performed acceptably with no further changes required to progress to the primary longitudinal study. The introduction of an electric hot knife made severance of the stereotactically guided catheter hub from the implanted portion both possible and transferred a low force onto the subject and implant.

Minor modifications to the catheter were required to aid handling during surgery. A dome head feature was added to enable handling with forceps.

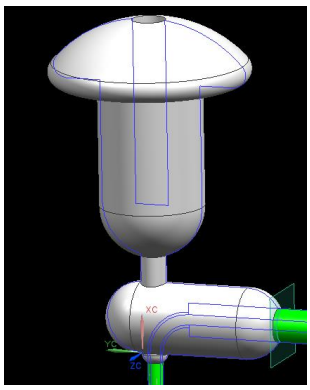

Figure 7-15. Revised design of the small animal model (SAM) catheter system following a design review and development of the form to improve on the usability of the device.

An increased curvature was added to the silicone port housing to minimise the risk or erosion over longer implantation periods.

The pilot study provided first-hand experience in implanting this novel catheter system. In addition to the opportunity to refine several aspects of design that may improve outcomes and de-risk a longer implantation study.

7.5.2 Tissue response to implant and CED infusions

The miniaturised catheter and subcutaneous access port developed for this study were successfully deployed to conduct monthly intermittent infusions in the rodent model. Subjects tolerated both the surgical procedures and the monthly re-accesses, with overall weight gain throughout the study with small, expected dips around the time of surgery and re-access.

While tissues naturally resides in a state of homeostasis, in response to traumatic injury, or more specifically injury following implantation of medical devices, a cascade of signalling cytokines drive the immune response through the stages of acute and chronic inflammation, ultimately leading to the formation of a fibrous capsule around the device (Anderson, 2001; Kuhn, 2005; Fawcett and Asher, 1999).

Within the CNS the fibrous capsule is formed by activated astroglia, which become hypertrophic in response to injury, dramatically increasing the number of their prominences. As a syncytium of interwoven cells, astroglia are recruited from the area surrounding an injury and migrate to the site to aid in the formation of the glial scar (Hayn, Deppermann and Koch, 2017).

Previously, investigations of stab wounds in the rat cortex identified that, in the absence of an implanted device, a glial scar would form in approximately 35 days, and was associated with an increase in the tortuosity and volume fraction of tissue around the wound (Roitbak and Sykova, 1999). The duration required for the formation of the fibrous capsule around an implanted catheter to reach a state of equilibrium is poorly defined, and is likely linked to the unique stimulus provided by the combination of the device design, materials and the nature and quality of the surgical intervention (Tian *et al.*, 2006; Williams, 2008). The level of trauma should be as low as practicably possible, as excess trauma has been shown to exacerbate reflux away from the target area (White *et al.*, 2011a).

H&E staining of the histological sections around the catheter track (Figure 7-6), indicate a local immune response to the presence of the implanted catheter. Single nucleated immunogenic cells cluster around the catheter track in high numbers at all time points, but no multinucleated cells were visible which may have indicated frustrated phagocytosis, sometimes seen in chronic implants (Anderson, 2001).

Levels of microglia and activated astroglia were elevated at 14 days (Figure 7-7 & Figure 7-9). Microglia levels subsided and remained low between 30 -90days (Figure 7-9) while GFAP levels dropped significantly at 30days post implant, they rose again at 60days and remained elevated until the end of the study (90days). The high levels of microglia observed around the catheter track after 14 days of catheter implantation would be consistent with previous reports of injured CNS models, as the function of the microglia is to respond to acute injury by migrating in large numbers to aid in the phagocytosis of foreign material. The reduction in microglia at 30 days post implant would be expected in the absence of continued injury or bacterial infection at the site of the implant.

Like microglia, astroglia, typically responsible for the maintenance of neurons and the regulation of the blood brain barrier, respond to injury by becoming reactive, increasing their expression of GFAP and becoming hypertrophic, ultimately forming the glial scar. It is therefore unexpected that the levels of GFAP, after spiking at 14days post implant, drop significantly at 30 days. Astroglial cells are however, known to efficiently and adaptably respond to environmental stimuli, migrating to sites of injury and upregulating intermediate filament proteins (Pekny and Nilsson, 2005; Okada *et al.*, 2018). Phenotypic changes in the evolution of astroglia from reactive astrocytes to scar forming astrocytes has been recently shown in the spinal cord indentation model (Okada *et al.*, 2018) with scar forming astrocytes isolated from tissue samples 14 days after injury. It is possible that the downregulation of GFAP observed around 30 days, could be a phenotypic change occurring in the astroglia as they become scar forming astrocytes, or as they increase the number and interweaving of prominences to wall off the implanted catheter. This delayed change may be in response to the presence of the implanted catheter which would not have been present in the previously reported literature.

As this effect is seen across the whole group at 30 days, it is prudent to query if the batch could have been negatively affected by an environmental stimulus. Given the acceptable performance of both H&E and IBA-1 stains in these same samples however, and that all GFAP stained slides were randomly processed within a single batch, such errors are low risk. A repeat study, while outside the scope of this work, would help to confirm such findings and could be expanded to investigate phenotyping the reactive astroglia.

The absence of a significant difference in the level of reaction seen between left and right hemispheres at all time points which received an infusion (30-90 days), indicate that the act of performing intermittent infusions in the CNS does not exacerbate the glial scar in the rodent model. This is of value as chronically implanted catheters can be used from the time of implant without inducing a markedly different reaction to that of the implanted device alone.

It is however necessary to perform baseline infusion to assess the implanted performance of any indwelling system. The timeframe for such test infusions now appears more important, as glial scar formation may be delayed in chronically implanted catheters, beyond the 2-4weeks previously highlighted by investigations of stab wounds in the rat cortex (Roitbak and Sykova, 1999) and used in a clinical capacity within this group (Whone *et al.*, 2019a). 6-8weeks may provide a distribution pattern more consistent with repeat, chronic infusions as the glial scar appears to be more stable at this time point. This 90 day study remains relatively short in duration compared to the chronic, service life of permanently implanted delivery systems, but provides a snapshot of a period during which healing occurs post-surgery/ injury. The immune response within a diseased subject may be different as neurodegenerative diseases are proinflammatory conditions which may exacerbate any reaction seen.

We have previously attempted to maintain catheter systems in the porcine model with poor outcomes due to the rapid skeletal and muscular growth of the model which displaces cranially anchored systems (Bienemann *et al.*, 2012). While it was possible to modulate the infusion distributions by actively controlling the infusion regime, further work is required to optimise infusions in a more suitable, readily accessible large chronic model.

7.5.3 Conclusions

As expected, the implantation of a miniaturised clinical polyurethane catheter system in the rat model induced an inflammatory immune response. Levels of microglia and GFAP, indicative of activated astrocytes, were elevated 14 days post implant, most markedly at the interface with the implanted catheter system. Levels of microglia continued to subside throughout the study while levels of GFAP fluctuated. GFAP levels at the catheter interface dropped significantly at 30 days before rising and staying high from 60 days post implant. The elevated GFAP level at 60 and 90 days were not significantly different, which indicates the stabilisation of the astrogliotic scar around the implanted device.

Clinically, modulation of infusions in the first months following implantation is likely required due to the continually changing nature of the microenvironment around the catheter. Visualisation of the distribution morphology *in vivo* will enable active manipulation of the infusion regime until a stabilisation in the distribution can be achieved.

Further work is required to investigate the distribution and optimisation of chronically implanted catheters in a stable large animal model.

Take home message

Test infusions visible under MRI conditions to map the coverage of a prescribed infusion regime may not be an accurate reflection of long-term performance until the microenvironment has stabilised.

Chronic intermittent infusions may not become stable until 2 months after the implantation of the catheter system as the body adapt to the presence of the medical device.

8 Optimisation of a chronically implanted catheter for the delivery of therapeutics to the brain

8.1 General discussion of thesis

At the outset, this project did not seek to design a new drug delivery system for the brain.

Such a system had already been developed for use in a *first-in-man* study investigating the chronic, intermittent delivery of GDNF to the brain for the treatment of Parkinson's disease (Whone *et al.*, 2019b; Whone *et al.*, 2019a). This project therefore sought to use this unique data source to investigate long term implanted catheters in the brain to evaluate performance and opportunities to optimise delivery for neurodegenerative diseases.

As highlighted in section 2 above, this approach was multidisciplinary and multifaceted, pulling in components of research from modelling, to gel studies and *in vivo* experimentation with post infusion imaging and immunohistopathology. A schematic was initially provided which outlined the specific questions posed at the outset of each chapter (Figure 2-13). This schematic has been updated with the outcomes of each body of work, highlighting how these feed into the overarching problem of optimisation of delivery in chronically implanted catheters (Figure 8-1).

Over the course of five years, between 2012-2017, 41 patients received three test infusions containing a gadolinium-based contrast agent, 40 weeks apart, in addition to their monthly drug administrations. These test infusions were reviewed to assess retention of the therapeutic in the target anatomy, but also provide a unique opportunity to chart the initial and ongoing performance of the implanted system. Since this trial has finished, gadolinium has fallen out of favour due to evidence of asymptomatic retention of linear and macrocyclic gadolinium molecules within the brain tissues (Kanda *et al.*, 2014). This study therefore represents one of the few comprehensive studies where direct mapping of a contrast agent was used over an extended period of time.

Assessment of device performance must be disconnected from drug efficacy in the first instance, as the trial of GDNF failed to meet its primary endpoint. Performance can therefore be idealised as coverage of a target anatomy, with 100 % coverage and retention representing best case (though this is an oversimplification as coverage must ultimately be linked to clinical benefit or therapeutic affect).

Surgical plans were reviewed against assessments of infusate distributions in the target anatomy. From this review, surgical planning guidelines were created which identified requirements for the placement of this particular device (i.e. the guide tube tip should be placed in excess of 3 mm into the target anatomy boundary with the tip of the catheter equal distance from the boundary. The catheter should be placed within the boundary of the structure wherever possible while maintaining the longest step length possible to maximise coverage).

Such planning guidance has been previously published for other device types (Yin *et al.*, 2011), whose mode of action is unique to the device design. These guidelines for surgical placement of the RSC have been utilised in subsequent clinical trials investigating alternative proteins for the treatment of Parkinson's disease.

These guidelines represented the variables which correlated most with increased coverage of the target anatomy during the first test infusions. Additional observations highlighted the desire to minimise variables in clinical trial forced a fixed volume to be administered in all subjects. The large variation in target volume however resulted in a maximum theoretical coverage of 56-93 %, where allowing for variation in the infusion volume could provide a theoretical maximum of 100 % coverage.

Comparison between and within subjects' data was often difficult and compounded by variations including diagnostic imaging time. While difficult to control in centres where large pieces of capital equipment are a shared resource, maintaining infusion to scan time would enable direct and fair comparison of distribution data, empowering users to compare the quality in the distribution of therapeutic over time (where imaging signal correlates with drug dispersal). Limitations on the image acquisition time for clinical trials not utilising gadolinium is of even greater importance as the contrast between infused fluid and the surrounding tissue is lower. This recommendation was implemented in a subsequent clinical trial and helped maintain a degree of control over the variation between assessments of infusion distributions.

Observations of the second and third test infusions noted changes in several of the patients' distribution volumes and locations. While some subjects maintained very good coverage, others experienced increased levels of reflux, with retention in the target anatomy dropping significantly without any obvious cause. Further investigation of the environment around the catheter was required.

Also, the development of the catheter system on route to clinical trial focused on the use of the catheter with a fixed step length of 3 mm. Comparison to other catheter designs was favourable, resulting in the selection of the recessed step catheter for clinical trial use (Gill *et al.*, 2013). Within the trial however, surgical plans used step lengths between 12 and 35 mm, warranting further characterisation of the device with this new mode of action.

A review of brain mimic materials to assess the catheter concluded that while agarose gels were mechanically dissimilar to brain, the permeability and translucency of agarose meant it was more suitable for *in vitro* testing of the catheter than opaque hydrogels which lacked the correct permeability, despite being more mechanically similar to brain tissue (section 4).

Assessment of the RSC in both gels and *in vivo* models confirmed the controlled reflux action of the catheter over a pre-clinically and clinically useful range (3-18 mm).

It was also observed that the reflux inhibition feature of the catheter assembly becomes overwhelmed at excessive infusion volumes or flow rates but is dependent on the length of the step between the guide tube and the catheter tip. In this way, modifications to the distribution morphology can be achieved by changes to the physical

embodiment of the catheter (chiefly the step length) and how it is driven (peak flow rate, ramp time, infusion volume). The combination of which are an effective way to optimise acute delivery, maximising coverage of the target anatomy. Following these observations, reductions in the peak flow rates used were implemented clinically both in investigational and humanitarian cases.

The creation of a finite element analysis model aided in the interpretation of infusion distribution patterns observed empirically. Despite higher flow rates creating large concentration gradients at the catheter-tissue interface, the lower infusion rates achieve a larger distribution of solutes at a lower concentration level. These observations are helpful to understand why higher volumetric flow rates of infused trypan blue created smaller distribution volumes in gels, but also provide a starting point for the assessment of drug specific applications where half-life or clinically useful concentrations can be reviewed and modelled.

The observations within the clinical trial of infusion distributions changing location within the anatomy over time was assessed through a review of the micro environment around catheters over time within a longitudinal rodent study. No difference was observed in the immune response between catheters that received infusions and those that did not, suggesting that CED does not exacerbate the formation or extent of the gliotic sock which surrounds the implanted catheter. Interestingly gliosis, expressed as GFAP levels, was observed to drop around 1 month following implant before rising to a stable level from 2 months onward. This delayed scar stabilisation may account for differences observed between clinical cases where the first test infusion differs from both subsequent test infusions that appear more stable.

Phenotypic changes in the astroglial cells, from reactive astrocytes to scar forming astrocytes observed in spinal cord damage studies (Okada *et al.*, 2018), may account for the changes in GFAP levels, and possibly the migration of infusate from the site of the initial test infusion in some subjects as the level of gliosis would be linked to the extent of the trauma caused during surgery. Further analysis is required to both repeat and interpret this observation, however the recommendation to minimise trauma during device implantation is advantageous to minimise incidence of haemorrhage and oedema which negatively affect the predictability of infusion distributions (White *et al.*, 2011a). Extending the period between initial implant and test infusion to 2 months is also a recommendation which may provide more robust long-term prediction of distribution information (both coverage and location) where prescriptive infusion regimes are used in place of real time infusion assessment.

Further work to limit reflux development over time might include the integration (adhesion) of the catheter into the surrounding tissue, intervention in the immune response to injury, affecting the cascade of chemicals which instigate the formation of the gliotic sleeve around the device, or the delivery of a media to degrade the scar once formed (e.g. chondroitin sulphate inhibitor).

Optimisation of a chronically implanted catheter for intraparenchymal delivery of therapeutics to the brain

Q – How does a catheter perform when chronically implanted?

Chapter 3 – Evaluation of a first in man chronic, intermittent convection enhanced delivery system
Purpose: Characterise the performance metrics of the recessed step catheter design used *in vivo*
Outcomes:

- The RSC was used to successfully perform monthly, intermittent infusions over 80weeks
- Longest step lengths achieved from posterior trajectory with significant improvements in the coverage of target structures at the first test infusion
- As the RSC uses controlled reflux (instead of a point source distribution), a balance of implant placement variables is thought to provide the best opportunity for optimising coverage
- Improvements to future study design identified to minimise variation within and between subject's data
- Subjects putamen volumes were normally distributed
- While some patients maintained good coverage over the study, retention of infusate in target structure generally deteriorated over time, with no obvious cause identified on post implant scans

Q – What materials can be used as brain mimics to further develop knowledge of the catheter function in vitro?

Chapter 4 – Evaluation of brain mimics for catheter design evaluation
Purpose: Identify an optimal brain mimic to further evaluate the recessed step catheter
Outcomes:

- Both composite hydrogel mixtures evaluated were discounted from further use through poor distributions during in vitro testing
- Agarose gels were selected for further use despite limitations (dissimilarities in mechanical properties with brain tissue)

Q – How does changing the catheter infusion or dimensional variables affect the infusion distribution and how can this be used towards optimisation?

Chapter 5 – In vitro and in vivo characterisation of the recessed step catheter distributions
Purpose: Execution of infusion study in gels and pigs comparing distribution characteristics obtained when modifications are made to the catheter features or the way it is driven (infusion rates)
Outcomes:

- Increasing the step length elongates the infusion distribution cloud and narrows the width
- Increasing the flow rate decreases the distribution volume and increases the risk of reflux, which is most pronounced in short step length configurations

Q – Can an in-silico model of the recessed step catheter be created and used to verify the characteristics observed within in vitro gel studies, and later built in to planning or analysis software?

Chapter 6 – Modelling of the recessed step catheter
Purpose: Create a computational model of porous flow from a recessed step catheter
Outcomes:

- FEBio used to create a biphasic finite element model of solvent flow through a porous substrate with 3, 6, 12 and 18mm step lengths at 0.1, 0.3 and 0.6ml/hr flow rates.
- Distribution profiles match those obtained empirically in agarose gel studies, with changes in profile associated with dispersal of low concentrations of solute in the porous substrate
- Model can be further developed for predictive, planning or investigational purposes

Q – Is the permeability of the micro environment around the catheter negatively affected by the implantation of the catheter or the continued intermittent infusions and how could this affect chronic optimisation?

Chapter 7 – Longitudinal study of inflammatory reaction to a chronically implanted catheter
Purpose: investigate the inflammatory reaction *in vivo* comparing active and inactive catheters over 90 days post implant
Outcomes:

- No difference in amount of scaring after implant whether catheters were inert or infused through
- The marker for scar tissue (GFAP) formation dropped markedly at 30days, and may be linked to phenotypic changes in the astroglial cells (reactive to scar forming astrocytes)
- Delay to test infusions beyond 4weeks may provide a more stable environment for distribution assessments post implant

Figure 8-1; Schematic of thesis chapters with primary outcomes.

8.1.1 Thesis conclusions and opportunities for further work

An assessment of distribution data from a long term clinical trial, infusing GDNF at monthly intervals, directly into the brains of Parkinson's disease patients was performed. It was found that large variations in the coverage of the putamen existed at each test infusion (spaced 9 months apart). Trajectory of catheter insertion into the putamen was shown to have a significant effect on coverage, with a posterior approach providing the greatest distribution within the putamen.

A review of the planned and actual placement of the catheter and its reflux inhibiting features, revealed that in isolation, the placement did not provide improvements in the coverage of the target anatomy. When combined and weighted equally however, the depth into the structure of the inhibiting feature, the distance from the catheter tip to the boundary, the length of the catheter step and the placement within the midline of the anatomy, contributed to improvements in the coverage of the putamen. This finding was implemented directly in surgical guidance, stating that a balance of these factors was more important that maximising a single factor at the expense of the others.

These recommendations are however a hypothesis for improved performance and offer the opportunity for further work, reviewing the efficacy of the planned implant position against initial and ongoing coverage of the target structure.

The time following infusions that diagnostic MRIs are taken was found to positively affect coverage but also introduced variation which prevented fair comparison within a subject's chronological data set. A reduction in the window to acquire MRI scans was subsequently implemented in a follow up clinical trial from 2 hrs to within 30 minutes, but ideally as soon as possible.

A comparison between brain mimic materials for infusion and distribution assessments identified that composite hydrogels which match the mechanical, viscoelastic properties of brain, and which have been shown to be porous, are not permeable. Composite hydrogels containing polyvinyl-alcohol and phytagel at *5 %PVA/0.59 %PHY* and *6 %PVA/0.85 %PHY* ratios failed to provide predictable distributions which matched empirical *in vivo* data preventing their use as a model for catheter and infusion development. Agarose gel (0.6 % by weight) remains, on balance, the best choice due to its low cost, easy manufacture and disposal and optical transparency which permit real time monitoring of infusion distributions using standard lighting and photographic media. Further work is required to identify mechanically similar, permeable mimic materials which have the same characteristics as brain tissues.

A parametric study of the recessed step catheter and its use found that manipulation of the distribution shape could be achieved by modifications to a combination of the step length and peak infusion flow rate using the *controlled reflux* method. Generally, longer steps could induce longer and narrower distribution clouds but decreasing the infusion flow rate would maintain the form but increase the volume covered. Short step lengths (3-6 mm) induced spherical distribution patterns which were again positively affected by reductions in the flow rate. Increases in the infusion flow rate to 0.6 ml/hr (10 µl/min) induced uncontrolled reflux beyond the step feature, occurring in greater

frequency as the step length decreased. The longest of the step length investigated (18 mm) did not experience uncontrolled reflux even at the highest flow rate used. Further work is required to investigate step lengths and flow rates beyond those investigated here. Specifically, the 'controlled reflux' action of the RSC continued throughout the 3-18 mm step length, only failing to reach the guide tube at the lowest flow rates and longest step lengths. Further work is required to identify operational 'controlled reflux' combinations between flow rate and step length.

The larger distributions observed at lower flow rates, when other variables are kept constant, was proven to be due to the greater dispersion of a low concentration of solutes within a finite element model mimicking the delivery of a solution into a porous, brain like material. Further work is required to integrate this type of predictive model into the surgical planning workflow/ software, in addition to the integration of voxel specific attributes (e.g. differences in permeability, porosity, directionality from grey/ white matter, microvasculature or CSF sinks).The inflammatory response of the body to foreign materials (e.g. a catheter), intermittent delivery of fluid and duration of implantation was compared in a longitudinal rodent study. No difference was observed in the level of gliosis (scaring) around the catheter track at any time point suggesting that the formation of the gliotic sock is not exacerbated by performing convection-enhanced delivery. A reduction in the level of GFAP was noted around 1 months before rising to previous levels at 2 months and staying high until the end of the trial at 3 months. This reduction in GFAP, a marker of gliosis, occurred around the same time as test infusions of chronically implanted drug delivery systems are performed to assess baseline coverage values in patients. A prolonged healing period as astroglial cells change from reactive to scar forming astrocytes was hypothesised as a potential cause of the reduction in the marker. Such a fluctuation in the stability of the wound around the catheter track may account for the variations seen in the clinical distribution patterns observed in several cases, where distribution stabilised later than the first test infusion, one month following surgery. Further analysis is required to both repeat and interpret this observation. Assessment of the stability of infusions from one month onwards would also provide supplemental confirmation of the stability of the microenvironment around the catheter for implementation of ongoing infusion parameter setting (e.g. infusion volume per catheter, peak flow rates and ramp times, etc.).

Chronic, intermittent delivery of therapeutics to the brain for neurodegeneration or other neurological conditions (e.g. neuro-oncology, spinal cord injury, lysosomal storage disorders, etc) is now possible using long-term implanted catheters with reflux inhibiting features for infusate retention.

Optimisation of these catheters is however multifaceted.

Consideration must be given to all aspects of implantation, recovery and use to maximise coverage of the intended target anatomy both acutely and chronically.

- Delivery instrumentation must enable low trauma, accurate insertion which avoids micro and macro haemorrhage where possible to minimise the extent of the gliosis which forms naturally around the implant in response to injury.

- Surgical planning must place implants using prescribed, device specific guidelines, positioning the reflux inhibiting and delivery features optimally within the structure boundaries. The exact position will be a function of the desired infusion volume, anatomy tissue type, local anisotropy and step length when using the RSC.
- Patient specific algorithms to accurately predict distribution are limited by the resolution of medical diagnostic imaging, however patient specific infusion volumes could provide a simple means of optimising coverage for discrete target anatomy.
- Empirical, device specific performance is valuable as a starting point when developing therapies for specific conditions to minimise iteration
- Where real time imaging to drive each infusion is not financially or logistically feasible, test infusions can provide useful baseline information on position and volume of coverage, but due to the natural healing which can be delayed due to the presence of the implanted catheter, up to 2 months recovery time may be required, and test scans should ideally occur at similar time intervals during/ post infusions.
- While higher flow rates are clinically desirable to minimise the duration of visits for patients to healthcare establishments, this must be balanced against the increased risk of undesirable reflux or poor retention of infusates in the target anatomy. The peak flow rates used are device specific. Within the GDNF clinical trial, flow rates up to 5 µl/min were used successfully with the RSC, and *in vitro* experiments highlighted the increased risk of reflux using 10 µl/min with short step lengths. Such a flow rate may however be appropriate when using longer step lengths but will be target dependant.

With the continued use of diagnostic imaging, reduced costs and accessibility may further enable users to drive the implanted systems real-time, allowing further optimisation of each infusion on a patient specific basis.

9 References

Anderson, J. M. (2001) 'Biological Responses to Materials', *Annual Review of Materials Research,* 31(1), pp. 81-110.

Bankiewicz, K. S., Eberling, J. L., Kohutnicka, M., Jagust, W., Pivirotto, P., Bringas, J., Cunningham, J., Budinger, T. F. and Harvey-White, J. (2000) 'Convection-enhanced delivery of AAV vector in parkinsonian monkeys; in vivo detection of gene expression and restoration of dopaminergic function using pro-drug approach', *Exp Neurol,* 164(1), pp. 2-14.

Bankiewicz, K. S., Sudhakar, V., Samaranch, L., San Sebastian, W., Bringas, J. and Forsayeth, J. (2016) 'AAV viral vector delivery to the brain by shape-conforming MR-guided infusions', *J Control Release,* 240, pp. 434-442.

Barua, N. U., Hopkins, K., Woolley, M., O'Sullivan, S., Harrison, R., Edwards, R. J., Bienemann, A. S., Wyatt, M. J., Arshad, A. and Gill, S. S. (2014) 'A novel implantable catheter system with transcutaneous port for intermittent convection-enhanced delivery of carboplatin for recurrent glioblastoma', *J Drug Delivery*.

Barua, N. U., Lowis, S. P., Woolley, M., O'Sullivan, S., Harrison, R. and Gill, S. S. (2013a) 'Robot-guided convection-enhanced delivery of carboplatin for advanced brainstem glioma', *Acta Neurochir (Wien),* 155(8), pp. 1459-65.

Barua, N. U., Woolley, M., Bienemann, A. S., Johnson, D., Wyatt, M. J., Irving, C., Lewis, O., Castrique, E. and Gill, S. S. (2013b) 'Convection-enhanced delivery of AAV2 in white matter--a novel method for gene delivery to cerebral cortex', *J Neurosci Methods,* 220(1), pp. 1-8.

Barua, N. U., Woolley, M., Bienemann, A. S., Johnson, D. E., Lewis, O., Wyatt, M. J., Irving, C., O'Sullivan, S., Murray, G., Fennelly, C., Skinner, P. and Gill, S. S. (2013c) 'Intermittent convection-enhanced delivery to the brain through a novel transcutaneous bone-anchored port', *J Neurosci Methods,* 214(2), pp. 223-32.

Bauer, H. C., Krizbai, I. A., Bauer, H. and Traweger, A. (2014) '"You Shall Not Pass"-tight junctions of the blood brain barrier', *Front Neurosci,* 8, pp. 392.

Bear, J. (1988) *Dynamics of fluids in porous media.* New York: Dover.

Belova, E., Shaffer, C. L. and Trapa, P. E. (2017) 'Insights from mathematical modeling for convection-enhanced intraputamenal delivery of GDNF', *Med Biol Eng Comput*.

Bienemann, A., White, E., Woolley, M., Castrique, E., Johnson, D. E., Wyatt, M., Murray, G., Taylor, H., Barua, N. and Gill, S. S. (2012) 'The development of an implantable catheter system for chronic or intermittent convection-enhanced delivery', *Journal of Neuroscience Methods,* 203(2), pp. 284-291.

Bobo, R. H., Laske, D. W., Akbasak, A., Morrison, P. F., Dedrick, R. L. and Oldfield, E. H. (1994) 'Convection-enhanced delivery of macromolecules in the brain', *Proc Natl Acad Sci U S A,* 91(6), pp. 2076-80.

Brady, M. L., Raghavan, R., Singh, D., Anand, P. J., Fleisher, A. S., Mata, J., Broaddus, W. C. and Olbricht, W. L. (2014) 'In vivo performance of a microfabricated catheter for intraparenchymal delivery', *J Neurosci Methods,* 229, pp. 76-83.

Budday, S., Nay, R., de Rooij, R., Steinmann, P., Wyrobek, T., Ovaert, T. C. and Kuhl, E. (2015) 'Mechanical properties of gray and white matter brain tissue by indentation', *J Mech Behav Biomed Mater,* 46, pp. 318-30.

Chen, M. Y., Lonser, R. R., Morrison, P. F., Governale, L. S. and Oldfield, E. H. (1999) 'Variables affecting convection-enhanced delivery to the striatum: a systematic examination of rate of infusion, cannula size, infusate concentration, and tissue-cannula sealing time', *J Neurosurg,* 90(2), pp. 315-20.

Chen, Z. J., Broaddus, W. C., Viswanathan, R. R., Raghavan, R. and Gillies, G. T. (2002) 'Intraparenchymal drug delivery via positive-pressure infusion: experimental and modeling studies of poroelasticity in brain phantom gels', *IEEE Trans Biomed Eng,* 49(2), pp. 85-96.

Chen, Z. J., Gillies, G. T., Broaddus, W. C., Prabhu, S. S., Fillmore, H., Mitchell, R. M., Corwin, F. D. and Fatouros, P. P. (2004) 'A realistic brain tissue phantom for intraparenchymal infusion studies', *J Neurosurg,* 101(2), pp. 314-22.

Cheng, S. and Bilston, L. E. (2007) 'Unconfined compression of white matter', *J Biomech,* 40(1), pp. 117-24.

ClinicalTrials.gov (2015) *National Institutes of health, clinicaltrials.gov - A service of the U.S. National Institutes of Health*. Online: National Institutes of Health. Available at: https://clinicaltrials.gov/ct2/home (Accessed: 10August2015 2015).

Dawe, R. and Erickson, R. (2006) 'Convection-enhanced delivery into agarose gel brain tissue phantoms'.

Debinski, W. and Tatter, S. B. (2009) 'Convection-enhanced delivery for the treatment of brain tumors', *Expert Rev Neurother,* 9(10), pp. 1519-27.

Dorsey, E. R., Constantinescu, R., Thompson, J. P., Biglan, K. M., Holloway, R. G., Kieburtz, K., Marshall, F. J., Ravina, B. M., Schifitto, G., Siderowf, A. and Tanner, C. M. (2007) 'Projected number of people with Parkinson disease in the most populous nations, 2005 through 2030', *Neurology,* 68(5), pp. 384-6.

Elenes, E. Y., Rausch, M. K. and Rylander, C. G. (2019) 'Parametric Study of the Design Variables of an Arborizing Catheter on Dispersal Volume Using a Biphasic Computational Model', *Journal of Engineering and Science in Medical Diagnostics and Therapy,* 2(3), pp. 031002-031002-9.

Fawcett, J. W. and Asher, R. A. (1999) 'The glial scar and central nervous system repair', *Brain Res Bull,* 49(6), pp. 377-91.

Fick, A. (1855) 'Ueber Diffusion', *Annalen der Physik,* 170(1), pp. 59-86.

Forte, A. E., Galvan, S., Manieri, F., Rodriguez y Baena, F. and Dini, D. (2016) 'A composite hydrogel for brain tissue phantoms', *Materials & Design,* 112(Supplement C), pp. 227-238.

Franceschini, G., Bigoni, D., Regitnig, P. and Holzapfel, G. A. (2006) 'Brain tissue deforms similarly to filled elastomers and follows consolidation theory', *Journal of the Mechanics and Physics of Solids,* 54(12), pp. 2592-2620.

Gash, D. M., Zhang, Z., Ovadia, A., Cass, W. A., Yi, A., Simmerman, L., Russell, D., Martin, D., Lapchak, P. A., Collins, F., Hoffer, B. J. and Gerhardt, G. A. (1996) 'Functional recovery in parkinsonian monkeys treated with GDNF', *Nature,* 380(6571), pp. 252-5.

Geuzaine, C. and Remacle, J.-F. (2009) 'Gmsh: A 3-D finite element mesh generator with built-in pre- and post-processing facilities', *International Journal for Numerical Methods in Engineering,* 79(11), pp. 1309-1331.

Gill, S. S., Patel, N. K., Hotton, G. R., O'Sullivan, K., McCarter, R., Bunnage, M., Brooks, D. J., Svendsen, C. N. and Heywood, P. (2003) 'Direct brain infusion of glial cell line-derived neurotrophic factor in Parkinson disease', *Nat Med,* 9(5), pp. 589-95.

Gill, T., Barua, N. U., Woolley, M., Bienemann, A. S., Johnson, D. E., Sullivan, S. O., Murray, G., Fennelly, C., Lewis, O., Irving, C., Wyatt, M. J., Moore, P. and Gill, S. S. (2013) 'In vitro and in vivo testing of a novel recessed-step catheter for reflux-free convection-enhanced drug delivery to the brain', *J Neurosci Methods,* 219(1), pp. 1-9.

Gimenez, F., Krauze, M. T., Valles, F., Hadaczek, P., Bringas, J., Sharma, N., Forsayeth, J. and Bankiewicz, K. S. (2011) 'Image-guided convection-enhanced delivery of GDNF protein into monkey putamen', *Neuroimage,* 54 Suppl 1, pp. S189-95.

Guarnieri, M., Carson, B. S., Sr. and Jallo, G. I. (2008) 'Catheters for chronic administration of drugs into brain tissue', *Methods Mol Biol,* 437, pp. 109-17.

Hayn, L., Deppermann, L. and Koch, M. (2017) 'Reduction of the foreign body response and neuroprotection by apyrase and minocycline in chronic cannula implantation in the rat brain', *Clin Exp Pharmacol Physiol,* 44(2), pp. 313-323.

Ivanchenko, O., Sindhwani, N. and Linninger, A. (2010) 'Experimental techniques for studying poroelasticity in brain phantom gels under high flow microinfusion', *J Biomech Eng,* 132(5), pp. 051008.

Kanda, T., Ishii, K., Kawaguchi, H., Kitajima, K. and Takenaka, D. (2014) 'High signal intensity in the dentate nucleus and globus pallidus on unenhanced T1-weighted MR images: relationship with increasing cumulative dose of a gadolinium-based contrast material', *Radiology,* 270(3), pp. 834-41.

Kim, J. H., Mareci, T. H. and Sarntinoranont, M. (2010) 'A voxelized model of direct infusion into the corpus callosum and hippocampus of the rat brain: model development and parameter analysis', *Med Biol Eng Comput,* 48(3), pp. 203-14.

Kowal, S. L., Dall, T. M., Chakrabarti, R., Storm, M. V. and Jain, A. (2013) 'The current and projected economic burden of Parkinson's disease in the United States', *Mov Disord,* 28(3), pp. 311-8.

Krauze, M. T., Saito, R., Noble, C., Tamas, M., Bringas, J., Park, J. W., Berger, M. S. and Bankiewicz, K. (2005) 'Reflux-free cannula for convection-enhanced high-speed delivery of therapeutic agents', *J Neurosurg,* 103(5), pp. 923-9.

Kuhn, L. T. (2005) '6 - BIOMATERIALS A2 - Enderle, John D', in Blanchard, S.M. and Bronzino, J.D. (eds.) *Introduction to Biomedical Engineering (Second Edition)*. Boston: Academic Press, pp. 255-312.

Kumpulainen, E., Kokki, H., Halonen, T., Heikkinen, M., Savolainen, J. and Laisalmi, M. (2007) 'Paracetamol (acetaminophen) penetrates readily into the cerebrospinal fluid of children after intravenous administration', *Pediatrics,* 119(4), pp. 766-71.

Kunwar, S., Chang, S., Westphal, M., Vogelbaum, M., Sampson, J., Barnett, G., Shaffrey, M., Ram, Z., Piepmeier, J., Prados, M., Croteau, D., Pedain, C., Leland, P., Husain, S. R., Joshi, B. H. and Puri, R. K. (2010) 'Phase III randomized trial of CED of IL13-PE38QQR vs Gliadel wafers for recurrent glioblastoma', *Neuro Oncol,* 12(8), pp. 871-81.

Lam, M. F., Foo, S. W., Thomas, M. G. and Lind, C. R. (2014) 'Infusion-line pressure as a real-time monitor of convection-enhanced delivery in pre-clinical models', *J Neurosci Methods,* 221, pp. 127-31.

Lam, M. F., Thomas, M. G. and Lind, C. R. (2011) 'Neurosurgical convection-enhanced delivery of treatments for Parkinson's disease', *J Clin Neurosci,* 18(9), pp. 1163-7.

Lang, A. E., Gill, S., Patel, N. K., Lozano, A., Nutt, J. G., Penn, R., Brooks, D. J., Hotton, G., Moro, E., Heywood, P., Brodsky, M. A., Burchiel, K., Kelly, P., Dalvi, A., Scott, B., Stacy, M., Turner, D., Wooten, V. G., Elias, W. J., Laws, E. R., Dhawan, V., Stoessl, A. J., Matcham, J., Coffey, R. J. and Traub, M. (2006) 'Randomized controlled trial of intraputamenal glial cell line-derived neurotrophic factor infusion in Parkinson disease', *Ann Neurol,* 59(3), pp. 459-66.

Langford, R. A., Hogg, M., Bjorksten, A. R., Williams, D. L., Leslie, K., Jamsen, K. and Kirkpatrick, C. (2016) 'Comparative Plasma and Cerebrospinal Fluid Pharmacokinetics of Paracetamol After Intravenous and Oral Administration', *Anesth Analg,* 123(3), pp. 610-5.

Leibinger, A., Forte, A. E., Tan, Z., Oldfield, M. J., Beyrau, F., Dini, D. and Rodriguez, Y. B. F. (2016) 'Soft Tissue Phantoms for Realistic Needle Insertion: A Comparative Study', *Ann Biomed Eng,* 44(8), pp. 2442-52.

Lewandowsky, M. (1909) 'Zur Lehre der Cerebrospinalflussigkeit', *Z. Klin. Med.,* 40, pp. 480-494.

Lewis, O., Woolley, M., Johnson, D., Rosser, A., Barua, N. U., Bienemann, A. S., Gill, S. S. and Evans, S. (2016) 'Chronic, intermittent convection-enhanced delivery devices', *J Neurosci Methods,* 259, pp. 47-56.

Lewis, O., Woolley, M., Johnson, D. E., Fletcher, J., Fenech, J., Pietrzyk, M. W., Barua, N. U., Bienemann, A. S., Singleton, W., Evans, S. L. and Gill, S. S. (2018) 'Maximising coverage of brain structures using controlled reflux, convection-enhanced delivery and the recessed step catheter', *J Neurosci Methods*.

Lewis, O., Woolley, M. and Johnson, D. F., J Fenech, J Keenan, B Potts, M Hobden, P Evans, SL 'Novel brain phantoms for neurological catheter development'. *World Congress of Biomechanics*, Dublin, Ireland.

Linninger, A. A., Somayaji, M. R., Erickson, T., Guo, X. and Penn, R. D. (2008a) 'Computational methods for predicting drug transport in anisotropic and heterogeneous brain tissue', *J Biomech,* 41(10), pp. 2176-87.

Linninger, A. A., Somayaji, M. R., Mekarski, M. and Zhang, L. (2008b) 'Prediction of convection-enhanced drug delivery to the human brain', *J Theor Biol,* 250(1), pp. 125-38.

Linninger, A. A., Somayaji, M. R., Zhang, L., Smitha Hariharan, M. and Penn, R. D. (2008c) 'Rigorous mathematical modeling techniques for optimal delivery of macromolecules to the brain', *IEEE Trans Biomed Eng,* 55(9), pp. 2303-13.

Lonser, R. R., Schiffman, R., Robison, R. A., Butman, J. A., Quezado, Z., Walker, M. L., Morrison, P. F., Walbridge, S., Murray, G. J., Park, D. M., Brady, R. O. and Oldfield, E. H. (2007a) 'Image-guided, direct convective delivery of glucocerebrosidase for neuronopathic Gaucher disease', *Neurology,* 68(4), pp. 254-61.

Lonser, R. R., Walbridge, S., Garmestani, K., Butman, J. A., Walters, H. A., Vortmeyer, A. O., Morrison, P. F., Brechbiel, M. W. and Oldfield, E. H. (2002) 'Successful and safe perfusion of the primate brainstem: in vivo magnetic resonance imaging of macromolecular distribution during infusion', *J Neurosurg,* 97(4), pp. 905-13.

Lonser, R. R., Walbridge, S., Murray, G. J., Aizenberg, M. R., Vortmeyer, A. O., Aerts, J. M., Brady, R. O. and Oldfield, E. H. (2005) 'Convection perfusion of glucocerebrosidase for neuronopathic Gaucher's disease', *Ann Neurol,* 57(4), pp. 542-8.

Lonser, R. R., Warren, K. E., Butman, J. A., Quezado, Z., Robison, R. A., Walbridge, S., Schiffman, R., Merrill, M., Walker, M. L., Park, D. M., Croteau, D., Brady, R. O. and Oldfield, E. H. (2007b) 'Real-time image-guided direct convective perfusion of intrinsic brainstem lesions. Technical note', *J Neurosurg,* 107(1), pp. 190-7.

Lopez, O. L. (2011) 'The growing burden of Alzheimer's disease', *Am J Manag Care,* 17 Suppl 13, pp. S339-45.

Lueshen, E., Tangen, K., Mehta, A. I. and Linninger, A. (2017) 'Backflow-free catheters for efficient and safe convection-enhanced delivery of therapeutics', *Med Eng Phys,* 45, pp. 15-24.

Messaritaki, E., Rudrapatna, S. U., Parker, G. D., Gray, W. P. and Jones, D. K. (2018) 'Improving the Predictions of Computational Models of Convection-Enhanced Drug Delivery by Accounting for Diffusion Non-gaussianity', *Front Neurol,* 9, pp. 1092.

Morrison, P. F., Laske, D. W., Bobo, H., Oldfield, E. H. and Dedrick, R. L. (1994) 'High-flow microinfusion: tissue penetration and pharmacodynamics', *Am J Physiol,* 266(1 Pt 2), pp. R292-305.

Mueller, S., Polley, M. Y., Lee, B., Kunwar, S., Pedain, C., Wembacher-Schroder, E., Mittermeyer, S., Westphal, M., Sampson, J. H., Vogelbaum, M. A., Croteau, D. and Chang, S. M. (2011) 'Effect of imaging and catheter characteristics on clinical outcome for patients in the PRECISE study', *J Neurooncol,* 101(2), pp. 267-77.

Nutt, J. G., Burchiel, K. J., Comella, C. L., Jankovic, J., Lang, A. E., Laws, E. R., Jr., Lozano, A. M., Penn, R. D., Simpson, R. K., Jr., Stacy, M. and Wooten, G. F. (2003) 'Randomized, double-blind trial of glial cell line-derived neurotrophic factor (GDNF) in PD', *Neurology,* 60(1), pp. 69-73.

Okada, S., Hara, M., Kobayakawa, K., Matsumoto, Y. and Nakashima, Y. (2018) 'Astrocyte reactivity and astrogliosis after spinal cord injury', *Neurosci Res,* 126, pp. 39-43.

Patel, N. K., Pavese, N., Javed, S., Hotton, G. R., Brooks, D. J. and Gill, S. S. (2013) 'Benefits of putaminal GDNF infusion in Parkinson disease are maintained after GDNF cessation', *Neurology,* 81(13), pp. 1176-8.

Pekny, M. and Nilsson, M. (2005) 'Astrocyte activation and reactive gliosis', *Glia,* 50(4), pp. 427-34.

Pekovic, S., Filipovic, R., Subasic, S., Lavrnja, I., Stojkov, D., Nedeljkovic, N., Rakic, L. and Stojiljkovic, M. (2005) 'Downregulation of glial scarring after brain injury: the effect of purine nucleoside analogue ribavirin', *Ann N Y Acad Sci,* 1048, pp. 296-310.

Raghavan, R., Brady, M. L., Rodriguez-Ponce, M. I., Hartlep, A., Pedain, C. and Sampson, J. H. (2006) 'Convection-enhanced delivery of therapeutics for brain disease, and its optimization', *Neurosurg Focus,* 20(4), pp. E12.

Raghavan, R., Brady, M. L. and Sampson, J. H. (2016) 'Delivering therapy to target: improving the odds for successful drug development', *Ther Deliv,* 7(7), pp. 457-81.

Raghavan, R. and Odland, R. M. (2017) 'Theory of porous catheters and their applications in intraparenchymal infusions', *Biomed Phys Eng Express,* 3(2).

Raven, P. H. and Johnson, G. B. (1996) *Biology.* Dubuque, IA: Wm. C. Brown Publishers.

Reese, T. S. and Karnovsky, M. J. (1967) 'Fine structural localization of a blood-brain barrier to exogenous peroxidase', *J Cell Biol,* 34(1), pp. 207-17.

Richardson, R. M., Kells, A. P., Martin, A. J., Larson, P. S., Starr, P. A., Piferi, P. G., Bates, G., Tansey, L., Rosenbluth, K. H., Bringas, J. R., Berger, M. S. and Bankiewicz, K. S. (2011) 'Novel platform for MRI-guided convection-enhanced delivery of therapeutics: preclinical validation in nonhuman primate brain', *Stereotact Funct Neurosurg,* 89(3), pp. 141-51.

Roitbak, T. and Sykova, E. (1999) 'Diffusion barriers evoked in the rat cortex by reactive astrogliosis', *Glia,* 28(1), pp. 40-8.

Rosenbluth, K. H., Luz, M., Mohr, E., Mittermeyer, S., Bringas, J. and Bankiewicz, K. S. (2011) 'Design of an in-dwelling cannula for convection-enhanced delivery', *J Neurosci Methods,* 196(1), pp. 118-23.

Saltzman, W. M. (2001) *Drug delivery : engineering principles for drug therapy.* Oxford [England]; New York: Oxford University Press.

Sampson, J. H., Archer, G., Pedain, C., Wembacher-Schroder, E., Westphal, M., Kunwar, S., Vogelbaum, M. A., Coan, A., Herndon, J. E., Raghavan, R., Brady, M. L., Reardon, D. A., Friedman, A. H., Friedman, H. S., Rodriguez-Ponce, M. I., Chang, S. M., Mittermeyer, S., Croteau, D. and Puri, R. K. (2010) 'Poor drug distribution as a possible explanation for the results of the PRECISE trial', *J Neurosurg,* 113(2), pp. 301-9.

Sampson, J. H., Raghavan, R., Brady, M. L., Provenzale, J. M., Herndon, J. E., 2nd, Croteau, D., Friedman, A. H., Reardon, D. A., Coleman, R. E., Wong, T., Bigner, D. D., Pastan, I., Rodriguez-Ponce, M. I., Tanner, P., Puri, R. and Pedain, C. (2007) 'Clinical utility of a patient-specific algorithm for simulating intracerebral drug infusions', *Neuro Oncol,* 9(3), pp. 343-53.

Sarntinoranont, M., Chen, X., Zhao, J. and Mareci, T. H. (2006) 'Computational model of interstitial transport in the spinal cord using diffusion tensor imaging', *Ann Biomed Eng,* 34(8), pp. 1304-21.

Singleton, W. G. B., Bieneman, A. S., Woolley, M., Johnson, D., Lewis, O., Wyatt, M. J., Damment, S. J. P., Boulter, L. J., Killick-Cole, C. L., Asby, D. J. and Gill, S. S. (2018) 'The distribution, clearance, and brainstem toxicity of panobinostat administered by convection-enhanced delivery', *J Neurosurg Pediatr*, pp. 1-9.

Slevin, J. T., Gerhardt, G. A., Smith, C. D., Gash, D. M., Kryscio, R. and Young, B. (2005) 'Improvement of bilateral motor functions in patients with Parkinson disease through the unilateral intraputaminal infusion of glial cell line-derived neurotrophic factor', *J Neurosurg,* 102(2), pp. 216-22.

Smith, J. H. and Humphrey, J. A. (2007) 'Interstitial transport and transvascular fluid exchange during infusion into brain and tumor tissue', *Microvasc Res,* 73(1), pp. 58-73.

Stockwell, J., Abdi, N., Lu, X., Maheshwari, O. and Taghibiglou, C. (2013) 'Novel Central Nervous System Drug Delivery Systems', *Chem Biol Drug Des*.

Sykova, E. and Nicholson, C. (2008) 'Diffusion in brain extracellular space', *Physiol Rev,* 88(4), pp. 1277-340.

Tian, D. S., Yu, Z. Y., Xie, M. J., Bu, B. T., Witte, O. W. and Wang, W. (2006) 'Suppression of astroglial scar formation and enhanced axonal regeneration associated with functional recovery in a spinal cord injury rat model by the cell cycle inhibitor olomoucine', *J Neurosci Res,* 84(5), pp. 1053-63.

Tortora, G. J. D., B.H. (2009) *Principles of anatomy and physiology.* 12th International student edition edn.: John Wiley & Sons.

W.H.O., W. H. O. (2006) *Neurological Disorders: Public Health Challenges.*

White, E., Bienemann, A., Malone, J., Megraw, L., Bunnun, C., Wyatt, M. and Gill, S. (2011a) 'An evaluation of the relationships between catheter design and tissue mechanics in achieving high-flow convection-enhanced delivery', *Journal of Neuroscience Methods,* 199(1), pp. 87-97.

White, E., Woolley, M., Bienemann, A., Johnson, D. E., Wyatt, M., Murray, G., Taylor, H. and Gill, S. S. (2011b) 'A robust MRI-compatible system to facilitate highly accurate stereotactic administration of therapeutic agents to targets within the brain of a large animal model', *Journal of Neuroscience Methods,* 195(1), pp. 78-87.

Whone, A., Luz, M., Boca, M., Woolley, M., Mooney, L., Dharia, S., Broadfoot, J., Cronin, D., Schroers, C., Barua, N. U., Longpre, L., Barclay, C. L., Boiko, C., Johnson, G. A., Fibiger, H. C., Harrison, R., Lewis, O., Pritchard, G., Howell, M., Irving, C., Johnson, D., Kinch, S., Marshall, C., Lawrence, A. D., Blinder, S., Sossi, V., Stoessl, A. J., Skinner, P., Mohr, E. and Gill, S. S. (2019a) 'Randomized trial of intermittent intraputamenal glial cell line-derived neurotrophic factor in Parkinson's disease', *Brain,* 142(3), pp. 512-525.

Whone, A. L., Boca, M., Luz, M., Woolley, M., Mooney, L., Dharia, S., Broadfoot, J., Cronin, D., Schroers, C., Barua, N. U., Longpre, L., Barclay, C. L., Boiko, C., Johnson, G. A., Fibiger, H. C., Harrison, R., Lewis, O., Pritchard, G., Howell, M., Irving, C., Johnson, D., Kinch, S., Marshall, C., Lawrence, A. D., Blinder, S., Sossi, V., Stoessl, A. J., Skinner, P., Mohr, E. and Gill, S. S. (2019b) 'Extended Treatment with Glial Cell Line-Derived Neurotrophic Factor in Parkinson's Disease', *J Parkinsons Dis*.

Williams, D. F. (2008) 'On the mechanisms of biocompatibility', *Biomaterials,* 29(20), pp. 2941-53.

Yin, D., Richardson, R. M., Fiandaca, M. S., Bringas, J., Forsayeth, J., Berger, M. S. and Bankiewicz, K. S. (2010) 'Cannula placement for effective convection-enhanced delivery in the nonhuman primate thalamus and brainstem: implications for clinical delivery of therapeutics', *J Neurosurg,* 113(2), pp. 240-8.

Yin, D., Valles, F. E., Fiandaca, M. S., Bringas, J., Gimenez, F., Berger, M. S., Forsayeth, J. and Bankiewicz, K. S. (2011) 'Optimal region of the putamen for image-guided convection-enhanced delivery of therapeutics in human and non-human primates', *Neuroimage,* 54 Suppl 1, pp. S196-203.

Yin, D., Valles, F. E., Fiandaca, M. S., Forsayeth, J., Larson, P., Starr, P. and Bankiewicz, K. S. (2009) 'Striatal volume differences between non-human and human primates', *J Neurosci Methods,* 176(2), pp. 200-5.

Zhang, L., Yang, M. and Jiang, M. (2012) 'Mathematical Modeling for Convection-Enhanced Drug Delivery', *Procedia Engineering,* 29, pp. 268-274.

10 Appendix A – Journal article submitted to the Journal of Neuroscience Methods

Chronic, intermittent convection-enhanced delivery devices

Authors: Owen Lewis[abc], Max Woolley[b], David Johnson[b], Anne Rosser[c], Neil U. Barua[b], Alison S. Bienemann[b], Steven S. Gill[b], Sam Evans[a]

[a] School of Medical Engineering, Queen's Building, Cardiff University, The Parade, Cardiff CF24 3AA

[b] Functional Neurosurgery Research Group, University of Bristol, School of Clinical Sciences, Learning & Research Building, Southmead Hospital, UK

[c]

Abstract

Background

Intraparenchymal convection-enhanced delivery (CED) of therapeutics directly into the brain has long been endorsed as a medium through which meaningful concentrations of drug can be administered to patients, bypassing the blood brain barrier. The translation of the technology to clinic has been hindered by poor distribution not previously observed in smaller pre-clinical models. In part this was due to the larger volumes of target structures found in humans but principally the poor outcome was linked to reflux (backflow) of infusate proximally along the catheter track. Over the past 10 years, improvements have been made to the technology in the field which has led to a small number of commercially available devices containing reflux inhibiting features.

New Method

While these devices are currently suitable for acute or short term use, several indications would benefit from longer term repeated, intermittent administration of therapeutics (Parkinson's, Alzheimer's, Amyotrophic lateral sclerosis, Brain tumours such as Glioblastoma Multiforme (GBM) and Diffuse intrinsic Pontine Glioma (DIPG), etc.).

Results

Despite the need for a chronically accessible platform for such indications, limited experience exists in this part of the field.

Comparison with existing method(s)

At the time of writing no commercially available clinical platform, indicated for chronic, intermittent or continuous delivery to the brain exists.

Conclusions

Here we review the improvements that have been made to CED devices over recent years and current state of the art for chronic infusion systems.

Highlights

- State of the art review of catheter designs for Convection-Enhanced delivery
- Analysis of the design features, materials and methods of use which could be applied to chronic intermittent drug delivery systems and clinical trials to minimise risk of trial failure and opportunities to optimise intraparenchymal distributions

Keywords

- Convection-Enhanced Delivery
- CED
- Optimisation
- Chronic
- Intermittent
- Catheter

1 Introduction

With global population and predicted lifespan increasing, the prevalence of neurological disease is set to rise. At present over 4.6 million patients have been identified with Parkinson disease (PD) in the top 10 populated countries of the west (*with an undefined global population*) while there are in excess of 20 million patients globally who suffer with Alzheimer disease (Kowal *et al.*, 2013; Dorsey *et al.*, 2007). Forecast burden models show predicted volumes of PD cases doubling within 15-25 years, while Alzheimer disease is predicted to triple (81.1 Million) by 2040 (Lopez, 2011; W.H.O., 2006). This will place a very high demand on healthcare resources all over the world.

As has previously been reported, oral and intravascular medication are ineffective against these types of pathologies given that <1 % of systemically administered drugs reach the brain (Stockwell *et al.*, 2013). A series of tight junctions in the endothelial layer of the vascular system provides a highly effective filtration system that prevents the transport of therapeutic molecules to the tissues and fluids of the brain. This filtration system is called the Blood Brain Barrier (BBB) (Bauer *et al.*, 2014).

Bypassing the BBB and delivering therapeutics directly to the parenchyma, offers the user the ability to introduce therapeutics locally, at doses and concentrations that would otherwise have to be delivered at toxic levels systemically. Bolus injection and the reliance on natural diffusion from the point of delivery, is not a valid administration paradigm as the spread of the therapeutic is limited to a few millimetres from the cannula. Delivery of infusate via a pressure driven regime amplifies the distances permeated by macromolecules and produces a more continuous concentration distribution (Bobo *et al.*, 1994; Morrison *et al.*, 1994). This technique, Convection-Enhanced Delivery (CED), replicates the bulk flow of fluid through the interstitial spaces observed in natural processes, such as vasogenic oedema, by increasing the pressure local to a point source. Therapeutic is driven homogenously into tissues beyond the infusion boundary that would be achieved by diffusion alone [Figure 1-1]. Intuitively, smaller molecules were associated with larger dispersions than bigger molecules however receptor binding, charge and other molecular properties also impact on the distribution of an infusate (Saito *et al.*, 2006).

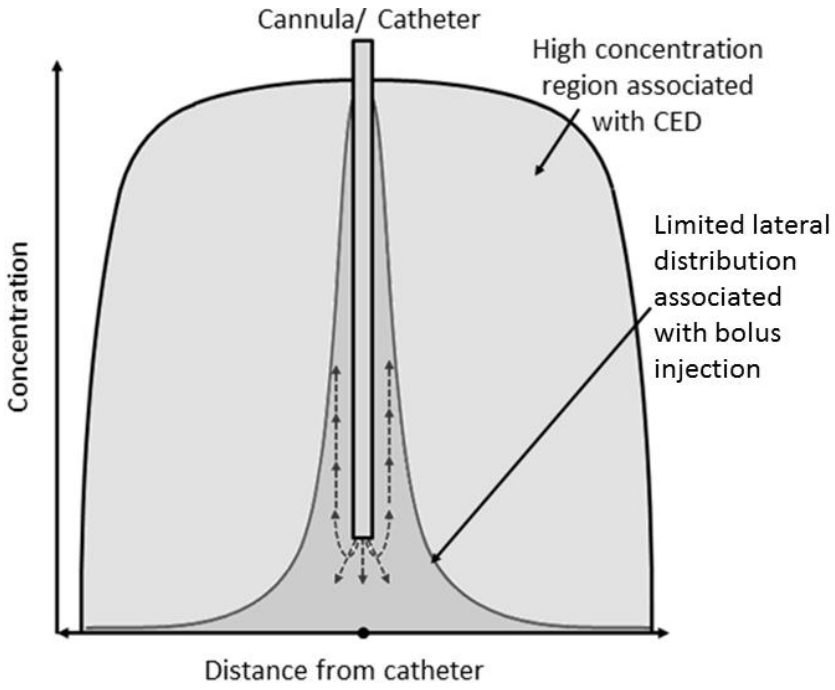

Figure 1-1. Graphic depiction comparing the distribution associated with Convection-Enhanced Delivery (CED) and bolus injection (reproduced and modified from (Lam, Thomas and Lind, 2011). Note that the region of high concentration has spread laterally a much larger distance from the catheter than simply injecting a bolus which is the signature of CED.

Despite positive results pre-clinically (Gash *et al.*, 1996) and in phase I clinician led studies (Gill *et al.*, 2003; Slevin *et al.*, 2005; Patel *et al.*, 2013) clinical translation of CED has been hampered by high profile failed studies (Lang *et al.*, 2006; Kunwar *et al.*, 2010). Retrospective investigations have found that overly ambitious study design, catheter target accuracy and predictability of distribution were major factors failing to achieve successful outcomes (Mueller *et al.*, 2011; Sampson *et al.*, 2010).

Recent improvements, notably to the delivery platform, has reinvigorated the application of clinical CED with eight active studies registered (ClinicalTrials.gov, 2015a). More studies that do not require registration may also be active.

A small number of devices have been commercialised which display good acute performance when used with the principles of CED (Brady et al., 2014; Richardson et al., 2011). Progress in this field has therefore focused on acute or short term infusions. These devices are suited to the delivery of small volume payloads for the delivery of viral vectors and stem cells, but little exists in the experience of chronic CED applications.

Chronic, intermittent delivery could be useful to treat a range of neurological diseases such as Alzheimer's, Parkinson's (Gill *et al.*, 2003), Gaucher Disease (Lonser *et al.*, 2005) among others where repeated infusions could maintain elevated levels of therapeutic within a target tissue, where it is quickly cleared or metabolised (e.g. chemotherapy). While the application of chronic CED may be useful in the treatment of brain tumours such as Glioblastoma Multiforme (GBM) and Diffuse Intrinsic Pontine Glioma (DIPG) tumours, targeting strategies will be key to place long term catheters in areas of likely recurrence. While direct targeting of a tumour will deplete its

core of dividing cells, the resulting necrotic core may act as a sump for further therapeutic delivered, preventing convection into the surrounding tissues. Catheters will need to be placed around the periphery of a tumour in areas of likely recurrence.

Broadening the knowledge of this niche has been hindered in part by the lack of commercially available chronic CED systems to undertake clinical research. Given the predicted volume of demand for intraparenchymal delivery options, including chronic administration systems, a new appreciation of the field must be generated. Novel, chronic systems will provide clinicians 'enabling technology' to treat patients and provide the pharmaceutical industry a new platform to develop therapeutics.

As highlighted in the following review, a large range of catheter profiles have been reported following use in CED infusions. Debinski and Tatter previously highlighted 5 categories of catheter design category [Figure 1-2]; End Port Cannula (EPC), Stepped Profiles Catheters (SPC), Multi-Port Catheters (MPC), Porous tipped catheters (PTC) and Balloon Tipped Catheters (BTC) (Debinski and Tatter, 2009). Designs are not limited to these categories however and numerous variations and overlaps exist.

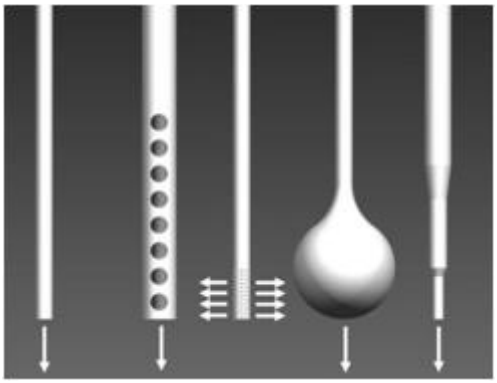

Figure 1-2. Device design groups used in CED studies (left to right); End Port Cannula, Multi-Port Cannula, Porous Tipped Catheters, Balloon Tipped Catheters and Stepped Profile Catheters,– image reproduced and modified from (Debinski and Tatter, 2009).

Here we review and consolidate information on catheter design, experience and materials which have been published when performing CED infusions in pre-clinical and clinical studies over the past 20 years. This review of the state of the art will guide the design and optimisation of new chronic intraparenchymal catheters and their use.

2 Intracranial CED devices

2.1 End port cannula (EPC)

Much of the earliest work which categorised the basic knowledge of CED was performed with EPC. While EPC are defined as having a singular external profile, no restriction is made to the material, devices can be rigid (e.g. fused silica, PEEK or steel hypotube) or flexible (e.g. Polyurethane, Silicone).

Bobo et al (1994) first defined the V_d/V_i ratio, a multiplication ratio used to describe the proportional increase in volume distributed in the brain (V_d) from the volume infused (V_i). Bobo observed that the V_d/V_i ratio was not constant for all infusions. Smaller molecules displayed larger distributions (Bobo *et al.*, 1994). Later studies highlighted that the ratio was also linked to the tissue type, as the interstitial fraction is lower in grey matter than white matter (Lieberman *et al.*, 1995). Larger volumes and faster infusion rates developed to infuse clinically relevant volumes in an acceptable timeframe. Increases in flow rates were however linked to increases in the amount of reflux (leakback/ backflow) along the catheter track (Chen *et al.*, 1999). Reflux is detrimental to CED as the loss of fluid around the point of distribution drops the local pressure, limiting further distribution. Leakages into unintended regions can lead to unwanted side effects (Nutt *et al.*, 2003; Tanner *et al.*, 2007). Investigation of infusion parameters affecting distribution identified that increases in cannula diameter strongly correlated to increases in the volume and distance of reflux (Chen *et al.*, 1999) [Figure 2-1] which was also predicted mathematically (Morrison *et al.*, 1999). Increasing the concentration of the infusate or delaying the start of an infusion (tissue-to-catheter sealing time) were discounted experimentally as having little to no effect on reflux. However, it was later shown that increases in tissue trauma (common with larger bore devices) positively correlated to volume and extent of reflux (White *et al.*, 2011a). The sealing times described by Chen would not have been long enough for healing mechanisms to reduce oedema associated with local trauma allowing the tissue to seal around the device.

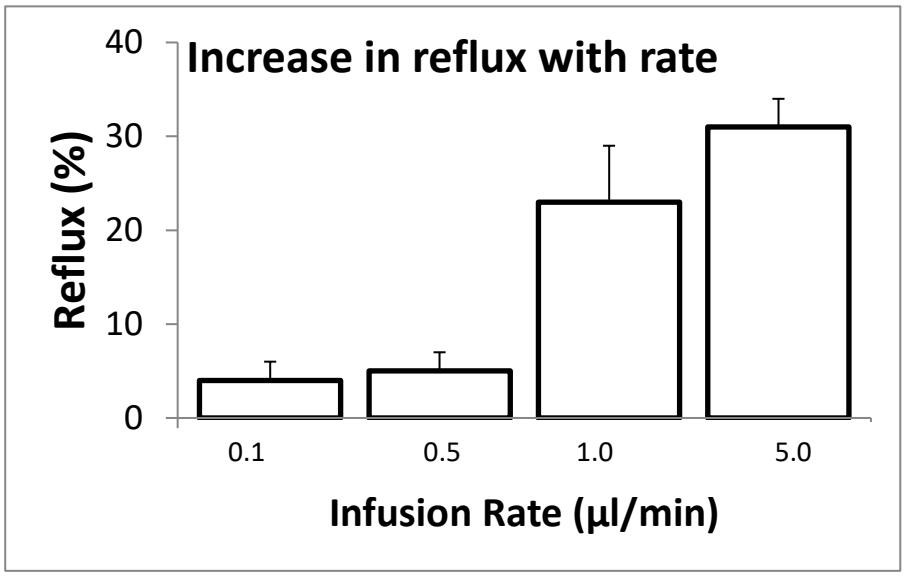

Figure 2-1. Increases in flow rate have been shown empirically to generate increases in reflux along the catheter track - graph reproduced and modified from Chen et al 1999.

2.2 Shunts and peritoneal catheters used for CED (including multi-port catheters [MPC])

Hydrocephalus shunts, designed for long term implantation in the brain are routinely used to deliver and aspirate liquids to and from the ventricles in the brain. They are made from flexible materials such as silicones or polyurethanes. Shunts typically come with an end port, fish mouth or multiport design and usually have a large bore (>1mm) to aid the rapid clearance of excess cerebro-spinal fluid (CSF). Shunts however may not be optimal for

CED as they lack functional features (i.e. small diameters, reflux inhibiting profiles, etc; discussed later) which are critical to effectively distribute infusates into the interstitial fluids of the brain through pressure driven means.

Large calibre, flexible end port style ventricular catheters (2-3mm outer diameter) that have been implanted in clinical trials to treat glioma have failed to distribute effectively and have been linked to poor distributions (Kunwar *et al.*, 2010; Tanner *et al.*, 2007). Cases treating Diffuse Intrinsic Pontine Glioma (DIPG), assumed spherical distribution but required a low flow rate,~1 μl/min to delivery (~6 ml in 100 hours), to minimise the risk of reflux. As no diagnostic tracer was used to confirm the distribution (as acknowledged by the author) it is not possible to evaluate the infusion effectively, however T2 weighted MRI scans indicated some elevated signal around the catheter tip (Anderson *et al.*, 2013).

In other phase I clinical trials, multi-port catheters were implanted into the striatum of patients with promising results (Slevin *et al.*, 2005). It was suggested that the increased number of holes may have aided delivery of therapeutics to the parenchymal tissues but as no post infusion imaging was performed on the distribution of these infusions it is impossible to fully qualify this assertion.

Subsequent investigations of MPC for CED in gel showed that they performed poorly (Raghavan *et al.*, 2006; Salvatore *et al.*, 2006) with preferential flow occurring from the proximal holes.

Investigations of multiport hydrocephalus shunts (Lin *et al.*, 2003) demonstrated that of the available eight holes along the device, 80% of the flow escaped from the most proximal three holes [Figure 2-2]. This was proven empirically and then supported through a Computational model.

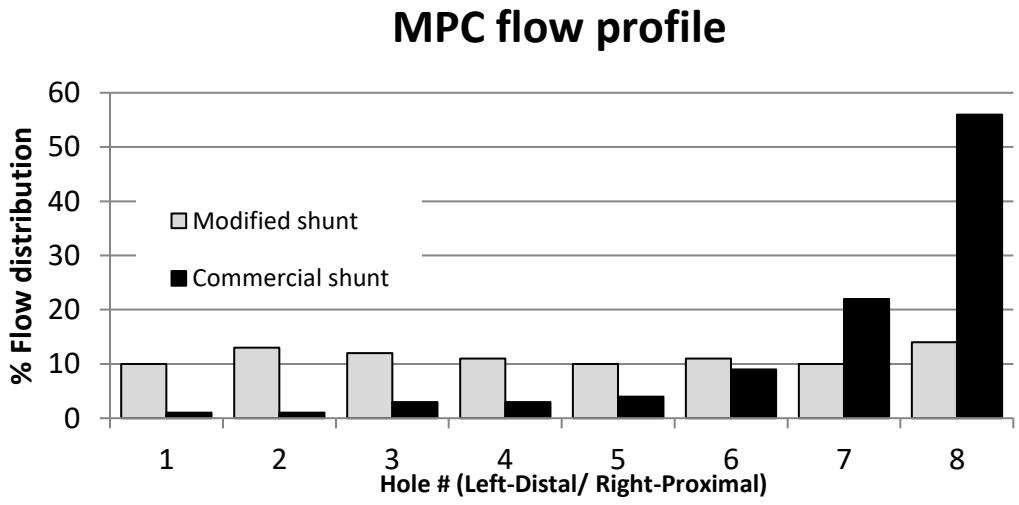

Figure 2-2. Graphical representation of uneven flow distribution within multiport hydrocephalus catheters (black) and a more even flow which could be achieved through modifications to the hole profiles and arrangement (white). The distal end is shown on the left of the graph – image reproduced and modified from (Lin et al., 2003).

Preferential flow seen in hydrocephalus devices might help explain the patterns of distribution seen in CED studies using these devices in the opposite flow direction.

2.3 Micro porous tipped cannula (PTC)

PTC are similar to MPC in that they have a number of holes along their outer wall but PTC have a much larger number of much smaller holes (≤0.45μm diameter). These holes make up the porous, ceramic walls in the tips of these devices. During an infusion, each pore experiences a very small volumetric flow which will drop the pressure within the core of the device by an equally small amount. By maintaining a high internal pressure more distal pores also experience a modest flow which contributes to the overall distribution along the length of the porous tip [Figure 2-3].

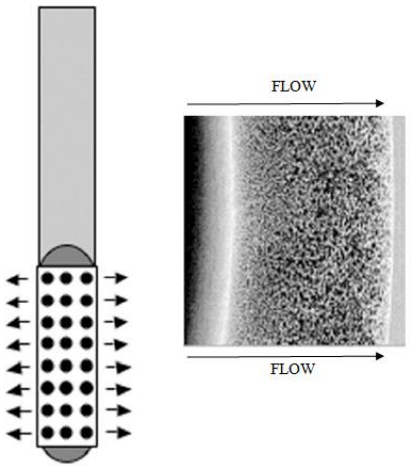

Figure 2-3. Microporous tipped cannula a) illustration of even flow possible over elongated portions of the device (note blocked tip), b) radial view of the cannula wall showing tortuous pathway for infusate through the porous wall – Images reproduced from (Oh et al., 2007).

When compared to EPC the PTC was shown to increase the distribution of infusate into the surrounding gel substrate and murine brain tissue (Oh *et al.*, 2007). A later study found that PTC cannula produced a comparable infusion profile to 3mm step profile cannula in vivo (Brady *et al.*, 2013). PTC are being commercialised for drug delivery by Twin Star Medical.

2.4 Balloon tipped catheters (BTC)

While not commonly used in CED trials, a small number of studies have shown that BTC may have use in treating oncology subjects who have undergone resection of their tumour mass. As the penumbra of a resection cavity is most at risk of metastasis, it has been argued that infusions targeting dividing cells should be administered preferentially into these areas. Intra-ventricular infusions have shown little diffusion of infusate beyond the ependymal layer of the ventricles (Nutt *et al.*, 2003) while catheters placed too close to a resection cavity have been linked to losses into these CSF spaces, dramatically stagnating further distribution into surrounding tissues (Sampson *et al.*, 2011).

A team at Emory University performed resections in canine subjects with the aim of investigating whether CED could be effectively used to distribute infusate into a tumour penumbra by first filling the resection cavity with a balloon (Olson *et al.*, 2008). The study infused continuously for 4 days at a rate of 83μl/hr and stated that in 2 of 3 cases 97-99% of the brain achieved coverage. The images of coverage [Figure 2-4] however do not appear to display the homogenous distribution profile associated with CED. The large coverage may be attributed to the large concentration of the MRI visible tracer - 75% saline/ 25% Gd-DTPA [Magnevist, Berlex] (Olson *et al.*, 2008) (Olson *et al.*, 2008) (Olson *et al.*, 2008) (Olson *et al.*, 2008) (Olson *et al.*, 2008) (Olson *et al.*, 2008) (Olson *et al.*, 2008) (Olson *et al.*, 2008) (Olson *et al.*, 2008) (Olson *et al.*, 2008) (Olson *et al.*, 2008) (Olson *et al.*, 2008) (Olson et al. 2008) and prolonged period of infusion, with gadolinium being carried along with natural parenchymal CSF turnover. Further work is required to expand the knowledge for this application.

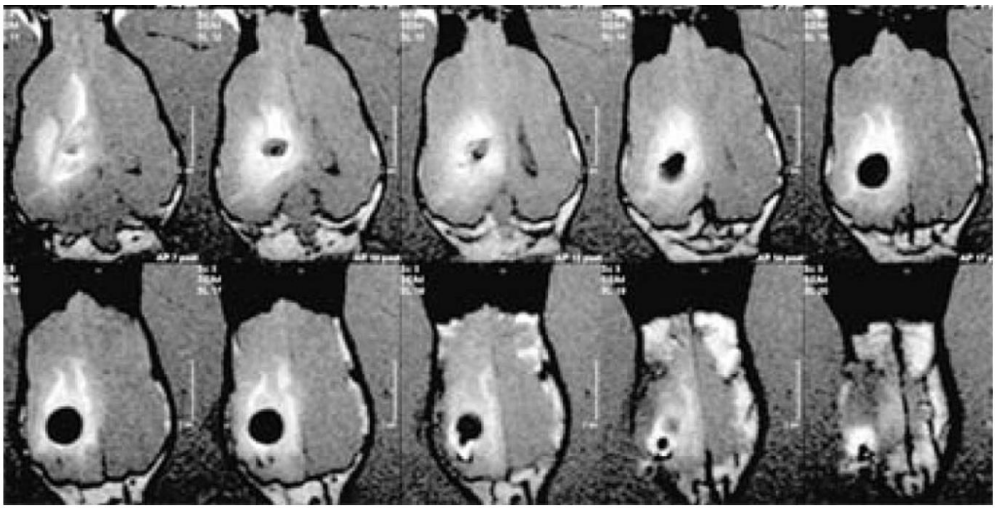

Figure 2-4. Infusions into the penumbra of a resection cavity using a 2 channel Gliasite® brachytherapy catheter, infusing 75% saline/ 25% Gd-DTPA Magnevist – image reproduced from (Olson et al., 2008).

2.5 Stepped Profile Cannula (SPC) assemblies

Several designs of SPC have been used to perform CED infusions in clinical and pre-clinical studies. Stepped profiles can be produced through the assembly of tubes at the time of implantation or within a monolithic assembly that is implanted as a single unit, although it can be argued that the later exhibits much less traumatic delivery characteristics for acute delivery.

Monolithic stepped profiles were pioneered by a team at the University of California, San Francisco (UCSF) showing that where end port cannula alone would have refluxed, the addition of stepped features would inhibit the progression of backflow (Krauze *et al.*, 2005; Sanftner *et al.*, 2005) [Figure 2-5].

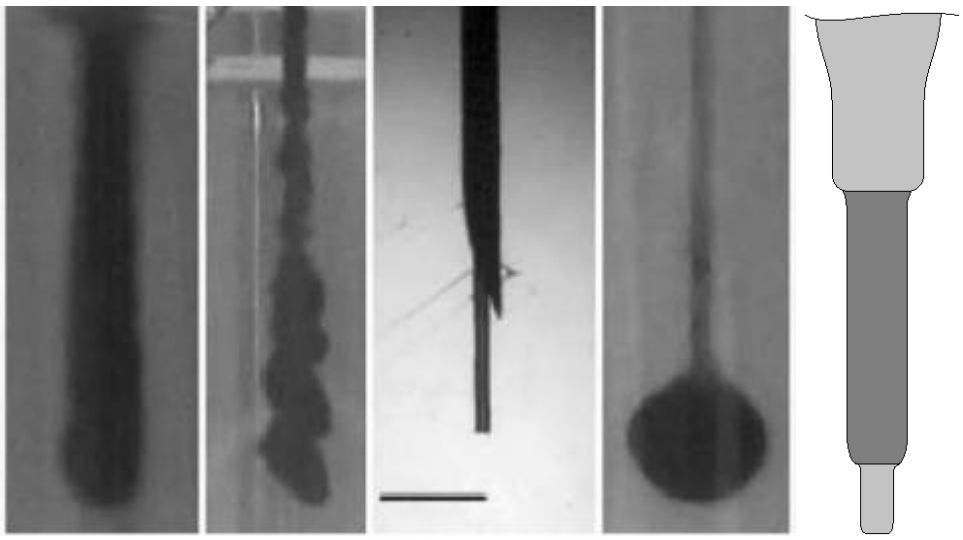

a) b) c) d) e)

Figure 2-5. Infusion profiles of end port cannula (a, b) and improvement possible through introduction of a reflux inhibiting feature (c, d) – images reproduced and modified from (Krauze et al., 2005), e) MRI interventions - SmartFlow cannula - commercial embodiment of the stepped profile cannula.

The distribution of the stepped profile was evaluated first in agarose gel containers and later histologically following infusions in the rat and primate model. Agarose gel is a standard phantom material for brain tissue which has been validated against the porcine brain model (Chen *et al.*, 2004). A monolithic SPC is being commercialised by MRI interventions Inc. which contains a ceramic, fused silica liner and a polymer sheath.

Research conducted at Cornell University utilised silicon industry technology to manufacture printed cannula tips containing dual lumen. These can be independently coupled to proximal tubing away from a delivery site enabling the delivery of a multitude of infusates in addition to the integration of sensor technology. This could be used during delivery to monitor the local environment or to actively monitor the infusate itself (flow rate, temperature, air in line, etc.)(Olbricht, Neeves and Foley, 2010). The tip design is being incorporated into a stepped profile cannula and commercialised by Alcyone Inc.

Investigations using the dual channel tip were conducted in the porcine model at varying flow rates with a number of infusates. When combined with a stepped profile design comparable distributions to other SPC were achieved. Infusion rates as high as 20μl/min were published for white (internal capsule) and grey (thalamus, putamen) matter targets but no investigation of tissue damage was conducted (Brady *et al.*, 2014). Earlier studies noted tissue damage at infusion rates in excess of 10μl/min when delivered from a cannula with a 102μm diameter bore. The authors speculated that the tissue damage may be attributed to the delivery of excessive volume however subsequent studies have successfully infused larger volumes (Chittiboina *et al.*, 2014) discounting the theory that volume alone is the cause of the observed tissue damage. It is therefore possible that the tissue damage found by the UCSF team may be linked to the fluid velocity at the tip of the catheter. At 10μl/min, a cannula with a 102μm internal diameter would eject a fluid stream at 5.1mm/s. Evaluating the smaller cannula outlet produced by the micro-fabricated dual

channel tips (30x53μm), a comparable flow rate may have produced a fluid jet travelling at over 10 times this rate. It is therefore essential that new cannula and catheter designs are tested not only for performance with diagnostic imaging but the infusion regimes must be validated at a cellular level to provide future users a set of safe operational parameters. Further investigation of this and other designs is therefore warranted.

Prior to the release of commercial alternatives, other groups treating DIPG clinically have pre-clinically investigated the use of FS components from Plastics one, a supplier of pre-clinical infusion systems, before implanting a similar device in humans. A large bore guide tube (16-18Gauge) is implanted into the brain stereotactically and is bonded into a burr hole formed in the cranium, with the distal tip 15-35mm short of the target. A primed silica catheter is then inserted to depth in the guide tube, with the tip located in the brainstem (Lonser *et al.*, 2002; Lonser *et al.*, 2007a; Lonser *et al.*, 2007b).

Monolithic SPC usually combine steel or ceramic tubing with fused silica (FS) liners. This rigid construction is advantageous for acute infusions as devices can be implanted with a stereotactic guide system which helps minimise macro-motion during insertion and infusion which is critical to reducing reflux (Chen *et al.*, 2004). Long term implantation of these monolithic assemblies is not feasible due to the rigidity of the cannula. The relative movement between the brain and the device will promote reflux but may also accelerate natural healing processes. We postulate that as the brain encases the device in a sheath of glial tissue the permeability around the cannula will drop which may further increase reflux.

A modified hybrid of the monolithic SPC (Figure 2-3) made from flexible tubing and a rigid, FS tip was investigated by the same team at UCSF, Medgenesis Therapeutics and Brainlab AG. This enabled the device to be implanted in a rigid state (to aid stereotactic delivery), before a delivery rod was removed leaving the flexible, indwelling device (with rigid tip) in situ. The flexible tubing outside the skull could then be routed beneath the skin to a distal exit point. Evidence of acute but not chronic intermittent infusions, in addition to images of the device were published (Rosenbluth *et al.*, 2011).

Similar, stepped catheter designs were fabricated in Medtronic sponsored studies. Needle tip catheters were used in a 10 day study in the porcine model, coupled to an implantable pump (Kim *et al.*, 2014) and later a 28 day study in adult primates (Fan *et al.*, 2015). Following a 3 or 7 day infusion (flow rate; 0.3 μl/min) of a Gd-DTPA solution into the brain, distribution volumes of 1.544±0.420 ml (V_d/V_i= 1.2) were recorded in the pig and 1.936±0.660 ml (V_d/V_i= 1.68) were recorded in the primate. The low distribution volumes may be accounted for by a high clearance rate of Gd-DTPA seen in other studies (Lonser *et al.*, 2007a)[Figure 2-6]. Acute infusions in the primates showed much higher V_d/V_i ratios (5.56+/-1.6) indicating clearance may be a major factor in low flow, continuous infusion.

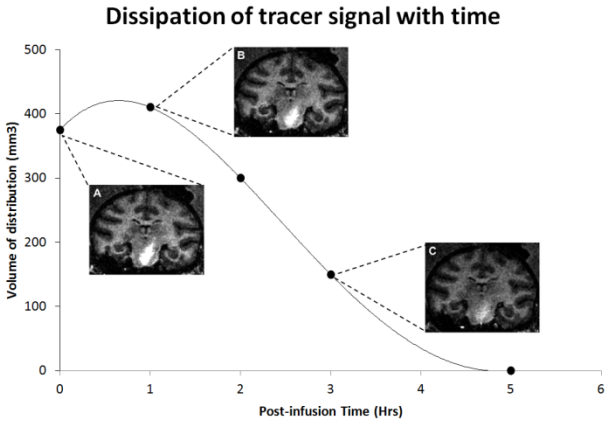

Figure 2-6. Decrease in the intensity of a gadolinium tracer in the brainstem following the end of an infusion – A) immediately after completion of the infusion, B) after 1 hour, C) after 3 hours - Note the initial increase in the distribution due to diffusion and clearance processes but the large drop by 3 hours post infusion (39% of the Vd at infusion end) - images reproduced and modified from (Lonser et al., 2007a).

In order to cover the larger human putamen (3.98±0.15 ml)(Yin *et al.*, 2009) using this system it may be necessary to implant multiple catheters with each attached to a pump. Alternatively, higher coverage ratios might be achieved by running the pump at a higher rate for a short period of time before natural clearance removes the infusate from the local area. Continuous infusions were shown to achieve larger overall infusions. A recent study of prolonged CED in the rat brainstem (Ho *et al.*, 2015) produced no neurological behavioural changes or signs of local toxicity. The relatively short period of the study (10 days) may not have provided sufficient time for the onset of local toxicity due to point source accumulation identified in other studies (Barua *et al.*, 2013c).

Flexible guide tube and catheter assemblies, suitable for long term implantation, were manufactured specifically for a phase I investigational study of Glial cell-line Derived Neurotrophic Factor (GDNF) at Frenchay hospital, Bristol, UK (Gill *et al.*, 2003). Sub 1mm diameter catheters and guide tubes were used to minimise the risk of reflux which had been shown to occur in larger diameter cannula (Chen *et al.*, 1999). The catheter was manufactured in Carbothane™, an aliphatic polyurethane which was later shown to be critical in achieving low blockage rates (Bienemann *et al.*, 2012). Despite promising clinical outcomes in a small number of cases, it was not possible to measure infusion performance of this system as MRI tracers such as gadolinium (Gd-DTPA) were not routinely used.

Successful intermittent infusions performed over 163 days in the porcine model were demonstrated by the University of Bristol, utilising a similar system to that described by Gill in 2003. Novel infusion regimes were used to deliver intermittently which differed from previous, longer term studies in which fluids were supplied continuously from an implanted reservoir pump (Bienemann *et al.*, 2012). The flexible guide tube assembly was further developed with the incorporation of a third cannula. Instead of a dual step design the central cannula is cut shorter than the outer tube, producing a recessed design [Figure 2-7,Figure 2-5].

We have identified that contrary to the initial description of CED as a point source event (Bobo *et al.*, 1994), infusions naturally involve a degree of reflux which can be incorporated into the infusion distribution model (Woolley *et al.*, 2013). Immediately following the start of an infusion, fluid passes into the interstitial spaces of the surrounding tissue as expected from the standard model. As the pressure continues to build however the contact forces between the outer wall of the catheter and the tissue surrounding it will reach a state of equilibrium. At this point fluid will pass into this space, passing up the outside of the catheter as reflux. As fluid escapes from the tip area the local pressure drops the contact forces high up the catheter track remain high which combined, stem the flow of fluid.

By embracing and this inevitable reflux, we have demonstrated it is possible to exert a degree of control over it. We have previously published evidence on the indwelling performance of the recessed step catheter (Gill *et al.*, 2013) over a month in the porcine model and subsequently within clinical glioblastoma cases (Barua *et al.*, 2014; Barua *et al.*, 2013a). While monolithic SPC utilise progressively larger diameters to inhibit and retard this flow acutely, no chronic infusion data is available therefore their efficacy cannot be stated. A chronic, pre-clinical infusion system and a similar chronic, clinical platform are being commercialised by Renishaw PLC.

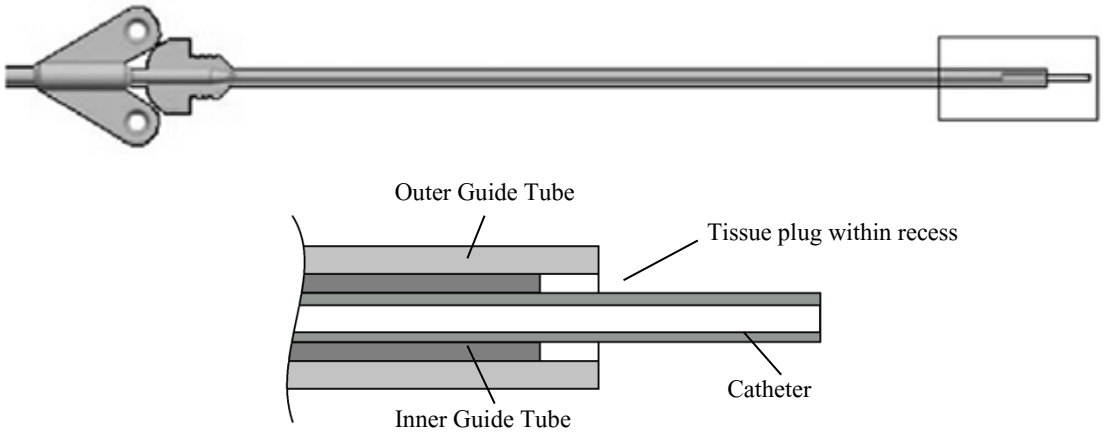

Figure 2-7. Assembled catheter design with a reflux inhibiting feature – a recessed step - images reproduced and modified from Gill et al. 2013.

A novel aspect of the assembled guide tube platform is the ability to modify the length of the step between the smallest diameter tube (catheter) and the outer guide tube specific to each target site. Together with the recessed step feature, it has been demonstrated that increasing the protruding step length has the effect of minimising the volume of reflux which travels beyond the flow inhibiting step feature, achieving a controlled form of reflux (Woolley *et al.*, 2013).

We have identified, and will subsequently present data (Lewis, 2015b), that it is possible to manipulate infusion morphology through modifications to the step length and the infusion regime of a recessed step catheter. The ability to modify infusion parameters permits non-surgically invasive optimisation of infusion distributions following implantation and potentially longer term.

For chronically implanted devices, attributes such as a 90^{O} bend in the tube at the skull surface, and access via a distal port, facilitate real time monitoring to make informed decisions on the progress of the infusion.

A novel accessory described by a team at the University of Wisconsin creates a 'valve tip' and prevents blockage by occluding the inner bore of the cannula with a solid rod during insertion. Following insertion the rod is retracted a short distance (~3-5mm) within the catheter where the inner bore opens slightly leaving room for fluid to pass around the rod (Sillay *et al.*, 2012). This design has the additional benefit of reducing the dead volume within implanted systems but will increase the pressure required to infuse. Comparisons to monolithic stepped cannula designs and also microporous tipped cannula showed that the 'valve tip' design produced comparable infusion profiles but no marked improvement in distribution (Brady *et al.*, 2013; Sillay *et al.*, 2012). This design would therefore only offer improved robustness and possibly reduced tissue trauma on entry.

3 A systems based approach

While this review has focused on catheter design for chronic intraparenchymal delivery, previous experience from clinical trials indicates that dealing with problem areas in isolation is the root cause of failures to tackle the clinical translation of CED.

Novel delivery platforms for chronic infusions should therefore be founded on the successes pioneered in the acute setting while incorporating lessons from previous, failed trials to consider new approaches. While a detailed review of other aspects of CED is beyond the scope of this review, here we acknowledge the inter-relationship between the catheter design and other variables. Chronic, repeated delivery is a complex problem with a number of interdependent elements that require consideration if optimised, reliable and repeatable intraparenchymal drug delivery is to be achieved, Woolley et al (2013).

This multi factorial approach to successful infusions, depicted as the pinnacle of the CED pyramid [Figure 3-1], relies on expertise and knowledge across several disciplines. Here it is believed that optimal CED can be attained if based on a solid foundation of effective stereotaxy, sophisticated surgical planning software, ridged stereotactic delivery instruments and appropriate, responsive infusion pumps.

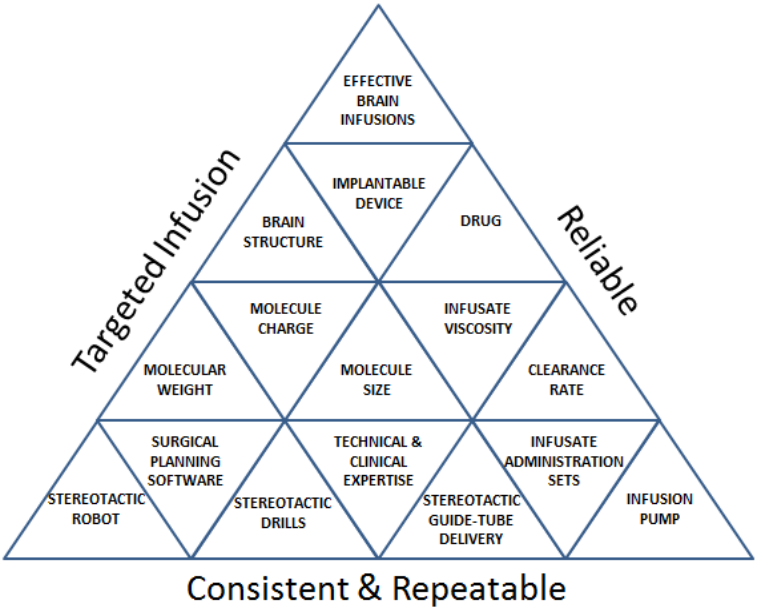

Figure 3-1. Pyramid of effective drug delivery to the brain – image reproduced and modified from (Woolley et al., 2013).

It seems likely that only once a solid platform is achieved can reflux resistant chronic drug delivery systems be implanted with the required accuracy to ensure that critical catheter features are positioned within target structures. The CED pyramid also illustrates the need to consider contributing factors that affect particular therapeutics, such as; molecular size, weight, charge, tissue affinity together with receptor binding, deactivation and potency levels to material and geometry used in the design of the implantable device.

Natural variations in the population as well as a changing internal environment over time due to healing processes present further complicating factors which demand individual attention and will require ongoing evaluation to optimise the infusion regimes to ensure the patient receives treatment where it is required.

4 Discussion

Following years of basic research which characterised the performance issues associated with CED systems, there is now a growing community which actively use the principles of CED in pre-clinical and clinical investigations of new and existing drugs.

Despite the immaturity of the knowledge surrounding successful implementation of CED systems and the ability to achieve acceptable coverage of target structures, CED continues to be practiced within a small number of research centres who accept the current limitations, enabling the implantation of infusion devices based on empirical, historic knowledge and experience of each device's prior performance.

A limited number of acute devices have received market approval, and fewer still have received authorisation for marketization as CED devices, but no commercially available system is currently indicated for chronic intraparenchymal delivery.

Drug device combination programs developing pharmaceuticals and improving catheter designs are likely to benefit from development within a systematic, lab to clinic process where first principles and empirical evidence combine to optimise the delivery. Translation of device design should start with distribution characterisation in an isotropic, homogenous substrate such as agarose gel to baseline performance. Distribution properties should then be confirmed pre-clinically within *in vivo* models before finally being translated to clinical indications.

While only an indicator of infusion morphology, we have found, and will subsequently be publishing, that agarose gel infusions offer baseline infusion morphology data which is specific to each device. Reflux inhibiting features can be trialled and gain a degree of supporting empirical evidence before it is trialled in the complex *in vivo* environment. Users must appreciate that gel data resents an excellent starting point which can inform clinical decisions but this is only a starting point and knowledge of the infusion distribution properties of the local structures (and more preferably, prior clinical experience) should be incorporated into the planning and implementation process. Published evidence of safe, achievable distributions in the *in-vivo* pre-clinical model should also form the basis of a CED practitioner's planning arsenal, specifically whilst this technique is being adopted and experience gained.

In order to enable optimisation of infusion systems following implantation, it is beneficial for flexibility to be built in to study or treatment protocols. It is now obvious that CED infusions must be visualised following the implantation of chronic infusion systems to confirm target acquisition and characterise the distribution achieved. Where poor target structure coverage or other undesirable distributions are observed, clinicians must be given the knowledge of how best to intervene and optimise the distribution. It is unacceptable to permit treatments or trials to fail where the technology exists, and can be easily implemented, to modify the input infusion regimes and improve outcomes for patients. Such a controllable infusion system will maximise clinical benefits and reduce the risk of adverse events while accelerating the development of new drugs to clinic. Pre-clinical correlation mapping of a pharmaceutical agent to imaging tracers should precede clinical use to ensure representative diagnostic imaging interpretations.

For chronic infusions, periodic mapping of the distribution, using diagnostic imaging tracers, will help characterise ongoing distribution of therapeutics within target tissues and permit intervention to optimise coverage.

Following the initial description of CED which used simple cannula, development of infusion parameters (flow rate, ramping regimes etc.) have preceded device development. Numerous infusion cannula and catheter systems have since been trialled for CED with varying degrees of success. Published distribution data indicates that each device performs differently and infusion parameters should be developed for each device to optimise distributions. All systems will benefit from further investigation and clinical use to generate a better understanding of their performance attributes. A small number of physical attributes appear critical across all designs which can be translated to that of a chronically implanted catheter system.

Larger diameters are linked to increased distance of undesirable reflux along the catheter track. Large diameter tubing is therefore undesirable for intraparenchymal delivery. Increases in infusion rates raise the local pressure around the infusion site and also increases the extent of reflux if the pressure surpasses that required to achieve bulk flow of the interstitial fluid. If reflux is observed then further distribution is limited as the additional infusate follows the path of least resistance around the catheter. Actively dropping an infusion rate may decrease the pressure local to the site of reflux and halt further progression.

From this review and from our own work, we have found that a reflux inhibiting feature is required to halt backflow along the catheter entry track. Simultaneously this maximises local interstitial pressure and achieves bulk flow of the therapeutic into the tissue volume.

For prolonged chronic indications it is essential that the catheter systems are made from a flexible material which can move with the brain during every day activities. All devices must be placed accurately without lateral macro motion as this can increase trauma and have a detrimental effect on the distribution.

In addition to physical features, certain practical and transferable attributes are essential for CED devices to facilitate this novel treatment regime.

If we accept that the local environment surrounding each catheter site is unique and each patient specific, then it is unlikely that a standard infusion regime will produce comparable distributions between patients. Catheter specific optimisation may be required to achieve acceptable coverage of the target structure. Therefore catheter designs need to be flexible so that specific features that inhibit reflux can be optimally placed in the intended target structure.

Devices must be compatible with imaging modalities such as MRI (or nuclear imaging in the cases of radio-labelled markers) to enable real time visualisation of distributions to verify acceptable coverage or intervene and implement a modified infusion regime to optimise the distribution. Until a standard model of repeatable delivery is achieved patient specific infusion regimes provide a practical method of providing patients with optimal coverage of targeted tissues (Healy and Vogelbaum, 2015). As an emerging field, CED will require specialist clinical infusion pumps and software that are capable of running at low infusion rates (0.1-10ul/min). Pump or pump software should have the functionality to house patient specific infusion regimes which can be categorised at test infusion milestones (e.g. first infusion).

There are a range of pre-clinical and clinical options for accessing intracranial catheter systems. Active, implantable osmotic pumps (Alzet®) are routinely used to continuously deliver infusate pre-clinically. More recently Alzet® have manufactured a programmable, micro infusion pump containing a 900µl reservoir which can be programmed to run intermittently using an on board micro-processor (iPrecio®) and a radial peristaltic pump. This micro pump has a maximum flow rate of 0.5µl/min. While not indicated for it, the low peak rate would be of limited clinic use to achieve CED.

Passive subcutaneous access ports (e.g. PinPorts/ Soloports, Instech Solomon, Portacath, Smiths Medical, Porthales, Tricumed Medizintechnik GmbH, etc.) provide a means of periodically accessing implanted catheter systems injecting into or cutting down to make the connection immediately prior to an infusion. While subcutaneous ports, osmotic and reservoir pumps can be connected to intracranial catheters, chronic infusion systems may benefit from having an externally accessible port to facilitate easy connection and prolonged attachment during infusions (several hours) with minimal implanted hardware (Barua *et al.*, 2013c; Barua *et al.*, 2014).

Despite a small number of commercially available reflux resistant catheter designs, and some stiff tipped indwelling catheters, no evidence of their chronic efficacy is available. Further work is required to develop knowledge of how to implant, optimise and maintain chronically implanted convection-enhanced delivery infusion systems.

5 Conclusions

Forecast burden models indicate that the growing and aging global population will cause a steep rise in the prevalence of neuro-oncology and neurodegenerative disease which will place a high demand on palliative healthcare resources.

Convection-Enhanced Delivery provides a paradigm for pharmaceutical and academic institutions to provide not only acute infusions of gene therapy but also chronic, intermittent infusions of proteins, neurotrophic factors, chemotherapeutics or other quickly metabolised molecules.

A small number of dedicated CED devices are starting to enter the marketplace but are targeted at acute, stereotactic delivery. No devices are commercially available which are indicated for chronic, intermittent CED to the brain parenchyma.

Targeted chronic catheter and study design should be developed to enable development of novel treatment regimes which can be based upon the principles developed within acute delivery systems.

All catheter designs have unique attributes which must be characterised to be used effectively. It should not be assumed that infusions parameters can be utilised uniformly across all commercially available catheter platforms.

Chronic infusion catheter systems will benefit from small diameters and the inclusion of reflux inhibiting features. To remain in the brain long term, catheters will need to be made from soft materials but still need to achieve excellent target accuracy which is likely to require a ‘systems based approach’ which tackles peripheral issues around the design of the catheter to ensure effective delivery.

Following implantation, and initial characterisation of the distribution, further periodic test infusions will be required to assess changes to the distribution pattern which may be caused by healing mechanisms and natural changes to the internal environment. In order to do this, device design must facilitate real-time imaging, enable alterations to infusion distribution and be minimally invasive whilst maximising the patient’s quality of life.

Further work is required to generate understanding of infusion distributions which can be achieved by utilising chronically implanted CED systems.

6 Acknowledgments

Special thanks go to the Functional Neurosurgery Group at Bristol University and Renishaw's Neurological Applications Department for collaborative work towards research work yet unpublished.

7 Disclosures

While undertaking the research for this review, O. Lewis, M. Woolley and D. Johnson were employees of Renishaw PLC.

S.S. Gill, N.U. Barua and A.S. Bienemann were consultants to Renishaw PLC.

O. Lewis is undertaking a part time PhD at Cardiff University which is funded by Renishaw PLC.

8 References

Anderson R C, Kennedy B, Yanes C L, Garvin J, Needle M, Canoll P, Feldstein N A and Bruce J N (2013) Convection-enhanced delivery of topotecan into diffuse intrinsic brainstem tumors in children. *J Neurosurg Pediatr* 11 (3) 289-295.

Barua N U, Hopkins K, Woolley M, O'Sullivan S, Harrison R, Edwards R J, Bienemann A S, Wyatt M J, Arshad A and Gill S S (2014) A novel implantable catheter system with transcutaneous port for intermittent convection-enhanced delivery of carboplatin for recurrent glioblastoma. *J Drug Delivery*.

Barua N U, Lowis S P, Woolley M, O'Sullivan S, Harrison R and Gill S S (2013a) Robot-guided convection-enhanced delivery of carboplatin for advanced brainstem glioma. *Acta Neurochir (Wien)* 155 (8) 1459-1465.

Barua N U, Woolley M, Bienemann A S, Johnson D E, Lewis O, Wyatt M J, Irving C, O'Sullivan S, Murray G, Fennelly C, Skinner P and Gill S S (2013b) Intermittent convection-enhanced delivery to the brain through a novel transcutaneous bone-anchored port. *J Neurosci Methods* 214 (2) 223-232.

Bauer H C, Krizbai I A, Bauer H and Traweger A (2014) "You Shall Not Pass"-tight junctions of the blood brain barrier. *Front Neurosci* 8 392.

Bienemann A, White E, Woolley M, Castrique E, Johnson D E, Wyatt M, Murray G, Taylor H, Barua N and Gill S S (2012) The development of an implantable catheter system for chronic or intermittent convection-enhanced delivery. *Journal of Neuroscience Methods* 203 (2) 284-291.

Bobo R H, Laske D W, Akbasak A, Morrison P F, Dedrick R L and Oldfield E H (1994) Convection-enhanced delivery of macromolecules in the brain. *Proc Natl Acad Sci U S A* 91 (6) 2076-2080.

Brady M L, Raghavan R, Alexander A, Kubota K, Sillay K and Emborg M E (2013) Pathways of infusate loss during convection-enhanced delivery into the putamen nucleus. *Stereotact Funct Neurosurg* 91 (2) 69-78.

Brady M L, Raghavan R, Singh D, Anand P J, Fleisher A S, Mata J, Broaddus W C and Olbricht W L (2014) In vivo performance of a microfabricated catheter for intraparenchymal delivery. *J Neurosci Methods* 229 76-83.

Chen M Y, Lonser R R, Morrison P F, Governale L S and Oldfield E H (1999) Variables affecting convection-enhanced delivery to the striatum: a systematic examination of rate of infusion, cannula size, infusate concentration, and tissue-cannula sealing time. *J Neurosurg* 90 (2) 315-320.

Chen Z J, Gillies G T, Broaddus W C, Prabhu S S, Fillmore H, Mitchell R M, Corwin F D and Fatouros P P (2004) A realistic brain tissue phantom for intraparenchymal infusion studies. *J Neurosurg* 101 (2) 314-322.

Chittiboina P, Heiss J D, Warren K E and Lonser R R (2014) Magnetic resonance imaging properties of convective delivery in diffuse intrinsic pontine gliomas. *J Neurosurg Pediatr* 13 (3) 276-282.

ClinicalTrials.gov (2015) *National Institutes of health, clinicaltrials.gov - A service of the U.S. National Institutes of Health.* https://clinicaltrials.gov/ct2/home Accessed: 10August2015

Debinski W and Tatter S B (2009) Convection-enhanced delivery for the treatment of brain tumors. *Expert Rev Neurother* 9 (10) 1519-1527.

Dorsey E R, Constantinescu R, Thompson J P, Biglan K M, Holloway R G, Kieburtz K, Marshall F J, Ravina B M, Schifitto G, Siderowf A and Tanner C M (2007) Projected number of people with Parkinson disease in the most populous nations, 2005 through 2030. *Neurology* 68 (5) 384-386.

Fan X, Nelson B D, Ai Y, Stiles D K, Gash D M, Hardy P A and Zhang Z (2015) Continuous intraputamenal convection-enhanced delivery in adult rhesus macaques. *J Neurosurg* 1-9.

Gash D M, Zhang Z, Ovadia A, Cass W A, Yi A, Simmerman L, Russell D, Martin D, Lapchak P A, Collins F, Hoffer B J and Gerhardt G A (1996) Functional recovery in parkinsonian monkeys treated with GDNF. *Nature* 380 (6571) 252-255.

Gill S S, Patel N K, Hotton G R, O'Sullivan K, McCarter R, Bunnage M, Brooks D J, Svendsen C N and Heywood P (2003) Direct brain infusion of glial cell line-derived neurotrophic factor in Parkinson disease. *Nat Med* 9 (5) 589-595.

Gill T, Barua N U, Woolley M, Bienemann A S, Johnson D E, Sullivan S O, Murray G, Fennelly C, Lewis O, Irving C, Wyatt M J, Moore P and Gill S S (2013) In vitro and in vivo testing of a novel recessed-step catheter for reflux-free convection-enhanced drug delivery to the brain. *J Neurosci Methods* 219 (1) 1-9.

Healy A T and Vogelbaum M A (2015) Convection-enhanced drug delivery for gliomas. *Surg Neurol Int* 6 (Suppl 1) S59-67.

Ho S L, Singh R, Zhou Z, Lavi E and Souweidane M M (2015) Toxicity evaluation of prolonged convection-enhanced delivery of small-molecule kinase inhibitors in naive rat brainstem. *Childs Nerv Syst* 31 (2) 221-226.

Kim I, Paek S, Nelson B D, Knight E J, Marsh M P, Bieber A J, Bennet K E and Lee K H (2014) Implementation of a chronic unilateral intraparenchymal drug delivery system in a swine model. *J Neurosci Methods*.

Kowal S L, Dall T M, Chakrabarti R, Storm M V and Jain A (2013) The current and projected economic burden of Parkinson's disease in the United States. *Mov Disord* 28 (3) 311-318.

Krauze M T, Saito R, Noble C, Tamas M, Bringas J, Park J W, Berger M S and Bankiewicz K (2005) Reflux-free cannula for convection-enhanced high-speed delivery of therapeutic agents. *J Neurosurg* 103 (5) 923-929.

Kunwar S, Chang S, Westphal M, Vogelbaum M, Sampson J, Barnett G, Shaffrey M, Ram Z, Piepmeier J, Prados M, Croteau D, Pedain C, Leland P, Husain S R, Joshi B H and Puri R K (2010) Phase III randomized trial of CED of IL13-PE38QQR vs Gliadel wafers for recurrent glioblastoma. *Neuro Oncol* 12 (8) 871-881.

Lam M F, Thomas M G and Lind C R (2011) Neurosurgical convection-enhanced delivery of treatments for Parkinson's disease. *J Clin Neurosci* 18 (9) 1163-1167.

Lang A E, Gill S, Patel N K, Lozano A, Nutt J G, Penn R, Brooks D J, Hotton G, Moro E, Heywood P, Brodsky M A, Burchiel K, Kelly P, Dalvi A, Scott B, Stacy M, Turner D, Wooten V G, Elias W J, Laws E R, Dhawan V, Stoessl A J, Matcham J, Coffey R J and Traub M (2006) Randomized controlled trial of intraputamenal glial cell line-derived neurotrophic factor infusion in Parkinson disease. *Ann Neurol* 59 (3) 459-466.

Lewis O (2015) Manipulating infusion morphology of chronically implanted convection-enhanced delivery catheters. *Journal of Drug Delivery (publication in writing)*.

Lieberman D M, Laske D W, Morrison P F, Bankiewicz K S and Oldfield E H (1995) Convection-enhanced distribution of large molecules in gray matter during interstitial drug infusion. *J Neurosurg* 82 (6) 1021-1029.

Lin J, Morris M, Olivero W, Boop F and Sanford R A (2003) Computational and experimental study of proximal flow in ventricular catheters. Technical note. *J Neurosurg* 99 (2) 426-431.

Lonser R R, Schiffman R, Robison R A, Butman J A, Quezado Z, Walker M L, Morrison P F, Walbridge S, Murray G J, Park D M, Brady R O and Oldfield E H (2007a) Image-guided, direct convective delivery of glucocerebrosidase for neuronopathic Gaucher disease. *Neurology* 68 (4) 254-261.

Lonser R R, Walbridge S, Garmestani K, Butman J A, Walters H A, Vortmeyer A O, Morrison P F, Brechbiel M W and Oldfield E H (2002) Successful and safe perfusion of the primate brainstem: in vivo magnetic resonance imaging of macromolecular distribution during infusion. *J Neurosurg* 97 (4) 905-913.

Lonser R R, Walbridge S, Murray G J, Aizenberg M R, Vortmeyer A O, Aerts J M, Brady R O and Oldfield E H (2005) Convection perfusion of glucocerebrosidase for neuronopathic Gaucher's disease. *Ann Neurol* 57 (4) 542-548.

Lonser R R, Warren K E, Butman J A, Quezado Z, Robison R A, Walbridge S, Schiffman R, Merrill M, Walker M L, Park D M, Croteau D, Brady R O and Oldfield E H (2007b) Real-time image-guided direct convective perfusion of intrinsic brainstem lesions. Technical note. *J Neurosurg* 107 (1) 190-197.

Lopez O L (2011) The growing burden of Alzheimer's disease. *Am J Manag Care* 17 Suppl 13 S339-345.

Morrison P F, Chen M Y, Chadwick R S, Lonser R R and Oldfield E H (1999) Focal delivery during direct infusion to brain: role of flow rate, catheter diameter, and tissue mechanics. *Am J Physiol* 277 (4 Pt 2) R1218-1229.

Morrison P F, Laske D W, Bobo H, Oldfield E H and Dedrick R L (1994) High-flow microinfusion: tissue penetration and pharmacodynamics. *Am J Physiol* 266 (1 Pt 2) R292-305.

Mueller S, Polley M Y, Lee B, Kunwar S, Pedain C, Wembacher-Schroder E, Mittermeyer S, Westphal M, Sampson J H, Vogelbaum M A, Croteau D and Chang S M (2011) Effect of imaging and catheter characteristics on clinical outcome for patients in the PRECISE study. *J Neurooncol* 101 (2) 267-277.

Nutt J G, Burchiel K J, Comella C L, Jankovic J, Lang A E, Laws E R, Jr., Lozano A M, Penn R D, Simpson R K, Jr., Stacy M and Wooten G F (2003) Randomized, double-blind trial of glial cell line-derived neurotrophic factor (GDNF) in PD. *Neurology* 60 (1) 69-73.

Oh S, Odland R, Wilson S R, Kroeger K M, Liu C, Lowenstein P R, Castro M G, Hall W A and Ohlfest J R (2007) Improved distribution of small molecules and viral vectors in the murine brain using a hollow fiber catheter. *J Neurosurg* 107 (3) 568-577.

Olbricht W L, Neeves K B and Foley C P (2010) Microfluidic probes in the treatment of brain-related diseases. *Drug News Perspect* 23 (8) 491-497.

Olson J J, Zhang Z, Dillehay D and Stubbs J (2008) Assessment of a balloon-tipped catheter modified for intracerebral convection-enhanced delivery. *J Neurooncol* 89 (2) 159-168.

Patel N K, Pavese N, Javed S, Hotton G R, Brooks D J and Gill S S (2013) Benefits of putaminal GDNF infusion in Parkinson disease are maintained after GDNF cessation. *Neurology* 81 (13) 1176-1178.

Raghavan R, Brady M L, Rodriguez-Ponce M I, Hartlep A, Pedain C and Sampson J H (2006) Convection-enhanced delivery of therapeutics for brain disease, and its optimization. *Neurosurg Focus* 20 (4) E12.

Richardson R M, Kells A P, Martin A J, Larson P S, Starr P A, Piferi P G, Bates G, Tansey L, Rosenbluth K H, Bringas J R, Berger M S and Bankiewicz K S (2011) Novel platform for MRI-guided convection-enhanced delivery of therapeutics: preclinical validation in nonhuman primate brain. *Stereotact Funct Neurosurg* 89 (3) 141-151.

Rosenbluth K H, Luz M, Mohr E, Mittermeyer S, Bringas J and Bankiewicz K S (2011) Design of an in-dwelling cannula for convection-enhanced delivery. *J Neurosci Methods* 196 (1) 118-123.

Saito R, Krauze M T, Noble C O, Tamas M, Drummond D C, Kirpotin D B, Berger M S, Park J W and Bankiewicz K S (2006) Tissue affinity of the infusate affects the distribution volume during convection-enhanced delivery into rodent brains: implications for local drug delivery. *J Neurosci Methods* 154 (1-2) 225-232.

Salvatore M F, Ai Y, Fischer B, Zhang A M, Grondin R C, Zhang Z, Gerhardt G A and Gash D M (2006) Point source concentration of GDNF may explain failure of phase II clinical trial. *Exp Neurol* 202 (2) 497-505.

Sampson J H, Archer G, Pedain C, Wembacher-Schroder E, Westphal M, Kunwar S, Vogelbaum M A, Coan A, Herndon J E, Raghavan R, Brady M L, Reardon D A, Friedman A H, Friedman H S, Rodriguez-Ponce M I, Chang S M, Mittermeyer S, Croteau D and Puri R K (2010) Poor drug distribution as a possible explanation for the results of the PRECISE trial. *J Neurosurg* 113 (2) 301-309.

Sampson J H, Brady M, Raghavan R, Mehta A I, Friedman A H, Reardon D A, Petry N A, Barboriak D P, Wong T Z, Zalutsky M R, Lally-Goss D and Bigner D D (2011) Colocalization of gadolinium-diethylene triamine pentaacetic acid with high-molecular-weight molecules after intracerebral convection-enhanced delivery in humans. *Neurosurgery* 69 (3) 668-676.

Sanftner L M, Sommer J M, Suzuki B M, Smith P H, Vijay S, Vargas J A, Forsayeth J R, Cunningham J, Bankiewicz K S, Kao H, Bernal J, Pierce G F and Johnson K W (2005) AAV2-mediated gene delivery to monkey putamen: evaluation of an infusion device and delivery parameters. *Exp Neurol* 194 (2) 476-483.

Sillay K, Schomberg D, Hinchman A, Kumbier L, Ross C, Kubota K, Brodsky E and Miranpuri G (2012) Benchmarking the ERG valve tip and MRI Interventions Smart Flow neurocatheter convection-enhanced delivery system's performance in a gel model of the brain: employing infusion protocols proposed for gene therapy for Parkinson's disease. *J Neural Eng* 9 (2) 026009.

Slevin J T, Gerhardt G A, Smith C D, Gash D M, Kryscio R and Young B (2005) Improvement of bilateral motor functions in patients with Parkinson disease through the unilateral intraputaminal infusion of glial cell line-derived neurotrophic factor. *J Neurosurg* 102 (2) 216-222.

Stockwell J, Abdi N, Lu X, Maheshwari O and Taghibiglou C (2013) Novel Central Nervous System Drug Delivery Systems. *Chem Biol Drug Des*.

Tanner P G, Holtmannspotter M, Tonn J C and Goldbrunner R (2007) Effects of drug efflux on convection-enhanced paclitaxel delivery to malignant gliomas: technical note. *Neurosurgery* 61 (4) E880-882; discussion E882.

W.H.O. W H O (2006) *Neurological Disorders: Public Health Challenges*.

White E, Bienemann A, Malone J, Megraw L, Bunnun C, Wyatt M and Gill S (2011) An evaluation of the relationships between catheter design and tissue mechanics in achieving high-flow convection-enhanced delivery. *Journal of Neuroscience Methods* 199 (1) 87-97.

Woolley M, Barua N U, Lewis O, Keane I, Johnson D E, Irving C, Kinch S, Moore P, Howell M, O'Sullivan S, Fennelly C, Pritchard G, Campbell S, Skinner P and Gill S S (2013) Factors Facilitating Optimised Intraparenchymal Drug Delivery – A Prescriptive Systems Approach. In *Partnership Opportunities in Drug Delivery*. Boston, USA.

Yin D, Valles F E, Fiandaca M S, Forsayeth J, Larson P, Starr P and Bankiewicz K S (2009) Striatal volume differences between non-human and human primates. *J Neurosci Methods* 176 (2) 200-205.

11 Appendix B - Journal article submitted to the Journal of Neuroscience Methods

Maximising coverage of brain structures using controlled reflux, convection-enhanced delivery and the recessed step catheter

Authors: Owen Lewis[abc], Max Woolley[bc], David Johnson[bc], Julia Fletcher[c], Johnathan Fenech[c], Mariusz W.Pietrzyk[bc], Neil U. Barua[bc], Alison S. Bienemann[bc], Will Singleton[b], Sam L. Evans[a], Steven S. Gill[bc]

[a] School of Engineering, Queen's Building, Cardiff University, The Parade, Cardiff CF24 3AA
[b] Functional Neurosurgery Research Group, University of Bristol, School of Clinical Sciences, Learning & Research Building, Southmead Hospital, UK
[c] Neurological Applications Department, Renishaw PLC, New Mills, Wotton-Under-Edge, Gloucestershire, UK GL12

Abstract

Background

The design and use of convection-enhanced delivery catheters remains an active field as clinical trials have highlighted suboptimal distribution as a contributory factor to the failure of those studies. Recent studies indicate limitations and challenges in achieving target coverage using conventional point source delivery.

New method

The recessed step catheter (RSC), developed by this group, does not function as a point source delivery device, but instead uses 'controlled reflux' of the infusate to a flow inhibiting recess feature. Here we investigate a range of clinically useful step lengths in agarose gel and investigate proof-of-principle *in vivo*(n=5). Infusion morphology was characterised in terms of length, width and distribution volume over a range of flow rates.

Results

For a fixed infusion volume, increases in catheter step length strongly correlated with increases in the length and volume of distribution ($r>0.90$, $p<0.001$) whilst there were small reductions in the width of distribution ($r<-0.62$, $p<0.001$). Step lengths below 6mm produced spherical distributions while steps above 12mm produced elongated distributions. Increasing peak flow rates resulted in significant reductions in distribution volume at each step length, and an increased risk of reflux beyond the step. Modifications to the infusion morphology using changes in step length were confirmed *in vivo*.

Conclusions

The combination of the recessed step and the ability to adjust the step length with this catheter design make it highly suitable for tailoring the distribution volume of the infusate to meet specific morphological target volumes in the brain.

Key words

Convection-Enhanced Delivery, Recessed-step-catheter, Parkinson's Disease, CED, DIPG, controlled reflux

Highlights

The recessed step catheter can be used to bypass the blood brain barrier in neurodegenerative or neuro-oncological indications to deliver therapeutics directly to target tissues

The variable step length can be used to control the shape of the distribution volume to match the target morphology.

Novel surgical trajectories could be employed to maximise coverage of neuroanatomical targets such as the striatum, thalamus or pons

Corresponding author: Dr Max Woolley, Renishaw Medical Solutions, Neurological Applications Department, New Mills, Wotton-Under-Edge, Gloucestershire UK, GL12 8JR max.woolley@renishaw.com

1 Introduction

Systemic routes of administration for macromolecules targeting neurological conditions have significant limitations for achieving therapeutic drug concentrations within the central nervous system (CNS). Transportation from the blood stream to neurological tissues is severely limited because of the blood brain barrier (Stockwell *et al.*, 2013). Direct delivery via a series of intracranially implanted catheters offers a promising alternative to this route as expensive or toxic substances can be administered at much lower doses than would be required systemically to achieve the same local concentration. It also allows drugs to be delivered to specific targeted tissues, and not widespread throughout the CNS.

Convection-Enhanced Delivery (CED) describes an improved method (over injection) to distribute a high concentration of macromolecules in parenchymal tissues. Low flow rates (>50 µl/min) generate pressure gradient from the point of infusion to minimise backflow (reflux) along the catheter tracks (Bobo *et al.*, 1994; Barua *et al.*, 2012; Gill *et al.*, 2013). Infusion concentrations are also elevated above that which could be achieved via diffusion alone, as the random path of diffusive molecules would take days/weeks to reach a similar distance from the site of infusion (Saltzman, 2001).

Despite initial description of the technique being published in 1994 no clinically available treatment utilising CED is currently available outside of investigational clinical trials, indicating the difficulty of translation from lab and pre-clinical trials into the clinic (Gill *et al.*, 2003; Lang *et al.*, 2006; Mueller *et al.*, 2011; Kunwar *et al.*, 2010; Warren Olanow *et al.*, 2015).

While higher than average placebo responses are a known phenomenon in neurological studies (Goetz *et al.*, 2008; Kunwar *et al.*, 2010), cited among the reasons for failure of these studies was the requirement for increased experience of the users, improved equipment and predictability of implanted devices.

The incorporation of predictive distribution models (Linninger *et al.*, 2008a; Linninger *et al.*, 2008b; Linninger *et al.*, 2008c) within the planning stage of neurosurgical procedures has been advocated and will no doubt provide a step change towards improved trial outcomes (Raghavan, Brady and Sampson, 2016). Underpinning such algorithms however must be an empirical knowledge of how each device performs. While not the only devices used for direct delivery, End Port Catheters (EPC) are often described as having an idealised, spherical distribution pattern which emanates from their tips (Ivanchenko, Sindhwani and Linninger, 2010). Investigations using devices with this aim have shown that this use is suboptimal in that multiple payloads are often required to deliver clinically meaningful infusion volumes (Sillay *et al.*, 2013; Bartus *et al.*, 2013). This increases the duration of the infusions but also the complexity of the implant as the device must be moved multiple times throughout a treatment. Further, anatomical structures of interest for some neurodegenerative pathologies, such as the putamen and caudate nucleus are themselves, not spherical but elongate. Despite axial trajectories for foetal cell deposition being described in 1995 (Breeze, Wells and Freed, 1995), implantation of CED catheters along this trajectory have not been discussed until recently (Bankiewicz *et al.*, 2016; Brady *et al.*, 2013) likely due to the surgical and anaesthetic challenges of

implantation and extended infusions associated with keeping patients in the prone position to access the long axis of targets such as the caudate nucleus or the putamen.

We developed a fully polymeric catheter device which uses image guided, robot assisted implantation remote from an MRI suite (Gill *et al.*, 2013; Lewis, 2015a; Barua *et al.*, 2013a) enabling implantation along almost any desired trajectory. Once implanted, real time scans are possible to track and optimise the infusion regimes. The recessed step catheter does not function as a point source distribution device but one that uses a form of "controlled reflux" (Woolley *et al.*, 2013; Singleton *et al.*, 2017). As the recess forms an inhibiting feature, fluid flows from the tip of the device around the boundary to the recess (along the catheter to the outer guide tube, defining the *step length* – *see* Figure 2-1), providing a potential mechanism for higher overall coverage in target structures within a single implantation procedure. The use and optimisation of chronically implanted catheters are however little known and further research is required for optimisation (Lewis *et al.*, 2016). Here we investigate and characterise the variable step length feature of the recessed step catheter to optimise the morphology of infusions as a means of maximising coverage of neuro-anatomical structures.

2 Materials and Methods

2.1 In vitro *evaluation*

2.1.1 Agarose gel and infusate preparation

Agarose gel (0.6%) was prepared by mixing molecular grade agarose gel (Severn Biotech LTD, UK) with concentrated Tris Borate-ETDA buffer (Severn Biotech, UK) and deionised water. The mixture was heated in a microwave for 5minutes, stirred and then heated further until all powder had fully dissolved. The heated solution was decanted into 50x50x150 clear, rectangular acrylic containers (Volume:375 ml) and left to cool and solidify to room temperature.

A 3mm acrylic lid was secured to the pot and used to simulate the skull, allowing the recessed step catheter to be press fit into the acrylic plate, mimicking the implantation procedure.

Trypan Blue powder (Sigma Aldrich®) was weighed and dissolved in deionised water to a concentration of 0.4% and used as a high visual contrast infusate.

2.1.2 Catheter

Recessed Step Catheters (neuroinfuse™, Renishaw PLC, UK) are formed in three parts using an Outer Guide Tube (OGT), Inner Guide Tube (IGT) and a sub-millimetre diameter catheter (Gill *et al.*, 2013; Lewis, 2015a), as illustrated in Figure 2-1. The device was prepared by cutting an OGT to 60mm and the IGT to 58.5mm creating a 1.5mm recess. Catheters were cut at lengths of 63, 66, 72, 78mm, creating step lengths of 3, 6, 12 and 18mm beyond the OGT.

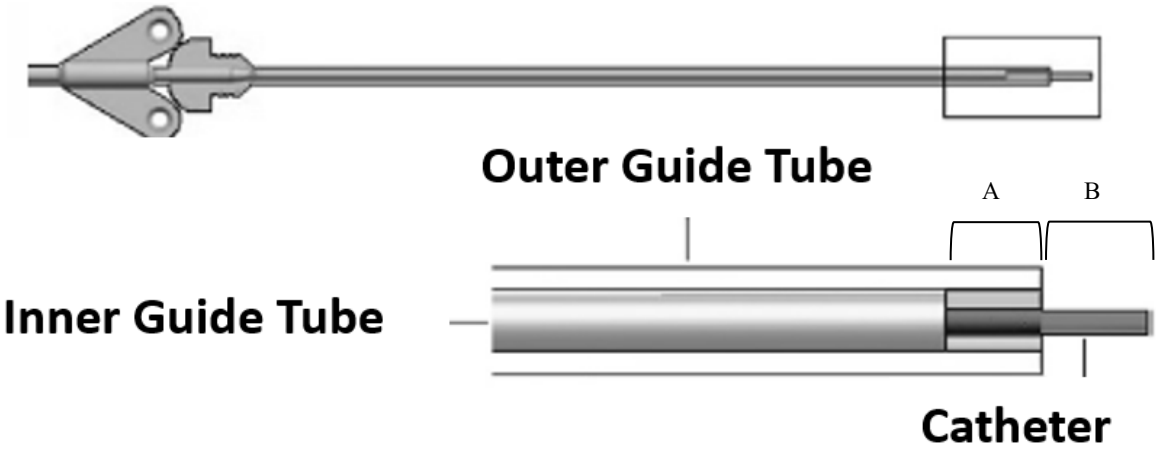

Figure 2-1. Fully implantable recessed step catheter assembly, inset showing a cut away view of the tubing and the formation of the recess (A), and step length (B).

2.1.3 Delivery tooling

As a polymeric device, each of the guide tube elements must be delivered over delivery rods to ensure they maintain target accuracy. The OGT is delivered over a tungsten carbide delivery rod and held just short of the final implantation position. The OGT is then advanced over the rod to create a tissue/ gel plug in the base of the assembly. The IGT is then passed over a steel rod while aspiration is used to minimise the introduction of air into the infusion area.

A 0.6mm diameter rod, is then used to penetrate the gel beyond the OGT to the depth of the catheter, creating a pre-form track for the unsupported catheter to maintain target accuracy.

2.1.4 Test set up

Agarose pots were held in a bespoke fixation rig (Figure 2-2). A human stereotactic frame (Radionics® CRW™, Integra Lifesciences Corp.) was used to aid delivery of guide rods and catheter elements into the gel. A DSLR camera (Model 1200D, Canon Inc) was attached to a laptop fitted with Digital Photo Professional (Canon, Inc) remote shooting software. Additional lighting was used as required to illuminate the infusion. B|Braun™ Perfusor Space syringe pumps were used to run *ramp and taper* infusion regimes (Figure 2-3).

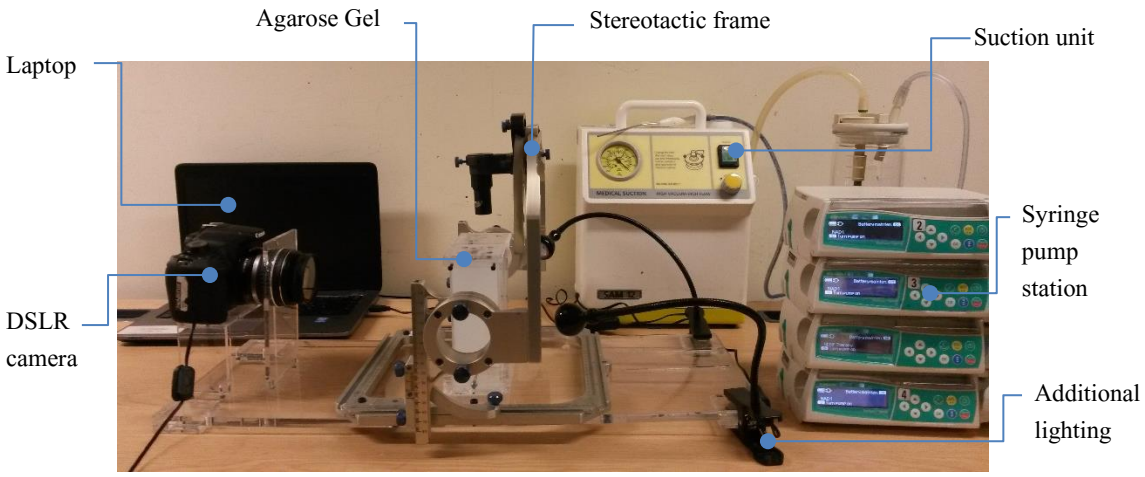

Figure 2-2. Schematic of gel infusion test set up.

2.1.5 Infusion volume and regime

A retrospective study of anonymised surgical plans from a backlist of some of the authors historical Deep Brain Stimulation (DBS) cases was performed to establish baseline volumes of two likely neurodegenerative target structures, the putamen and the caudate nucleus. 143 Parkinson's disease patients were analysed using an auto-segmentation tool (within Renishaw's neuroinspire™ surgical planning software) for anatomical structures.

Average putamen volumes were 4.30±0.03 ml (range: 2.89-5.94 ml) which compares favourably to a smaller study conducted using only 11 cases which found average putamen volumes of 4.02±0.23 ml (range: 3.01-5.29 ml) (Yin *et al.*, 2009)

Average caudate nucleus volumes were 2.90±0.03 ml (range 2.03-4.64 ml) which was similar to previously published data (3.5±0.26 ml) from the same source.

Interstitial space in grey matter accounts for ~20 % of the volume fraction (Roitbak and Sykova, 1999), published values for infusions into the rat striatum confirm a V_d/V_i ratio of 5±0.2 (mean ± standard deviation)(Chen *et al.*, 1999).

Targeting complete coverage of the average putamen would therefore require an infusion volume of at least 0.8 ml (800 µl), or 0.4 ml (400 µl) split over 2 catheters.

Slowly increasing the interstitial pressure at the target site by stepping or ramping the infusion rate from low to high minimises the risk of overwhelming inhibition features such as a step or recesses (Bankiewicz *et al.*, 2000; Bienemann *et al.*, 2012; Gill *et al.*, 2013; Barua *et al.*, 2013b).

Syringe pumps (Perfusor® Space, B|Braun) were programmed with three linear ramp and taper profiles delivering a fixed infusion volume of 400 µl, ramping from zero to the peak flow rate (Q) over 40mins (Figure 2-3). Total infusion times were 1hr (Q=0.6 ml/hr[10 µl/min]), 1hr40mins (Q=0.3 ml/hr[5 µl/min]) and 4hrs21mins (Q=0.1 ml/hr[1.3 µl/min]) which were all considered clinically translatable.

A minimum of 9 repeats for each step length at each flow rate were performed (n=108).

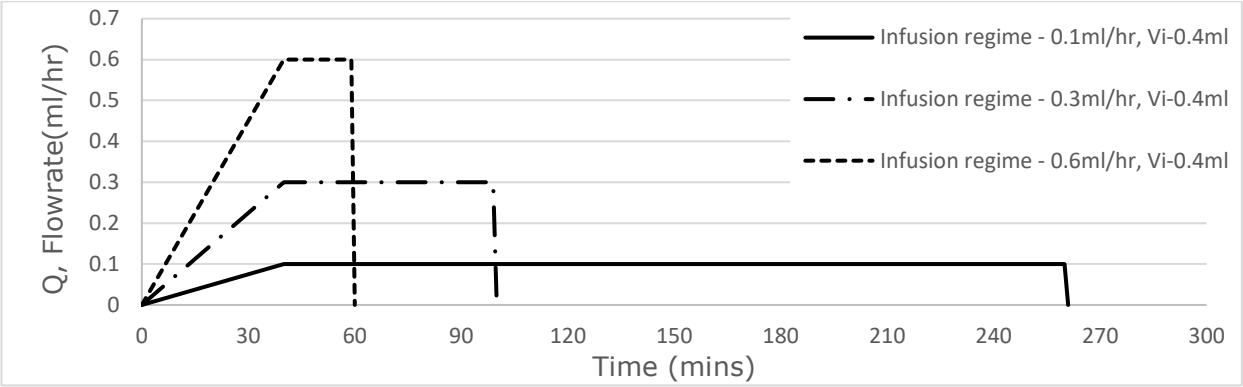

Figure 2-3. Investigational, clinically translatable infusion regimes for intermittent delivery.

2.1.6 Infusion image acquisition rig

Following completion of the infusion (<10mins) the agarose gels were emptied into a bespoke cutting matrix. 150mm long skin grafting blades (Swann Morton) were used to section the gel into 3mm slices. Slices containing the midline of the distribution cloud were laid onto a graduated platform (Figure 2-4). Compressive distortions were minimised as the gel was smoothed to the known cross-sectional dimensions. A diffusion light box was placed over the rig prior to image acquisition with a Canon camera (described above) to provide uniform and consistent lighting of the samples.

Images of the infused gel were recorded within approximately 10minutes following completion of the infusion to minimise diffusion effects.

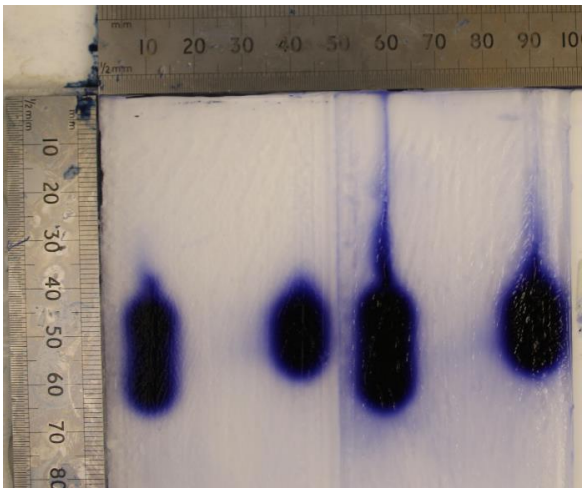

Figure 2-4. Infusion imaging rig showing well demarcated infusion clouds within 3mm thick slices of agarose gel against a graduated border.

2.1.7 Image analysis

Images were loaded into the image segmentation toolbox of Matlab 9.2 (The Mathworks, Inc., Natick, Massachusetts, United States). Infusion areas were magnified to fill the screen and the manual polygon plotter tool used to profile the boundary of the infusion, creating a segmented binary image with the same dimensions as the base image. The binary image was exported to the workspace. Pixel width was calibrated for each image using the inbuilt steel rules which formed part of the imaging rig. Distribution Volume (V_d) was calculated on a pixel line

basis as a cylindrical volume; Infusion width was halved, creating a radius while the height was the calibrated pixel height. Calculations were repeated for each line and the sum total provided the V_d. Maximum distribution length and width were also recorded.

Sectioned gel slices displayed a clear profile boundary for the distributions as a dark, saturated core with a weaker, diffuse boundary. The band of diffuse infusate was routinely 1-2mm in width and inherently variable. To minimise subjectivity, manual profiles were created for each infusion at the border of the highly saturated core region. Analysed volumes are therefore likely to underestimate total coverage but provide a more direct comparison between tests.

2.2 In vivo *evaluation*

2.2.1 Surgical procedures

Surgical procedures were performed in accordance with the Animals (Scientific Procedures) Act (1986) under specific UK Home Office project and personal licence (project licence number 30/2909) at a licensed establishment. Study protocols were pre-approved by the University of Bristol Ethical Review board. Bilateral infusions into the grey matter (putamen or thalamus) of 5 large white landrace pigs were conducted using the recessed step catheter (n=12 infusions). Outer guide tubes were placed within the boundary of the target structure and the catheter tip was implanted to sufficient depth to create a series of increasing step lengths to a maximum of 12mm (restricted by the size of the thalamus in the porcine model).

Anaesthesia, head fixation, MRI scanning and stereotactic procedures were performed as previously described (White *et al.*, 2011b; Barua *et al.*, 2013c).

2.2.2 Test infusions

Artificial cerebrospinal fluid (aCSF) was prepared with a 2mM concentration of gadolinium based contrast agent (GBCA), Magnevist® (Bayer) and loaded into a fixed volume reservoir. Infusion volumes to the putamen were typically 120 µl while infusions into the larger thalamus were typically 200 µl.

Real time (sequential T1 weighted) MRI scans were performed by placing the fixed volume reservoirs downstream of 6 m access lines which could extend into the bore of the scanner, allowing the infusion pumps to remain in the control room. Ramped infusion regimes were used as described above with flow rates peaking at 0.18-0.3 ml/hr.

2.3 Statistical analysis

With sample groups larger than two we used a one-way ANOVA to establish statistically significant differences in mean populations of V_d, distribution width and length between flow rates and between step lengths.

Pearson correlation coefficients were calculated for the distribution volume, width and length at each infusion flow rate over the step length groups.

3 Results

3.1 In vitro *infusion morphology: Distribution length and width*

In the gel model, as expected, there was a very strong correlation between increased step length (SL) and increased length of the distribution (Figure 3-1a: Q1[r=0.95, p<0.001], Q5[r= 0.98, p<0.001], Q10[r=0.98, p<0.001]) as infusions refluxed to the flow inhibiting feature. Increases of the distribution length also resulted in a numerically small but significant drop in the maximum distribution width at each step length (Figure 3-1b: Q1[r=-0.89, p<0.001], Q5[r=-0.83, p<0.001], Q10[r=-0.60, p<0.001]).

Average distribution lengths were significantly reduced when increasing the infusion flow rate (Q) at each of the step lengths investigated (SL(3mm); $F(2,27)=31.6$, $p<0.001$, SL(6mm); $F(2,29)=25.3$, $p<0.001$, SL(12mm); $F(2,30)=19.7$, $p<0.001$, SL(18mm); $F(2,29)=9.5$, $p<0.001$). Average distribution width was also significantly reduced when increasing the infusion flow rate (Q) at each of the step lengths investigated (SL(3mm); $F(2,27)=116.0$, $p<0.001$, SL(6mm); $F(2,29)=49.9$, $p<0.001$, SL(12mm); $F(2,30)=75.2$, $p<0.001$, SL(18mm); $F(2,29)=46.8$, $p<0.001$).

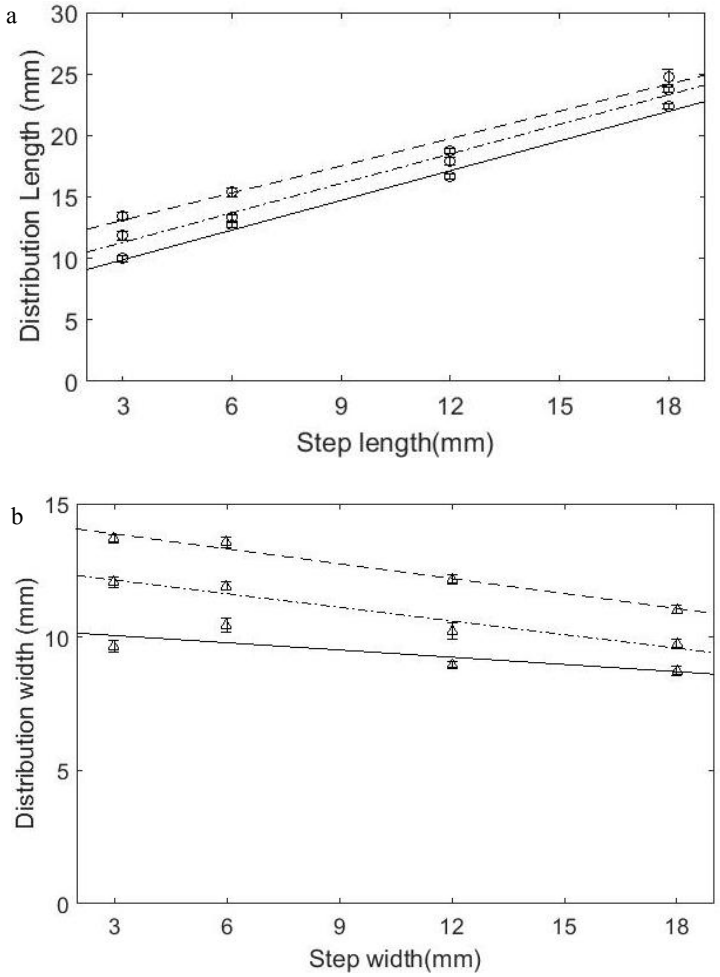

Figure 3-1. a) Q1 (top), Q5 (middle) and Q10 (bottom) trendlines for distribution length versus step length, b) Q1 (top), Q5 (middle) and Q10 (bottom) trendlines for distribution width versus step length.

3.2 In vitro *infusion morphology: Distribution volume*

Increasing the RSC step length resulted in a significant increase in the volume covered across all infusion flow rates tested (Q1[r=0.66, p<0.001], Q5[r=0.74, p<0.001], Q10[r=0.78, p<0.001]). Average distribution volumes were analysed immediately after the completion of the infusion. Vd was significantly reduced when the infusion flow rate (Q) at each step length was increased (SL(3mm); F(2,27)= 71.3, p<0.001, SL(6mm); F(2,29)= 65.4, p<0.001, SL(12mm); F(2,30)= 103.6, p<0.001, SL(18mm); F(2,29)= 69.4, p<0.001) (Figure 3-2).

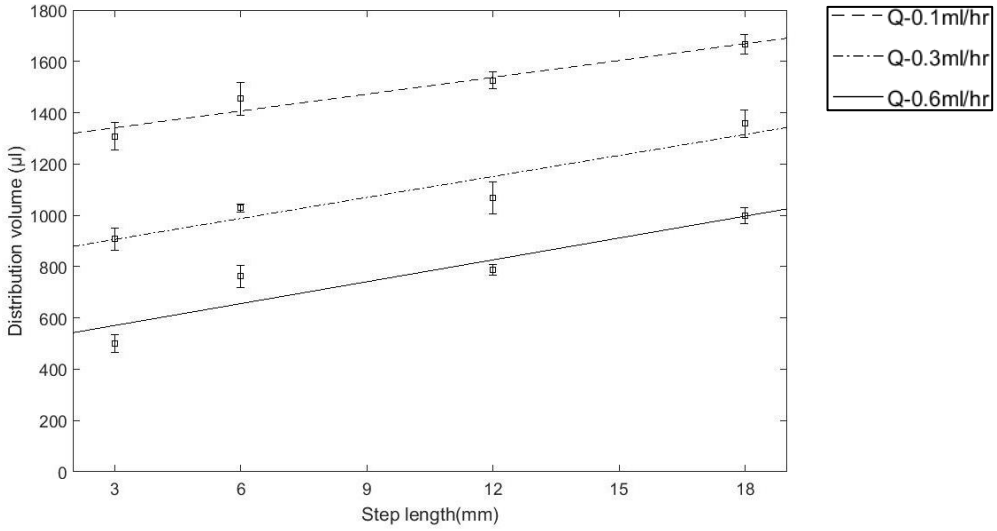

Figure 3-2. Q1 (top), Q5 (middle) and Q10 (bottom) trendlines for distribution volumes versus step length.

3.3 In vivo *infusion morphology: Length and width*

In vivo infusions were grouped into two volumes; 120 µl for the putamen and 200 µl for the thalamus. Infusions into the porcine grey matter show a strong correlation for a linear rise of distribution length as the catheter step length is increased (Vi(120 µl): R=0.90, p=0.006, Vi(200 µl): R=0.84, p=0.03) (Figure 3-3a). While the distribution widths reduce in both infusion volumes, the magnitude of the change is non-significant in the putamen (Vi(120 µl): R=-0.62, p=0.13, Vi(200 µl):R=-0.82, p=0.05)(Figure 3-3 b).

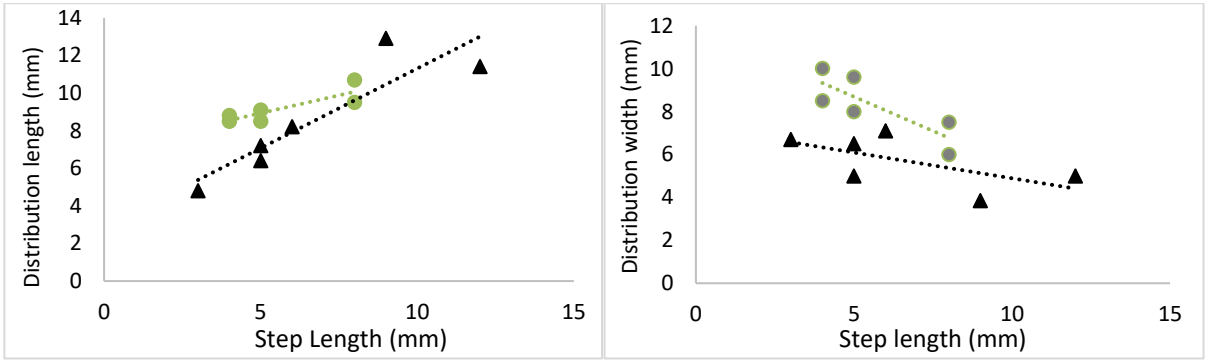

b) b)

Figure 3-3. a) Length of infusions achieved in the porcine grey matter; triangles=120µl (at 5µl/min), circles = 200µl (at 3µl/min); b) width of distributions achieved in the porcine white matter; triangles=120µl (at 5µl/min), circles = 200µl (at 3µl/min).

As the 120µl infusions reached a slightly higher peak flow rate of 0.3ml/hr, a shorter distribution length and smaller width may be anticipated in line with the results of the gel experiments. All infusions refluxed back to the inhibiting step in a predicable fashion across all lengths tested (3-12mm) (Figure 3-4a-d).

3.4 In vivo *infusion morphology: distribution volume*

All infusions showed small numerical increases in coverage as the step length increased, but failed to show significance (Vi(120µl):R=0.77, p=0.27, Vi(200µl):R=0.77, p=0.07) (Figure 3-4e).

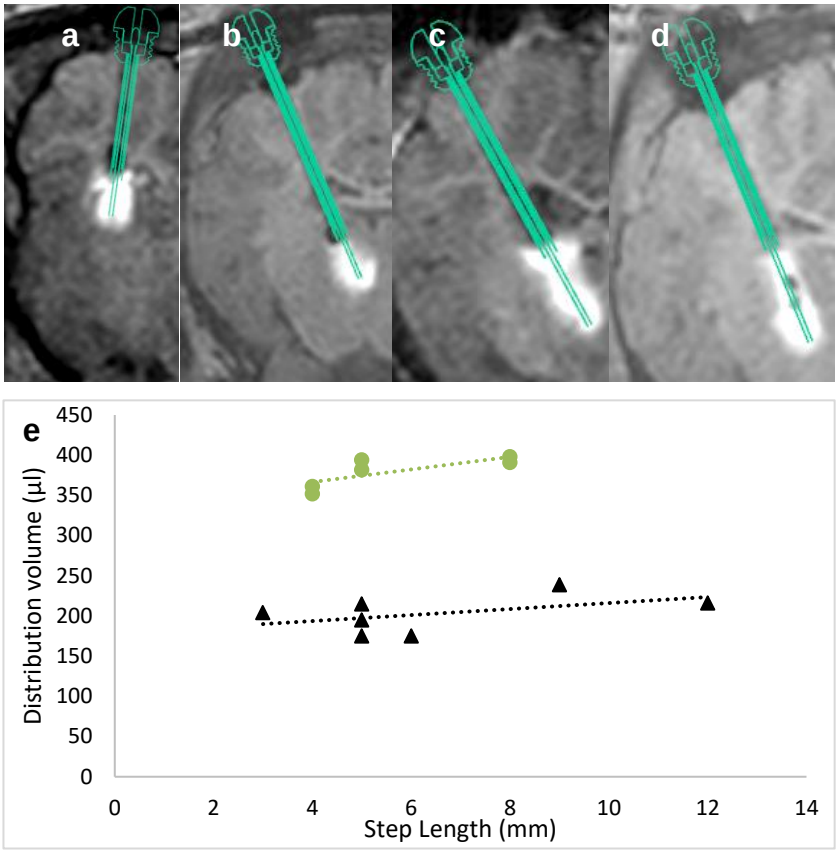

Figure 3-4. in vivo MRI scans of infusions using the recessed step catheter in the porcine model - a) 5mm step in putamen, b) 6mm step in thalamus, c) 8mm step in thalamus, d) 12mm step in thalamus, e) distribution volume achieved from infusions into the porcine grey matter; triangles=120µl (at 0.3ml/hr) circles = 200µl (at 0.18ml/hr).

4 Discussion

4.1 Controlled reflux

Following initiation of the infusion regime, the line pressure rose until fluid passed from the distal tip of the catheter. The initial reflux was instantaneous, passing from the tip of the catheter immediately to the recessed step (Figure 4-1b). Once flow was retarded below the step, a stable pressure region is believed to establish and fluid flow pathways were initiated radially along the step region (Figure 4-1c-e). Convection continued until a critical point is reached where local pressures required to continue infusions radially from the step, exceed those provided by the flow inhibitor and secondary reflux commences around the outer guide tube (Figure 4-1f).

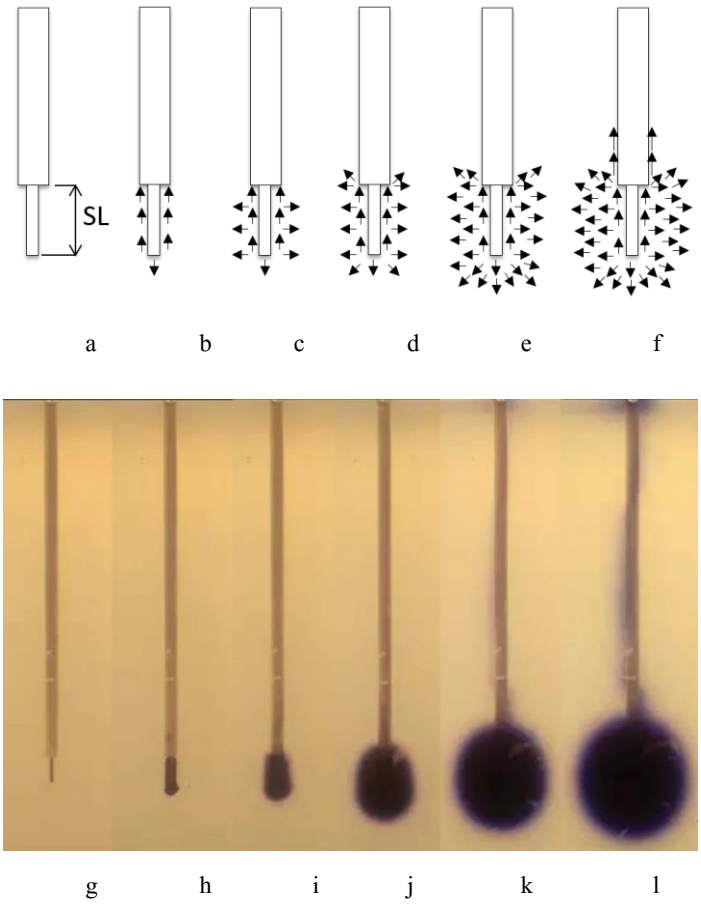

Figure 4-1. The stages of controlled reflux; a) implanted device – SL=Step Length, b) initial reflux, c) ramped/ stepped increase in the flow rate leading to containment of flow front at the inhibition feature and establishment of lateral flow pathways, d) peak flow rate achieved and stable convection reached, e) optimal limit of delivery, f) overload – pressure exceeds inhibition feature limit.

4.2 Controlling infusion morphology

The increase of backflow with increases in catheter diameter and infusion flow rate are by now, well-known phenomena (Chen *et al.*, 1999). The substrate porosity is known to expand at the point of influx which is thought to create pathways for fluid flow and reflux (Lueshen *et al.*, 2017). Controlled reflux (Woolley *et al.*, 2013) is therefore attained by embracing this inevitable event and restricting it below a flow inhibiting feature (Figure 2-1 and Figure 4-1). The first evidence of a recessed step was previously described by this group (Gill *et al.*, 2013). Unlike monolithic alternatives however, the recessed step catheter can be cut and assembled to suit patient target anatomy giving a fully variable step length. Here we investigated the modification of the step length beyond the previously used standard of 3mm (Krauze *et al.*, 2005; Gill *et al.*, 2013). This investigation in the gel model has identified the predictable behaviour of the RSC to create distribution clouds with increasing lengths in a robust way, utilising the controlled reflux method (Figure 4-2a-b) which could be used to maximise coverage of pre-clinical or human intraparenchymal structures.

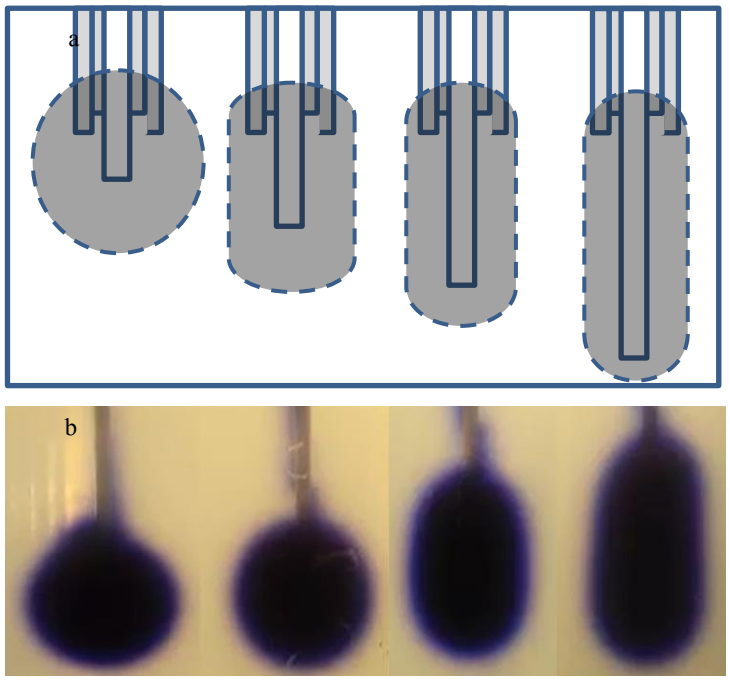

Figure 4-2. a) Schematic of distribution morphology characteristics associated with increasing the step length of the recessed step catheter, b) actual distributions associated with increasing step lengths.

Unlike point source delivery devices, the RSC infusion cloud length closely matches that of the step length. Conversely and logically, the longer infusion clouds which share a fixed input volume, narrowed as a consequence, limiting lateral coverage which is typical of point source CED infusions. Less obvious was the reduction in coverage volumes which resulted from infusions into short step length assemblies. With an infusion volume (V_i) of 400µl for each experiment, a distribution volume (V_d) between 1600-2000µl may have been anticipated given a V_d/V_i ratio of 4:1-5:1. The mean infusion volumes recorded here range from 550-1700µl. As spherical distributions must convect to a larger radial distance than those spread over a region of a longer step length, spherical distributions must have higher concentration cores at the end of an infusion.

These characteristic profiles identified in the gels were also observed *in vivo*, with infusate refluxing in a controlled manner to the step before stabilising and distributing laterally. As might be expected, infusions into live tissues are less uniform than in homogenous gels however linear increases in distribution length and a reduction in width were observed across the small number of catheters tested which demonstrates proof of principle.

We observed that secondary reflux occurred most often in tests utilising short step lengths (3-6mm) and the highest flow rate (0.6ml/hr). This may help explain the difficulty in directly translating pre-clinical results to clinic, as smaller infusion volumes would typically be infused to cope with the smaller anatomy of, for example, rodent, porcine and primate models, resulting in less reflux. Generally, faster flow rates are regarded as more desirable in human applications as shorter duration infusions are more cost effective and preferred by both clinicians and patients (Bankiewicz *et al.*, 2016). It is of interest to note therefore that the trends observed in this study indicate that faster rates are associated with smaller distributions at the end of the infusion and increased rates of undesirable reflux, while previous studies have highlighted the risks of tissue damage at high flow rates (Krauze *et al.*, 2005).

It is noteworthy that the infusion duration at 0.1ml/hr takes more than 3hrs longer than at 0.6ml/hr providing more time for fluid pathways to develop in the substrate. High concentration gradients will of course continue to distribute after the end of the infusion, but through the action of residual pressure and diffusion alone. *In vivo*, such action would be subject to loss mechanisms (e.g. metabolism, drug half-life, perivascular losses and cerebrospinal fluid turnover). High concentration, homogenous coverage of a large area is therefore of primary interest. A compromise must therefore be struck between the preferred, short infusion times resulting in smaller distribution volumes, or longer infusion times that provide greater coverage, reduced risk of reflux but greater risk of unavoidable losses via natural clearance mechanisms.

Our evaluation used previously published image segmentation methods to measure distribution volumes from areas of high concentration in gel slices (Gill *et al.*, 2013). Advanced techniques could provide further real time image processing of the concentration profiles under investigation (Sindhwani *et al.*, 2011).

As previously discussed, maximising coverage of target structures can be better achieved if the distribution morphology more closely matches that of the target. Dividing the length to the width of each distribution respectively, normalises the distribution morphology in to two distinct types; Spherical and Cylindrical.

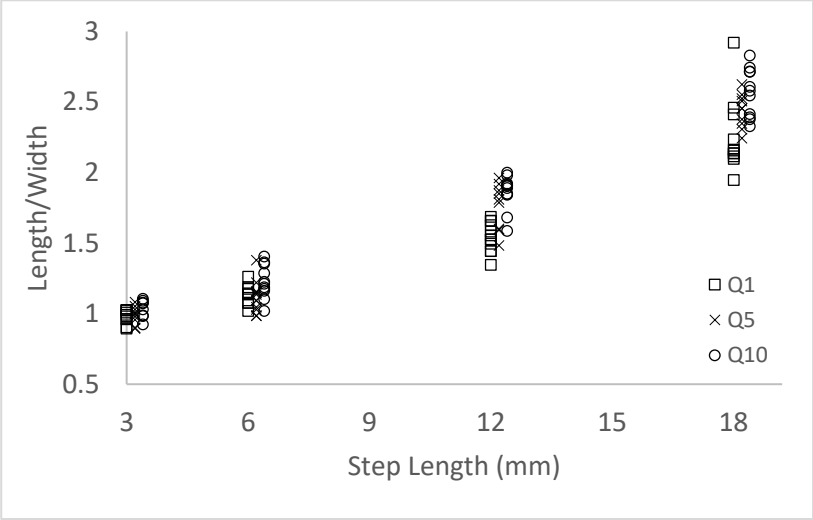

Figure 4-3. Distribution morphology aspect ratio.

The shorter step lengths, 3 and 6mm, produce a spherical like distribution with a length/width ratio of 1:1 to 1:1.5 (for comparable, clinically relevant infusion volumes), which would account for the point source distributions historically expected from CED devices. Increasing the step length above 12mm resulted in distribution aspect ratios of 2:1 or 3:1 (Figure 4-3).

Application of the RSC characteristics to clinical indications would see safe trajectories being chosen based on maximising the catheter step length within the target structure, providing patient specific opportunities to maximise target coverage. While *in vivo* loss pathways, clearing mechanisms and reflux remain real world challenges, this basic empirical model of distribution morphologies can provide a useful tool when planning catheter implantation targets and trajectories.

We have demonstrated the action of controlled reflux along the step region of the RSC for a range of step lengths both through in vitro gel and in vivo experimentation. While this is immediately applicable to surgical planning decision making, the specific characteristics of the RSC can now be included within predictive models of distribution of anisotropic flow in the brain (Linninger *et al.*, 2008a; Linninger *et al.*, 2008b; Linninger *et al.*, 2008c).

Spherical distributions may continue to suit small, pre-clinical targets or clinical targets such as the pons or thalamus while elongate, cylindrical distributions would match structures like the putamen, caudate nucleus or hippocampus (etc.). Further, by using the elongate, lozenge shaped infusion clouds which are associated with longer step lengths, fewer catheters could be used simultaneously to infuse into multiple targets, as catheters can be implanted and infused in separate stages. This may be over simplistic however, as the target tissue volume is not homogeneously distributed throughout structures like the putamen. The anterior aspect of the putamen is wider and taller than in the posterior of the structure. Preferential surgical planning strategies may combine the placement of a shorter stepped catheter vertically, down into the anterior portion while further catheters with much longer steps could be placed along the long, midline axis of the structure, from an anterior or posterior approach (e.g. Figure 4-4). Further, by implanting multiple catheters (Figure 4-4a-c), simultaneous infusions can reduce the overall administration time while the choice of trajectory and infusion regime maximise target coverage.

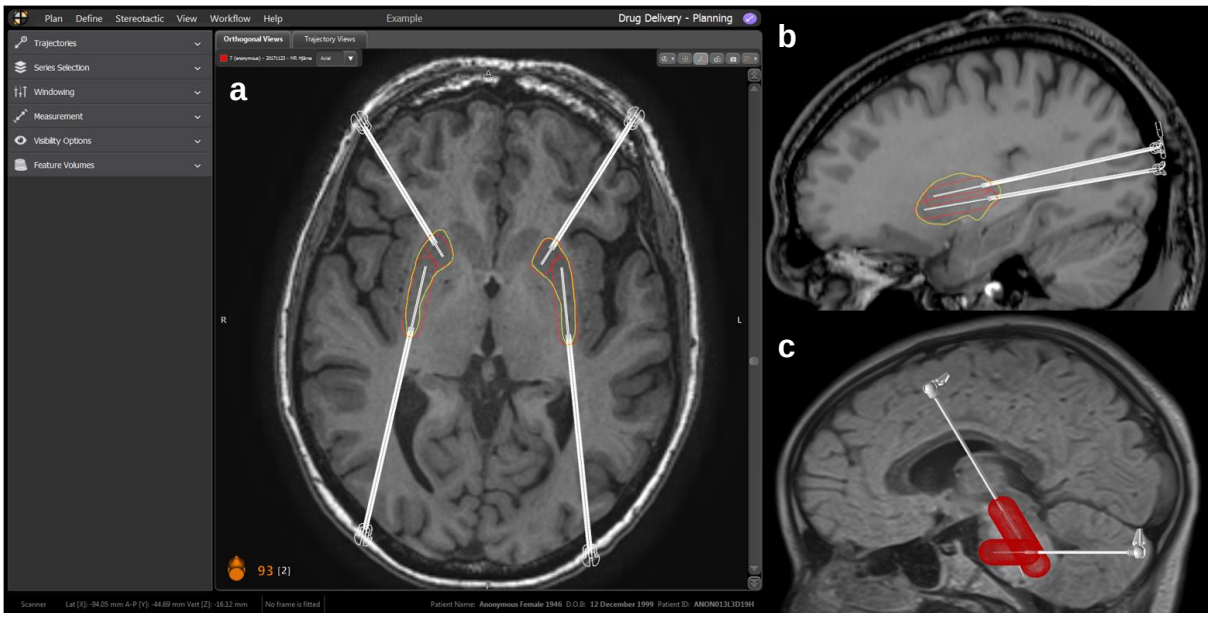

Figure 4-4. Examples of surgical trajectories aiming to maximise target structure coverage using the RSC, a) Example drug delivery surgical plan within neuro\|inspire™ (Renishaw plc, UK), putamen (yellow outlines) coverage is targeted with an empirical infusion distribution planning guide (red outlines) delivered via four catheters (white outlines), b) alternative, vertically stacked RSC entering the putamen via a posterior trajectory, c) transfrontal and transcerebellar catheter trajectories aimed at maximising coverage in the brain stem for indications such as Diffuse Intrinsic Pontine Glioma (DIPG).

4.3 Intervening in refluxing infusions

As described above, we observed secondary reflux at the highest frequency in experiments with short step lengths and high flow rates. Once a reflux pathway is established, large volumes are continually lost down this path of least resistance.

As an additional investigational endpoint, we investigated the ability of the user to recover an out of control refluxing catheter as it became visible in the gel model. Twelve infusions were performed using 3, 6 and 12mm steps with infusions ramped to the fastest flow rate (0.6ml/hr) in 40mins. Secondary reflux occurred routinely within the first 30mins after initiating the infusion (Figure 4-5 a-f), which may account in part for the lower distribution volumes seen. Once observed, the user intervened in the infusion regime, dropping the infusion rate to 0.1ml/hr or initiating a new ramp profile to 0.1ml/hr. In both cases the secondary reflux was halted at the initially observed level and the remaining distribution volume continued to develop as desired below the recessed step (Figure 4-5 g-l). This practical recovery method will prove useful to ensure predictable V_d's are attained even if a patient's anatomy is so heterogeneous that the desired distribution morphology proves difficult to achieve.

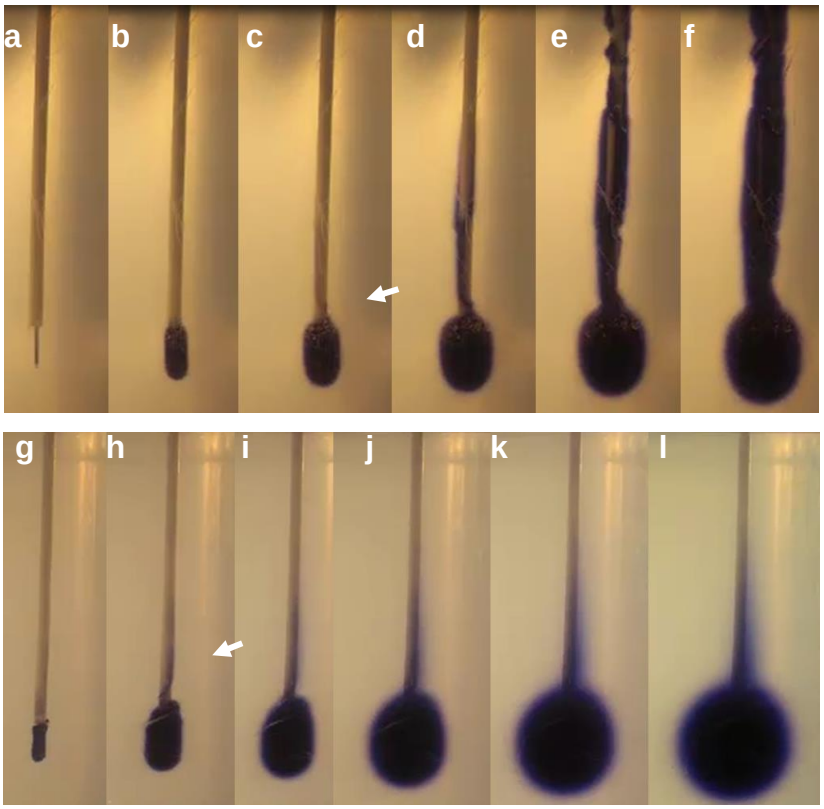

Figure 4-5. Progression of infusion distributions: a-f) standard 40minute ramp run to peak rate of 0.6ml/hr (arrow indicates initiation of visible secondary reflux), g-l) standard 40minute ramp run to peak rate of 0.6ml/hr halted and dropped to lower rate after visible reflux begins.

Our preliminary investigations suggest that priming the flow pathways ahead of increasing flow rates may yield favourable outcomes but further work is required to optimise this paradigm. As there is inherent variability within neurodegenerative populations our investigations would discourage the use of a *"one size fits all"* approach, and real time or post-infusion imaging would augment a treatment regime which enables the clinician to "drive" the

implanted system based on real feedback. Implanted catheters could then be optimised with initial infusion parameters, but fully implanted MRI compatible systems also offer the ability to maintain long term performance through periodic test infusions.

5 Conclusions

We have demonstrated how the recessed step catheter and the "controlled reflux" technique can be used to optimise the distribution morphology of infusates within an idealised, homogeneous gel model and demonstrated proof of this principle *in vivo* in porcine grey matter structures.

We have also demonstrated a practical method to recover 'out-of-control' refluxing catheters that may be affected by the heterogenous and isotropic nature of the parenchyma.

The drive towards ever faster flow rates to minimise the burden on clinical time must be balanced against the increased risk of losses due to reflux and reduced distribution volumes. Further work is required to investigate optimal controlled reflux regimes for maximising V_d.

Real time or post-infusion imaging offers users the opportunity to fine tune infusion regimes, as we have demonstrated that reducing infusion rates can offer improved distribution volumes and an opportunity to actively control infusion morphology. Real time or post infusion imaging therefore remains critical to CED treatments in order to optimise distributions in an inherently variable patient population. A fully MRI compatible implant will enable periodic infusion modulation to maximise coverage in the desired target anatomy over time or optimise catheters placed in unavoidable, leakage pathway areas of the parenchyma.

Further work is required to understand how these observations may be translated to acute and chronic infusions in the human diseased brain. The challenge to clinicians utilising CED systems remains the integration of current knowledge of surgical planning techniques and the integration of expensive real-time imaging for the benefit of long term optimisation of target coverage. These device specific characteristics should be incorporated into predictive computational models to provide user specific solutions in the surgical planning workflow.

Continued investment in CED platforms is resulting in more robust designs being available for investigational and clinical trial use. Continued research to optimise acute and chronic CED devices, as well as their infusion regimes, is necessary to maximise the coverage of neuroanatomical structures and provide the best chance of success in neurodegenerative and neuro-oncological treatments and investigational studies. Development and use of similar devices for in vitro laboratory assessment, prior to pre-clinical and clinical studies is essential to translate the learning and experiences gained in to clinical practice.

6 Acknowledgements

Special thanks go to the staff at the Translational Biomedical Research Centre, Bristol, UK.

7 References

Anderson, J. M. (2001) 'Biological Responses to Materials', *Annual Review of Materials Research,* 31(1), pp. 81-110.

Anderson, R. C., Kennedy, B., Yanes, C. L., Garvin, J., Needle, M., Canoll, P., Feldstein, N. A. and Bruce, J. N. (2013) 'Convection-enhanced delivery of topotecan into diffuse intrinsic brainstem tumors in children', *J Neurosurg Pediatr,* 11(3), pp. 289-95.

Bankiewicz, K. S., Eberling, J. L., Kohutnicka, M., Jagust, W., Pivirotto, P., Bringas, J., Cunningham, J., Budinger, T. F. and Harvey-White, J. (2000) 'Convection-enhanced delivery of AAV vector in parkinsonian monkeys; in vivo detection of gene expression and restoration of dopaminergic function using pro-drug approach', *Exp Neurol,* 164(1), pp. 2-14.

Bankiewicz, K. S., Sudhakar, V., Samaranch, L., San Sebastian, W., Bringas, J. and Forsayeth, J. (2016) 'AAV viral vector delivery to the brain by shape-conforming MR-guided infusions', *J Control Release,* 240, pp. 434-442.

Bartus, R. T., Baumann, T. L., Brown, L., Kruegel, B. R., Ostrove, J. M. and Herzog, C. D. (2013) 'Advancing neurotrophic factors as treatments for age-related neurodegenerative diseases: developing and demonstrating "clinical proof-of-concept" for AAV-neurturin (CERE-120) in Parkinson's disease', *Neurobiol Aging,* 34(1), pp. 35-61.

Barua, N. U., Bienemann, A. S., Hesketh, S., Wyatt, M. J., Castrique, E., Love, S. and Gill, S. S. (2012) 'Intrastriatal convection-enhanced delivery results in widespread perivascular distribution in a pre-clinical model', *Fluids Barriers CNS,* 9(1), pp. 2.

Barua, N. U., Hopkins, K., Woolley, M., O'Sullivan, S., Harrison, R., Edwards, R. J., Bienemann, A. S., Wyatt, M. J., Arshad, A. and Gill, S. S. (2014) 'A novel implantable catheter system with transcutaneous port for intermittent convection-enhanced delivery of carboplatin for recurrent glioblastoma', *J Drug Delivery*.

Barua, N. U., Lowis, S. P., Woolley, M., O'Sullivan, S., Harrison, R. and Gill, S. S. (2013a) 'Robot-guided convection-enhanced delivery of carboplatin for advanced brainstem glioma', *Acta Neurochir (Wien),* 155(8), pp. 1459-65.

Barua, N. U., Woolley, M., Bienemann, A. S., Johnson, D., Wyatt, M. J., Irving, C., Lewis, O., Castrique, E. and Gill, S. S. (2013b) 'Convection-enhanced delivery of AAV2 in white matter--a novel method for gene delivery to cerebral cortex', *J Neurosci Methods,* 220(1), pp. 1-8.

Barua, N. U., Woolley, M., Bienemann, A. S., Johnson, D. E., Lewis, O., Wyatt, M. J., Irving, C., O'Sullivan, S., Murray, G., Fennelly, C., Skinner, P. and Gill, S. S. (2013c) 'Intermittent convection-enhanced delivery to the brain through a novel transcutaneous bone-anchored port', *J Neurosci Methods,* 214(2), pp. 223-32.

Bauer, H. C., Krizbai, I. A., Bauer, H. and Traweger, A. (2014) '"You Shall Not Pass"-tight junctions of the blood brain barrier', *Front Neurosci,* 8, pp. 392.

Bear, J. (1988) *Dynamics of fluids in porous media.* New York: Dover.

Belova, E., Shaffer, C. L. and Trapa, P. E. (2017) 'Insights from mathematical modeling for convection-enhanced intraputamenal delivery of GDNF', *Med Biol Eng Comput*.

Bienemann, A., White, E., Woolley, M., Castrique, E., Johnson, D. E., Wyatt, M., Murray, G., Taylor, H., Barua, N. and Gill, S. S. (2012) 'The development of an implantable catheter system for chronic or intermittent convection-enhanced delivery', *Journal of Neuroscience Methods,* 203(2), pp. 284-291.

Bobo, R. H., Laske, D. W., Akbasak, A., Morrison, P. F., Dedrick, R. L. and Oldfield, E. H. (1994) 'Convection-enhanced delivery of macromolecules in the brain', *Proc Natl Acad Sci U S A,* 91(6), pp. 2076-80.

Brady, M. L., Raghavan, R., Alexander, A., Kubota, K., Sillay, K. and Emborg, M. E. (2013) 'Pathways of infusate loss during convection-enhanced delivery into the putamen nucleus', *Stereotact Funct Neurosurg,* 91(2), pp. 69-78.

Brady, M. L., Raghavan, R., Singh, D., Anand, P. J., Fleisher, A. S., Mata, J., Broaddus, W. C. and Olbricht, W. L. (2014) 'In vivo performance of a microfabricated catheter for intraparenchymal delivery', *J Neurosci Methods,* 229, pp. 76-83.

Breeze, R. E., Wells, T. H., Jr. and Freed, C. R. (1995) 'Implantation of fetal tissue for the management of Parkinson's disease: a technical note', *Neurosurgery,* 36(5), pp. 1044-7; discussion 1047-8.

Budday, S., Nay, R., de Rooij, R., Steinmann, P., Wyrobek, T., Ovaert, T. C. and Kuhl, E. (2015) 'Mechanical properties of gray and white matter brain tissue by indentation', *J Mech Behav Biomed Mater,* 46, pp. 318-30.

Chen, M. Y., Lonser, R. R., Morrison, P. F., Governale, L. S. and Oldfield, E. H. (1999) 'Variables affecting convection-enhanced delivery to the striatum: a systematic examination of rate of infusion, cannula size, infusate concentration, and tissue-cannula sealing time', *J Neurosurg,* 90(2), pp. 315-20.

Chen, Z. J., Broaddus, W. C., Viswanathan, R. R., Raghavan, R. and Gillies, G. T. (2002) 'Intraparenchymal drug delivery via positive-pressure infusion: experimental and modeling studies of poroelasticity in brain phantom gels', *IEEE Trans Biomed Eng,* 49(2), pp. 85-96.

Chen, Z. J., Gillies, G. T., Broaddus, W. C., Prabhu, S. S., Fillmore, H., Mitchell, R. M., Corwin, F. D. and Fatouros, P. P. (2004) 'A realistic brain tissue phantom for intraparenchymal infusion studies', *J Neurosurg,* 101(2), pp. 314-22.

Cheng, S. and Bilston, L. E. (2007) 'Unconfined compression of white matter', *J Biomech,* 40(1), pp. 117-24.

Chittiboina, P., Heiss, J. D., Warren, K. E. and Lonser, R. R. (2014) 'Magnetic resonance imaging properties of convective delivery in diffuse intrinsic pontine gliomas', *J Neurosurg Pediatr,* 13(3), pp. 276-82.

ClinicalTrials.gov (2015a) *National Institutes of health, clinicaltrials.gov* - https://clinicaltrials.gov/ct2/home (Accessed: 10August2015 2015).

ClinicalTrials.gov (2015b) *National Institutes of health, clinicaltrials.gov - A service of the U.S. National Institutes of Health*. Online: National Institutes of Health. Available at: https://clinicaltrials.gov/ct2/home (Accessed: 10August2015 2015).

Dawe, R. and Erickson, R. (2006) 'Convection-enhanced delivery into agarose gel brain tissue phantoms'.

Debinski, W. and Tatter, S. B. (2009) 'Convection-enhanced delivery for the treatment of brain tumors', *Expert Rev Neurother,* 9(10), pp. 1519-27.

Dorsey, E. R., Constantinescu, R., Thompson, J. P., Biglan, K. M., Holloway, R. G., Kieburtz, K., Marshall, F. J., Ravina, B. M., Schifitto, G., Siderowf, A. and Tanner, C. M. (2007) 'Projected number of people with Parkinson disease in the most populous nations, 2005 through 2030', *Neurology,* 68(5), pp. 384-6.

Dumont, T. M. (2016) 'Prospective Assessment of a Symptomatic Cerebral Vasospasm Predictive Neural Network Model', *World Neurosurg,* 94, pp. 126-130.

Elenes, E. Y., Rausch, M. K. and Rylander, C. G. (2019) 'Parametric Study of the Design Variables of an Arborizing Catheter on Dispersal Volume Using a Biphasic Computational Model', *Journal of Engineering and Science in Medical Diagnostics and Therapy,* 2(3), pp. 031002-031002-9.

Fan, X., Nelson, B. D., Ai, Y., Stiles, D. K., Gash, D. M., Hardy, P. A. and Zhang, Z. (2015) 'Continuous intraputamenal convection-enhanced delivery in adult rhesus macaques', *J Neurosurg*, pp. 1-9.

Fawcett, J. W. and Asher, R. A. (1999) 'The glial scar and central nervous system repair', *Brain Res Bull,* 49(6), pp. 377-91.

Fick, A. (1855) 'Ueber Diffusion', *Annalen der Physik,* 170(1), pp. 59-86.

Forte, A. E., Galvan, S., Manieri, F., Rodriguez y Baena, F. and Dini, D. (2016) 'A composite hydrogel for brain tissue phantoms', *Materials & Design,* 112(Supplement C), pp. 227-238.

Franceschini, G., Bigoni, D., Regitnig, P. and Holzapfel, G. A. (2006) 'Brain tissue deforms similarly to filled elastomers and follows consolidation theory', *Journal of the Mechanics and Physics of Solids,* 54(12), pp. 2592-2620.

Gash, D. M., Zhang, Z., Ovadia, A., Cass, W. A., Yi, A., Simmerman, L., Russell, D., Martin, D., Lapchak, P. A., Collins, F., Hoffer, B. J. and Gerhardt, G. A. (1996) 'Functional recovery in parkinsonian monkeys treated with GDNF', *Nature,* 380(6571), pp. 252-5.

Geuzaine, C. and Remacle, J.-F. (2009) 'Gmsh: A 3-D finite element mesh generator with built-in pre- and post-processing facilities', *International Journal for Numerical Methods in Engineering,* 79(11), pp. 1309-1331.

Gill, S. S., Patel, N. K., Hotton, G. R., O'Sullivan, K., McCarter, R., Bunnage, M., Brooks, D. J., Svendsen, C. N. and Heywood, P. (2003) 'Direct brain infusion of glial cell line-derived neurotrophic factor in Parkinson disease', *Nat Med,* 9(5), pp. 589-95.

Gill, T., Barua, N. U., Woolley, M., Bienemann, A. S., Johnson, D. E., Sullivan, S. O., Murray, G., Fennelly, C., Lewis, O., Irving, C., Wyatt, M. J., Moore, P. and Gill, S. S. (2013) 'In vitro and in vivo testing of a novel recessed-step catheter for reflux-free convection-enhanced drug delivery to the brain', *J Neurosci Methods,* 219(1), pp. 1-9.

Gimenez, F., Krauze, M. T., Valles, F., Hadaczek, P., Bringas, J., Sharma, N., Forsayeth, J. and Bankiewicz, K. S. (2011) 'Image-guided convection-enhanced delivery of GDNF protein into monkey putamen', *Neuroimage,* 54 Suppl 1, pp. S189-95.

Goetz, C. G., Laska, E., Hicking, C., Damier, P., Muller, T., Nutt, J., Warren Olanow, C., Rascol, O. and Russ, H. (2008) 'Placebo influences on dyskinesia in Parkinson's disease', *Mov Disord,* 23(5), pp. 700-7.

Guarnieri, M., Carson, B. S., Sr. and Jallo, G. I. (2008) 'Catheters for chronic administration of drugs into brain tissue', *Methods Mol Biol,* 437, pp. 109-17.

Hayn, L., Deppermann, L. and Koch, M. (2017) 'Reduction of the foreign body response and neuroprotection by apyrase and minocycline in chronic cannula implantation in the rat brain', *Clin Exp Pharmacol Physiol,* 44(2), pp. 313-323.

Healy, A. T. and Vogelbaum, M. A. (2015) 'Convection-enhanced drug delivery for gliomas', *Surg Neurol Int,* 6(Suppl 1), pp. S59-67.

Ho, S. L., Singh, R., Zhou, Z., Lavi, E. and Souweidane, M. M. (2015) 'Toxicity evaluation of prolonged convection-enhanced delivery of small-molecule kinase inhibitors in naive rat brainstem', *Childs Nerv Syst,* 31(2), pp. 221-6.

Ivanchenko, O., Sindhwani, N. and Linninger, A. (2010) 'Experimental techniques for studying poroelasticity in brain phantom gels under high flow microinfusion', *J Biomech Eng,* 132(5), pp. 051008.

Kanda, T., Ishii, K., Kawaguchi, H., Kitajima, K. and Takenaka, D. (2014) 'High signal intensity in the dentate nucleus and globus pallidus on unenhanced T1-weighted MR images: relationship with increasing cumulative dose of a gadolinium-based contrast material', *Radiology,* 270(3), pp. 834-41.

Kim, I., Paek, S., Nelson, B. D., Knight, E. J., Marsh, M. P., Bieber, A. J., Bennet, K. E. and Lee, K. H. (2014) 'Implementation of a chronic unilateral intraparenchymal drug delivery system in a swine model', *J Neurosci Methods*.

Kim, J. H., Mareci, T. H. and Sarntinoranont, M. (2010) 'A voxelized model of direct infusion into the corpus callosum and hippocampus of the rat brain: model development and parameter analysis', *Med Biol Eng Comput,* 48(3), pp. 203-14.

Kowal, S. L., Dall, T. M., Chakrabarti, R., Storm, M. V. and Jain, A. (2013) 'The current and projected economic burden of Parkinson's disease in the United States', *Mov Disord,* 28(3), pp. 311-8.

Krauze, M. T., Saito, R., Noble, C., Tamas, M., Bringas, J., Park, J. W., Berger, M. S. and Bankiewicz, K. (2005) 'Reflux-free cannula for convection-enhanced high-speed delivery of therapeutic agents', *J Neurosurg,* 103(5), pp. 923-9.

Kuhn, L. T. (2005) '6 - BIOMATERIALS A2 - Enderle, John D', in Blanchard, S.M. and Bronzino, J.D. (eds.) *Introduction to Biomedical Engineering (Second Edition)*. Boston: Academic Press, pp. 255-312.

Kumpulainen, E., Kokki, H., Halonen, T., Heikkinen, M., Savolainen, J. and Laisalmi, M. (2007) 'Paracetamol (acetaminophen) penetrates readily into the cerebrospinal fluid of children after intravenous administration', *Pediatrics,* 119(4), pp. 766-71.

Kunwar, S., Chang, S., Westphal, M., Vogelbaum, M., Sampson, J., Barnett, G., Shaffrey, M., Ram, Z., Piepmeier, J., Prados, M., Croteau, D., Pedain, C., Leland, P., Husain, S. R., Joshi, B. H. and Puri, R. K. (2010) 'Phase III randomized trial of CED of IL13-PE38QQR vs Gliadel wafers for recurrent glioblastoma', *Neuro Oncol,* 12(8), pp. 871-81.

Lam, M. F., Foo, S. W., Thomas, M. G. and Lind, C. R. (2014) 'Infusion-line pressure as a real-time monitor of convection-enhanced delivery in pre-clinical models', *J Neurosci Methods,* 221, pp. 127-31.

Lam, M. F., Thomas, M. G. and Lind, C. R. (2011) 'Neurosurgical convection-enhanced delivery of treatments for Parkinson's disease', *J Clin Neurosci,* 18(9), pp. 1163-7.

Lang, A. E., Gill, S., Patel, N. K., Lozano, A., Nutt, J. G., Penn, R., Brooks, D. J., Hotton, G., Moro, E., Heywood, P., Brodsky, M. A., Burchiel, K., Kelly, P., Dalvi, A., Scott, B., Stacy, M., Turner, D., Wooten, V. G., Elias, W. J., Laws, E. R., Dhawan, V., Stoessl, A. J., Matcham, J., Coffey, R. J. and Traub, M. (2006) 'Randomized controlled trial of intraputamenal glial cell line-derived neurotrophic factor infusion in Parkinson disease', *Ann Neurol,* 59(3), pp. 459-66.

Langford, R. A., Hogg, M., Bjorksten, A. R., Williams, D. L., Leslie, K., Jamsen, K. and Kirkpatrick, C. (2016) 'Comparative Plasma and Cerebrospinal Fluid Pharmacokinetics of Paracetamol After Intravenous and Oral Administration', *Anesth Analg,* 123(3), pp. 610-5.

Leibinger, A., Forte, A. E., Tan, Z., Oldfield, M. J., Beyrau, F., Dini, D. and Rodriguez, Y. B. F. (2016) 'Soft Tissue Phantoms for Realistic Needle Insertion: A Comparative Study', *Ann Biomed Eng,* 44(8), pp. 2442-52.

Lewandowsky, M. (1909) 'Zur Lehre der Cerebrospinalflussigkeit', *Z. Klin. Med.,* 40, pp. 480-494.

Lewis, O. 'A systems based approach to drug delivery - a method that works', *SNO-SCIDOT Joint Conference on Therapeutic Delivery to the CNS*, San Antonio, Texas, USA.
Lewis, O. (2015b) 'Manipulating infusion morphology of chronically implanted convection-enhanced delivery catheters', *Journal of Drug Delivery (publication in writing)*.
Lewis, O., Woolley, M., Johnson, D., Rosser, A., Barua, N. U., Bienemann, A. S., Gill, S. S. and Evans, S. (2016) 'Chronic, intermittent convection-enhanced delivery devices', *J Neurosci Methods,* 259, pp. 47-56.
Lewis, O., Woolley, M., Johnson, D. E., Fletcher, J., Fenech, J., Pietrzyk, M. W., Barua, N. U., Bienemann, A. S., Singleton, W., Evans, S. L. and Gill, S. S. (2018) 'Maximising coverage of brain structures using controlled reflux, convection-enhanced delivery and the recessed step catheter', *J Neurosci Methods*.
Lewis, O., Woolley, M. and Johnson, D. F., J Fenech, J Keenan, B Potts, M Hobden, P Evans, SL 'Novel brain phantoms for neurological catheter development'. *World Congress of Biomechanics*, Dublin, Ireland.
Lieberman, D. M., Laske, D. W., Morrison, P. F., Bankiewicz, K. S. and Oldfield, E. H. (1995) 'Convection-enhanced distribution of large molecules in gray matter during interstitial drug infusion', *J Neurosurg,* 82(6), pp. 1021-9.
Lin, J., Morris, M., Olivero, W., Boop, F. and Sanford, R. A. (2003) 'Computational and experimental study of proximal flow in ventricular catheters. Technical note', *J Neurosurg,* 99(2), pp. 426-31.
Linninger, A. A., Somayaji, M. R., Erickson, T., Guo, X. and Penn, R. D. (2008a) 'Computational methods for predicting drug transport in anisotropic and heterogeneous brain tissue', *J Biomech,* 41(10), pp. 2176-87.
Linninger, A. A., Somayaji, M. R., Mekarski, M. and Zhang, L. (2008b) 'Prediction of convection-enhanced drug delivery to the human brain', *J Theor Biol,* 250(1), pp. 125-38.
Linninger, A. A., Somayaji, M. R., Zhang, L., Smitha Hariharan, M. and Penn, R. D. (2008c) 'Rigorous mathematical modeling techniques for optimal delivery of macromolecules to the brain', *IEEE Trans Biomed Eng,* 55(9), pp. 2303-13.
Lonser, R. R., Schiffman, R., Robison, R. A., Butman, J. A., Quezado, Z., Walker, M. L., Morrison, P. F., Walbridge, S., Murray, G. J., Park, D. M., Brady, R. O. and Oldfield, E. H. (2007a) 'Image-guided, direct convective delivery of glucocerebrosidase for neuronopathic Gaucher disease', *Neurology,* 68(4), pp. 254-61.
Lonser, R. R., Walbridge, S., Garmestani, K., Butman, J. A., Walters, H. A., Vortmeyer, A. O., Morrison, P. F., Brechbiel, M. W. and Oldfield, E. H. (2002) 'Successful and safe perfusion of the primate brainstem: in vivo magnetic resonance imaging of macromolecular distribution during infusion', *J Neurosurg,* 97(4), pp. 905-13.
Lonser, R. R., Walbridge, S., Murray, G. J., Aizenberg, M. R., Vortmeyer, A. O., Aerts, J. M., Brady, R. O. and Oldfield, E. H. (2005) 'Convection perfusion of glucocerebrosidase for neuronopathic Gaucher's disease', *Ann Neurol,* 57(4), pp. 542-8.
Lonser, R. R., Warren, K. E., Butman, J. A., Quezado, Z., Robison, R. A., Walbridge, S., Schiffman, R., Merrill, M., Walker, M. L., Park, D. M., Croteau, D., Brady, R. O. and Oldfield, E. H. (2007b) 'Real-time image-guided direct convective perfusion of intrinsic brainstem lesions. Technical note', *J Neurosurg,* 107(1), pp. 190-7.
Lopez, O. L. (2011) 'The growing burden of Alzheimer's disease', *Am J Manag Care,* 17 Suppl 13, pp. S339-45.
Love, S., Plaha, P., Patel, N. K., Hotton, G. R., Brooks, D. J. and Gill, S. S. (2005) 'Glial cell line-derived neurotrophic factor induces neuronal sprouting in human brain', *Nat Med: Vol. 7*. United States, pp. 703-4.
Lueshen, E., Tangen, K., Mehta, A. I. and Linninger, A. (2017) 'Backflow-free catheters for efficient and safe convection-enhanced delivery of therapeutics', *Med Eng Phys,* 45, pp. 15-24.
Messaritaki, E., Rudrapatna, S. U., Parker, G. D., Gray, W. P. and Jones, D. K. (2018) 'Improving the Predictions of Computational Models of Convection-Enhanced Drug Delivery by Accounting for Diffusion Non-gaussianity', *Front Neurol,* 9, pp. 1092.
Morrison, P. F., Chen, M. Y., Chadwick, R. S., Lonser, R. R. and Oldfield, E. H. (1999) 'Focal delivery during direct infusion to brain: role of flow rate, catheter diameter, and tissue mechanics', *Am J Physiol,* 277(4 Pt 2), pp. R1218-29.
Morrison, P. F., Laske, D. W., Bobo, H., Oldfield, E. H. and Dedrick, R. L. (1994) 'High-flow microinfusion: tissue penetration and pharmacodynamics', *Am J Physiol,* 266(1 Pt 2), pp. R292-305.
Mueller, S., Polley, M. Y., Lee, B., Kunwar, S., Pedain, C., Wembacher-Schroder, E., Mittermeyer, S., Westphal, M., Sampson, J. H., Vogelbaum, M. A., Croteau, D. and Chang, S. M. (2011) 'Effect of imaging and catheter characteristics on clinical outcome for patients in the PRECISE study', *J Neurooncol,* 101(2), pp. 267-77.

Nutt, J. G., Burchiel, K. J., Comella, C. L., Jankovic, J., Lang, A. E., Laws, E. R., Jr., Lozano, A. M., Penn, R. D., Simpson, R. K., Jr., Stacy, M. and Wooten, G. F. (2003) 'Randomized, double-blind trial of glial cell line-derived neurotrophic factor (GDNF) in PD', *Neurology,* 60(1), pp. 69-73.

Oh, S., Odland, R., Wilson, S. R., Kroeger, K. M., Liu, C., Lowenstein, P. R., Castro, M. G., Hall, W. A. and Ohlfest, J. R. (2007) 'Improved distribution of small molecules and viral vectors in the murine brain using a hollow fiber catheter', *J Neurosurg,* 107(3), pp. 568-77.

Okada, S., Hara, M., Kobayakawa, K., Matsumoto, Y. and Nakashima, Y. (2018) 'Astrocyte reactivity and astrogliosis after spinal cord injury', *Neurosci Res,* 126, pp. 39-43.

Olbricht, W. L., Neeves, K. B. and Foley, C. P. (2010) 'Microfluidic probes in the treatment of brain-related diseases', *Drug News Perspect,* 23(8), pp. 491-7.

Olson, J. J., Zhang, Z., Dillehay, D. and Stubbs, J. (2008) 'Assessment of a balloon-tipped catheter modified for intracerebral convection-enhanced delivery', *J Neurooncol,* 89(2), pp. 159-68.

Patel, N. K., Pavese, N., Javed, S., Hotton, G. R., Brooks, D. J. and Gill, S. S. (2013) 'Benefits of putaminal GDNF infusion in Parkinson disease are maintained after GDNF cessation', *Neurology,* 81(13), pp. 1176-8.

Pekny, M. and Nilsson, M. (2005) 'Astrocyte activation and reactive gliosis', *Glia,* 50(4), pp. 427-34.

Pekovic, S., Filipovic, R., Subasic, S., Lavrnja, I., Stojkov, D., Nedeljkovic, N., Rakic, L. and Stojiljkovic, M. (2005) 'Downregulation of glial scarring after brain injury: the effect of purine nucleoside analogue ribavirin', *Ann N Y Acad Sci,* 1048, pp. 296-310.

Raghavan, R., Brady, M. L., Rodriguez-Ponce, M. I., Hartlep, A., Pedain, C. and Sampson, J. H. (2006) 'Convection-enhanced delivery of therapeutics for brain disease, and its optimization', *Neurosurg Focus,* 20(4), pp. E12.

Raghavan, R., Brady, M. L. and Sampson, J. H. (2016) 'Delivering therapy to target: improving the odds for successful drug development', *Ther Deliv,* 7(7), pp. 457-81.

Raghavan, R. and Odland, R. M. (2017) 'Theory of porous catheters and their applications in intraparenchymal infusions', *Biomed Phys Eng Express,* 3(2).

Raven, P. H. and Johnson, G. B. (1996) *Biology.* Dubuque, IA: Wm. C. Brown Publishers.

Reese, T. S. and Karnovsky, M. J. (1967) 'Fine structural localization of a blood-brain barrier to exogenous peroxidase', *J Cell Biol,* 34(1), pp. 207-17.

Richardson, R. M., Kells, A. P., Martin, A. J., Larson, P. S., Starr, P. A., Piferi, P. G., Bates, G., Tansey, L., Rosenbluth, K. H., Bringas, J. R., Berger, M. S. and Bankiewicz, K. S. (2011) 'Novel platform for MRI-guided convection-enhanced delivery of therapeutics: preclinical validation in nonhuman primate brain', *Stereotact Funct Neurosurg,* 89(3), pp. 141-51.

Ridgeway, C. D., Gu, C., Ripplinger, K., Detwiler, D., Ji, M., Soghrati, S. and Luo, A. A. (2020) 'Prediction of location specific mechanical properties of aluminum casting using a new CA-FEA (cellular automaton-finite element analysis) approach', *Materials & Design,* 194, pp. 108929.

Roitbak, T. and Sykova, E. (1999) 'Diffusion barriers evoked in the rat cortex by reactive astrogliosis', *Glia,* 28(1), pp. 40-8.

Rosenbluth, K. H., Luz, M., Mohr, E., Mittermeyer, S., Bringas, J. and Bankiewicz, K. S. (2011) 'Design of an in-dwelling cannula for convection-enhanced delivery', *J Neurosci Methods,* 196(1), pp. 118-23.

Saito, R., Krauze, M. T., Noble, C. O., Tamas, M., Drummond, D. C., Kirpotin, D. B., Berger, M. S., Park, J. W. and Bankiewicz, K. S. (2006) 'Tissue affinity of the infusate affects the distribution volume during convection-enhanced delivery into rodent brains: implications for local drug delivery', *J Neurosci Methods,* 154(1-2), pp. 225-32.

Saltzman, W. M. (2001) *Drug delivery : engineering principles for drug therapy.* Oxford [England]; New York: Oxford University Press.

Salvatore, M. F., Ai, Y., Fischer, B., Zhang, A. M., Grondin, R. C., Zhang, Z., Gerhardt, G. A. and Gash, D. M. (2006) 'Point source concentration of GDNF may explain failure of phase II clinical trial', *Exp Neurol,* 202(2), pp. 497-505.

Sampson, J. H., Archer, G., Pedain, C., Wembacher-Schroder, E., Westphal, M., Kunwar, S., Vogelbaum, M. A., Coan, A., Herndon, J. E., Raghavan, R., Brady, M. L., Reardon, D. A., Friedman, A. H., Friedman, H. S., Rodriguez-Ponce, M. I., Chang, S. M., Mittermeyer, S., Croteau, D. and Puri, R. K. (2010) 'Poor drug distribution as a possible explanation for the results of the PRECISE trial', *J Neurosurg,* 113(2), pp. 301-9.

Sampson, J. H., Brady, M., Raghavan, R., Mehta, A. I., Friedman, A. H., Reardon, D. A., Petry, N. A., Barboriak, D. P., Wong, T. Z., Zalutsky, M. R., Lally-Goss, D. and Bigner, D. D. (2011) 'Colocalization of gadolinium-diethylene triamine pentaacetic acid with high-molecular-weight molecules after intracerebral convection-enhanced delivery in humans', *Neurosurgery,* 69(3), pp. 668-76.

Sampson, J. H., Raghavan, R., Brady, M. L., Provenzale, J. M., Herndon, J. E., 2nd, Croteau, D., Friedman, A. H., Reardon, D. A., Coleman, R. E., Wong, T., Bigner, D. D., Pastan, I., Rodriguez-Ponce, M. I., Tanner, P., Puri, R. and Pedain, C. (2007) 'Clinical utility of a patient-specific algorithm for simulating intracerebral drug infusions', *Neuro Oncol,* 9(3), pp. 343-53.

Sanftner, L. M., Sommer, J. M., Suzuki, B. M., Smith, P. H., Vijay, S., Vargas, J. A., Forsayeth, J. R., Cunningham, J., Bankiewicz, K. S., Kao, H., Bernal, J., Pierce, G. F. and Johnson, K. W. (2005) 'AAV2-mediated gene delivery to monkey putamen: evaluation of an infusion device and delivery parameters', *Exp Neurol,* 194(2), pp. 476-83.

Sarntinoranont, M., Chen, X., Zhao, J. and Mareci, T. H. (2006) 'Computational model of interstitial transport in the spinal cord using diffusion tensor imaging', *Ann Biomed Eng,* 34(8), pp. 1304-21.

Sillay, K., Hinchman, A., Kumbier, L., Schomberg, D., Ross, C., Kubota, K., Brady, M., Brodsky, E., Miranpuri, G. and Raghavan, R. (2013) 'Strategies for the delivery of multiple collinear infusion clouds in convection-enhanced delivery in the treatment of Parkinson's disease', *Stereotact Funct Neurosurg,* 91(3), pp. 153-61.

Sillay, K., Schomberg, D., Hinchman, A., Kumbier, L., Ross, C., Kubota, K., Brodsky, E. and Miranpuri, G. (2012) 'Benchmarking the ERG valve tip and MRI Interventions Smart Flow neurocatheter convection-enhanced delivery system's performance in a gel model of the brain: employing infusion protocols proposed for gene therapy for Parkinson's disease', *J Neural Eng,* 9(2), pp. 026009.

Sindhwani, N., Ivanchenko, O., Lueshen, E., Prem, K. and Linninger, A. A. (2011) 'Methods for determining agent concentration profiles in agarose gel during convection-enhanced delivery', *IEEE Trans Biomed Eng,* 58(3), pp. 626-32.

Singleton, W. G. B., Bieneman, A. S., Woolley, M., Johnson, D., Lewis, O., Wyatt, M. J., Damment, S. J. P., Boulter, L. J., Killick-Cole, C. L., Asby, D. J. and Gill, S. S. (2018) 'The distribution, clearance, and brainstem toxicity of panobinostat administered by convection-enhanced delivery', *J Neurosurg Pediatr*, pp. 1-9.

Singleton, W. G. B., Woolley, M., Lewis, O., Johnson, D. E., Irving, C, Pritchard, G., Moore, P., Kinch, S., Howell, M., Selby, J. P., Fletcher, J., Skinner, P., Bienemann, A. S., Harcourt-Brown, T., Barua, N. U. and Gill, S. S. 'Development of new CED devices'. *SCIDOT-SNO*, San Francisco, USA.

Slevin, J. T., Gerhardt, G. A., Smith, C. D., Gash, D. M., Kryscio, R. and Young, B. (2005) 'Improvement of bilateral motor functions in patients with Parkinson disease through the unilateral intraputaminal infusion of glial cell line-derived neurotrophic factor', *J Neurosurg,* 102(2), pp. 216-22.

Smith, J. H. and Humphrey, J. A. (2007) 'Interstitial transport and transvascular fluid exchange during infusion into brain and tumor tissue', *Microvasc Res,* 73(1), pp. 58-73.

Souweidane, M. M., Kramer, K., Pandit-Taskar, N., Zhou, Z., Haque, S., Zanzonico, P., Carrasquillo, J. A., Lyashchenko, S. K., Thakur, S. B., Donzelli, M., Turner, R. S., Lewis, J. S., Cheung, N. V., Larson, S. M. and Dunkel, I. J. (2018) 'Convection-enhanced delivery for diffuse intrinsic pontine glioma: a single-centre, dose-escalation, phase 1 trial', *Lancet Oncol,* 19(8), pp. 1040-1050.

Stockwell, J., Abdi, N., Lu, X., Maheshwari, O. and Taghibiglou, C. (2013) 'Novel Central Nervous System Drug Delivery Systems', *Chem Biol Drug Des*.

Sykova, E. and Nicholson, C. (2008) 'Diffusion in brain extracellular space', *Physiol Rev,* 88(4), pp. 1277-340.

Tanner, P. G., Holtmannspotter, M., Tonn, J. C. and Goldbrunner, R. (2007) 'Effects of drug efflux on convection-enhanced paclitaxel delivery to malignant gliomas: technical note', *Neurosurgery,* 61(4), pp. E880-2; discussion E882.

Tian, D. S., Yu, Z. Y., Xie, M. J., Bu, B. T., Witte, O. W. and Wang, W. (2006) 'Suppression of astroglial scar formation and enhanced axonal regeneration associated with functional recovery in a spinal cord injury rat model by the cell cycle inhibitor olomoucine', *J Neurosci Res,* 84(5), pp. 1053-63.

Tortora, G. J. D., B.H. (2009) *Principles of anatomy and physiology.* **12th International student edition** edn.: John Wiley & Sons.

Vidotto, M., Pederzani, M., Castellano, A., Pieri, V., Falini, A., Dini, D. and De Momi, E. (2020) 'Integrating Diffusion Tensor Imaging and Neurite Orientation Dispersion and Density Imaging to Improve the Predictive Capabilities of CED Models', *Annals of Biomedical Engineering*.

W.H.O., W. H. O. (2006) *Neurological Disorders: Public Health Challenges.*

Warren Olanow, C., Bartus, R. T., Baumann, T. L., Factor, S., Boulis, N., Stacy, M., Turner, D. A., Marks, W., Larson, P., Starr, P. A., Jankovic, J., Simpson, R., Watts, R., Guthrie, B., Poston, K., Henderson, J. M., Stern, M., Baltuch, G., Goetz, C. G., Herzog, C., Kordower, J. H., Alterman, R., Lozano, A. M. and Lang, A. E. (2015) 'Gene delivery of neurturin to putamen and substantia nigra in Parkinson disease: A double-blind, randomized, controlled trial', *Ann Neurol,* 78(2), pp. 248-57.

White, E., Bienemann, A., Malone, J., Megraw, L., Bunnun, C., Wyatt, M. and Gill, S. (2011a) 'An evaluation of the relationships between catheter design and tissue mechanics in achieving high-flow convection-enhanced delivery', *Journal of Neuroscience Methods,* 199(1), pp. 87-97.

White, E., Woolley, M., Bienemann, A., Johnson, D. E., Wyatt, M., Murray, G., Taylor, H. and Gill, S. S. (2011b) 'A robust MRI-compatible system to facilitate highly accurate stereotactic administration of therapeutic agents to targets within the brain of a large animal model', *Journal of Neuroscience Methods,* 195(1), pp. 78-87.

Whone, A., Luz, M., Boca, M., Woolley, M., Mooney, L., Dharia, S., Broadfoot, J., Cronin, D., Schroers, C., Barua, N. U., Longpre, L., Barclay, C. L., Boiko, C., Johnson, G. A., Fibiger, H. C., Harrison, R., Lewis, O., Pritchard, G., Howell, M., Irving, C., Johnson, D., Kinch, S., Marshall, C., Lawrence, A. D., Blinder, S., Sossi, V., Stoessl, A. J., Skinner, P., Mohr, E. and Gill, S. S. (2019a) 'Randomized trial of intermittent intraputamenal glial cell line-derived neurotrophic factor in Parkinson's disease', *Brain,* 142(3), pp. 512-525.

Whone, A. L., Boca, M., Luz, M., Woolley, M., Mooney, L., Dharia, S., Broadfoot, J., Cronin, D., Schroers, C., Barua, N. U., Longpre, L., Barclay, C. L., Boiko, C., Johnson, G. A., Fibiger, H. C., Harrison, R., Lewis, O., Pritchard, G., Howell, M., Irving, C., Johnson, D., Kinch, S., Marshall, C., Lawrence, A. D., Blinder, S., Sossi, V., Stoessl, A. J., Skinner, P., Mohr, E. and Gill, S. S. (2019b) 'Extended Treatment with Glial Cell Line-Derived Neurotrophic Factor in Parkinson's Disease', *J Parkinsons Dis*.

Williams, D. F. (2008) 'On the mechanisms of biocompatibility', *Biomaterials,* 29(20), pp. 2941-53.

Woolley, M., Barua, N. U., Lewis, O., Keane, I., Johnson, D. E., Irving, C., Kinch, S., Moore, P., Howell, M., O'Sullivan, S., Fennelly, C., Pritchard, G., Campbell, S., Skinner, P. and Gill, S. S. 'Factors Facilitating Optimised Intraparenchymal Drug Delivery – A Prescriptive Systems Approach'. *Partnership Opportunities in Drug Delivery*, Boston, USA.

Yin, D., Richardson, R. M., Fiandaca, M. S., Bringas, J., Forsayeth, J., Berger, M. S. and Bankiewicz, K. S. (2010) 'Cannula placement for effective convection-enhanced delivery in the nonhuman primate thalamus and brainstem: implications for clinical delivery of therapeutics', *J Neurosurg,* 113(2), pp. 240-8.

Yin, D., Valles, F. E., Fiandaca, M. S., Bringas, J., Gimenez, F., Berger, M. S., Forsayeth, J. and Bankiewicz, K. S. (2011) 'Optimal region of the putamen for image-guided convection-enhanced delivery of therapeutics in human and non-human primates', *Neuroimage,* 54 Suppl 1, pp. S196-203.

Yin, D., Valles, F. E., Fiandaca, M. S., Forsayeth, J., Larson, P., Starr, P. and Bankiewicz, K. S. (2009) 'Striatal volume differences between non-human and human primates', *J Neurosci Methods,* 176(2), pp. 200-5.

Zhan, W., Rodriguez, Y. B. F. and Dini, D. (2019) 'Effect of tissue permeability and drug diffusion anisotropy on convection-enhanced delivery', *Drug Deliv,* 26(1), pp. 773-781.

Zhang, L., Yang, M. and Jiang, M. (2012) 'Mathematical Modeling for Convection-Enhanced Drug Delivery', *Procedia Engineering,* 29, pp. 268-274.